2018

STUDY OF THE EFFECT OF STERIC BULK OF SIDE CHAINS ON THE PROPERTIES OF CONJUGATED POLYMERS

Bei Zhang
University of Kentucky, beiz0001@gmail.com
Author ORCID Identifier:
https://orcid.org/0000-0003-4140-6894
Digital Object Identifier: https://doi.org/10.13023/ETD.2018.146

STUDENT AGREEMENT:

I represent that my thesis or dissertation and abstract are my original work. Proper attribution has been given to all outside sources. I understand that I am solely responsible for obtaining any needed copyright permissions. I have obtained needed written permission statement(s) from the owner(s) of each third-party copyrighted matter to be included in my work, allowing electronic distribution (if such use is not permitted by the fair use doctrine) which will be submitted to UKnowledge as Additional File.

I hereby grant to The University of Kentucky and its agents the irrevocable, non-exclusive, and royalty-free license to archive and make accessible my work in whole or in part in all forms of media, now or hereafter known. I agree that the document mentioned above may be made available immediately for worldwide access unless an embargo applies.

I retain all other ownership rights to the copyright of my work. I also retain the right to use in future works (such as articles or books) all or part of my work. I understand that I am free to register the copyright to my work.

REVIEW, APPROVAL AND ACCEPTANCE

The document mentioned above has been reviewed and accepted by the student's advisor, on behalf of the advisory committee, and by the Director of Graduate Studies (DGS), on behalf of the program; we verify that this is the final, approved version of the student's thesis including all changes required by the advisory committee. The undersigned agree to abide by the statements above.

Bei Zhang, Student

Dr. Mark D. Watson, Major Professor

Dr. Mark A. Lovell, Director of Graduate Studies

STUDY OF THE EFFECT OF STERIC BULK OF SIDE CHAINS ON THE PROPERTIES OF CONJUGATED POLYMERS

DISSERTATION

A dissertation submitted in partial fulfillment of the requirements for the degree of

Doctor of Philosophy in the College of Arts and Sciences

at the University of Kentucky

By

Bei Zhang

Lexington, Kentucky

Director: Dr. Mark D. Watson, Professor of Chemistry

Lexington, Kentucky

2018

ABSTRACT OF DISSERTATION

STUDY OF THE EFFECT OF STERIC BULK OF SIDE CHAINS ON THE PROPERTIES OF CONJUGATED POLYMERS

Donor-acceptor conjugated polymers opened a new era for conjugated polymer research due to the abundant selection and combination of different conjugated units. This class of polymers function as semiconductor materials with potential application in plastic consumer electronics. The frontier molecular orbital energies of the polymers are generally determined by the selection of donor and acceptor units in the backbone structure, and their substituents. The side chains attached to the backbone not only affect the solubility of the materials, but also their self-assembly and morphological characteristics, which indirectly govern optoelectronic properties. It is important therefore to consider backbone architectures and the side chains together, to control (opto)-electronic properties for specific applications, while also maintaining solution processability without disrupting solid-state packing.

The research presented in this dissertation focuses largely on the side chains: how the bulk and position of side chains affect the (opto)-electronic properties of select donor-acceptor (D-A) conjugated polymers. More precisely the intent is to vary the size and position of branches in the alkyl side chains of donor-acceptor polymers, in the attempt to solubilize poorly soluble polymers, without disrupting self-assembly of the polymer backbones into close π-stacks. After an introductory chapter 1, chapter 2 mainly focuses on the synthesis and structure-property study of polymers with 2,3,5,6-tetrafluorobenzene (TFB) as the acceptor motif and benzo[1,2-b:4,5-b′]dithiophene (BDT) as donor units carrying solubilizing substituents. TFB units were chosen based on previous observations that this acceptor unit imparts particularly poor solubility to various donor-acceptor copolymers. The current study indicates that bulky branches placed close to the polymer backbone could solubilize the PBDTTFB copolymers without altering the absorption profile and oxidation potentials. Optical, wide-angle x-ray diffraction (WAXD) and solubility studies shows that solubility is closely related to branching size and position. As the branch size in increased, the solubility of these polymers undergoes a step-change.

The third chapter mainly focusses on the structure-property study of D-A polymers with thienopyrroledione (TPD) as acceptor. Unlike TFB, this acceptor can carry additional side chains that can compete with the space-filling demands of the donor unit side chains. As donor, the rigid BDT unit was compared with 3,3’-dialkoxy-2,2’bithiophene (RO2T2) units which have a similar size, but contain a “swiveling” central σ-bond. Bulkiness of side

chains attached to the T2 units should be expected to have a more severe impact, possibly causing the two thiophene units of the T2 units to twist out of plane. It was demonstrated that alkoxy side chains with bulky branches in close proximity to the polymer backbones does not disrupt conjugation in these polymers. The UV-Vis absorption spectra of RO2T2-TPD polymers were red-shifted (more than 120 nm) in comparison to PBDTTPD polymers due to the smaller Eg (energy gap), which might be attributed to the expected higher energy HOMO imparted by the donor unit. The π-π stacking of polymers with BDT units was little affected by the bulky side chains. However, the π-π stacking of polymers with RO2T2 units was much more sensitive to side-chain bulk, with high degree of order and close π-π stacking only if proper local free spacing exists for side-chain interdigitation.

Chapter 4 reports efforts to study polymers from the same set of RO2T2 monomers studied in Chapter 3, but without acceptor units that might otherwise drive self-assembly. RO2T2 homopolymers were synthesized via the Grignard metathesis (GRIM) method. Further, copolymers were prepared with RO2T2 units alternating with thiophene, thieno[3,2-b]thiophene or bithiophene. The spectroscopic studies suggest these polymers with bulky side chains exhibit some varying level of backbone conjugation. Somewhat surprisingly, despite an expected decrease in the strength of intermolecular donor-acceptor interactions, the solubilities were in some cases low, but varied with volume fraction of side chains. Further, even for polymers that appear to easily dissolve, aggregation in solution is so extensive as to give ensembles “too large” for characterization by GPC and or solution NMR. Oxidation potentials seem essentially insensitive to any of the structural variables (governed mostly by the backbone RO2T2 units).

KEYWORDS: Donor-Acceptor conjugated polymers, fluorinated arene, benzo[1,2-b:4,5-b′]dithiophene (BDT), 3,3’-dialkoxy bithiophene, thiopheneimide (TPD).

Bei Zhang

Student’s Signature

03/07/2018

Date

STUDY OF THE EFFECT OF STERIC BULK OF SIDE CHAINS ON THE PROPERTIES OF CONJUGATED POLYMERS

By

Bei Zhang

Dr. Mark D. Watson

Director of Dissertation

Dr. Mark A. Lovell

Director of Graduate Studies

03/07/2018

Date

ACKNOWLEDGMENTS

Time passes very quickly, often so quickly that you are surprised. It would not have been possible to complete my PhD and write my dissertation without the help of many individuals.

First and foremost, I would express my gratitude to my PhD advisor and mentor: Prof. Mark D. Watson, who guided me during my PhD study and research. I deeply appreciate all his support, encouragement, and direction in my academic and personal life. He is nice and patient, so I can discuss with him whenever I had obstacles. He challenged me to think broadly and deeply to pursue ideas, I'm grateful for him for everything I learnt throughout my graduate career.

It's my great pleasure to acknowledge to all my committee members: Professor Mark S. Meier, Professor Dongsheng Yang and Professor Zach J. Hilt for their valuable suggestions and encouragements. I also offer my sincere appreciation to Professor Joseph Brill who was the outside examiner of my final defense examination.

I would like to mention with great appreciation, Mr. John Layton and Dr. Sean Parkin for their support in NMR and X-ray diffraction experiments, respectively. Also I must acknowledge Art Sebesta for his enormous support in repairing electronic and many other instruments and Jeff Babbitt for his help of repair glassware and make new Soxhlet device.

I thank Dr. Daijun Feng, Soledad Yao and Zhen Fang for their help and support in the lab. Also thanks Daudi Saang'onyo, Dr. Aman Preet Kaur and Harsha Attanayake for their help about NMR and spectroelectrochemical experiment.

Words are powerless to express my gratitude to my family. I would like to thank my parents, Shulong Zhang and Yuxia Du, for all their love and encouragement along with my growth.

TABLE OF CONTENTS

LIST OF TABLES

LIST OF FIGURES

LIST OF SCHEMES

LIST OF ABBREVIATIONS

A	Acceptor
BDT	Benzodithiophene
BHJ	Bulk heterojunction
BuLi	n-butyllithium
Bu_3SnCl	Tributyltin chloride
CV	Cyclic voltammetry
D-A	Donor-Acceptor
D	Donor
DCM	Dichloromethane
DEK	3-pentanone
DSC	Differential scanning calorimetry
DPV	Differential-pulse voltammetry
ECD	Electrochromic device
Eg	Energy gap
EtOAc	Ethyl acetate
EtOH	Ethanol
eV	Electron volts
Fc/Fc+	ferrocene/ferrocenium
FF	Fill factor
FMO	Frontier molecular orbitals
GPC	Gel permeation chromatography
HH	Head-to-head
HT	Head-to-tail
HOMO	Highest occupied molecular orbitals
J_{SC}	Short-circuit current density
LUMO	Lowest occupied molecular orbitals
MEK	Methyl ethyl ketone
MeCN	Acetonitrile
Me_3SnCl	Trimethyltin chloride
$Ni(dppp)Cl_2$	1,3-Bis(diphenylphosphino)propane nickel(II) chloride
OSCs	Organic solar cell
OLED	Organic light-emitting diodes
OFET	Organic field effect transistors
OPVs	Organic Photovoltaic device
PA	Polyacetylene
P3HT	Poly(3-hexylthiophene)
P3ATs	Poly(3-alkyl)thiophenes
PCBM	[6,6]-phenyl-C_{61}-butyric acid methyl ester
PCE	Power conversion efficiency
PEDOT	Poly(3,4-ethylenedioxythiophene)

PDI	Polydispersity index
PSC	Polymer solar cell
PVD	Photovoltaic devices
T2	3,3’-dialkoxy-2,2’-bithiophene
THF	Tetrahydrofuran
TFB	Tetrafluorobenzene
TPD	Thieno[3,4-c]pyrrole-4,6-dione
Voc	Open circuit voltage
WAXD	2-D wide angle x-ray diffraction

Chapter 1: Introduction to Organic Semiconductors

The new area of semiconducting polymer was developed quickly after the pioneering work of MacDiarmid, Heeger, Shirakawa who found polyacetylene as the first semiconducting polymer.[1] Nowadays semiconducting polymers have more complex molecular structures such as donor–acceptor co-polymers.[2]

1.1 Brief History of Conjugated Polymers

Polyacetylene (PA), the first conducting polymer, is unstable in air. Through the efforts of many scientists, more stable aromatic conjugated polymers such as polythiophene,[3] polypyrrole,[4] and polyaniline[5] were created through oxidative electrochemical synthesis methods. These conjugated polymers, recognized as first generation of conjugated polymers, have very poor solubility due to lack of side chains (Figure 1.1). The requirements to develop conjugated polymers that combined electrical properties as semiconductors and other physical properties of traditional polymers lead to the second generation of conjugated polymers with much better processability. Through introduction of alkyl side chains to improve the solubility, poly(3-alkyl)thiophenes (P3ATs) which have better processability were synthesized through one-step oxidation reaction.[6,7,8] A hypothetical isomer-free (regioperfect) P3AT is shown in Figure 1.1. However, the control of regularity is poor during the electropolymerization of poly(3-alkyl)thiophenes as a result of the low symmetry of 3-alkylthiophene, where coupling could occur randomly at the 2- and 5-positions which leads to structural irregularity. These regio-irregular P3ATs give poor conductivity due to disordered self-assembly and twisted backbones which limits inter- and intramolecular charge transport. The first regio-regular rr-P3AT synthesis was completed by McCullough and coworkers in 1992.[9] Then Rieke developed a similar method using

organozinc chemistry to synthesize rrP3ATs shortly after that.[10] The details about these methods will be introduced in the synthetic methods part. The rrP3ATs, especially the rr-P3HT (Figure 1.1, R = n-hexyl) benchmark are still widely studied conjugated polymers until today.

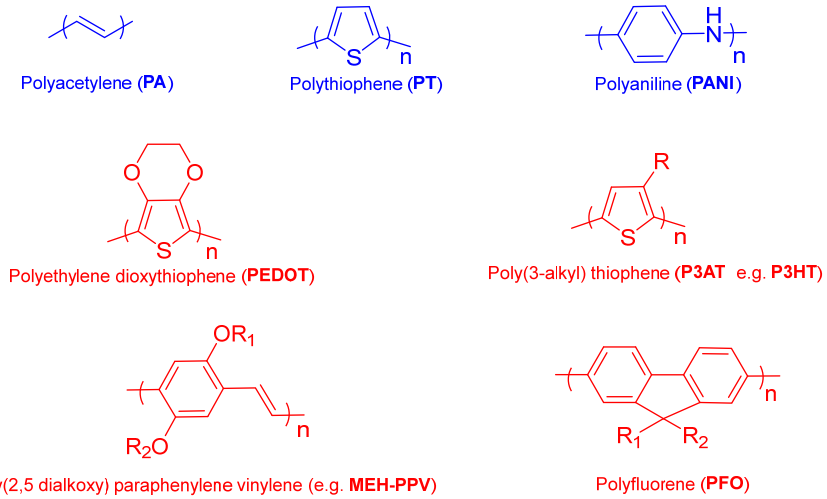

Figure 1.1: First (blue) and Second (red) Generation conjugated polymers, R = alkyl group.

In order to develop conjugated polymers with more tunable electronic and optical properties to apply for polymeric light-emitting diodes and photovoltaic cells, the third generation of conjugated copolymers evolved around the donor-acceptor (D-A) approach. The push-pull structure using the combination of electron-donor units (D) and electron-acceptor units (A) allow very fine control over (opto)electronic and other properties.[11] The D-A copolymers open a new era for conjugated polymers research in recent years, as a result of the abundant selection of conjugated building blocks with different frontier molecular orbital (FMO) energies .

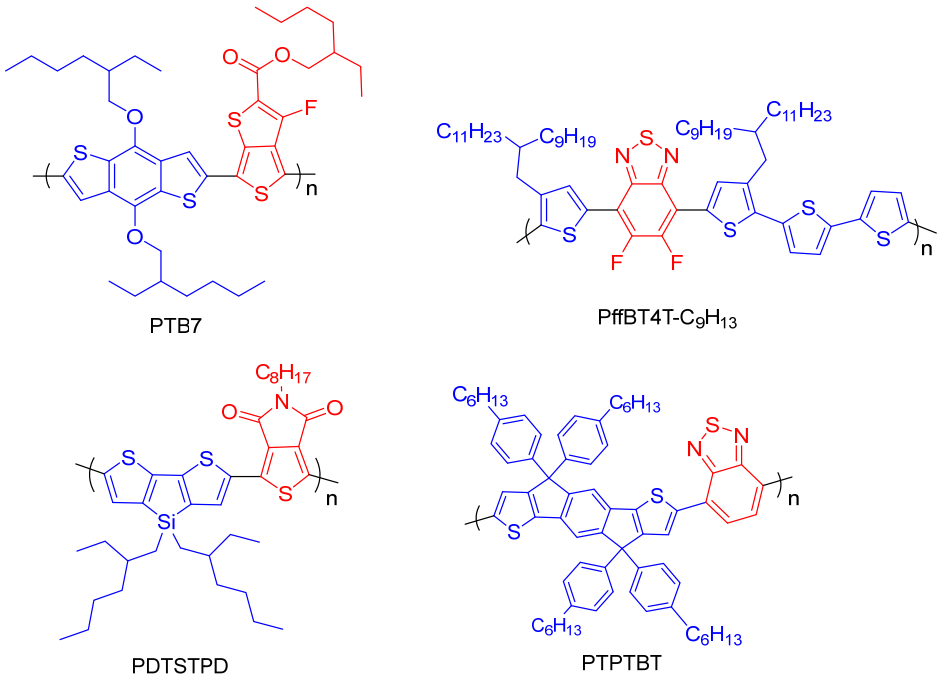

Figure 1.2: Third Generation (donor-acceptor) conjugated polymers (donor blue, acceptor red).

The Advantage and Outlook of Conjugated Polymers

Compared with inorganic semiconductors which are "harder" and more brittle, organic electronic materials can be softer and more flexible.[12] Although this point has been excessively used to promote the promise of organic electronic materials, its value is not so clear given the flexibility of inorganic materials on the length scale (nanometers) of components in electronic devices. Perhaps some advantage will be realized from "self-healing" of "softer" organic electronic components after suffering fractures. Complementary device fabrication techniques are offered through solution processing of organic materials. So it is possible to make a large scale device fabrication through ink-jets and other solution-based methods. The composition of organic electronic materials can be finely defined through synthesis, providing approaches to tuning (opto)electronic properties, complementary to the approaches that are used to finely tune

inorganic materials. The research of conjugated polymers as semiconductor materials, have potential applications in the area of organic light-emitting diodes (OLEDs),[13] organic field effect transistors (OFETs),[14] photovoltaic devices (PVDs),[15] electrochromic devices (ECDs)[16] and sensors.[17] Before the semiconductor materials can be applied in commercial devices, we need to consider not only the performance, processability and stability, but also the cost. To successfully exploit the research results for commercial application, much more attention should be paid to inexpensive and accessible materials, and reducing the complexity of device fabrication.[18]

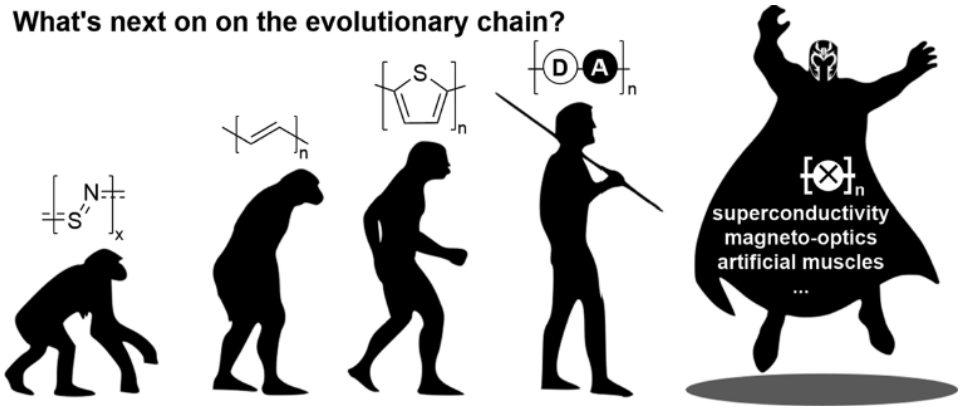

Figure 1.3: Key examples during conjugated polymer development. (Adapted with permission from Ref. [19] Copyright 2017 American Chemical Society)

A. G. MacDiarmid used to frequently say "We live in a materials-limited world."[19] This indicated the technology development was limited by new materials.[19] What's next for the conjugated polymers development? There is no answer yet, but functional materials continue to have a profound impact on new technologies and our daily life (see figure 1.3).[19] Recent study has shown that regioregular poly(3-hexylthiophene) films have unexpectedly high Verdet constant (describes the strength of the Faraday effect for a particular material) of 6.25 $\times 10^4$ deg/(T m),[20] which is comparable to state-of-the-art commercial terbium

gallium garnet (V = 7.68 × 10^4 deg/(T m)), materials developed specifically for their magneto-optical properties. This unpredicted and large magneto-optical properties can be used for detecting the magnetic signals associated with brain activity (normally requires superconducting detectors and a large cryogenic device to be placed around the subject's stationary head[21]), enable new generations of control systems that couple brain activity to mechanical or electronic systems. [19]

1.2 Frontier Molecular Orbital Engineering of Conjugated Polymers

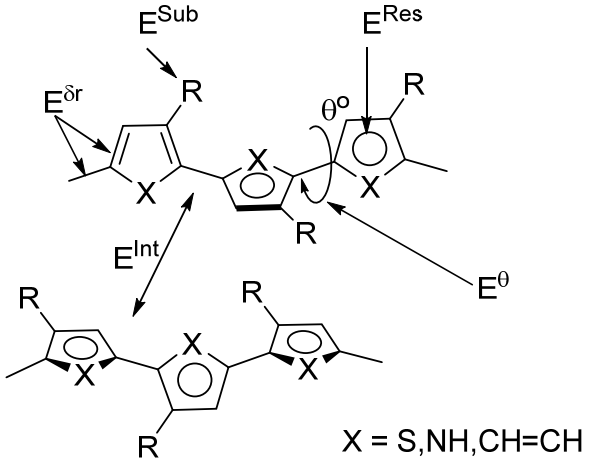

Figure 1.4: Schematic representation of five parameters (E^{δ}, E^{θ}, E^{res}, E^{sub}, and E^{int}) relative to the energy gap (Eg) of an organic semiconductor. [22]

Energy-gap (Eg, or HOMO-LUMO gap) control is an important approach to achieving desired physical and (opto)electronic properties for organic materials. Based on theoretical and experimental evidence, Ronacali[22,23] summarized and ascribed the Eg to five contributions:

1) bond length alternation (BLA) ($E^{\delta r}$), related to the difference between single and double bond lengths. Decreased BLA is correlated to decreased energy gap, for example,

increases contribution of quinoid structure (decreased BLA, see figure 1.5) to the overall resonance description.[24] Of course an increased contribution from the quinoidal resonance contributor would also affect the backbone planarity and therefore E^{θ} (see below),illustrating the interdependence of all these factors.

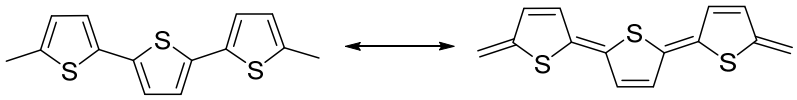

Figure 1.5: Representative aromatic and quinoid resonance forms. [25]

2) interannular rotations from single bond of aromatic cycles, twisting of the polymer backbone from its planarity (E^{θ}), orbital overlap varies approximately with the cosine of the twist angle, any departure from coplanarity will result in an increase in Eg. So in order to get smaller Eg, it is quite important to keep planar structure and/or limit the single bond rotation.

3) the aromatic resonance energy of the π-systems (E^{res}), there is a competition between π-electron confinement within the aromatic rings and delocalization along the conjugated backbone chain. Typically, highly delocalized π-electrons are essential to achieve optimal electronic properties.[26]

4) the effect of substituents (E^{Sub}) on the conjugated backbone, involves the grafting of electron-donating or -withdrawing substituents that will respectively increase the HOMO energy level (E_{HOMO}) or lower the LUMO level (E_{LUMO}).[27,28]

5) inter or intramolecular interactions in the solid state (E^{int}).[29]

The concept of Eg control plays an important role during the development of new conjugated polymers. For example, low energy gap polymers (Eg of 1.5 eV) has been

recognized as the "ideal" conjugated polymer for solar cell application.[30,31] In order to get low energy gap polymers coupled with low HOMO energy levels for solar cell application, the so called "weak donor-strong acceptor" strategy was successfully used by You.[32,33]

1.3 Conjugated Polymers and Applications in Devices

Conjugated polymers developed very quickly in these recent years, many novel conjugated polymers were created and used in several different devices. A brief introduction/summary of some important applications follows.

1.3.1 In Polymer Solar Cells

As one of the most promising ways to solving today's energy crisis and associated environmental issues, solar energy has attracted more and more interests.[15] Among several different kinds of solar cells, organic photovoltaic (OPV) devices are one of those being heavily researched.[34] Their potential processability through fast roll-to-roll production and possibly low-cost are making them a potential alternative to traditional inorganic solar cells.[12]

Parameters of Organic Semiconductor Materials for OPV Application

The performance of OPV can be partially characterized using a current-voltage curve like that depicted in figure 1.6. When no light is present, the current flow is zero because there is no exciton formation in the absence of light and therefore the charge-carrier concentration is "too low". When irradiated, the OPV begins to generate excitons and dissociated excitons to

free charge carriers can generate electrical current. From the current-voltage (*I-V*) curve, we can obtain the maximum power point (P_{max}), on the I-V curve (I_{max}, V_{max}) where the maximum power is produced. FF is the fill factor and P_{in} is the energy of incident light. This is illustrated in the diagram as the area of the rectangle.[15] The power conversion efficiency (η_e) of an OPV can be calculated using the following equation.[35]

$$\eta_e = \frac{V_{oc} \times I_{sc} \times \mathrm{FF}}{P_{in}}$$

$$FF = \frac{P_{max}}{P_{in}} = \frac{I_{max} \times V_{max}}{I_{sc} \times V_{oc}}$$

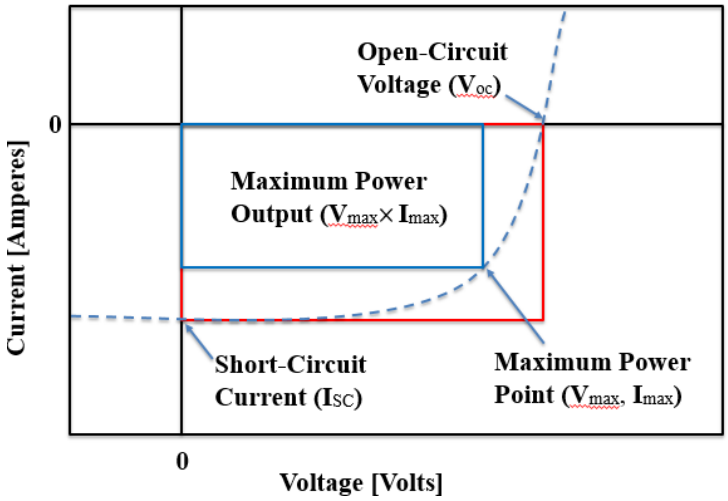

Figure 1.6: Current-voltage (*I-V*) curve of an ideal solar cell under illumination (blue line). V_{oc} is open circuit voltage, I_{sc} is short circuit current, I_{max} and V_{max} are the current and voltage at the maximum power point.

Since the first introduction of donor-acceptor heterojunctions for polymer solar cells by Heeger [36] in 1995, the BHJ (bulk heterojunctions) dominated the research. The BHJ contains conjugated polymer as donor material (or hole-transport material), usually PCBM as acceptor material (or electron-transport material). Donor and acceptor here refers to two separate materials, as opposed to the donor and acceptor molecular building blocks for D-A copolymers discussed above. The two materials are combined to form an

interpenetrating network with nanophase separation and the morphology control between the donor and acceptor is also crucial. Some important developments will be introduced in following paragraphs.

Conjugated Polymer Donor

Through the rational design of conjugated polymers, the power conversion efficiency (PCEs) of polymer solar cells has improved rapidly (from below 1% to over 11%) in the past years, though it is unclear at this point whether this trend will continue upwards, and whether other challenges will be overcome in order to actually commercialize.[37,38] In order to match solar spectrum in visible and near-infrared region (increasing Jsc), smaller Eg of the conjugated backbones was engineered (usually donor/acceptor structure polymer).[39] Here donor/acceptor refers to the D and A units along the conjugated polymer material, as opposed to the complementary donor and acceptor materials used to form the BHJ. In addition, suitable LUMO and HOMO energy levels are vital for facilitating the exciton dissociation at the donor/acceptor interface and for getting higher Voc of the PSC devices. Finally, sufficient intermolecular π-π interaction is important to enhance the charge transport efficiency across a large number of molecules (increase Jsc) and to increase FF of the devices.[39]

Hundreds of different kinds of backbones were developed for the BHJ (bulk heterojunctions) solar cells. The conjugated backbone is quite important for highly efficient photovoltaic materials and thus achieving the high power conversion efficiency (PCEs). It will affect the

electronic properties of the conjugated polymers, such as frontier orbitals: the highest occupied molecular orbitals (HOMO), the lowest unoccupied molecular orbitals (LUMO).[40]

Acceptor Materials in BHJs

The first BHJ[36] was introduced by Heeger as a blend of MEH-PPV (conjugated polymer, Figure 1.1) and PCBM (Figure 1.7)soon after PCBM was prepared by Wudl in 1995.[41] PCBM represents a milestone in the development of BHJ and is still widely studied today, although the search for other acceptor materials goes on.

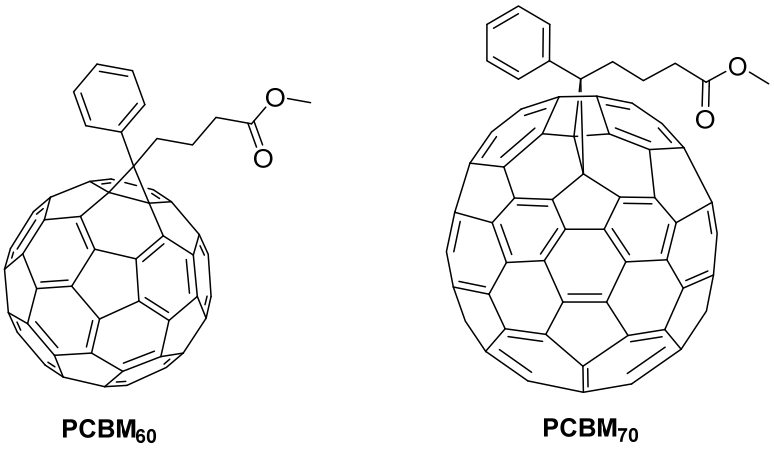

Figure 1.7: The structure of PCBMs.

Developing novel acceptors which can absorb more light is another approach to increase PCE. Compared with $PCBM_{60}$, $PCBM_{70}$ exhibits broader absorption, and replacing C60 derivatives with C70 derivatives often enhances J_{SC}. However, fullerene derivatives are hard to made chemical modification and expensive, also it is not easy to tune the energy level to match more polymers. Therefore, various novel non-fullerene acceptor materials are being pursued to replace the fullerene derivatives.[42,43] Examples of non-fullerene acceptor

materials include polymeric acceptors[44,45] and small-molecule acceptors. The small-molecule acceptors include perylene diimide (PDI)[46] and naphthalene diimide (NDI) derivatives[47] (see figure 1.8 left), indacenodithiophene (IDT)-based (see figure 1.8 right)[48,49] and diketo-pyrrolopyrrole (DPP)-based acceptor[50] according to their structure.

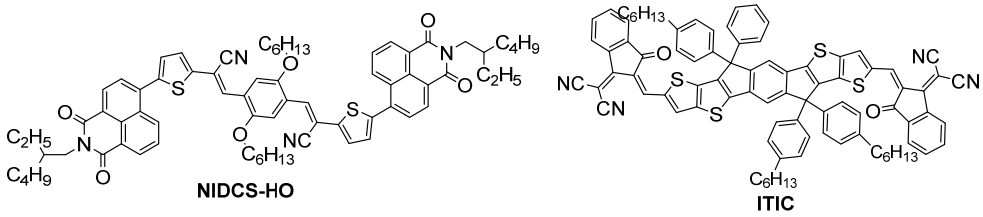

Figure 1.8: Examples of small-molecule non-fullerene acceptor.

Based on the small-molecule acceptor ITIC, Li found that the efficiency could reach 9.5% due to complementary absorption both from donor and acceptor, well-matched energy level between donor and acceptor phases, and proper nanoscale blend morphology.[51] With slightly modified IDIC acceptor and polymer based on BDT, Hou and coworkers even boosted the efficiency to about 12%, which is highest among the polymer solar cells.[49]

Morphology Control

For bulk heterojunction devices, charge separation can be relatively efficient after the materials absorb light, due to extensive interfaces between donor and acceptor material. In order to improve efficiency, the electron and hole must be transported through the acceptor (usually PCBM) and donor (conjugated polymer) phases within the exciton life time, then collected by the cathode and anode. Several researches found nanoscale morphology is critical to the performance of BHJ. The proper nanoscale (domain sizes on the 10−20 nm

length scale), bicontinuous and interpenetrating network and a large interfacial area is a prerequisite to achieve high efficiencies.[52]

Understandably, the morphology is affected not only by the structure of the polymers but also by various device fabrication methods, such as the choice of solvents, [53] solvent additives,[54,55] thermal[56,57,58,59], solvent annealing[60, 61] and mass ratio of the donor: acceptor components.[62, 63]

1.3.2 In Electrochromic Devices (ECDs)

Electrochromism is the reversible change in the color of a material with the change of external voltage. For conjugated polymers, the chromic phenomena are the result of reversible change in the absorption or transmission properties. In cases with low driving voltage of electrochromic materials, this technology has several potential applications, such as smart windows for building to save energy, self-dimming rearview mirrors to prevent glaring for cars, electronic displays[64] and paper (e-papers),[65] smart sunglasses[66] and wearable fabrics[67]. The electrochromic device has already used in the so called "magic sunroof" for cars from a report by Josh Rubin in 2011 (see figure 1.9).

Figure 1.9: Magic sunroof through the color control.

1.3.3 In Field Effect Transistors (FETs)

Field-effect transistors (FET) works as an electron valve or switch, using an electric field to control the current. Poly crystalline silicon (c-Si), as inorganic semiconductor materials, form highly ordered three-dimensional crystal structure[68] and have field-effect mobilities more than 10 $cm^2/(V\ s)$. Compared with inorganic based FETs, the charge carrier mobilities of the organic-based analogues (OFETs) are often lower, but polymer (PDPPTtTT) OFETs have exhibited very high mobility (up to 10.5 $cm^2/(V\ s)$).[27]

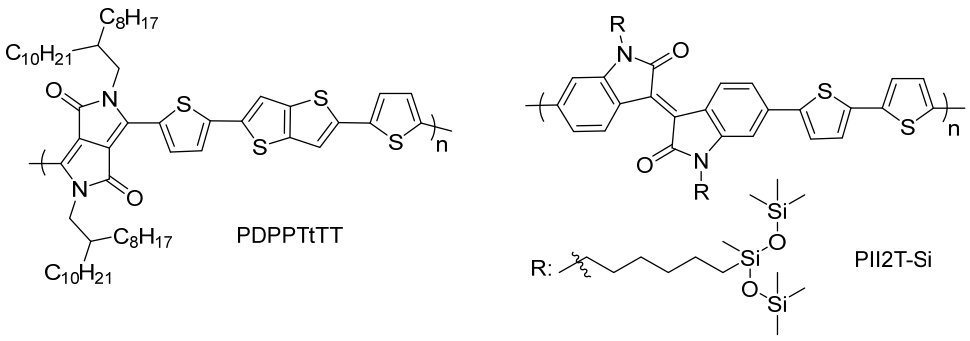

Figure 1.10: Examples of polymers used for OFETs.

Design Strategies for OFETs

Bao and coworkers described some design strategies for OFETs, including chemical approach (molecular consideration, or bottom-up approach), physical approach (molecular packing and morphology control during processing, or top-down approach) and theoretical approach (computer-aided structure−property research).[69] Here, I will just introduce some basic ideas from molecular level about OFETs. Intermolecular charge transport dominates the charge transport rate as the charge carriers have to move from one molecule to adjacent individual molecules. So the charge transport properties of organic solids are highly depending on molecular arrangements (packing). Thus closer π-π stacking and maximum

molecular orbital overlap is essential for higher charge carrier mobility. Solubilizing side-chains are quite important, not only affecting the solubility and processability of the polymer, but the charge transport. The length and position of the side chain affect the molecular packing and thin film morphology, thus charge transport property.

1.4 General Synthetic Methods for Conjugated Polymers

For conjugated polymer synthesis, forming sp- or sp^2-C-C bonds is the key step.[70] The most representative synthetic steps can be facilitated by a transition metal catalyst,[71] which couples two aryl groups via appropriate reactive functional groups.

1.4.1 Stille Cross-couplings

The first cross-coupling reactions using an organotin (organostannane) were reported by Eaborn[72] et al. in 1976. J. K. Stille[73] and co-workers reported the use of palladium-catalyzed cross-coupling in the preparation of ketones from acyl chlorides and organo-stannanes. After this, the Stille reaction became one of the most useful protocols for forming sp^2 carbon-carbon bonds. As many other transition-metal mediated coupling reactions, the catalytic cycle for Stille coupling can be seen from figure 1.11. Here L, represent ligand; R can be alkenyl, alkynyl or aryl group and finally X is Br, I, Cl (Halogen) or pseudohalogen such as triflate (-OTf). The general mechanism involving 1) oxidative addition of the aryl halide onto the Pd (0), 2) transmetallating the organostannane into the catalytic cycle (considered the rate-determining step),[74] and finally 3) reductive elimination step, which yield the coupled units and allows the regenerated palladium catalyst go back to

the catalytic cycle. As we see from the figure 1.11, if a Pd (II) species is used, then sacrificial organostannane monomers can convert this to the active Pd (0) species.

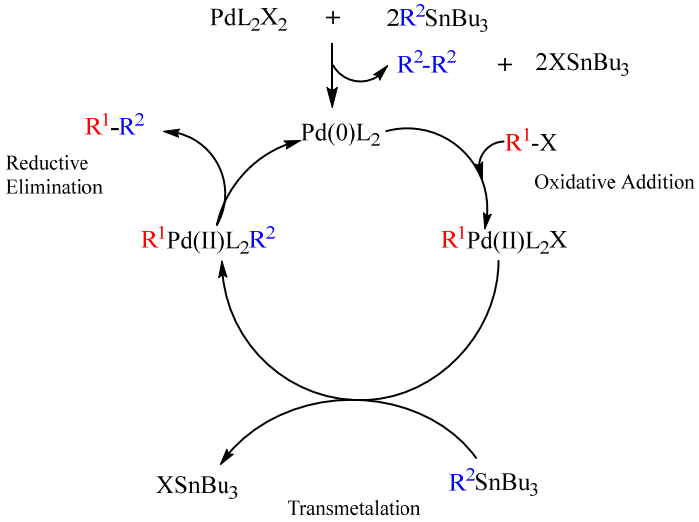

Figure 1.11: General mechanism of the Stille reaction.

As one of the most effective synthetic methods, the Stille reaction plays an important role in different kinds of conjugated polymers synthesis.[75] The reason is that the compatibility of this reaction with various functional groups, and also mild conditions. However, Stille reaction uses toxic distannylated monomers and generates stoichiometric toxic tin waste during the reaction. This could even be a big obstacle especially for large scale process. Distannylated monomers sometimes are difficult to isolate from the reagent trialkyltin chlorides, often making monomer purification difficult.

For the catalyst, our group has followed the prescription[76,77,78] of other groups[79] to use a combination of $Pd_2(dba)_3$ (1.5 mol% relative to the monomer) and tri(o-tolyl)-phosphine ligand (12 mol% relative to the monomer), which was found quite a good system for electron-rich thiophene monomer. This Pd (0) source can be stored for long periods at room temperature and it easily handled in air (unlike, e.g. $Pd(PPh_3)_4$, and precludes the necessity

for sacrificial monomer required when starting with Pd (II) species. The ideal solvent for the palladium-catalyzed polymerization should stabilize the catalyst and at the same time keep the growing polymeric molecules in solution in order to maximize molecular weights of the resulting polymer.[80] Also the solvent can dictate the upper reaction temperature, and therefore the reaction rate. Most of the polymers were prepared using Stille cross-couplings reaction in this work.

1.4.2 Suzuki Cross-couplings

Suzuki cross-coupling reaction is quite useful in organic synthesis for building the C-C bond and would be our method of choice if not for its limitations when the substrates are thiophene-based.[81] Many different compounds such as pharmaceuticals or fine chemicals have been obtained by Suzuki reaction. After modifications, this reaction can even be automated; some complex nature product was synthesized through this reaction.[82] Suzuki reaction was also successfully used for large scale synthesis, hundreds of kilograms' intermediates was obtained with high yield with this method.[83] This reaction is so useful from lab scale to industry scale, one reason being that the organo-borane reactants are so easy to prepare and store, at the same time the reaction is efficient and easy to handle.

Compared with Stille reaction using toxic distannylated monomers, Suzuki reaction would seem superior. However, there are only a few examples[84] to form thiophene based copolymers under Suzuki conditions. The reason is that thienyl boronic acids (and derivatives) are somewhat unstable[85] and tend to deboronate (lose the necessary functional

group) during the reaction, severely limiting the molecular weight as each deboronated reactive position becomes a polymer terminus. The molecular weights and yields could not be high enough[86] due to the chain termination. However, recently Ingleson and coworkers found that Suzuki polymerization with certain thienyl boronate esters can give high molecular weights polymers, comparable to polymers produced from Stille method.[87] Hopefully broad scope will be demonstrated such that the Stille method can be completely replaced.

1.4.3 McCullough Cross-Coupling and Grignard Metathesis Method (GRIM)

Among the many different conjugated polymers, polythiophenes and thiophene-based polymers are the most well studied and play a vital role for the conjugated polymers research, not only for theory research but also for synthesis and devices study.[88] When 3-alkylthiophenes are coupled, almost always via the 2- and 5-positions, there are 3 different regiochemical outcomes[89] (see figure 1.12 top):

- 2,5', or head–tail (HT), coupling.
- 2,2', or head–head (HH), coupling
- 5,5', or tail–tail (TT), coupling

The first poly alkylthiophens which were obtained via chemical and electrochemical methods were regioirregular, and therefore could not form ordered solid-state phases due to uncontrolled head-to-head (HH) and tail-to-tail (TT) couplings.

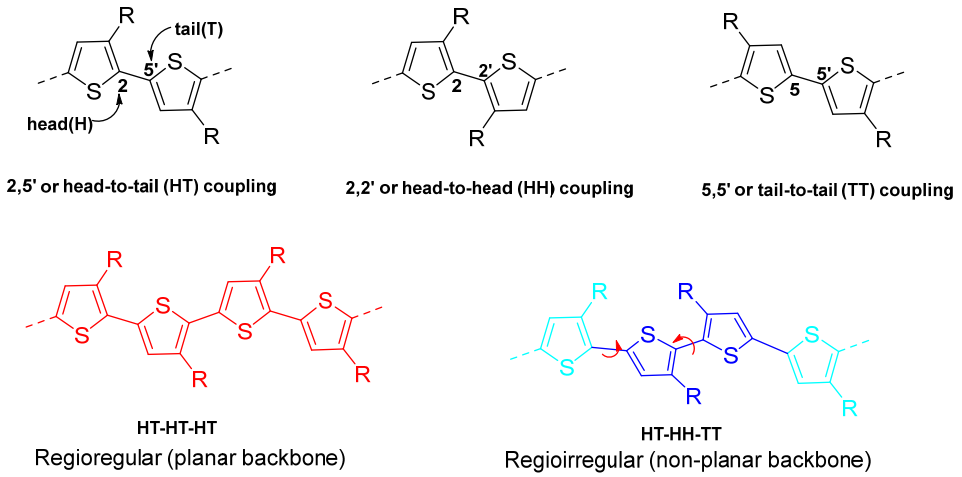

Figure 1.12: Regioisomeric couplings of 3-alkylthiophenes (top) and regioregular and regioirregular P3AT (bottom). [89]

The first HT rrP3AT synthesis was reported by McCullough and coworkers in 1992.[9] Then Rieke developed a similar method using organic zinc to synthesize rrP3ATs shortly after that (Scheme 1.1).[10] Over the succeeding few years, McCullough and others expanded the chemical synthesis of rrP3ATs, using a method that came to be known as the Grignard metathesis (GRIM) method (Scheme 1.1).[90,91] The advantage of this method is that the use of both cryogenic temperatures and highly reactive metals is unnecessary; allowing more practical synthesis of rrP3ATs (as well as a broad range of heterocycle-based polymers).[89] This method involves the magnesium-halogen exchange (forming a mixture of intermediates 2 and 3, Scheme 1.1) between 2,5-dibromo-3-alkylthiophene and an alkyl Grignard reagent.

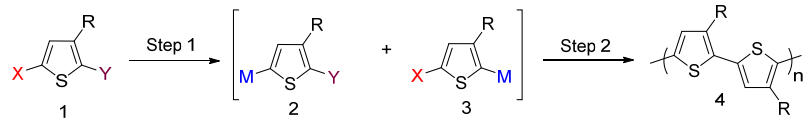

Method	X,Y	Step 1	M (ratio/ 2:3)	Step 2	HT Regioregularity
Mccullough	H, Br	i) LDA/THF, -40 ºC, 40 min ii) $MgBr_2.Et_2O$ -60 ºC to -40 ºC,	MgBr (~98: ~2)[a]	Ni(dppp)Cl_2, -5 to 25 ºC,18 h	98-100 %
Rieke	Br, Br	Zn*/THF, -78 ºC to rt, 4 h	ZnBr (90: 10)	Ni(dppe)Cl_2, -5 to rt, 24 h	97-100 %
GRIM	Br, Br	R′MgX[b]/THF, rt to reflux , 1 h	MgX′ (~95: ~5)	Ni(dppp)Cl_2, rt or reflux, <1 h	>99 %

a) X for intermediate 3 is Br (not H) in this case. b) R′ = Alkyl, X′ = Cl, Br

Scheme 1.1: Typical methods for the synthesis of regioregular poly(3-alkylthiophene)s. [89]

For McCullough method, the experiment result shows that relative high molecular weight forms very quickly and presence of Ni(0) , so the regioregular polymerization process follows a chain growth mechanism, as proposed in figure 1.13.[92]

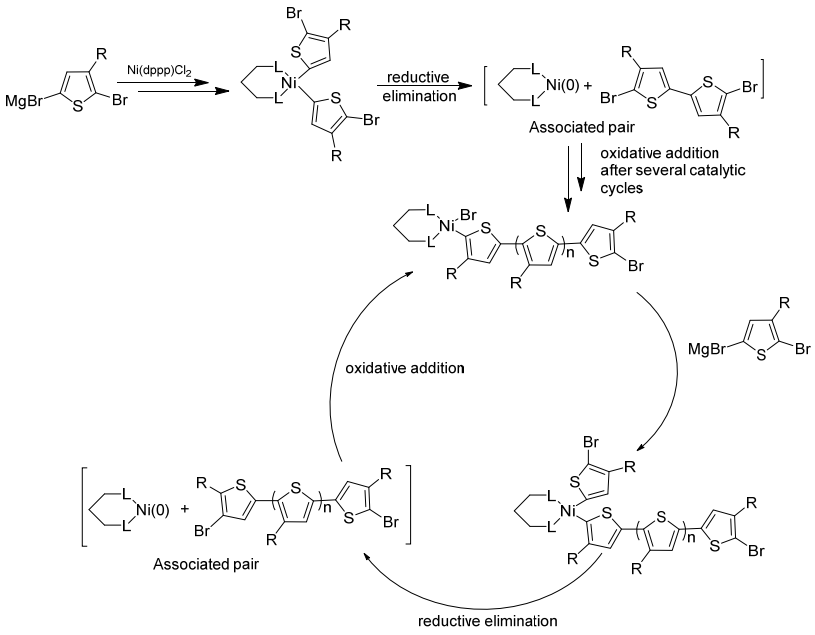

Figure 1.13: Proposed mechanism for the nickel-initiated cross-coupling polymerization.

1.4.4 Direct (hetero)arylation polymerization (DHAP) method

As we can see from the above methods, the key aryl carbon-carbon bond formation step in each one requires that one arene coupling partner is substituted with a (pseudo)halogen (I, Br, OTf, etc.), while the other contains an active moiety such as -$B(OR)_3$, -SnR_3, -ZnR, or -MgX. More recently, an alternative approach termed direct (hetero)arylation (Figure 1.14) has been reported, and seems quite interesting as it combines C-H activation and oxidative coupling while eliminating the need for two different reactive functional groups.[93,94,95] T.J. Marks and coworkers synthesized PBDT-TPD and PTB7 via this method, and the results show that it could give polymers of with yields and molecular weight comparable to Stille method. The devices made from the DHAP method have comparable or superior photovoltaic performances versus Stille-derived samples.[96]

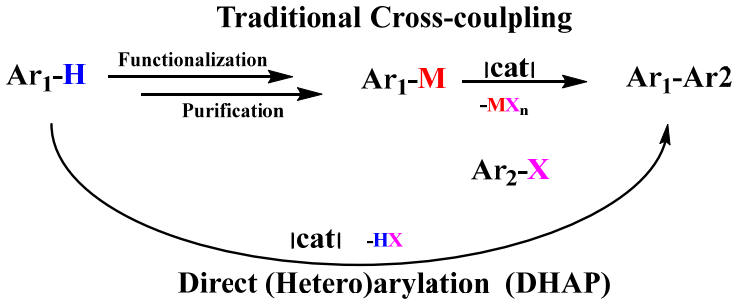

Figure 1.14: Comparison of traditional cross-coupling reactions with direct (hetero)arylation. [94]

During the studies reported in this dissertation, the DHAP method was evaluated and showed some promise, but to maintain focus on obtaining the synthetic targets more traditional methods continued to be followed. There are still some challenges to overcome for broad application of the DHAP method. Ill-defined branched and network polymer architectures result from some monomers with more than one reactive C-H bond.[97] Also, for each sterically/electronically different monomer, the reaction condition such as catalyst,

ligand, acid, base and solvent need to be varied in order to get higher molecular weight and yield, while minimizing side reactions leading to ill-defined structures.

1.5 Methods for Characterizing the Properties of Conjugated Polymers

This section summarizes the methods used by our group and others for characterizing the optical properties, FMO energies, and solid state ordering of the polymers[98,99]

1.5.1 Optical Spectroscopy

Optical spectroscopy, especially UV-Vis spectroscopy, is a useful tool for gaining a preliminary understanding of the (opto)electronic properties as well as some indirect information about the molecular assembly in polymer solutions and thin-films. The onset of absorption (λ_{onset}) is generally used to estimate the Eg of a given material as illustrated in figure 1.15.

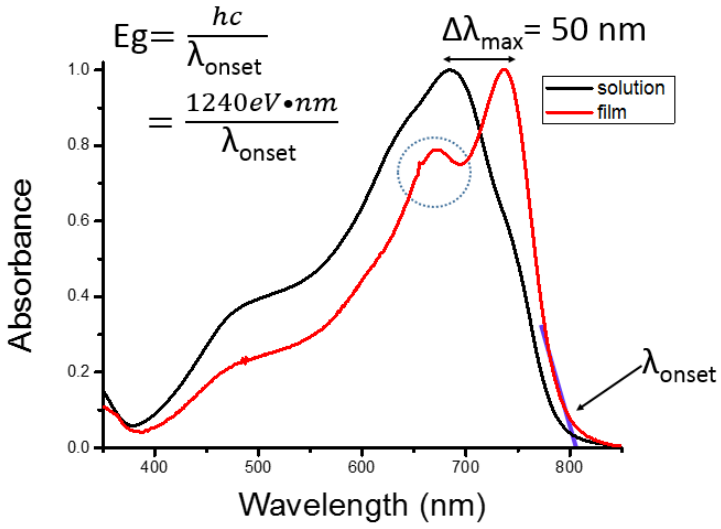

Figure 1.15: Example of UV-Vis spectra of a D-A polymer illustrating the estimation of Eg from a polymer thin-film, the difference in absorption maxima ($\Delta\lambda_{max}$) between the solution and thin-film spectra and the presence of fine structure (circled region) suggestive of a narrowing of population of states.

This method must be used with caution as onset of absorption does not necessarily correspond to the formation of free charge carriers, rather a bound electron-hole pair is formed. As is very common in this field, we use voltametric methods to estimate FMO energy levels. In many cases the energy gap estimated by electrochemical methods such as differential pulse voltammetry (DPV) yields higher values of Eg when compared to the optical energy gaps obtained from UV-Vis spectroscopy.[100,101] In many cases reduction waves are not observed in electrochemical voltammograms of p-type semiconductors (or oxidization peaks for n-type). The term Eg, used for the remainder of this dissertation refers to the optical energy gap estimated from the onset of UV-Vis absorption of a thin film.

Comparison of the solution and solid-state absorption spectra provides information about differences or similarities in the two states. Here, it should be clear that species in "solution" might be ensembles of molecules (aggregates), rather than fully solvated single polymer chains. For example, similar solution and thin-film absorption profiles implies similarities in the two states, whether the peaks are broad and featureless (dissolved polymers in solution - similar to amorphous polymers in the solid state) or structured (ordered and/or π-stacked and/or more planarized backbones). A large red-shift in the absorption profile (as illustrated as $\Delta\lambda max$ in figure 1.15) upon going from solution to the solid state implies a large difference between the two states. The red-shifts in going from solution to the solid state are thought to be a product to increased backbone planarity, increased conjugation and increased intermolecular orbital overlap relative to polymers dissolved in solution. Finally, fine structure (circled region in figure 1.15) is sometimes

observed in thin-films of conjugated polymers. The fine structure is generally attributed to "inter-chain" interactions of π-stacked polymer backbones in the solid state and/or a narrowing of populations of states, implying polymers displaying fine structure in their absorption spectra are relatively ordered.[98]

1.5.2 Electrochemistry

Voltammetric techniques are widely used by materials researchers to estimate FMO energy levels. Most commonly, a sweep technique, known as cyclic voltammetry (CV) is used to estimate E_{HOMO} and E_{LUMO}. This technique involves application of forward and reverse linear potential scans through a working electrode immersed in an electrolyte solution, also containing the redox active species of interest. If the material has accessible oxidations, an anodic wave appears in the forward positive scan, and a corresponding cathodic wave can be observed on the reverse scan, showing that the oxidation is reversible under the experimental conditions. The voltammetric instrument consists of a three-electrode system. One of the three electrodes is working electrode, which potential is varied linearly with time. The second electrode is reference electrode. Here no current go through this reference electrode and potential remains constant throughout the experiment. The third electrode is counter electrode which conduct current via the electrolyte solution to the working electrode. In our group, to estimate FMO energy levels, we basically use pulse voltammetric technique known as differential-pulse voltammetry (DPV) instead of CV. Compared to CV, this DPV technique is more sensitive. DPV measures the current at a time when the difference between the faradaic current and the interfering charging current is large. Voltammetric methods adapted to measure the oxidation and reduction potentials of conjugated polymers

typically involve solvent-casting of the polymer material onto the working electrode. The onsets of oxidation and reduction are used to estimate the E_{HOMO} and E_{LUMO}, respectively. The oxidation potential provides a relative estimate of the energy of HOMO which can consider as the ionization potential, the minimum energy required to remove an electron from an atom or molecule in a vacuum. According to these definitions it is clear that the energy values we obtain from this voltammetric technique are approximations because the HOMO/LUMO energies are scaled in vacuum, but our reduction/oxidation potentials are estimated in thin films.[98-99] Values close to those obtained by ultraviolet photoelectron spectroscopy (UPS) can be obtained if the thin films are first carefully "broken in". "Breaking in" involves first cycling the voltage a few times, approaching but not crossing the oxidation or reduction onset observed from a scan of a sacrificial film that was not broken in, thus "gently" bringing electrolyte into the film. Without breaking in, the thin-film voltammetric methods tend to "overshoot", giving onset of oxidation/reduction values with absolute values that are too large. For example, a large number of publications cite a E_{HOMO} value for the benchmark P3HT polymer which is too "deep" to correspond to observed device performance metrics (e.g. poor air stability in OFETs) and significantly deeper than that estimated by UPS. In-house DPV experiments on broken-in P3HT films gives an E_{HOMO} estimate which almost perfectly matches that estimated from UPS.

1.5.3 Wide Angle X-ray Diffraction (2D-WAXD) Patterns of Polymers

Supramolecular self-assembly is a very important aspect to obtain high device performance. Compared to inorganic semiconductors with long-range 3-dimensional order, "soft" organic

semiconductor materials like conjugated polymers show comparatively lower device performance partly due to their assembly by intermolecular interactions (as opposed to directly bonded networks) and relatively short range order. Also unlike inorganics, the electrons in organic materials are tightly bound to atoms lowering their free movement. Basically all these organics are insulators without any free charge carriers. The supramolecular arrangements of all polymers reported here were investigated by 2D-WAXD from aligned fibers. Unlike small molecules, it is not easy to obtain single crystals from polymers. Powder diffraction patterns can be obtained, giving some information about the spacing between semi-regularly arranged

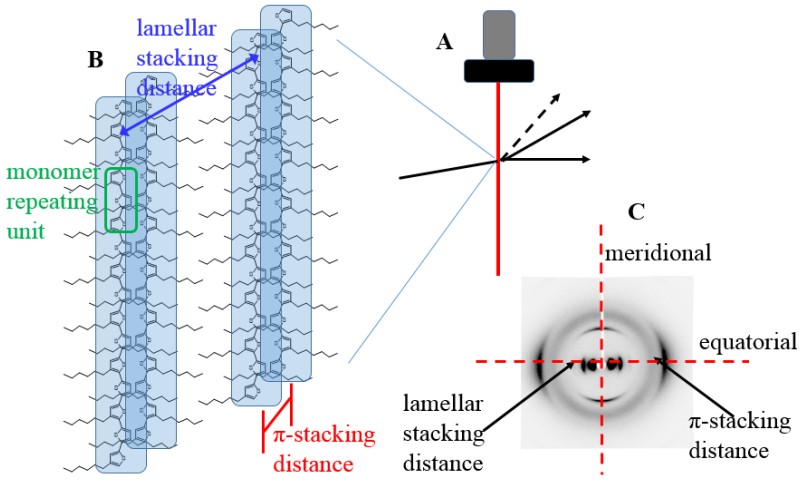

Figure 1.16: Schematic diagram illustrating a WAXD experiment. A) Alignment of polymer fibers through extruder. B) Illustration of lamellar packing of side chains and π-stacking of polymer backbones. C) 2D-WAXD pattern of a mechanically aligned polymer fiber.

molecules. To improve the utility of WAXD, scientists use polymer fibers, with polymer backbones aligned along the axis of the fiber. Here we used home built piston-operated mini-extruder to prepare polymer fibers. The polymer fibers obtained after passing through a die by mechanical force were mounted perpendicular to the incident X-ray beam and

diffracted x-rays were collected by an area detector. Polymer fiber was mounted perpendicular to the incident X-ray beam, so diffraction maxima along the meridian (vertical axis) provide information about repeating elements along the backbone and diffraction maxima along the equator (horizontal) convey the lamellar spacing and π-stacking. But it is important to note that these values are upper limits, exceeding the actual stacking distance if the polymer backbones are tilted away along the normal stacking axis.[98-99]

1.6 Side Chains on Donor (D) Acceptor (A) Conjugated Polymers

As conjugated polymers could be seen as one kind of mesogen, it is useful to see the meaning of mesogen– a unit which leads to a mesophase (state of order between disordered liquid and ordered crystal)

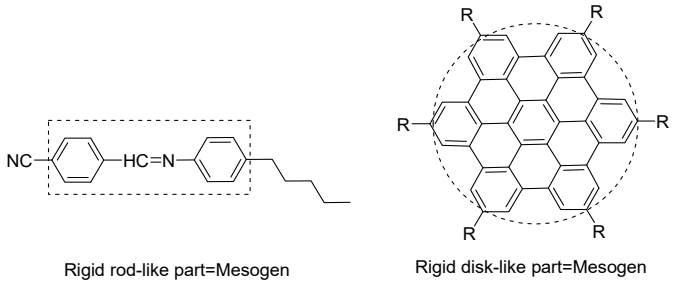

Figure 1.17: Examples of mesogenic structures.

Generally, the concept of mesogen is from liquid crystalline materials, which usually consists of a rigid part (named mesogen) and one or more flexible parts (figure 1.17). The rigid part can induce order along one or more dimensions, whereas the flexible parts induce fluidity or disorder in the liquid crystal. Many years of research have shown that the

chemical makeup and relative volume-fraction of flexible substituents strongly direct phase formation. Here we use nematic liquid crystal and discotic liquid crystal as examples.[102,103]

The figure 1.18 shows the shape of a typical nematic (rod-like) liquid crystal molecule. It consists of two or more ring systems (mesogen) and an alkyl chain, which provides a differentiation in short-range molecular forces that contribute to form the nematic phase. The long side chain strongly influences the physical and thermal properties of the liquid crystal phases. The thermal robustness (which is some indication of how stable the phase is) of the liquid crystal phase is strongly influenced by the volume fraction of flexible side chain.

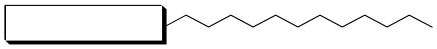

Figure 1.18: Typical shape of a nematic liquid crystal molecule.

Cyanobiphenyl (CB) compounds are typical nematic molecules, the properties could be found from table 1.1. Here the cyanobiphenyl (CB) compounds have the same two ring systems (mesogen), but different size of side chains.

There is no observable mesophase (just melt directly from crystal to liquid) if the volume fraction of flexible side chain is too small (such as 2CB). Every CB liquid crystal with different side chain has its own phase transition temperature(s) as we can see from table 1.[105] T_{NI} (temperature at which point the liquid crystals change from the nematic state to an isotropic state) is lower for compounds with an even number of carbons in the substituents compared to homologues with a similar, but even number of carbons in the substituents.

Table 1.1: Properties of CB compounds [104]

Name	Structure	Crystal phase	T (^{O}C)	Nematic phase	T (^{O}C)	Isotropic phase
2CB	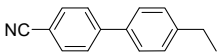		75.0			
4CB	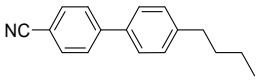		48.0		(16.5)	
5CB	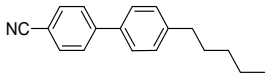		24.0		35.0	
6CB	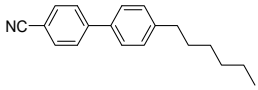		24.5		29.0	
7CB	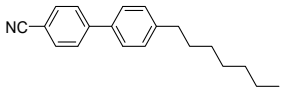		30		43.0	
8CB	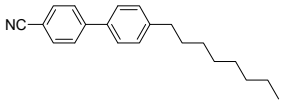		21.5		40.5	

For triphenylene-based discotic LCs (see figure 1.19), the properties are sensitive to structural variation.[103] 'Removal' of one of the alkoxy substituents eliminates the mesophase behavior. However, the effect is subtler, and replacement of one alkoxy with a (planar) polarizing group restores the mesophase behavior. Extension of this mesogenic core, particularly by appropriate polarizing α-substitution, further stabilizes the mesophase (higher clearing temperatures for CN substituent).[103]

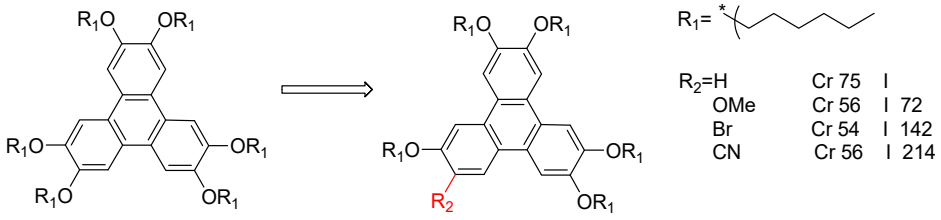

Figure 1.19: Modifications to the extended core of alkoxytriphenylenes. [103]

Not only does the volume fraction of flexible part (the side-chain) control self-assembly of mesogenic conjugated polymers, but the distribution of the side-chains along the mesogen also plays an important role. A prominent example is pBTTT (figure 1.20), which has a OFET charge-mobility of 0.37cm^2/(V s) after annealing.[20] Unlike P3HT and other polymers that have side chains attached to the backbone very close to each other on every aromatic unit, pBTTT polymers have alternating substituted and non-substituted units, that allowed the side chains from neighboring polymers to interdigitate. Melting of interdigitated semicrystalline alkane side chains lead to mesophase transition.[20] This transition is not observed in semiconducting polymers such as regioregular poly(3-hexylthiophene) (rr-P3HT).

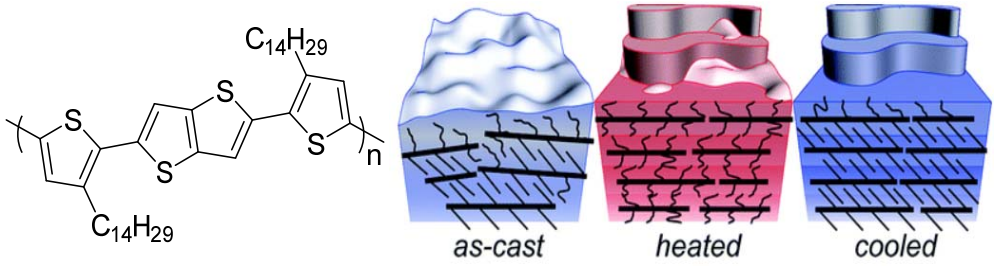

Figure 1.20: pBTTT and it phase state before and after annealing.

Turning to crystalline acenes, the self-assembly is very sensitive to relative volume fraction of substituent. Here use pentacenes as example (see figure 1.21), the sizes of substituents also affect a lot to the solid state arrangement (crystal packing).

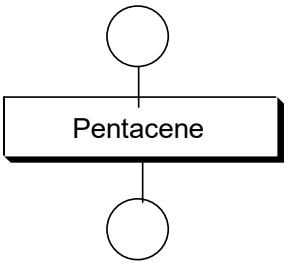

Figure 1.21: Typical shape of substituted pentacene.

Pentacene was widely studied for FET (field effect transistor) devices.[106] Anthony's group adding alkyne directly to the aromatic ring and found the packing is very sensitive to the relative volume fractions of rigid core and the substituents.[107] The results show that if use ethyl or n-propyl substituent, leads to a 1-D, "slipped-stack" arrangement. For i-propyl group, the substituent diameter very close to half the length of the acene, the material adopts a 2-D "bricklayer" arrangement. This fits in well with prior observations of increasing dimensionality of the order in small-molecule mesophases (e.g. for triphenylenes[108,109] and hexabenzocoronenes[110]) as the bulkiness of substituents is increased, reaching some ratio where the space-filling demands of different parts of the molecule are commensurate to direct the packing molecular registry along additional dimensions. Even stepping away from organic electronic materials, one can consider extensive studies of the effect on packing of the size and spacing of substituents along the backbones of polyethylene chains.[111,112]

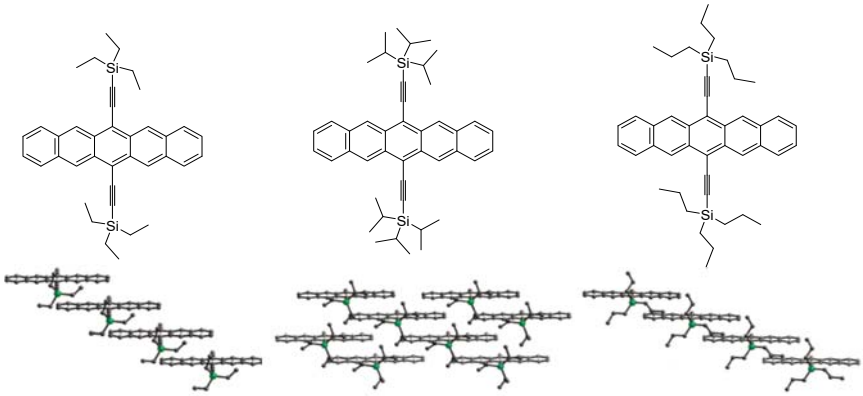

Figure 1.22: Substituted pentacene derivatives and their solid-state packing. [107]

Considering the above summarized excerpts from the broader body of knowledge concerning the effect of the size and position of substituents on the properties of other types of materials, we might ask what is known for conjugated polymers? Generally, a

conjugated polymer can be divided into two constituting components: the conjugated backbone and the side chains. So conjugated polymers could be seen as "long" mesogens and self-assemble with nanophase-separated core and side chains like other mesogens. This is further enhanced by donor-acceptor interactions in D-A polymers. Compared to the side chains, researchers paid much more attention to the backbone at the early stages of D-A polymers design. Side chains were generally thought of primarily as a way to improve the solubility when designing conjugated polymers even though a lot of side chains have been used over the years. But the importance of side chains, including benefits of using branched chains are becoming more apparent for some polymers.[40,113] Just as the size of side chains are closely related to properties of nematic liquid crystals, some recent studies focus on side chains and show us that polymer side chains not only affect the solubility but affect PCEs of OSCs a lot.[114,115]

In 2010, four groups reported the same structure of PBDTTPD polymers (see figure 1.23).[116,117,118,119] Different PCE performances varying from 4.1% to 6.8% in solar cells were reported, probably due primarily to differences in device fabrication processes, as well as likely differences in polymer molecular weights, molecular weight distributions, purity, etc.

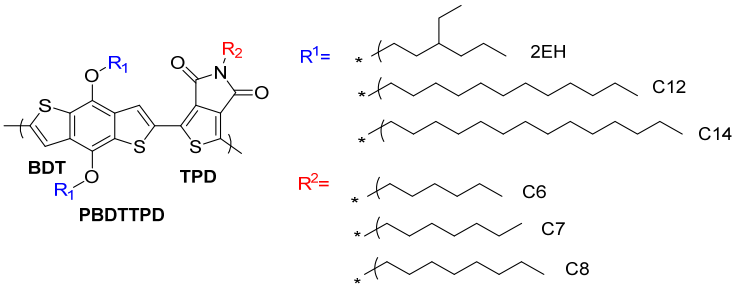

Figure 1.23: PBDTTPD derivatives bearing alkyl side chains with various lengths and branching. [120]

Base on the research of PBDTTPD polymers, Beaujuge's group examined the effect of side chain substitutions for both material self-assembly and solar cell performance. PCEs of 8.5% can be achieved when branched-alkyl-substituted BDTs and N-heptyl-substituted TPD-based polymers blend with $PC_{71}BM$ in standard BHJ devices. The authors point out that when the BDT donor has linear side chains, the absence of a preferential "face-on" polymer orientations relative to the substrate lead to a dramatic drop in BHJ device PCEs (<4.2%). What's more, a fine modulation of the linear N-alkyl side chain on TPD acceptor motifs does not significantly affect the "face-on" backbone orientation but can improve the device performance.[120]

Most of the side chains used for conjugated polymer are alkyl sidechains.[113] Alkyl side chains can be divided into linear and branched alkyl chains. For linear alkyl chain, some side chains（e.g. C6, C8, C10, C14 with even number of carbons）were used much more than others. For branched alkyl chain, the choice is usually (EH, HD, BO) especially EH (figure 1.24).[113] One reason these particular branched chains are so commonly used is that the starting materials are commercially available as alcohols and bromides which can be readily attached to monomers used for conjugated polymer synthesis.

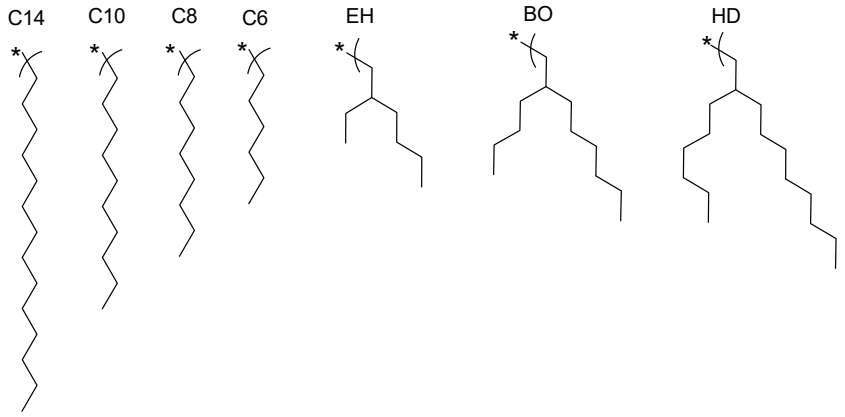

Figure 1.24: Commonly used alkyl side chains in conjugated polymers.

Here we want to more systematically study the effect of side-chain branching on D-A conjugated polymer properties. The designed D-A polymers have donor units with variably bulky side chains, combined with acceptors carrying either no side chains, short side chains or long side chains. This project is part of a systematic study to understand the effects of side chains on D-A polymer properties and hopefully establish some design rules, such as effect of volume fraction and distribution in space of side chains on optoelectronic properties and self-assembly. We step back from the much larger number of variables associated with device studies, and focus the structure-property studies on a simple, small set of property studies. The initial donor units chosen for study are BDT and bithiophene (T2) because the donor footprint is pretty similar, but the BDT has a rigid benzene ring linking two thiophenes, while the T2 has a flexible single bond (Dr. Daijun Feng in our group prepared the majority of the T2 polymers while this work focuses on BDT). Because the T2 units can twist out of plane around the central σ-bond to accommodate the space-filling demands of side chains while the BDT unit cannot, we expect significant differences in the sensitivity of the (opto)electronic properties and self-assembly of the two types of polymers to space-filling demands of the side chains.

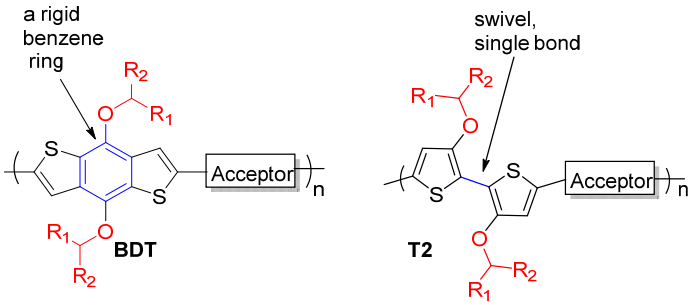

Figure 1.25: Initial synthetic targets in this study: polymers bearing different bulky alkyl side chains on rigid (benzodithiophene, BDT) or "swivel" (bithiophene, T2) donor units, and acceptor units.

As shown earlier in figure 1.24, most published branched side chains carry the branch at the β-position. One reason to choose side chains with α-position branch is that it could improve solubility. It is possible that we achieve higher solubility but with a lower volume fraction of side chain by distributing the volume of branches closer to the backbone. We can systematically alter the size of side chains to research their influence on BDT polymers. The solubility is one of the vital parameters for polymers used in OSCs during device manufacturing, though this receives little serious attention in the literature. Many of the highest performing polymers can be solvent-processed only with halogenated solvents. Our group's experience working with an industrial partner suggests that the need for halogenated solvents eliminates a polymer from consideration.

So in this whole research period the prime goals were,

To systematically investigate the effects of side chains on D-A polymer properties, such as the optical, electronic and self-assembly.

Study the differences in the sensitivity of the (opto)electronic properties and self-assembly of polymers to space-filling demands of the side chains.

1.7 Summary of Dissertation

As stated earlier the main focus of this dissertation is to get an idea of the structure property relationships of conjugated polymers, with primary focus on the side chains. The whole dissertation consists of six chapters, including this introduction.

Chapter 2 mainly focused on D-A copolymers with BDT as donor and 2,3,5,6-tetrafluorobenzene (TFB) as acceptor. Here the main priority goes to the effect of substituents where only the donor carries side chains. Further, our group has noted through previous preparation of many TFB-based D-A polymers that TFB often imparts very low solubility, making it a prime target for the current study. Systematic delineation of the requirements to solubilize these polymers without disrupting "close" π-stacking could lead to design rules to guide efforts concerning other polymer. How does different substituent size (the length of branch side chain) on the BDT affect the optical, electronic and solid-state packing arrangement of the resulting PBDTTFB polymers. Through change of chain length and branching position of alkoxy side chain on BDT, a systematic study was conducted on PBDTTFB polymers. The study reveals the branching effects on (i) solubility, (ii) aggregation tendency, and (iii) (opto)electronic properties in an overall consistent picture.

Chapter 3 mainly focuses on thiophene-imide (TPD) based D-A polymers. Studies of this acceptor had been underway in our group following our publications of other imide-fused arenes as acceptors, but study of TPD was essentially dropped when the aforementioned "tip of the iceberg" barrage of publications appeared from other groups, indicating that this

acceptor would be sufficiently studied by others. We return to the TPD unit here because, unlike TFB, it can carry side chains which can be varied in size.

Chapter 4 is mainly dedicated to 3,3'-dialkoxy bithiophene (RO2T2) donor units, which were prepared by a synthesis method (see details in chapter 3) through Ni catalyzed Grignard reagent coupling, which is an improvement over prior methods that suffered due to relatively unstable intermediate building blocks. After combining RO2T2 units in copolymer backbones with several different size spacer thiophene (T), thienothiophene (TT) and bithiophene (BT) units, we get several different polymers. These other units are normally considered as donor units, but when combined with the RO2T2 unit have such a shallow HOMO level, they may as well be considered as acceptors here. From DPV experiments we found that the E_{HOMO} was almost same for all these polymers, as dictated by the shallow HOMO of the RO2T2 unit. Structure proof via traditional techniques (e.g. solution NMR) of most of the polymers reported here is severely limited or even completely precluded due to extensive aggregation in solution. We rely on the large body of evidence for the well-defined nature of the polymer synthesis reactions (e.g. Stille coupling, GRIM method) to support the assumption that the polymer backbone structures are as predicted.

Chapter 5 proposes some novel polymers which may be developed later. Finally, the last chapter describes all the necessary experimental details of material synthesis, the structure and purity of the building blocks as ascertained by NMR and GCMS, and material characterization techniques such as TGA, DSC, WAXD and DPV etc.

Chapter 2: Influence of Side Chains on The Properties of Alternating Donor-Acceptor Co-polymers Based on BDT Donor and Tetrafluorobenzene Acceptor Units

2.1 Introduction

Benzo[1,2-b:4,5-b′]dithiophene (BDT) related materials have played an important role in organic semiconductor research especially organic solar cells research.[121] BDT's utility has been variously attributed to its molecular geometry, electronic properties (e.g. frontier molecular orbital energy levels) and versatile modification, which paves the way to adjust the (opto)electronic properties through derivation. BDT-based molecules[122] were synthesized during the 1980s; after that they were used as organic field-effect transistor (OFET) materials.[123] Hole mobility as high as 0.4 $cm^2/(V\ s)$ was achieved in 2007 based on BDT polymers.[124] In 2008, Hou and coworkers synthesized several conjugated polymers based on BDT unit and successfully used them in polymer solar cells.[125] Since then, BDT became one of the most successful building blocks for organic solar cells applications; some of the copolymers achieved milestone power conversion efficiency (PCEs) in the development of polymer solar cells (PSCs).

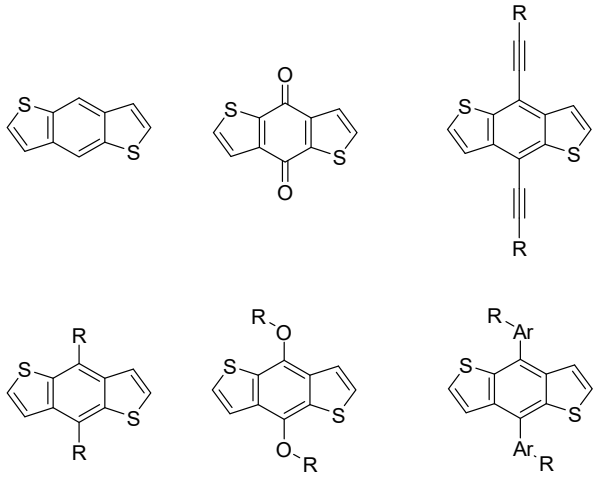

Figure 2.1: BDT and some derivatives.

The BDT unit is a fused system of benzene and thiophene units permitting attachment of side chains to the central benzene ring, distal from the thiophene positions that are coupled to form the polymer backbone, all coming together to minimize inhibition of close and regular face-to-face π-stacking for BDT-based conjugated polymers.[126] The E_{HOMO} level is deeper than comparably sized thiophene oligomers which enhance OFET stability and can positively impact PSC metrics. Moreover, it is quite easy to modify with various types of side chains (see figure 2.1) to improve the solubility and tailored (opto)electronic properties. Finally, the structural symmetry of the BDT monomers eliminates the regioregularity issues associated with lower symmetry units like 3-alkyl thiophenes.[127]

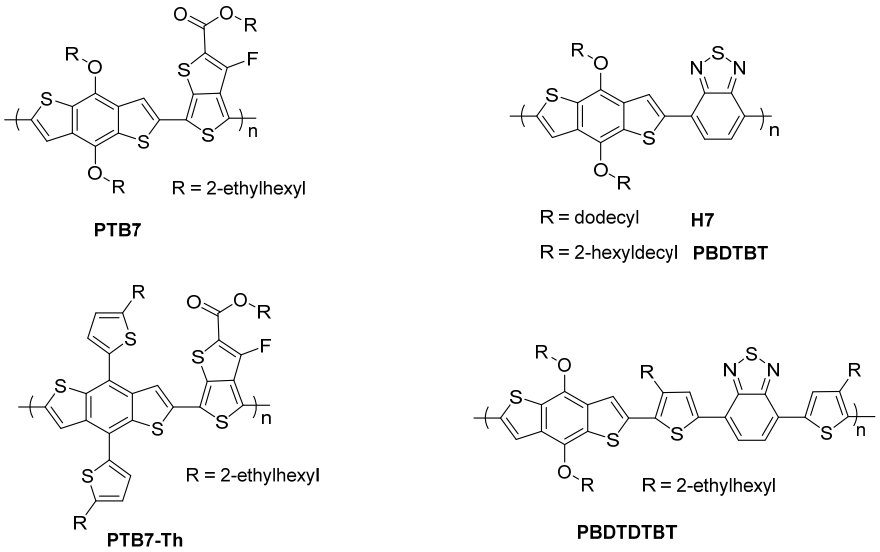

Figure 2.2: BDT-based polymers studied as solar cell components .

By varying the acceptor combined with BDT donor, several D-A polymers were created with proper energy levels and energy gaps, which ensure the polymer energy levels match the PCBM energy level and harvest more light during application in OSCs device.[125] For example, H7 created by combining strongly electron-accepting benzothiadiazole units with BDT.[125] Perhaps initially surprising, the strongest UV-Vis light absorption for H7 is only

591 nm. This turned out to be due to the poor solubility of H7, which causes premature precipitation during polymer growth, therefore, low molecular weight as the linear side chains on the BDT are insufficient for solubility. Compared with H7, the absorption profile of its PBDTBT analogue carrying longer and branched side chains is red shifted, with λ_{max} at 650 nm, a result of its more-solubilizing side chains facilitating higher molecular weight.[128] However, the PCE of these two polymers is not very high and was attributed to the low hole mobility. Through introducing thiophene bridges between the BDT and TBT units to give PBDTDTBT, higher PCE of 7.4% was obtained which is much higher than PBDTBT although these two polymers have similar HOMO levels and absorption ranges. The reason why PBDTDTBT has better performance was attributed to the increase in the absorption coefficient and four orders of magnitude higher hole mobility.[128] However, the extremely large number of additional variables associated with actual devices somewhat limits the weight of such attributions.

One of the polymer named PTB7 developed by Yu's group in 2010 has attracted a lot of attention due to the impressive device performance.[24] Although the choice of building blocks by most research groups seems to follow a plug-n-play approach, followed by claims that the best outcomes were envisaged beforehand, one can propose some explanations for the performance of this device rooted in the molecular structure (although serendipity in choice of the device fabrication conditions plays a possibly larger role). The mode of fusion of the two thiophene rings in thieno[3,4-b]thiophene (TT) units might increase the relative contribution of polymeric quinoidal character to the overall resonance description. Electron-withdrawing carbonyl groups can further modify the FMO energy levels, although

they surely influence a number of inter-related variables (solubility, pre-assembly in solution, interface energetics, subtle shifts in packing arrangements, etc.) so as to preclude sober claims concerning any primary cause of better device performance. This polymer does exhibit strong absorption from 550 to 750 nm, matching the highest photon flux region of the solar spectrum. A fluorine atom was included to further modify the properties. After solvent annealing to control the morphology, a PCE of 7.4% was achieved with BHJ blend of PTB7 and $PCBM_{70}$, which was the highest for polymer solar cell during that time.[24] After that Chen and coworkers observed better performance after attaching the 2-ethylhexyl-thienyl group to the BDT to form the PTB7-Th.[129] As the extension of the conjugated length, PTB7-Th has broad and strong visible absorption properties, lead to PCE of 9.35% for PTB7-Th : $PCBM_{70}$ blend. Recently Li even boosted the PCE of PTB7-Th : $PCBM_{70}$ blend to 10.8% with binary solvent additives.[130]

Some research groups have developed an approach to produce molecules that combine some features of crystalline small-molecules (e.g. precisely defined molecular structure and purity) with some features of polymers (e.g. film-forming and mode of phase-separation in BHJs). Chen and coworkers designed the acceptor−donor−acceptor (A-D-A) oligomeric molecules named DR3TBDT (Figure 2.3) with BDT as donor units. A PCE of 7.38% was obtained from the DR3TBDT-based solar cells.[131] After switching the BDT substituents from alkoxy to thioether groups, the PCE of the resulting DR3TSBDT was boosted to 9.95% upon thermal annealing and solvent vapor annealing.[132] Upon changing the BDT substituents to alkyl-thienyl groups, BTR was acquired with strong intermolecular interactions, as evidenced by its nematic liquid crystalline (LC) behavior. The hole

mobilities of BTR film exhibited up to 0.1 $cm^2/(V\ s)$ in OFET devices without intensive optimization indicating that either this structure modification was beneficial, or that the first attempted fabrication conditions were serendipitously well-suited for this particular molecular structure. The solution-processed BHJ solar cells based on BTR and $PCBM_{71}$ demonstrated efficiency up to 9.3%.[133]

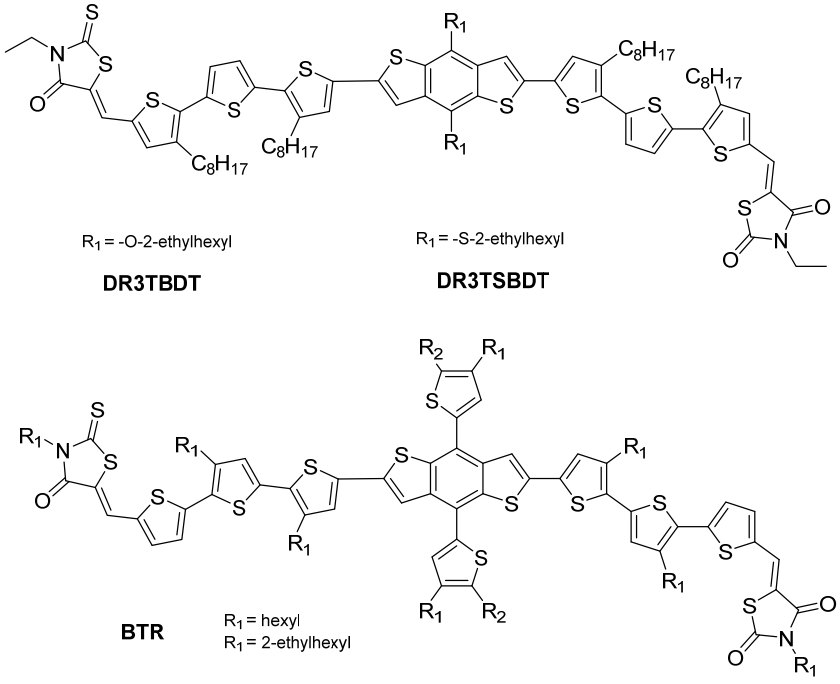

Figure 2.3: Small molecules used for OSCs based on BDT.

As we can see from the above example, sides chains were chosen to improve solubility. Most branched alkyl side chains used in these materials are branched at the β-position, no matter whether BDT-based polymers or small molecules. It is rare that branches are closer to the polymer backbone (α-position).[134] In 2011, Coffin's group reported PBDTTB polymers with various branching side chain on the BDT part (see figure 2.4).[135] The results showed that by moving the ethyl branch one position closer to the polymer backbone, the relative molecular weight (estimated by GPC) is dramatically increased to 68.8 kg/mol (for

1EH polymer) compare to 3.4 kg/mol (for 2EH polymer). It is reasonable to assume that the more poorly soluble 2EH polymer prematurely precipitates during polymerization, limiting polymer growth.

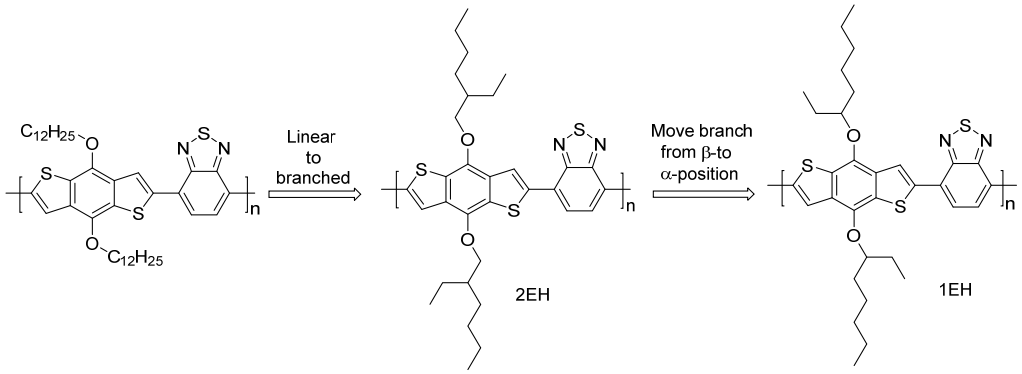

Figure 2.4: PBDTBT derivatives bearing alkyl side chains with various branching.[135]

Turning our attention to which acceptor to use in the current study, we considered 1,2,4,5-Tetrafluorobenzene (TFB), a "strong" electron-accepting unit, which is usually introduced into polymer to affect the ionization potentials and enhance π-stacking. Through increasing the random incorporation (1-15 mole %) of TFB within the backbones of polythiophenes, the HOMO level of polymer was raised along with increased ambient operational stability of OFETs (suppressed redox chemistry with atmosphere)..[136] Sommer and coworkers combined TFB with NDI to formed a polymer exhibit high electron mobilities.[137] TFB can be introduced as a non-alkylated spacer, also enhancing pi-stacking through attractive intramolecular interactions (π-πF) between fluorinated and non-fluorinated units.[138] Our group's prior studies also indicate that TFB units tend to impart very low solubility to conjugated polymers. So keeping these findings in mind, the project reported in this chapter focused on D-A polymers composed of BDT with TFB units. We also want to compare the BDT-TFB copolymers to analogues carrying identical

branched side chains, but with 3,3'-dialkoxy-2,2'-bithiophene (RO2T2) as the donor. BDT and RO2T2 units have relatively similar footprints, but drastically different flexibility (Figure 2.5). Dr. Daijun Feng in our group prepared the majority of the PRO2T2TFB polymers. Series of each copolymer with systematically varied side chains were prepared. Again, the initial polymer backbones chosen for study have acceptor unit of TFB because our past experience shows that such polymers usually have very poor solubility. If we can make these highly insoluble polymers become soluble in non-halogenated solvents at room temperature (through altering the size of the side chains) without disrupting π-π stacking and conjugation, then we can perhaps propose some design rules for solubilizing other polymers.

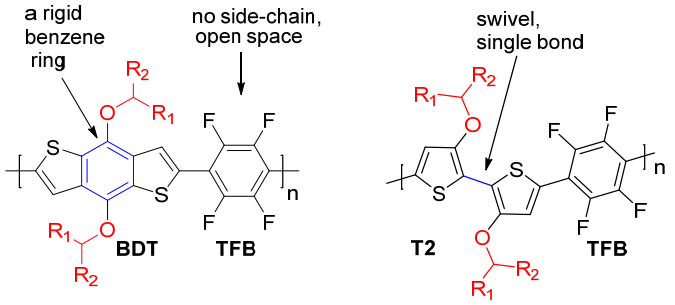

Figure 2.5: Polymers bearing different bulky alkyl side chains on rigid (benzodithiophene, BDT) or "swivel" (bithiophene, RO2T2) donor units, and TFB acceptor units.

The summarized initially outlined goals of the study include:

1. Assess effect of donor side-chain branching on properties of D-A polymers when acceptor has no side chains. Vary the length of the BDT alkoxy side chains while holding the size of their α-branches constant (α-methyl).
2. Assess effect of donor side-chain branching on properties of D-A polymers when acceptor has no side chains. Hold the length of the BDT side chain constant (tridecyloxy) while varying the size of the α-branch.

3. Pending outcome of the above. Assess the effect of donor side-chain branches at α vs β position. Choose the minimally sterically bulky side chain that imparts sufficient solubility (determined from goals 1 and 2) and move branch to β position. The solubility should substantially drop if the branch was the smallest one that could impart solubility when placed at the α-position.

2.2 Synthesis of Monomers and Donor-Acceptor Polymers Based on TFB Unit

2.2.1 Synthesis of Polymers with α-Methyl Branch

At the beginning of this study, the focus was on varying the length of the donor (BDT) alkoxy side chains while holding the size of their α-branches constant (α-methyl), resulting in the PBDTTFB polymers shown in figure 2.6.

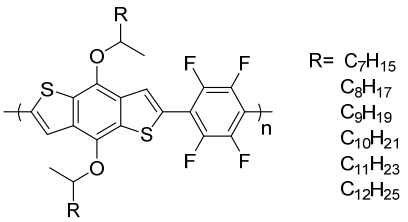

Figure 2.6: PBDTTFB polymers with methyl branch at α-position prepared in this study.

These PBDTTFB polymers were synthesized with a methyl branch at α position of the BDT side chains. The solubility apparently increased to some degree with size of R group (from heptyl to dodecyl). But even the polymer with 1-methyl-tridecyloxy side chains was still poorly soluble (less than 0.3 mg/ml in toluene). This indicates that an α-methyl branch is too small. So here we changed the focus to constant side-chain length (tridecyloxy side chain) while varying the size of the α-branch.

2.2.2 Evaluate the Solvent during the Polymerization

The Stille reaction was used for the polymerization and it is well known that the solvent plays a vital role in this reaction. For the polymerization, the solvent cannot only affect the catalysts stability but the molecular weights of the resulting polymer. The ideal solvent for the palladium-catalyzed polymerization should be able to stabilize the catalyst and at the same time be able to keep the polymeric molecules in solution.[18] THF is one of the good solvents for the Stille reaction according to the literature.[18] At the beginning, we choose THF as the solvent for the polymerization. However, the BDTTFB copolymers under study here are very poorly soluble in THF. Compared to THF, toluene can provide much better solubility, so identical polymerizations were run in THF and in toluene to compare. The molecular weight of the toluene-soluble fraction from each was estimated by GPC, and the results show us that higher molecular weights could be obtained for the polymerization in toluene than THF. The polymers precipitate earlier as they grow in less effective solvent THF and therefore retarding growth. The other reason is that we can run polymerization in toluene at higher temperature. Therefore, for all the further polymerization, we choose toluene as the solvent.

2.2.3 Synthesis of Polymers with constant length Tridecyloxy Side Chain and Varying α-Branch Size

From the above result, we moved to holding the length of the BDT side chain constant (tridecyloxy) while varying the size of the α-branch. 1,4-Dibromotetrafluorobenzene is commercially available and all the BDT monomers were synthesized following reported procedures after preparing the alkyl tosylates required for each side chain (Scheme 2.1). Commercially available thiophene-3-carboxylic acid was used as starting material. After

treating with oxalyl chloride in dichloromethane, the resulting acyl chloride was reacted with diethyl amine to give N,N-diethylthiophene-3-carboxamide, which was purified by distillation under vacuum to give colorless oil, in total yield over two steps near 90%. The thiophene was then selectively deprotonated at the 2-position with nBuLi in THF and resulting ambident species formed the BDT quinoid compound. The BDT quinoid compound can be purified by recrystallization from acetic acid to give yellow powder. The quinoid compound was reduced to diol by zinc in NaOH solution, and then an excess of alkyl tosylate was added with catalytic amount of tetrabutylammonium bromide (TBAB). It is worth to note that in this step the reaction time needed for acceptable conversion (from overnight to two days) depends on the bulk of side chains. Here in order to get different branch size of alkyl p-toluenesulfonate, the corresponding alcohol was made by simply reacting n-dodecyl Grignard reagent with various aldehydes. After purifying the BDT compounds using column chromatography, trimethyltin groups were introduced to provide the needed functionality for Stille polymerization (for further details please refer to the experimental section). Due to higher health risks, trimethyltin groups are to be avoided whenever possible, but became necessary here due to greater difficulty in purifying tributyltin derivatives.

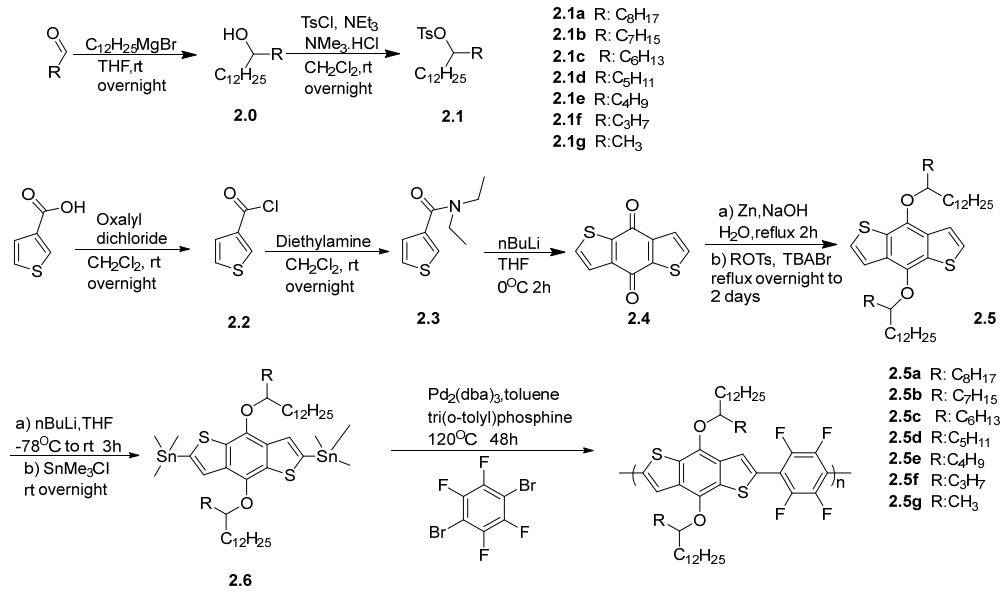

Scheme 2.1: Synthesis scheme of PBDTTFB polymers.

Purity of all the monomers were checked by using ^{1}H NMR, ^{13}C NMR and all these give satisfactory spectra. The structures of polymers and characterization (molecular weights, optical data) are listed in table 2.1. Most of the yields are good to moderate. The relative molecular weights are moderately high for most of the polymers as estimated by GPC (Gel Permeation Chromatography) using polystyrene standards.

2.2.4 Properties of PBDTTFB Polymers

Here in order to easy distinguish these polymers by name without having to refer to a figure, we give a systematic name to each of the polymers. As we see from figure 2.7, the "αC#" suffix after the PBDTTFB acronym indicates the location (α) and length of the branch (from C1 to C8). After polymerization, the resulting polymers were precipitated in methanol containing hydrochloric acid and the solid collected in a Soxhlet thimble. The color of these polymers are red to dark red. Each polymer was separated into different molecular weight fractions by sequential Soxhlet extraction with increasingly better solvents in the sequence:

acetone, 3-pentantone, pentane (or hexane) and $CHCl_3$ (depends on the solubility). Most published procedures proceed from acetone directly to hydrocarbon, but we were seeking here to get a finer separation. Later chapters will discuss further refinement of this approach with more solvents and a custom Soxhlet extractor designed by us to allow extraction with a given solvent but at different temperatures.

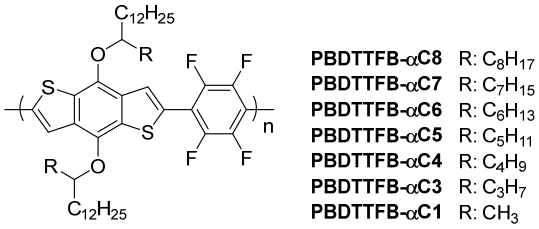

Figure 2.7: PBDTTFB polymers structure and related name.

The summary of PBDTTFB polymers is in table 2.1 (here the data is for the highest molecular weight fraction for each polymer. The end group for these polymers should be proton (the tin functional group will lose during the work up with strong acid) or bromide. For PBDTTFB-αC4, the number-average molecular weight (M_n) is about 11KDa (about 13 repeat unit) with a polydispersity of ca. 1.5 by using gel-permeation chromatography against polystyrene standards. M_n of PBDTTFB-αC5 is about 18KDa and M_n of PBDTTFB-αC7 is about 27KDa, M_n of PBDTTFB-αC8 is about 17KDa. The only exception is PBDTTFB-αC6 (M_n is about 5KDa), possibly from the lower monomer purity, also indicated by the Soxhlet solvent (Soxhlet from 3-pentanone). The M_n of PBDTTFB-αC3 and PBDTTFB-αC1 could not be evaluated due to very low solubility. For the sake of more valid comparison, the least number of structural variables (including M_n) is desirable. As will be shown from the results below, the low M_n of PBDTTFB-αC6 does not detract from the conclusions that can be drawn from this study. Further, the GPC

was equipped with a photodiode array detector. The PDA allows sequential collection of UV-Vis absorption profiles as the size distribution of each polymer eluted, demonstrating that each soluble polymer had reached the "effective conjugation length" (ECL). This is the length beyond which the UV-Vis absorption profile no longer shifts with each additional monomer unit.

Table 2.1: Properties of PBDTTFB polymers

Polymer	M_n [a] (kDa)	M_w (kDa)	PDI [b]	λ_{max}(abs) (nm) [c]	λ_{max}(film) (nm) [e]	λ_{onset} (film) (nm) [e]
PBDTTFB-αC8	16.9	22.1	1.31	505	521	558
PBDTTFB-αC7	26.9	36.4	1.35	508	522	552
PBDTTFB-αC6	5.3	8.8	1.92	505	521	563
PBDTTFB-αC5	17.8	28.7	1.61	507	522	554
PBDTTFB-αC4	11.1	16.8	1.52	508	521	559
PBDTTFB-αC3	N/A[d]	N/A[d]	N/A	521	522	554
PBDTTFB-αC1	N/A[d]	N/A[d]	N/A	514	515	550

a: Gel Permeation Chromatography (GPC) versus polystyrene standards.

b: PDI = polydispersity index = M_w/M_n.

c: $1x10^{-5}$ M in $CHCl_3$.

d: Polymer has poor solubility in $CHCl_3$ at ambient temperature so could not estimate the molecular weight via GPC measurement.

e: Pristine film spun-cast from 1 mg/ml $CHCl_3$ solution.

2.3 Effect of Side Chains Length on Solubility of PBDTTFB Polymers

The relative solubility of each polymer in toluene at room temperature was evaluated by serial dilution. Initial samples were prepared with 10 mg polymer per mL Toluene, swirled by hand to dissolve, stirred magnetically if dissolution had not yet occurred, and then left to stand. If the sample was not transparent to the naked eye, it was diluted, stirred, and left to stand again. This process was repeated until a clear solution was obtained. The clear solution was passed through a 0.45 μ filter to check (just by naked eye) whether colored material was retained in the filter.

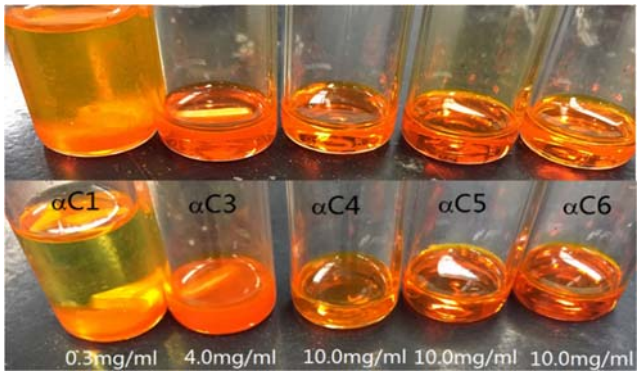

Figure 2.8: Solution of PBDTTFB polymers in toluene under ambient light: top (stirring then stand for 1 hour), bottom (stirring then stand for two days).

As we can see in figure 2.8, from left to right, the sample were PBDTTFB-αC1 (0.3 mg/ml), PBDTTFB-αC3 (4.0 mg/ml), PBDTTFB-αC4 (10.0 mg/ml), PBDTTFB-αC5 (10.0 mg/ml), PBDTTFB-αC6 (10.0 mg/ml). After stirring for 2 hours, PBDTTFB-αC3 solution was standing there for another 1 hour, seemed almost clear at about 4.0 mg/ml. However, after standing for 2 days of PBDTTFB-αC3 solution, it was cloudy again.

Table 2.2: Solubility test of PBDTTFB polymers

Polymer	Soxhlet solvent[a]	Solubility in toluene
PBDTTFB-αC8	Pentane	>10.0 mg/ml (quickly)
PBDTTFB-αC7	Pentane	>10.0 mg/ml (quickly)
PBDTTFB-αC6	Pentane	>10.0 mg/ml (quickly)
PBDTTFB-αC5	Pentane	>10.0 mg/ml (quickly)
PBDTTFB-αC4	Pentane	>10.0 mg/ml (quickly)
PBDTTFB-αC3	$CHCl_3$	<4.0 mg/ml (need stir)
PBDTTFB-αC1	$CHCl_3$	<0.3 mg/ml

[a] Soxhlet extraction solvent to extract highest MW fraction - through series of acetone, 3-pentanone, pentane, hexane and $CHCl_3$ (depends on the solubility).

The result of solubility test of PBDTTFB polymers are summarized in table 2.2. PBDTTFB-αC1 with the smallest α-branch having very poor solubility, giving cloudy suspension even with a concentration as low as 0.3 mg/ml in toluene. No

further dilution was evaluated. For PBDTTFB-αC3, solubility is better, but less than 4.0 mg/ml and stirring is necessary help this polymer soluble in toluene. Compare to PBDTTFB-αC3, the solubility of PBDTTFB-αC4 is much better, it is easy to make the 10.0 mg/ml solution clear just swirling by hand. For all other polymers, the solubility is at least 10.0 mg/ml. No higher concentrations were prepared, as this is already high enough for typical device fabrication. There is a step-change in solubility on increasing from PBDTTFB-αC3 to PBDTTFB-αC4. It is striking that Dr. Feng formerly in our group made a similar observation at the same branch size for the analogous ROT2TFB polymers (same acceptor, but RO2T2 donor carrying the same side chains). From the solubility test we determined that with a C13 side chain, the α branch should be C4 or longer for good room-temperature solubility.

The solubility difference of the PBDTTFB polymers also can be seen from the Soxhlet solvent required to extract the highest molecular weight fraction. After removing the lower molecular weight fraction through Soxhlet (using solvent such as acetone and 3-pentantone), the highest molecular weight fraction is extracted from the Soxhlet with the given solvents in table 2.2. For PBDTTFB-αC1 and PBDTTFB-αC3, the highest MW fraction required $CHCl_3$, but pentane is sufficient for all other PBDTTFB polymers. It is important to note that since Soxhlet extraction is a continuous extraction technique where the solvent is recycled, extraction of a fraction into a given solvent does not imply good solubility in that

solvent. A polymer fraction might be extracted into recycling hexanes, and yet show very poor solubility in hexanes and even in more powerful solvents extending up to boiling halogenated aromatics.

2.4 Effect of Side Chain Length on Polymer Optical, Electronic and Self Assembly

2.4.1 Optical Properties of Polymers

Changes in optoelectronic properties were evaluated with UV-Vis absorption spectra in solution and thin film (Figure 2.9). For consistency, molar concentrations are based on the molecular weight of the repeating units, not the polymer molecular weight. In good solvent (chloroform), it seems that PBDTTFB polymers with α-branch ≥ C4 are well solvated with decreased polymer-polymer interactions. PBDTTFB-αC3 has an obvious red shift (about 13 nm) relative to the other polymers with bigger branch, likely as a result of more extensive aggregation and less solvation, consistent with the solubility test in toluene. The red-shift of the "solution" absorption profile of PBDTTFB-αC1 relative to the polymers with larger side-chains branches should then be at least as large as that for PBDTFB-αC3 due to its poorer solubility (less than 0.3 mg/ml in toluene), but this was not observed. It is likely that the molecular weight of PBDTTFB-αC1 is limited during the polymerization (cannot be checked by GPC due to poor solubility) as a result of early precipitation during reaction. Shorter polymer backbone will absorb higher energy light and thus blue-shifted.

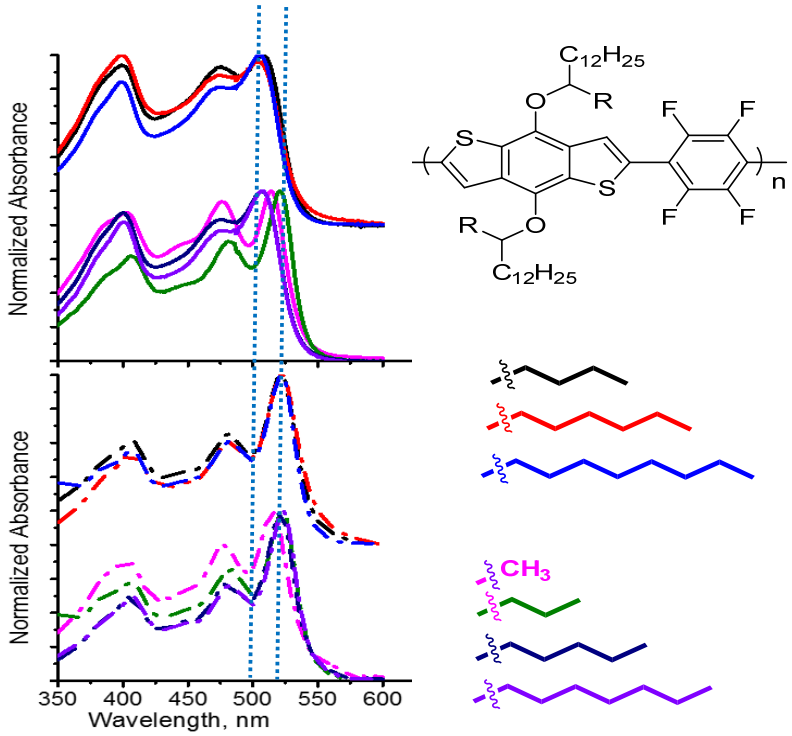

Figure 2.9: Normalized absorption spectra of PBDTTFB polymers at RT in solution (1.0 x 10^{-5} M, $CHCl_3$,top, solid line), and film (spun-cast from 1 mg/ml $CHCl_3$. bottom, dash line). Concentrations in solution are based on molecular weight of the repeating unit. The spectra from polymers with even and odd number of carbons in the side-chain branch are offset rather than all overlapping, to aid visualization. Vertical dashed lines are likewise included purely as visual aids.

All the polymers except PBDTFB-αC1 have essentially the same absorption profile in the solid state, and are red-shifted compared to solution, likely a result of similar π-π stacking arrangements for each polymer, which is supported by WAXD results (see below). However, we see a slight blue shift in absorption profile in solution (compared to solid-state) when the α branch is ≥ C4. This suggests decreased aggregation in solution when the α branch is ≥ C4, consistent with increased solubility. Therefore, C4 is the minimum size branch needed to induce "high" solubility, and at least for the examples prepared so far, π-stacking in the solid state

is not disturbed with increasing size of the branch (see WAXD results below). Interestingly, there is almost no shift for the UV−vis absorption profiles of PBDTFB-αC3 and PBDTFB-αC1 on going from "solution" to film. It is possible that PBDTFB-αC3 and PBDTFB-αC1 are extensively π-π stacked even when placed in $CHCl_3$ at 1.0 x 10^{-5} M. This is another evidence of the poor solubility of PBDTFB-αC3 and PBDTFB-αC1.

2.4.2 Self Assembly (Wide Angle X-ray Diffraction Patterns) of Polymers

The above results demonstrate that these polymers can be rendered highly soluble. The next question is whether bulky side chains required for solubility are too bulky to allow close π-stacking in the solid state. Oriented polymer fibers, obtained via passing through a die by mechanical force, were mounted perpendicular to an incident X-ray beam and diffracted x-rays were collected by an area detector. As polymer fiber was mounted perpendicular to the incident X-ray beam, diffraction maxima along the meridian (vertical axis) provided information about repeating elements along the backbone and diffraction maxima along the equator (horizontal) reflect the lamellar spacing and π-stacking. If any off-meridianal (neither on equator nor meridian) diffraction maxima were observed, this would indicate registry of repeating elements along more dimensions. As it is, diffraction maxima are seen only along the equator and meridian, the assembly can be considered as essentially lamellar arrangement of featureless lathe shapes (backbones) nanophase-separated from pendant alkyl chains. Some diffraction along the meridian does correspond

to repeating variation in electron density due to the defined backbone with alternating BDT and TFB repeating units.

WAXD Calibration with AgBeh

Table 2.3: The scattering angles and the d-spacings of AgBeh (CuKα radiation) [a]

hkl	2θ°	d(Å) (know)	d(Å) (experiment)
001	1.513	58.380	NA
003	4.537	19.460	20.175
004	6.051	14.595	15.230
005	7.565	11.676	12.070
006	9.081	9.730	10.100
007	10.607	8.340	8.655
008	12.128	7.298	7.605
009	13.651	6.487	6.770
010	15.230	5.817	6.025
011	16.754	5.293	5.470
013	19.800	4.484	4.725
015	22.846	3.890	3.965
017	25.893	3.513	3.575

[a] Reprint from reference Lee, B. et al. J. Appl. Cryst. 2006. 39, Page 750.

To accurately estimate the π-stacking distance, silver behenate (AgBeh, $CH_3(CH_2)_{20}COO{\cdot}Ag$) powder was used as a standard, the reason is that AgBeh is stable under ambient conditions and when exposed to X-rays.[139] AgBeh forms regular plate-like crystals with the lattice spacing 58.38 Å, giving a set of well-defined (0 0 l) diffraction peaks at 2θ values down to 1.5° when using CuKα radiation.[140,141]

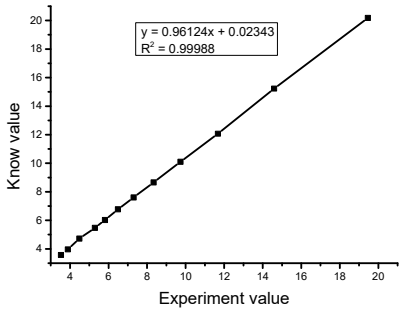

Figure 2.10: Calibration curve of AgBeh (x-axis is the experiment value; y-axis is the known value).

For diffraction peaks, the value of lattice spacing of AgBeh is already known, and the experimental values can be calculated from Bragg's equation ($\lambda = 2d\sin\theta$). Here the λ equals to 1.542 Å (CuKα radiation) for checking/adjusting the values automatically put forth by the instrument software. Some of the AgBeh diffraction peaks were not utilized as they were too weak to see. The experimental values for 2θ were taken directly from the instrument computer. Based on the known and experimental d-spacing values, a calibration curve was made, where x axis is the experimental value, and y axis the known value. After input all the points, a linear equation was produced and used for correcting the d-spacings taken from polymer fibers.

In the polymer fiber diffractograms, the 1st, 2nd, 3rd, and even 4th order reflections on the equator could be seen, suggesting relatively long range lamellar order normal to the aligned polymer backbones. The lamellar distance of these polymers are fairly similar, between 22.8-25 Å, due to the unvaried length of (tridecyloxy) side chain. There is however a small and steady increase in the lamellar spacing with increasing

space-filling demands of the branch, which are competing for the space between polymer backbones. Additionally, with the increase of branch size, the π-stacking distance increases, though only very slightly. When α branch is ≥ C4, close π-stacking (about 3.7 Å) was still seen for all α-branch PBDTTFB polymers, and the total increase in stacking distance from C4 to C7 is only 0.03 Å, which can't be considered significant.

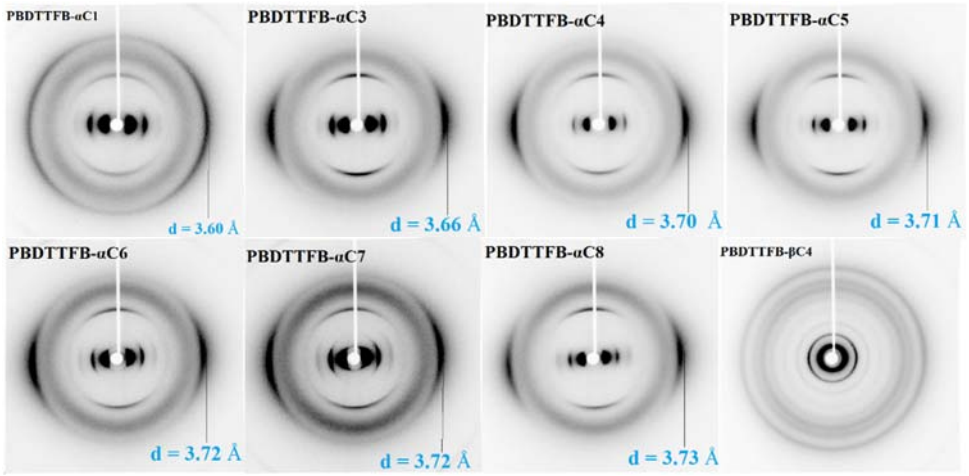

Figure 2.11: Fiber WAXD diffractograms of PBDTTFB polymers.

All the results taken together show that these otherwise very poorly soluble polymers can be solubilized with an α-branch having a minimum size of 4 carbons, while not disrupting close π-stacking in the solid state. Having established this fact, a derivative with the C4 branch moved to the β-position was prepared (see below). The diffraction pattern for PBDTTFB-β4 polymer carrying its C4 branch at the β-position, consists of concentric rings, as opposed to arcs centered around the equator and meridian. This reveals that the polymer backbones were not aligned during extrusion. The likely reason is that this polymer, which was very poorly soluble (< 0.5 mg/mL in toluene), was not aligned during extrusion. The polymer

was rather hard and brittle, and therefore resistant to plastic deformation that can transmit the shear throughout the sample.

Table 2.4: Data collected from diffraction patterns in figure 2.11

Polymer	Lamellar spacing L,L/2 (Å)	"d"(before calibration) π-spacing (Å)	"d"(after calibration) π-spacing (Å)
PBDTTFB-αC8	24.95, 12.87	3.86	3.73
PBDTTFB-αC7	24.45, 12.75	3.85	3.72
PBDTTFB-αC6	23.78, 12.34	3.85	3.72
PBDTTFB-αC5	23.79, 12.09	3.84	3.71
PBDTTFB-αC4	23.53, 11.76	3.82	3.70
PBDTTFB-αC3	23.01, 11.91	3.78	3.66
PBDTTFB-αC1	22.75, 11.13	3.72	3.60

Compare with PBDTTFB polymers, the stacking behavior of RO2T2TFB polymers (prepared by Dr. Feng) as a function of branch size is quite different. For ROT2TFB polymers, the π-π stacking distance was more sensitive to the increasing size of α-branch side chains. Upon increasing the branch-size to C5, the π-π stacking distance increased from values similar to those observed here to just under 4 Å (3.96 Å). The point of side-chain attachment is actually a little closer to the center long axis of the RO2T2 donor unit, and the donor unit is able to twist to accommodate space filling demands, unlike BDT.

2.4.3 Electrochemistry of Polymers

Voltammetric methods adapted to measure the oxidation and reduction potentials of conjugated polymers typically involve deposition of the polymer material onto the working electrode. The onsets of oxidation and reduction are used to estimate the E_{HOMO} and E_{LUMO}, respectively. E_{HOMO} provides a relative estimate of the ionization potential, the minimum energy required to remove an electron from an atom or

molecule in the gas phase. We know that our reduction/oxidation potentials obtain from this voltammetric technique are estimates as the test was from thin films, while, the HOMO/LUMO energies are scaled in vacuum.

Table 2.5: Electrochemical and optical data for polymers

Polymer	E_{ox} (V) [a]	E_{HOMO} (eV) [b]	E_{LUMO} (eV) [c]	E_g^{opt} (eV) [d]
PBDTTFB-αC8	0.88∓0.05	-5.68∓0.05	-3.46∓0.05	2.22
PBDTTFB-αC7	0.88∓0.05	-5.68∓0.05	-3.41∓0.05	2.25
PBDTTFB-αC6	0.85∓0.08	-5.65∓0.08	-3.44∓0.08	2.20
PBDTTFB-αC5	0.87∓0.07	-5.67∓0.07	-3.45∓0.07	2.25
PBDTTFB-αC4	0.83∓0.08	-5.63∓0.08	-3.41∓0.08	2.22
PBDTTFB-αC3	0.85∓0.05	-5.65∓0.05	-3.40∓0.05	2.25
PBDTTFB-αC1	0.85∓0.05	-5.65∓0.05	-3.40∓0.05	2.25

Experimental conditions: 0.1 M $(n\text{-}Bu)_4N.PF_6$ in anhydrous acetonitrile as supporting electrolyte, platinum disc as working electrode, platinum wire as counter electrode, silver wire as reference electrode and Fe/Fe+ (-4.8 eV vs vacuum) as reference, scanning rate: 50 mV/s; All measurements conducted on solution-cast thin films under nitrogen. [a]Corrected E_{ox} value respect to Fc/Fc+. [b]E_{HOMO} = -[4.8+(E_{ox}-Fc/Fc+)], E_{ox} calculated using onset of DPV measurements (Oxidation peak). [c]$E_{LUMO} = Eg^{opt} + E_{HOMO}$. [d] Eg^{opt} Optical band gap estimated from the absorption edge of the film. Each of the sample run 3 times. We test Fc before each polymer test and polish the electrode then test Fc again, each time the difference is less than 20 mV.

As we can see from table 2.5, the HOMO/LUMO energies of PBDTTFD polymers are all similar. At least for the examples prepared so far, the oxidation potential is insensitive to the size of the side-chain branch. This is in good agreement with the other observations so far.

2.5 Effect of Side Chains Position on Properties of PBDTTFB Polymers

2.5.1 Synthesis of β-branch monomer and PBDTTFB polymer

We have determined the critical α-branch length for solubility from above results, the solubility for PBDTTFB-αC4 is more than 10.0 mg/ml in toluene, substantially greater than with a branch size of 3 carbons. Then we want to see the effect of moving the branch to

β-position, so we can compare the branching position effect on the polymers. Here, we have the PBDTTFB-βC4 polymer with β-butyl branch (Figure 2.12).

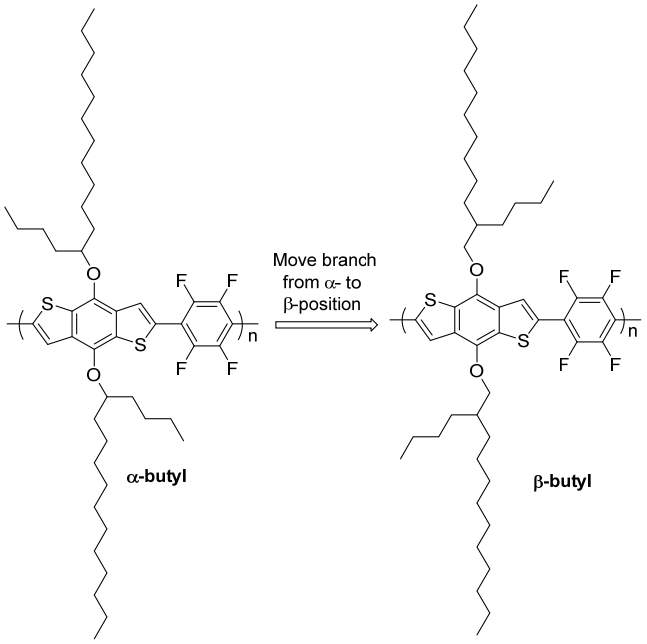

Figure 2.12: PBDTTFB polymers bearing alkyl side chains with various branching.

The polymer synthesis is identical to other PBDTTFB polymers as summarized in scheme 2.2.

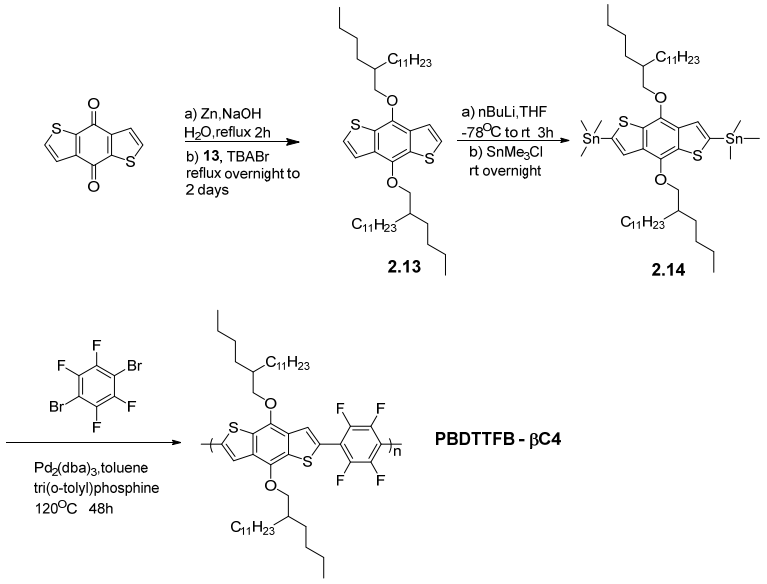

Scheme 2.2: Synthesis scheme of β-branched PBDTTFB polymer.

In order to get the β-branched alcohol intermediate, we exploit the malonic ester synthesis, starting from commercially available diethyl 2-butylmalonate. The 2-butyl-2-undecylmalonate (compound **2.8**) is quite easy to prepare. Surprisingly, the subsequent ester hydrolysis and decarboxylation was somewhat challenging (see details from experimental section). After various attempts under different conditions, hydrolysis was effective with KOH in isopropyl alcohol and water to give 2-butyl-2-undecylmalonic acid (compound **2.9**), which could be used for the next step without purification.

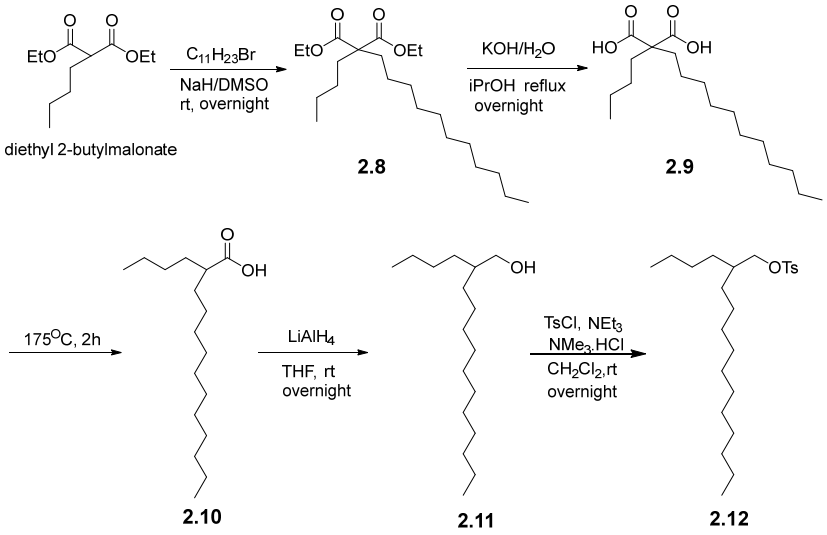

Scheme 2.3: Synthesis scheme of β-branched alcohol and related β-branched alkyl-OTs.

Here the key step was decarboxylation to remove one carboxylic acid group. After several attempts under the typical conditions of reflux the 2-butyl-2-undecylmalonic acid in strong acid (see experimental section), it seems removal of one carboxylic acid does not work in the acid solution. However, by just heating the sample directly to high temperature (about 175 ^{O}C) without solvent, the reaction generated a lot of bubbles (releasing of CO_2) and formed the desired 2-butyltridecanoic acid. This is a good example of solvent-free organic synthesis. As we know the solvent-free organic synthesis is a highly useful technique,

especially during the large scale synthesis process.[142] There is some report that microwave-assisted decarboxylation of malonate derivatives with the help of imidazole.[143] Until very recently, Escalante reported the microwave-assisted decarboxylation of malonic acid derivatives without solvent.[144] After purification of 2-butyltridecanoic acid via column chromatography, reduction with $LiAlH_4$ gave the 2-butyltridecan-1-ol which could be converted with p-toluenesulfonyl chloride to give the requisite compound 14 for alkoxylating BDT.

2.5.2 Properties of PBDTTFB-βC4 polymer

After getting PBDTTFB-βC4, we test the solubility and UV-Vis absorption spectra. The solubility test using toluene as solvent. Compared to PBDTTFB-αC4 which has good solubility (more than 10.0 mg/ml in toluene), the solubility of PBDTTFB-βC4 is quite poor, less than 1.0 mg/ml, and requires stirring help to solubilize. Also we can see the obvious solubility difference from solvents used for Soxhlet. The highest molecular weight fraction of the α-branch product can be Soxhlet extracted into pentane. However, the β-branch product required chloroform.

Table 2.6: Solubility test of PBDTTFB-C4 polymers

Polymer	Soxhlet solvent[a]	Solubility in toluene
PBDTTFB-αC4	Pentane	>10.0 mg/ml (quickly)
PBDTTFB-βC4	$CHCl_3$	< 1.0 mg/ml (need stir)

[a] Soxhlet extraction solvent to extract highest MW fraction - through acetone, 3-pentanone, pentane, hexane and $CHCl_3$ (depends on the solubility).

As we can see from solubility test and figure 2.13, solubility of these polymers is quite sensitive to the side chains position, the α-branch polymer has much better solubility than

β-branch polymer: PBDTTFB-αC4 (<1.0 mg/ml) can only suspension in toluene, but PBDTTFB-βC4 polymer form solution easily (10.0 mg/ml) in toluene.

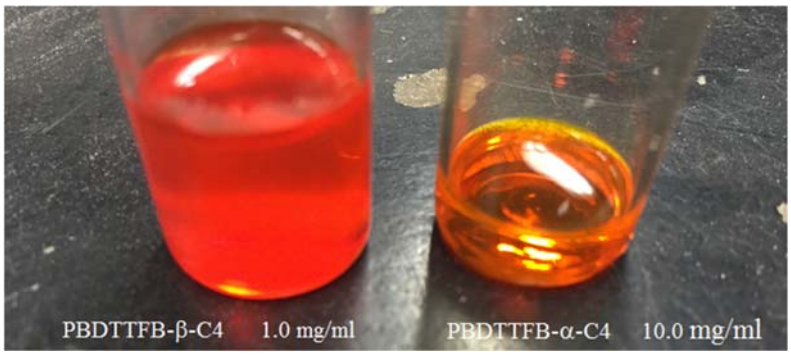

Figure 2.13: Solution of PBDTTFB polymers in toluene under ambient light.

UV-Vis absorption spectra in chloroform and thin film were compared. Compare to PBDTTFB-αC4, the UV-Vis absorption profile of PBDTTFB-βC4 chloroform has a red shift (about 10 nm), consistent with the solubility test.

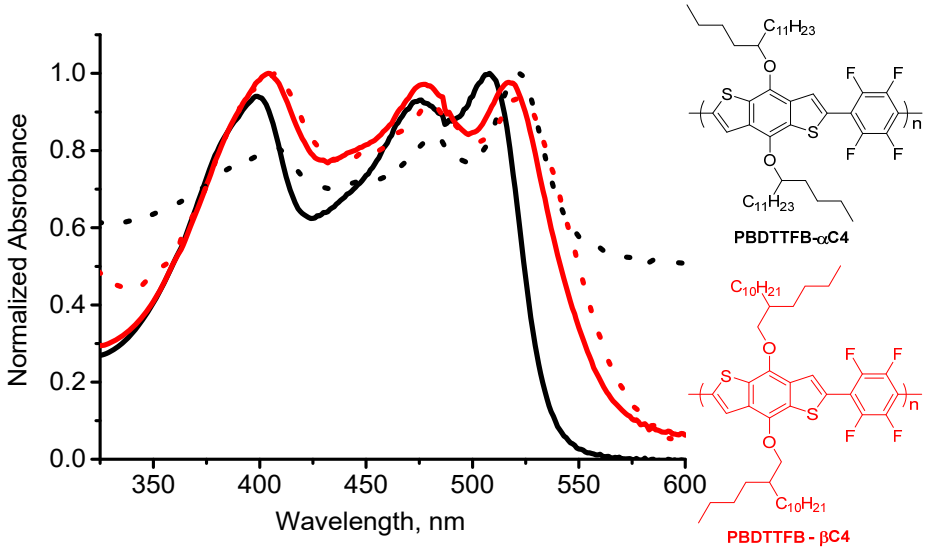

Figure 2.14: Normalized absorption spectra of PBDTTFB-C4 (1.0 x 10^{-5} M) in $CHCl_3$ at room temperature (solid line), and film spun-cast from 1 mg/ml $CHCl_3$ (dash line).

The results show us that branch position strongly affects the solubility of PBDTTFB polymers. For PBDTTFB-αC4 polymer, solubility was higher than 10.0 mg/ml in toluene; but for PBDTTFB-βC4 polymer, solubility was less than 1.0 mg/ml in toluene.

2.6 Thermal Analysis of Polymers

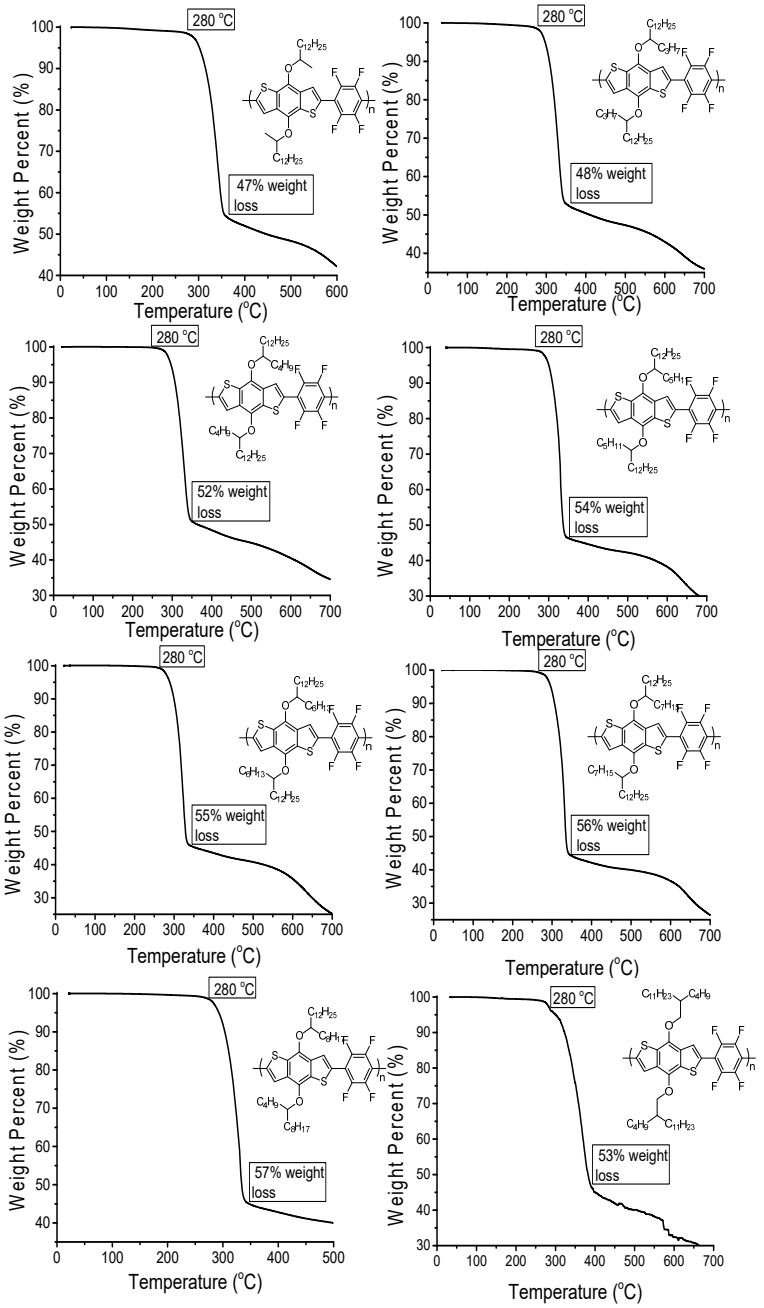

Figure 2.15: Thermogravimetic analyses of PBDTTFB polymers under N_2.

Thermogravimetric analyses (TGA) of conjugated polymer are generally not as relevant as they might be for polymers that will be employed in other applications. In any case, the TGA traces show a steep weight loss under nitrogen with onset near ~280 ºC. The weight loss is step-wise, with the % weight loss in the first step corresponding well to the weight percent of side chains (see table 2.7). This is not surprising given that the secondary-alkyl ether linkages should be succeptable to thermal elimination.

Table 2.7: Thermogravimetic analyses of PBDTTFB polymers

Polymer	Weight ratio of Side chains	Percent of weight loss [a]
PBDTTFB-αC1	51%	47%
PBDTTFB-αC3	53%	48%
PBDTTFB-αC4	56%	52%
PBDTTFB-αC5	58%	54%
PBDTTFB-αC6	59%	55%
PBDTTFB-αC7	60%	56%
PBDTTFB-αC8	61%	57%
PBDTTFB-βC4	56%	53%

[a] Here means the prominent weight loss of polymers after heating up to 300 ºC.

According to differential scanning calorimetry (DSC), none of the polymers undergo observable thermal transitions up to180 ºC.

2.7 Conclusions

To understand about how branch side chains size related to overall polymer properties we did a systematic study by changing the length and position of branches in alkoxy side chains.

From this study it was clearly shown that it is possible solubilize the PBDTTFB polymers without strongly altering the absorption profile, oxidation potentials, and solid-state

π-stacking. The solubility test and UV−vis absorptions test (in solution and film) both prove that BDT polymers undergo step-change in solubility when going from C3-C4 α branch. Unlike the ROT2TFB polymers, the absorption profiles for the BDTTFB polymers are relatively insensitive to the size of side chain branch. The absorption profiles (and π-stacking distance estimated from WAXD) of RO2T2TFB polymers changed significantly with the increase of side chain branch size. It is striking, though given the structrural differences for the two donors being compared, that ROT2TFB-based polymers also undergo step-change in solubility when going from C3-C4 α branch.

Thermogravimetric analyses (TGA) shows that all polymers are stable up to about ~280 ºC. None of the polymers showed any melting transition up to 180 ºC during differential scanning calorimetry study (DSC).

As predicted, when an α-branch with the minimal size necessary to impart good solubility is moved the β position, the solubility drops dramatically.

Chapter 3: Thiophene-Imide (TPD) and BDT, 3,3'-dialkoxy-Bithiophene Based Alternating Donor-Acceptor Co-polymers

3.1 Introduction

Having established (chapter 2) that the extremely poorly soluble copolymers of BDT with TFB could be solubilized with appropriately sized α-branches in the side chains without disrupting π-stacking, our focus shifted to replacing TFB with another acceptor that could carry side chains (unlike TFB). Can the large space-filling demands of such bulky side chains on the donor units still be accommodated within a tight π-stacked arrangement if the acceptor also carries side chains competing for space? Ideally, we would use one acceptor for all these studies to minimize variables, but we cannot attach side chains to TFB, and still have TFB. There are a number of reasons to choose thiophene-imide (TPD) as acceptor, but for the purposes of this study, one primary reason is that we can attach a single alkyl chain of varying size.

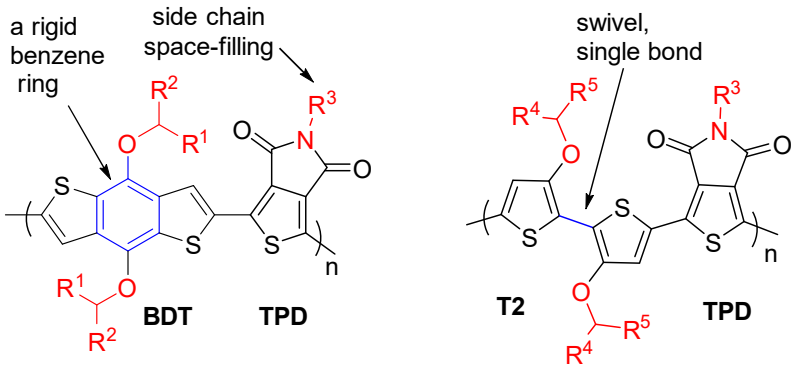

Figure 3.1: Polymers bearing different bulky alkyl side chains on rigid BDT or "swivel" RO2T2 donor units, and acceptor units (TPD) with side chains.

Switching to TPD from TFB acceptor introduces variables in addition to incorporation of alkyl chains on the acceptor so direct comparison between the results in this chapter and

those in chapter 2 are somewhat limited. Some introduction to additional factors affecting backbone planarity, π-stacking, and optoelectronic properties follows.

Extending π-electron systems while maintaining sufficient π-orbital overlap has been a main focus during the development of organic electronics, as this is a common strategy to achieve high-mobility organic materials. One way to control planarity is through restricting the rotation of neighboring aromatic rings by additional covalent bonds. Various bridge atoms (see figure 3.2) were included to restrict the rotation of biphenyl to form fluorene,[145] silafluorene[146] and carbazole,[147] which are important building blocks for OLED[148] and hole transport materials,[149] also used for OSCs.[150] Bridge atoms C,[151] Si,[152] Ge[153] and S[154] were also used in the bithiophene ring system. The building block not only changes due to the planarity, but the energy levels and π-electron delocalization are adjusted through choice of bridge atoms. However, one has to consider the additional synthetic steps for some of these molecules, which could limit practicality.

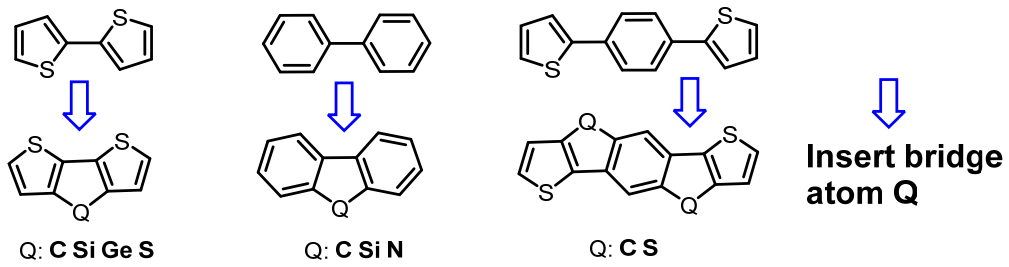

Figure 3.2: Planarity control through bridge atoms. The bottom row of structures includes examples of each structure immediately above, but with a bridge atom added.

Another strategy which employs noncovalent through-space intramolecular interactions, also called noncovalent conformational locks has been successfully used to increase the planarity and rigidity of extended π-electron systems.[26]

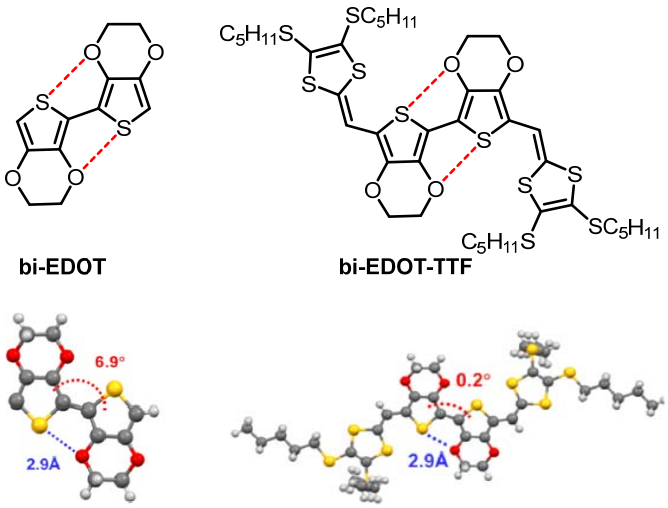

Figure 3.3: Planarity control through noncovalent conformational locks (data collected from crystal structure). [155]

Noncovalent intra- and intermolecular chalcogen-sulfur interactions have been known for some time. A lot of research shows us that the weak interaction is quite important for organic semiconductors as it will affect self-assembly, charge transport, and molecular recognition.[26] Through research of the crystal structure of 2,2'-bi(3,4-ethylenedioxy)thiophene (EDOT) (see figure 3.3, left) and a bis(EDOT) derivative (see figure 3.3, right), Roncali and coworkers found that the distances between oxygen and sulfur (2.92 Å) are significantly shorter than the sum of the van der Waals radii of the two atoms (3.25 Å), and contributes to other driving forces for the π-conjugated structure to be in a relatively planar conformation with a small dihedral angle between the thiophene rings.[155] The contribution of differing space-filling demands and crystal packing forces cannot be excluded, and probably contribute to the differing dihedral angles for the two molecules. The solution UV−vis spectrum of bi-EDOT-TTF shows a strong enhancement of the fine structure with the emergence of two main absorbance bands, in

accord with a fully planar rigid conformation of the molecule through conformational locking. [156]

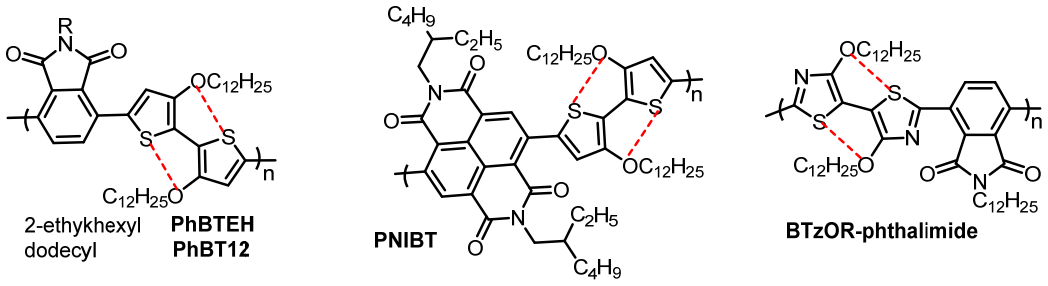

Figure 3.4: **Polymers with O···S conformational locks.**

Recently there were several reports showing HH linkages in bithiophene (T2) linkages do not necessarily preclude the backbone conjugation. A previous researcher from our group, Yongfeng Wang reported that, contrary to the "convential wisdom" at the time, the head-to-head (HH) linkages in polymers with 3,3'-dialkyl bithiophene (3,3'-R2T2) units, when combined with TFB acceptor units, did not intrinsically preclude co-planarity as shown by WAXD (wide angle X-ray diffraction) and uv-vis absorption studies.[138] An exact polymer analogue, but with the fluorine atoms deleted (benzene in place of TFB) was amorphous with no regular π-stacking in the solid state, and markedly more soluble. Backbone planarization is enhanced due to the intermolecular D-A interactions and intramolecular S-F interactions. PhBT12 (Figure 3.4), the first reported D-A polymeric semiconductor based on RO2T2 units was reported by Xugang Guo in our group, and worked as hole transporting materials with OTFT mobilities of ~0.2 $cm^2/(V\ s)$.[77] UV-vis absorption test indicating increased backbone planarization and π-stacking in the solid state. The reason behind this is the O···S interaction. The same strategy was used to design PNIBT, a D-A copolymer based on RO2T2 and strongly electron-deficient building block

naphthalene diimide (NDI).Ambipolar transistors with electron mobility of 0.04 $cm^2/(V\ s)$ and a hole mobility of 0.003 $cm^2/(V\ s)$ were prepared from PNIBT.[157] This polymer was independently developed and extensively studied, with many advancements in device studies largely headed by Fachetti (Polyera Corp) and others. Lately, Guo also designed BTzOR-phthalimide copolymer based on dialkoxybithiazole which has weak electron-donating ability, the device test show that hole mobility as high as 0.25 cm2/(V s) with enhanced device ambient stability (stability of the derived device against oxygen and moisture).[158]

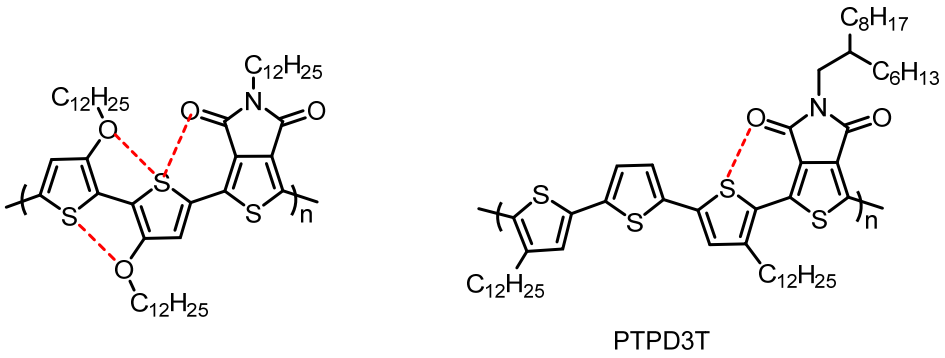

PTPD3T

Figure 3.5: TPD polymers with O···S interaction.

Thieno[3,4-c]pyrrole-4,6-dione (TPD) unit possesses compact, symmetric, and planar structure with an alkyl-substituted imide fused on thiophene. The TPD unit worked as electron acceptor due to the imide group, at the same time alkyl chains on the imide nitrogen can tune the solubilities of polymers. TPD unit should have less steric repulsion with adjacent backbone rings than some other aryl imides like those listed above. As our group was moving from those to TPD, it became clear that TPD would receive sufficient attention from other groups. The pioneer work of PBDTTPD polymers by Leclerc using TPD unit, through carefully tune the side chains and applied as PSCs with PCEs more than

8%. Another advantage of PBDTTPD polymers is that the stability of these materials allows for BHJ solar cell application after material purification which removes organic impurities.[159] Through combination of the common donor dithienosilole-(germole)[160] and terthiophene, the TPD-based polymers exhibit PCEs > 8% in BHJ solar cells. Guo and coworkers even found that a remarkable FFs (fill factor) approaching 80% was achieved for PTPD3T (see figure 3.5 right) polymers which attribute to substantial charge carrier mobility, highly ordered and π-face-on oriented microstructures with close π–π stacking.[161] Our group first copolymerized RO2T2 units with TPD to get polymer and used them for OTFTs (see figure 3.5 left).[162] All the above should explain the motivation for returning to TPD as an acceptor in the fundamental studies here.

As we achieved the goals to determine the type of side chains to impart solubility of polymers at the same time maintain the π-π stacking in D-A polymers with TFB as acceptor (much free volume surrounding acceptor without side chains), then we want to check if there still can be π-stacking with bulky branched side chains on donor when there are also space-filling side chains on the acceptor. Therefore, PBDTTPD polymers were chosen as the TPD part is a very strong acceptor which also has an easily modified alkyl side chain. So in chapter 3, I will combine BDT and RO2T2 units, like those reported in chapter 2, with TPD unit to form polymers and compare their solubilities, optoelectronic properties and solid-state packing. The TPD carries either a very small methyl group or larger n-octyl. Initial ideas to investigate TPD with no alkyl chain (R^3 = H) were not followed as this introduces the additional variable of H-bonding, which would not be present for the analogues carrying alkyl groups at the imide nitrogen.

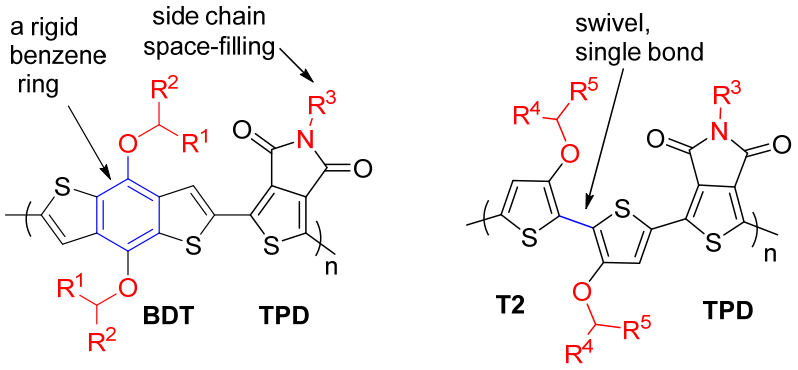

Figure 3.6: Polymers bearing different bulky alkyl side chains on rigid (benzodithiophene, BDT) or "swivel" (bithiophene, RO2T2) donor units, and acceptor units with (TPD) side chains.

So the main goals which we are testing:

1. Compare donor units of BDT and RO2T2, which has a similar donor size, but different linkage as in chapter 2.
2. Assess effect of donor side-chain branching on properties of D-A polymers when acceptor has side chains with varying space-filling demands.

3.2 Synthesis of Monomers and Polymers Based on TPD Acceptor Unit

3.2.1 Synthesis of TPD and PBDTTPD Polymers

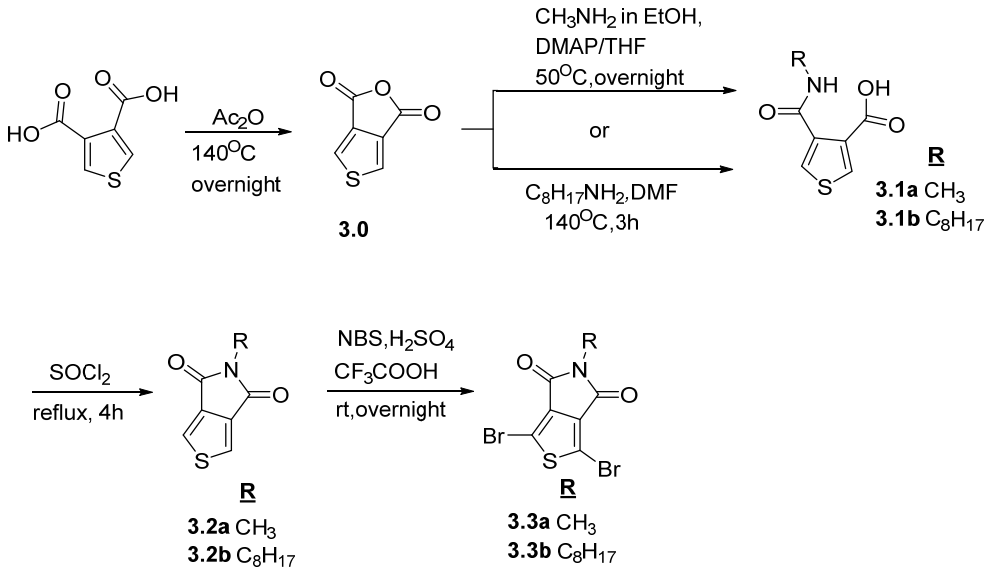

Scheme 3.1: Synthesis scheme of N-alkyl derivatives of TPD.

TPD monomers were prepared following published procedures[163] as depicted in scheme 3.1. Commercially available thiophene-3,4-dicarboxylic acid was dehydrated in refluxing acetic anhydride to form the corresponding anhydride. The anhydride was converted to imide in a two-step procedure by first reacting with amine (methyl or n-octyl amine) to give an amic acid. Unlike for pthalimides, imide ring closure does not occur in situ, but requires a second step involving an acid chloride intermediate. Until this step it was fine to use the crude product for all the reactions. The close ring product can be easily purified using column chromatography and further purified by recrystallization. As the imide group deactivates the thiophene ring towards electrophilic bromination, relatively harsh conditions were used to introduce bromine to the acceptor.

The PBDTTPD polymers (scheme 3.2) were prepared by Stille polymerization and fractionated by Soxhlet extraction using different solvents (depend on the solubility). The synthesis of the BDT monomers was described in chapter 2.

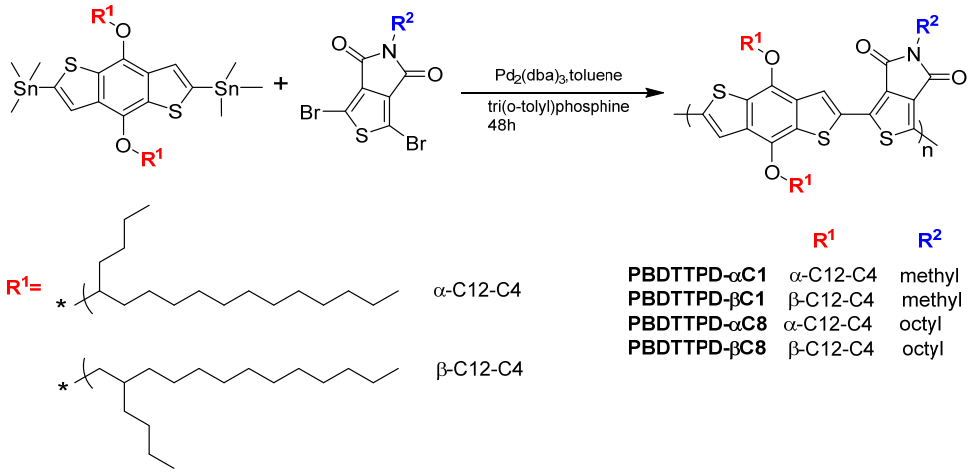

Scheme 3.2: Synthesis of PBDTTPD polymers.

For PBDTTPD-βC1 polymer, the highest molecular weight fraction was extracted with hexane; for the other three polymers, the highest molecular weight fraction was extracted with high temperature 3-pentanone, which is a poorer solvent, so these polymers have higher solubility.

3.2.2 Synthesis of 3,3'-dialkoxy-2,2'-Bithiophene (RO2T2) and PRO2T2TPD polymers

PRO2T2TPD polymers (scheme 3.3) were prepared by Stille polymerization and fractionated as described for the PBDTTPD polymers.

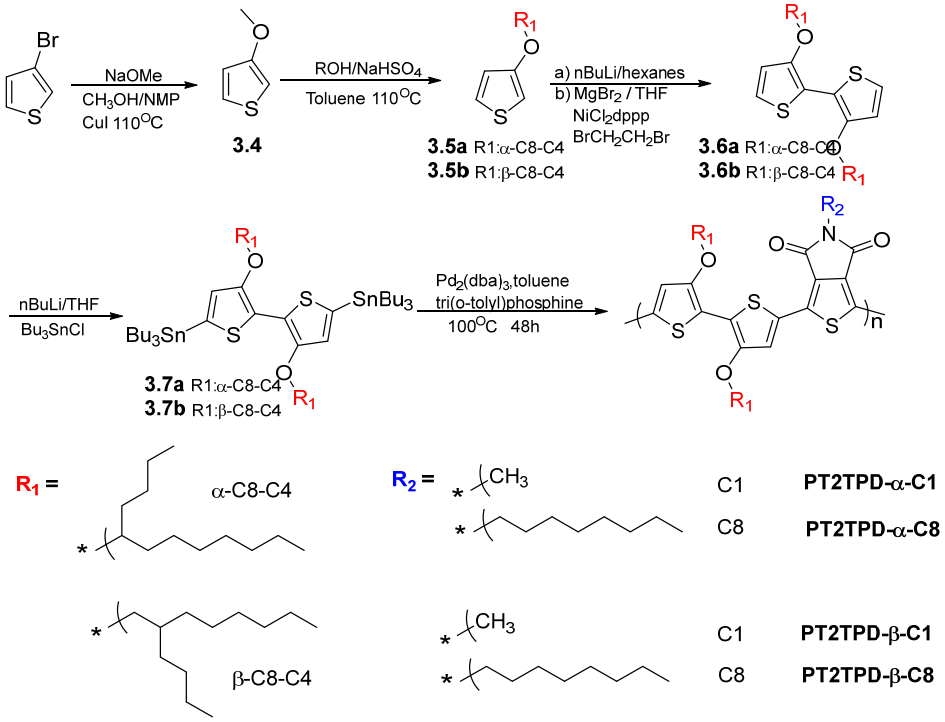

Scheme 3.3: Synthesis scheme of PRO2T2TPD polymers.

Synthesis of 3,3'-dialkoxy-2,2'-Bithiophene (RO2T2)

Improvements to published synthetic procedures for RO2T2 monomers were employed here (some of these improvements were developed by Dr. Daijun Feng in our group and are as yet unpublished). 3-Alkoxy-thiophenes carrying branched side chains were synthesized

according the procedure of reference, with one important modification.[164,165] The 3-bromide-thiophene reacted with NaOMe in mixed solvent (methanol and N-methyl-2-pyrrolidone) using CuI as catalyst. Typical conditions for exchanging the methoxy group with α-branched alkoxy chains suffered due to extensive elimination from the secondary alcohols. Acceptable yields of 3-alkoxy-thiophenes (6) could be obtained when $NaHSO_4$ was employed. The subsequent coupling to RO2T2 is a critical step.

There are various methods to prepare RO2T2 (scheme 3.2), each with their own drawbacks. Our group previously followed a route of first brominating 3-alkoxythiophene, then coupling the 2-bromo-3-alkoxythiophene under Yamamoto coupling condition, which required more than a stoichiometric amount of $Ni(cod)_2$.[76] Alternatively 2-bromo-3-alkoxythiophene can be converted to Grignard reagent via Grignard metathesis, and subsequently coupled to another equivalent of 2-bromo-3-alkoxythiophene with catalytic $Ni(dppp)Cl_2$.[166] The total yield of this reaction for RO2T2 is under 30%. A major drawback for either of these approaches is that 2-bromo-3-alkoxythiophene is somewhat unstable, undergoing an autopolymerization process with loss of HBr.[167] Our group often stored this intermediate in solution and at low temperature to minimize decomposition. Marks and McCulloch reported a method which bypasses 2-bromo-3-alkoxythiophene through oxidative coupling of 2-lithio-3-alkoxythiophene with stoichiometric $Fe(acac)_3$, but the yield is only moderate.[168,169] At least when applied to the target monomers in our study, this reaction produced regiosomers that were difficult to separate.

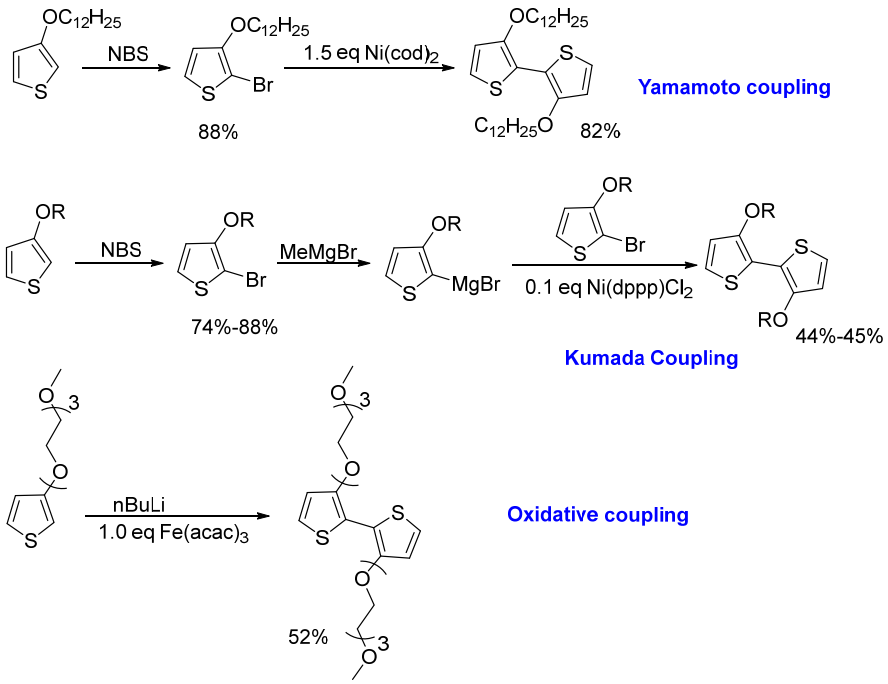

Scheme 3.4: Reported synthesis scheme of 3,3'-dialkoxy-2,2'-bithiophene (RO2T2).

Based on the modifications of previously published procedures, Dr. Feng in our group found that deprotonation of 3-alkoxythiophenes can be rendered regiospecific to the 2-position if carried out with nBuLi in hexanes at low temperature. Metallation was highly selective, but not regiospecific, if carried out in more typical ether solvents. Transmetallation with anhydrous $MgBr_2$ to form Grignard reagents prior to oxidative homocoupling with Ni catalyst eliminated the issues with regioisomers.

Conditions and Mechanism for Ni-catalyzed Grignard Regent Homocoupling

The Ni-catalyzed oxidative homo-coupling reaction under different conditions were carefully checked, the resulting yields are shown in Table 1. As this reaction in one pot process, the reagent and temperature were examined during the Grignard regent formed step.

For oxidized coupling step, experiments were carried out in different conditions including oxidant, catalysts loading and time in order to investigate their effect on yields.

Table 3.1: Ni-catalyzed homocoupling of RMgBr under different conditions

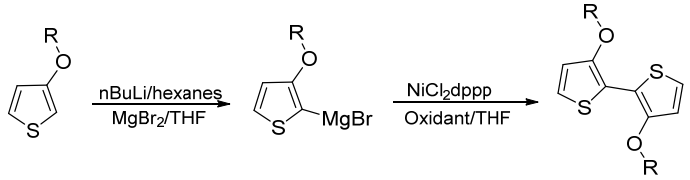

Entry	Reagent	T [°C]	Oxidant	Catalysts loading [%]	Time [h]	Yield [%]
1	$MgBr_2$	70	$BrCH_2CH_2Br$	10	12	63
2	$MgBr_2$	70	$BrCH_2CH_2Br$	5	12	61
3	$MgBr_2$	70	$BrCH_2CH_2Br$	3	12	60
4	$MgBr_2\,Et_2O$	70	$BrCH_2CH_2Br$	3	12	32
5	$MgBr_2$	70	$ClCH_2CH_2Cl$	3	12	55
6	$MgBr_2$	70	none	3	12	5
7	$MgBr_2$	25	$BrCH_2CH_2Br$	3	12	48
8	$MgBr_2$	70	$BrCH_2CH_2Br$	3	6	55
9	$MgBr_2$	70	$BrCH_2CH_2Br$	3	24	61

After treated the starting material (3-alkoxythiophene) with nBuLi at -20^{O}C, the solution was added to $MgBr_2$ at room temperature, then raised the temperature during coupling step increased the yield (entry 3 vs entry7). Compared to commercially available anhydrous $MgBr_2\,Et_2O$, the yield is greatly improved with freshly prepared $MgBr_2$. As we can see from the table, the catalyst loading could be decreased from 10 mol% to 3 mol% with little penalty (Table 2, entry 3). Inexpensive 1,2-dibromoethane or the chloro derivative seem to function equally well as stoichiometric oxidant. A reaction time of 12 hours is sufficient, and not significantly improved upon longer reaction time (entry 3, 8,9). Thus, in the presence of 3 mol% $Ni(dppp)Cl_2$ and 2.5 equiv. of $MgBr_2$, the homo-coupling of the Grignard reagent was completed in 12 h (entry 3), to afford the target RO2T2 in about 60% yield (also about 20% of starting materials was recovered). The oxidative Grignard reagent

homo-coupling reaction is quite useful considering the one-pot synthesis which avoids unstable intermediates and additional purification, also with fair yield under only 3% of catalysts.

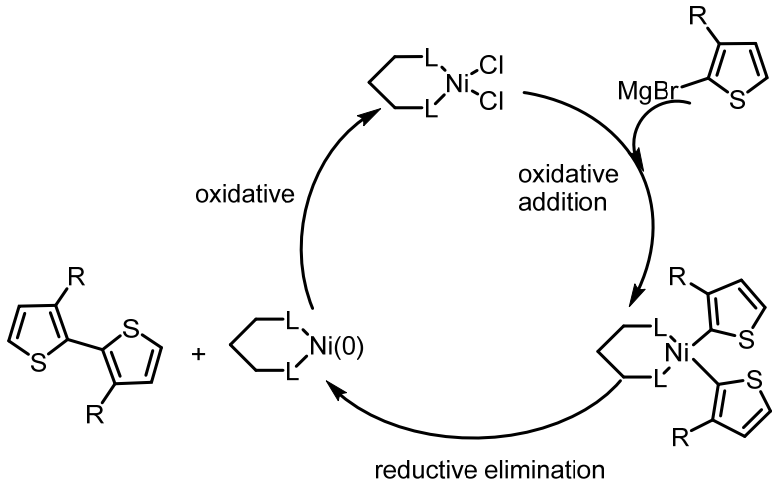

Figure 3.7: The proposed mechanism for oxidative coupling in RO2T2 synthesis.

For this reaction, it was found that the target RO2T2 was formed even without oxidant (entry 6) to regenerate the catalytic species, although in a yield similar to the initial catalyst loading. According to this result, the possible mechanism for the Ni-catalyzed cross-coupling is the same as the McCullough Cross-Coupling method, but no polymer was formed as there is only one functional group on the Grignard intermediate.

Properties of BDT and RO2T2 Copolymers with TPD

The summary of TPD polymers is in table 3.2 (data is for the highest molecular weight fraction for each polymer). The PBDTTPD polymers exhibited relatively very high solubility (more than 10 mg/ml in hexane). This rendered the typical Soxhlet fractionation procedures ineffective, as the whole distribution of polymer sizes were extracted with the

initial one or two solvents. Instead of just proceeding from acetone to hexane, we used the sequence acetone (dimethyl ketone), MEK (methyl ethyl ketone) and DEK (diethyl ketone, or 3-pentanone), before proceeding to hydrocarbons. To further tune extraction selectivity, a Soxhlet extractor was designed to allow each solvent to be employed for extraction at different temperatures. The extraction chamber was jacketed (external heat exchanger, Figure 3.8) and a modified condenser with "cold-finger" (internal heat exchanger) was employed. The temperature of water circulating through both of these was controlled to dictate the temperature in the extraction chamber, rather than just allowing the temperature to be determined by typical recycling distillation into the extraction chamber. For PBDTTPD-βC1 polymer (expected to be least soluble), the highest molecular weight fraction was extracted with hexane. The highest molecular weight fractions for the other 3, more soluble polymers were extracted with high temperature 3-pentanone, which is a poorer solvent, so these polymers have higher solubility.

Figure 3.8: The specially-design Soxhlet extractor with water-jacket (left) and traditional Soxhlet extractor (right).

Attempted analysis of these polymers by GPC revealed an unusual phenomenon that precluded estimation of relative molecular weights, despite their high solubility. Separation in a GPC column occurs primarily due to size, thus another common name is size exclusion chromatography. The stationary phase is composed of solvent-swollen particles with pores of varying dimensions. Smaller analytes will have longer retention times, while larger ones will have shorter retention times as they are excluded from any smaller pores. For example, the retention time in our GPC system is about 12.6 minutes for a polystyrene standard with M_n= 200 kD, but the retention time is about 19.7 minutes for the polystyrene standard with M_n 1.7 kD. The expected minimum retention time for our GPC system (based on standard column parameters provided by manufacturers) is estimated to be 11 – 12 minutes. This should correspond to total exclusion from pores in the packing material. Surprisingly, all the polymers reported here elute with retention time less than 12 minutes (some even about 8 to 9 minutes)! This phenomenon has been reported elsewhere and has been referred to as "super elution" in a couple of publications from one research group.[170,171] We have yet to find other published reports of this phenomenon. According to those authors, super elution could occur when species are so large that not only are they excluded from the pores in the gel, but they are also excluded from the somewhat confined paths near interfaces between adjacent stationary phase particles and cannot follow along irregular particle surfaces, instead following the actual most direct path through the column. This is not commonly observed as species this large are not typically injected. A cocktail was prepared containing polystyrene standards and a PDBTTPD polymer to confirm that

the standards eluted at the expected times during the same injection that this "super elution" occurred.

Table 3.2: Properties of BDT vs 3,3'-RO2T2 TPD Polymers

Polymer	λ_{max}(abs) (nm) [a]	λ_{max}(film) (nm) [b]	λ_{onset} (film) (nm) [b]
PBDTTPD-αC1	604	606	675
PBDTTPD-αC8	605	611	675
PBDTTPD-βC1	599	607	685
PBDTTPD-βC8	598	610	675
PRO2T2TPD-αC1	699	724	784
PRO2T2TPD-αC8	697	728	780
PRO2T2TPD-βC1	733	741	802
PRO2T2TPD-βC8	694	737	798

a: $1x10^{-5}$ M in $CHCl_3$.

b: Pristine film spun-cast from 1 mg/ml $CHCl_3$ solution.

How could we have species so large? Stille polymerization is a type of step-growth polymerization, so it follows Carothers equation:

$$\overline{Xn} = 1/(1-\rho)$$

where $\overline{Xn}$ = number-average degree of polymerization and ρ = conversion of the bond-forming reaction. Even if it was possible to obtain the unrealistically high 99% conversion (unreachable partly due to increasingly slow polymerization kinetics with increasing molecular weight and competing destannylation/debromination), this still gives a degree of polymerization far too small to correspond to the GPC elution times (several million g/mol). At the unreachable ρ = 0.99, then $\overline{Xn}$ = 100. Taking the highest molecular weight repeat unit here to be approximately 0.9 kDa, $\overline{Xn}$ = 100 would correspond to M_n of only 90 kDa. It is fairly common for GPC to overestimate the M_n of conjugated polymers by a factor in the range of 2, since the conjugated polymers are less flexible than the polystyrene standards used for calibration, but what we observe here

reflects an overestimation of orders of magnitude relative to what is achievable. We would certainly not expect any polymer with M_n of several million D to easily dissolve, we can propose that the polymers should have M_n in the range typically obtainable by Stille polymerization (5-40 kDa) but aggregate extensively in "solution". If the polymers aggregate in the manner that can be reasonable expected based on their structures, with face to face π-stacking of the polymer backbones, then board-shaped ensembles are formed and their surfaces are completely coated with solubilizing side chains.

3.3 Effect of BDT vs 3,3'-RO2T2 Donor on Polymer Optical, Electronic Properties and Self Assembly

3.3.1 Optical Properties of Polymers

Four PBDTTPD polymers with an identical polymer backbone repeating unit but different side chains were synthesized and investigated. UV-Vis absorption spectra of the PBDTTPD polymers (1.0×10^{-5} M) in chloroform could be seen from figure 3.7. The absorption of film was also tested; the film was spun-cast from 1 mg/ml chloroform solution.

All PBDTTPD polymers show typically dual band absorption. Interestingly, the UV-vis absorption of PBDTTPD in solution is very similar to that obtained in the film state, possibly indicating similar states. The fine structure of UV-vis absorption clearly indicates the rigidness backbone of the resulted PBDTTPD polymers. This is due to the narrowing of the assessable population of states (vibrational and rotational energy levels). The λmax is about 600 nm for PBDTTPD polymers, which is about 90 nm red-shifted compare to PBDTFB polymers relative to the TFB analogues reported in chapter 2. The structural

variables differentiating the TFB and TPD analogues should severely limit any direct comparison.

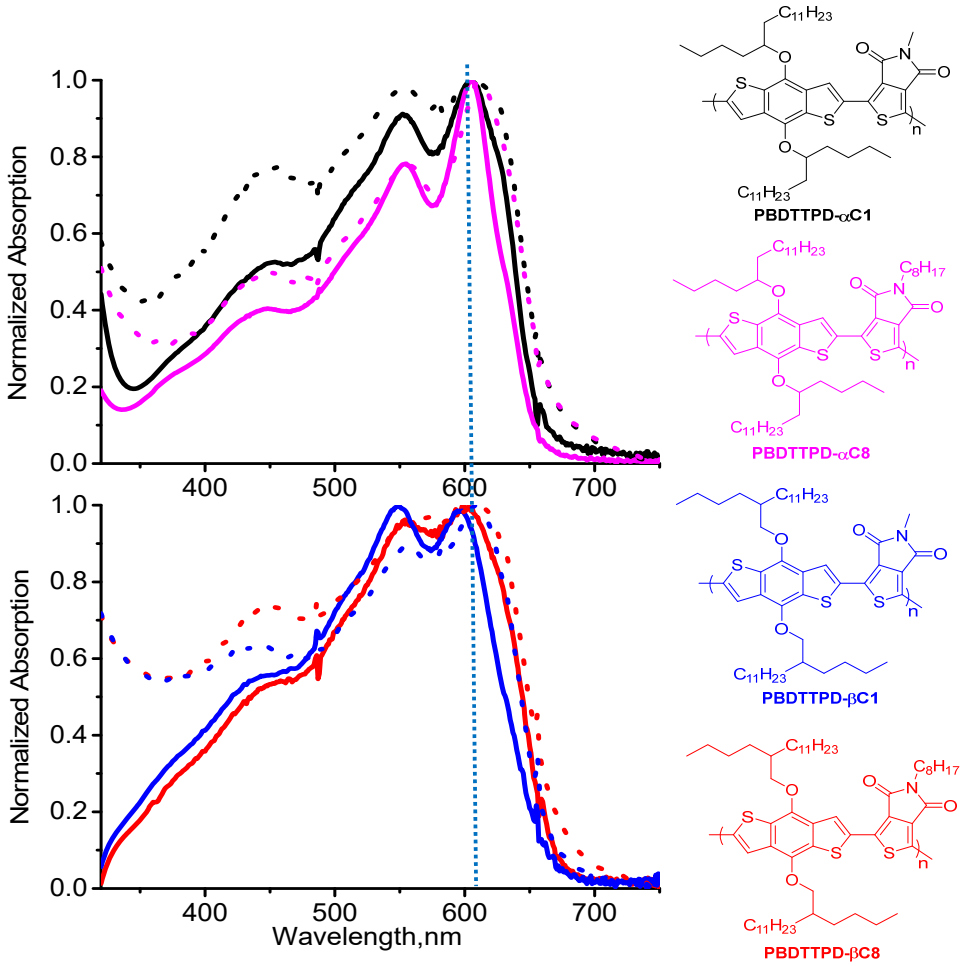

Figure 3.9: Normalized absorption spectra of PBDTTPD polymers at RT in solution (1.0 x 10^{-5} M, $CHCl_3$) (solid line), and film (spun-cast from 1 mg/ml $CHCl_3$) (dash line).

UV-Vis absorption spectra of the different Mw (molecular weight) Soxhlet fractions of PBDTTPD polymers (1.0 x 10^{-5} M) in chloroform were also tested. Although we were unable to estimate M_n from GPC, it is quite clear that the absorption spectra red-shifted and

the contribution of the longer wavelength absorption feature increased with successive Soxhlet fractions, indicating progressively higher M_n.

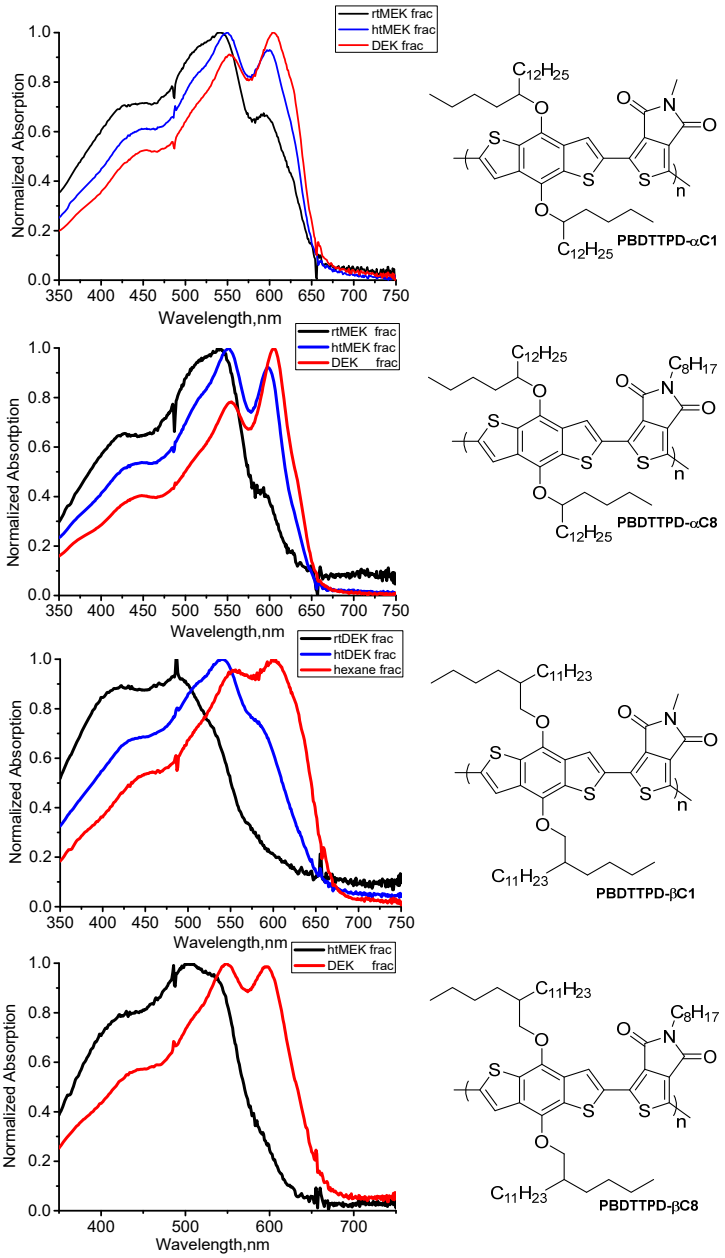

Figure 3.10: Normalized absorption spectra of PBDTTPD polymers fraction at RT in solution (1.0 x 10^{-5} M, $CHCl_3$). MEK = methyl ethyl ketone, DEK= 3-pentanone, rt and ht indicate whether the extraction was conducted at controlled room temperature or the higher "natural" temperature of Soxhlet extraction.

UV-Vis absorption spectra of the PRO2T2TPD polymers (1.0 x 10^{-5} M) in chloroform could be seen from figure 3.11. The absorption of film was also tested; the film was spun-cast from 1 mg/ml chloroform solution.

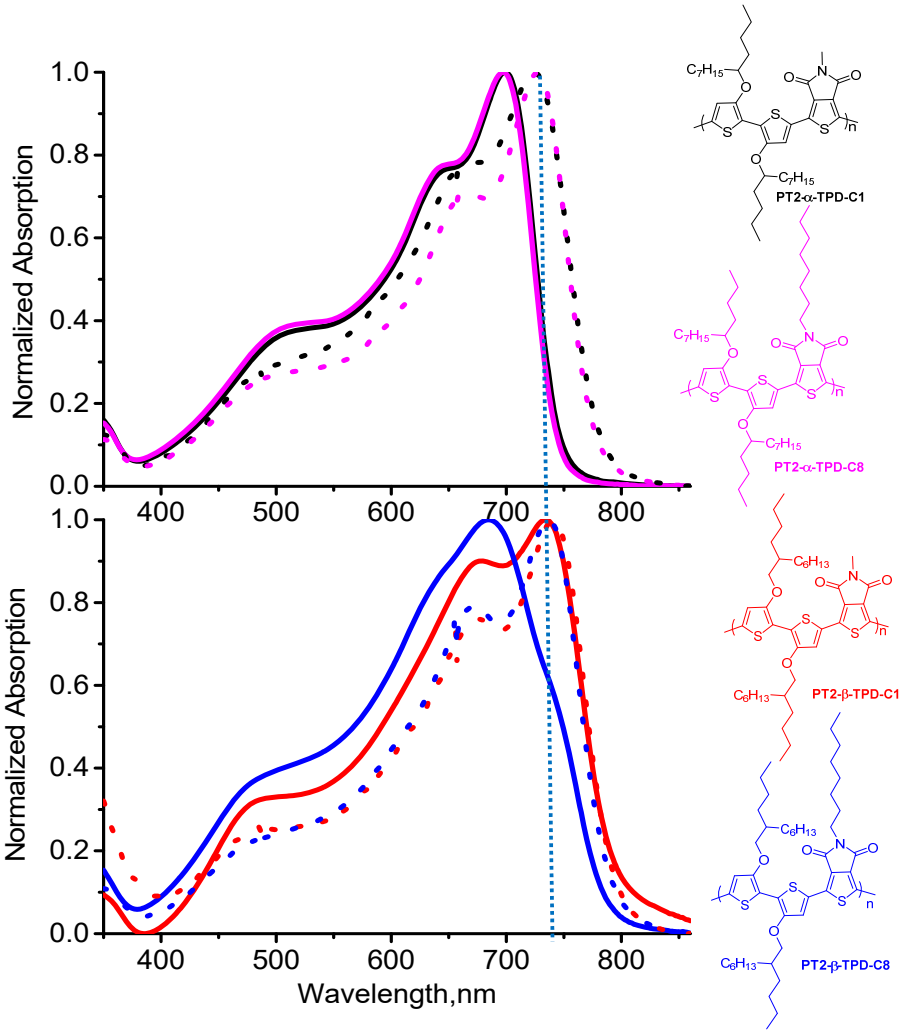

Figure 3.11: Normalized absorption spectra of RO2T2TPD polymers at RT in solution (1.0 x 10^{-5} M, $CHCl_3$) (solid line), and film (spun-cast from 1 mg/ml $CHCl_3$) (dash line).

The absorption maxima of PRO2T2TPD-βC1 polymers is red-shifted and more fine structured absorption in solution relative to other PRO2T2TPD polymers, indicating enhanced intermolecular interactions and a higher degree of ordering. In the case of PRO2T2TPD-βC1polymers, the alkyl-chain branching point is further away from the

RO2T2 core, together with the small methyl substitution in TPD give the least space-filling competition (and likely least solubilizing power), which allows stronger intermolecular interaction of the backbone, leading to enhanced molecular aggregation in solution. Therefore, aggregation could form in solution for PRO2T2TPD-βC1 as the stronger intermolecular interactions, the solid-state absorption of PRO2T2TPD-βC1 is pretty similar compare with its solution absorption. The much ordered structure of PRO2T2TPD-βC1 was also proved by XRD result, show clear π-π stacking. For polymers with α-branch side chains, the proximity of the alkyl-chain branching position to the T2 core possibly hinders the π-π stacking and aggregation in solution; this is overcome by intermolecular forces in the solid state, thus causing a significant red shift in film UV-Vis absorption relative to the solution absorption. For PRO2T2TPD-βC8, larger octyl substitution in TPD hinders side-chain interdigitation and intermolecular interaction, so the UV-Vis absorption behavior was similar to α-branch polymers.

The change of donor RO2T2 leads to about 100 nm and 120 nm red-shifts in the PRO2T2TPD λ_{max} in comparison to those of PBDTTPD solutions and thin films, respectively. Furthermore, the Eg^{opt} of PRO2T2TPD were 0.2 eV smaller than that of PBDTTPD, reflecting the much stronger electron-donating ability of the RO2T2 unit (more shallow E_{HOMO}). The electron-rich character of the dialkoxybithiophene decreases the energy gap of PRO2T2TPD polymers.

As for the PBDTTPD polymers the absorption profiles for successive Soxhlet fractions of PRO2T2TPD-α-C8 polymer red-shift supporting that these fractions are progressively

higher molecular weight. No such trend was seen in the only two fractions retained for PRO2T2TPD-α-C1.

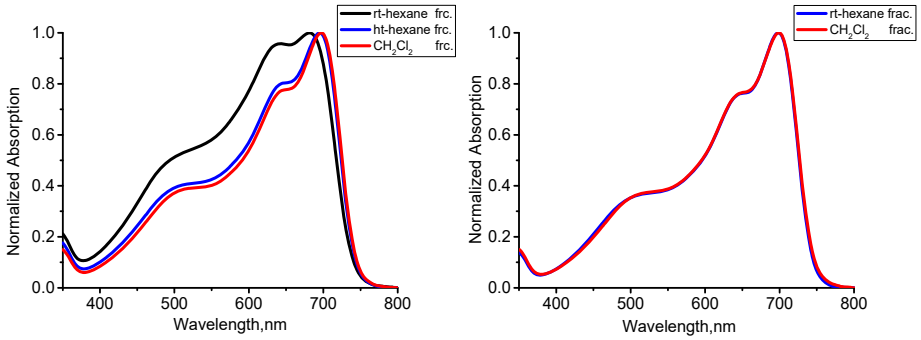

Figure 3.12: Normalized absorption spectra of PRO2T2TPD-α-C8 (left) and PRO2T2TPD-α-C1(right) polymers fraction at RT in solution (1.0 x 10^{-5} M, $CHCl_3$).

3.3.2 Self Assembly (Wide Angle X-ray Diffraction Patterns) of Polymers

The 1st, 2nd order reflections on the equator could be seen from the WAXD pictures, suggesting lamellar order, although not long range. The π-stacking distance is about 3.75Å (after calibration with AgBeh, the detail can be found from chapter 2) for PBDTTPD polymers with α branch, about 3.70 Å for PBDTTPD polymers with β branch, which is larger than published PBDTTPD polymers (3.6 Å) [119] owing likely to the bulk of the side chain. The π-stacking distance are smaller for β branch polymers compared to α branch, but the difference is rather small. However, the size of substituent on the acceptor seems to have even smaller effect on the π-stacking.

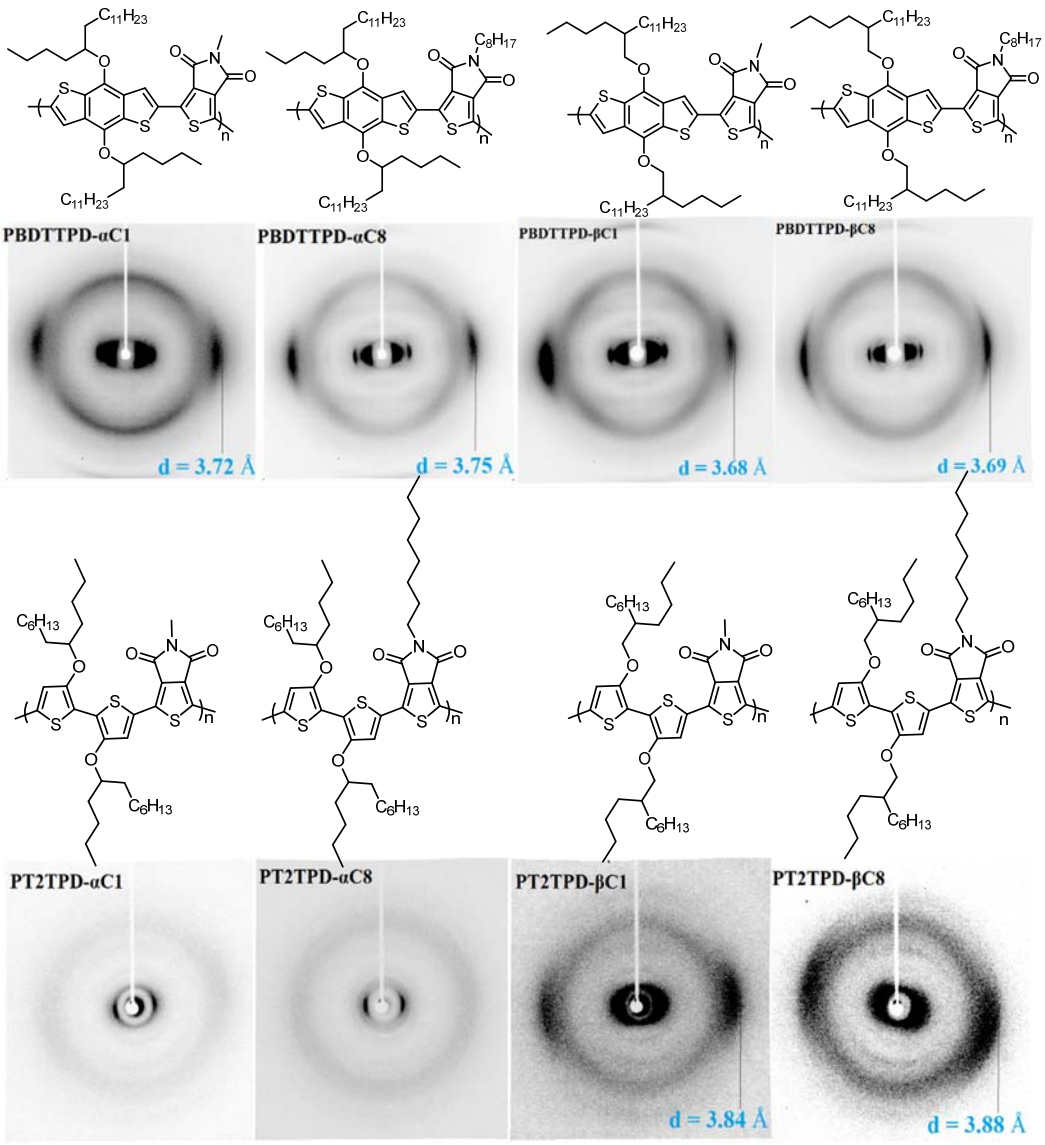

Figure 3.13: Fiber WAXD diffractograms of polymers.

The WAXD results for the PRO2T2TPD polymers are quite different from PBDTTPD polymers. The PRO2T2TPD polymers with α-branched sides chains on RO2T2 unit show no π-π stacking no matter the size of substituent on the TPD part, which is similar to the analog polymer with linear side chains reported by our group before.[162] However, The PRO2T2TPD polymers with β-branched sides chains on T2 unit show some kind of π-π stacking even considering the bulk of the sides chains. Compared to π-π stacking about 3.88

Å for PRO2T2TPD-βC8, the stronger π-π stacking about 3.84 Å was found for PRO2T2TPD-βC1 polymers, likely due to a higher degree of side-chain interdigitation, enabled by the large local free volume as the small methyl substitution in TPD. The π-π stacking lead to aggregation in solution, which was proved by the obvious red-shifted absorption of PRO2T2TPD-βC1.

3.3.3 Electrochemistry of Polymers

Table 3.3: Electrochemical and optical data for polymers

Polymer	E_{ox} (V) [a]	E_{HOMO} (eV) [b]	E_{LUMO} (eV) [c]	E_g^{opt} (eV) [d]
PBDTTPD-αC1	0.74∓0.03	-5.54∓0.03	-3.71∓0.03	1.83
PBDTTPD-αC8	0.78∓0.02	-5.58∓0.02	-3.75∓0.02	1.83
PBDTTPD-βC1	0.78∓0.01	-5.58∓0.01	-3.77∓0.01	1.81
PBDTTPD-βC8	0.79∓0.02	-5.59∓0.02	-3.76∓0.05	1.83
PRO2T2TPD-αC1	0.39∓0.01	-5.19∓0.01	-3.61∓0.01	1.58
PRO2T2TPD-αC8	0.47∓0.02	-5.27∓0.02	-3.68∓0.02	1.59
PRO2T2TPD-βC1	0.38∓0.01	-5.18∓0.01	-3.63∓0.01	1.55
PRO2T2TPD-βC8	0.40∓0.02	-5.20∓0.02	-3.65∓0.02	1.55

Experimental conditions: 0.1 M $(n\text{-}Bu)_4N.PF_6$ in anhydrous acetonitrile as supporting electrolyte, platinum disc as working electrode, platinum wire as counter electrode, silver wire as reference electrode and Fe/Fe+ (-4.8 eV vs vacuum) as reference, scanning rate: 50 mV/s; All measurements conducted on solution-cast thin films under nitrogen. [a]Corrected E_{ox} value respect to Fc/Fc+. [b]E_{HOMO} = -[4.8+(E_{ox}-Fc/Fc+)], E_{ox} calculated using onset of DPV measurements (Oxidation peak). [c]E_{LUMO} = E_g^{opt} + E_{HOMO}. [d] E_g^{opt} Optical band gap estimated from the absorption edge of the film. Each of the sample run 3 times. We test Fc before each polymer test and polish the electrode then test Fc again, each time the difference is less than 20 mV.

As we can see from table 3.3, moving the branching position away (β-branch) from the polymer backbones seems to not affect the HOMO energy level either in PBDTTPD polymers or PRO2T2TPD polymers. The result is different from reported reference where the branching point was related to HOMO level.[172] For our polymers, the HOMO energy level is insensitive to branch point of the side-chain. Compare with PRO2T2TPD polymers with much shallower HOMO level (about

0.55 eV) as the strong electron-donating alkoxy group from RO2T2, the alkoxy groups on BDT have lower electron-donating ability.

3.4 Thermal Analysis of Polymers

Thermogravimetric analyses (TGA) shows that PBDTTPD polymers with α branch side chain began to decompose at about 130 ºC. However, PBDTTPD polymers with β branch side chain are stable up to about ~330 ºC. This huge difference of thermal stability might come from the branch position of these polymers, the α branch side chain have lower thermal stability in these polymers. But it should be point out that the thermal stability of α branch side chain polymers were fair enough considering the operating temperature of plastic electronic devices.

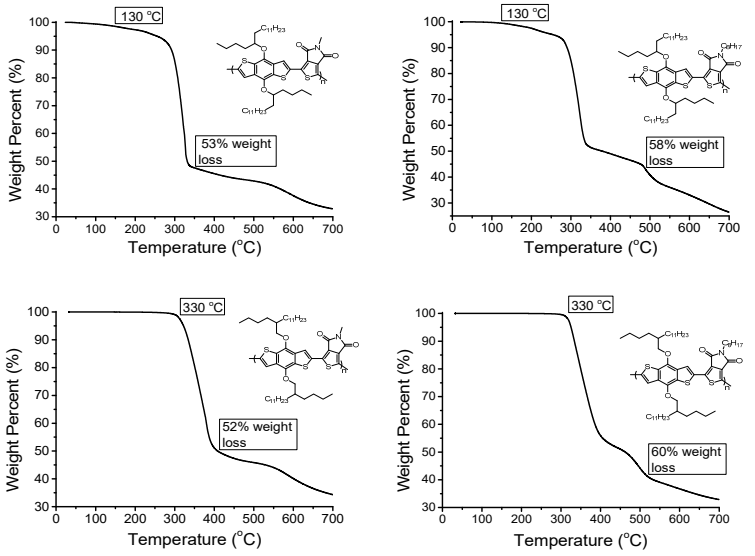

Figure 3.14: Thermogravimetic analyses of PBDTTPD polymers.

When compare with the percent of weight loss, it is very similar to the weight ratio of side chains. It clearly indicates the elimination of alkoxy side chains grafted on BDT unit and N-substituents on TPD unit happened first during heating process.

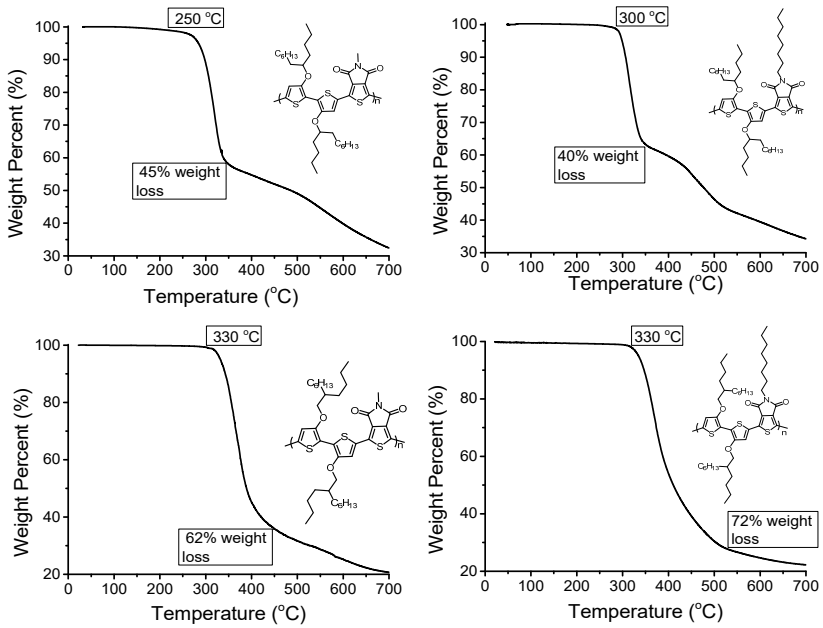

Figure 3.15: Thermogravimetic analyses of PRO2T2TPD polymers.

Thermogravimetric analyses (TGA) shows that PRO2T2TPD polymers with α branch side chain are stable up to about ~250 °C and ~300 °C. PBDTTPD polymers with β branch side chain are even stable, up to about ~330 °C. The percent of weight loss might as the result of loss side chains, which happen first during heating process.

None the polymers showed any melting transition up to 180 °C or any transitions in the cooling scans during differential scanning calorimetry study (DSC).

3.5 Conclusions

A more expeditious synthesis of 3,3'-dialkoxy-2,2'-bithiophene (RO2T2) through oxidative Grignard reagent homo-coupling reaction was investigated. This reaction eliminates the necessity for relatively unstable 2-bromo-3-alkoxy thiophene intermediates. Within detection limits, the critical thiophene coupling reaction appears regiospecific (not suffering

from regioisomers that complicate other coupling methods) and gives fair yield (about 60%) using only 3 mol % of catalytic Ni species.

Given that TFB units (chapter 2) tend to impart low solubility to D-A copolymers, it not surprising that we see increased solubility in this chapter when the TFB unit is replaced with TPD units. However, perhaps the most interesting observation in this chapter is that more soluble TPD-based polymers seem to aggregate much more extensively in solution as indicated by their "super elution" in the GPC. The reasons for this can perhaps be determined with future computational studies of intermolecular interactions. Without those calculations, one can speculate about the cause, but it is just speculation.

Based on the RO2T2 monomers and BDT monomers, PRO2T2TPD and PBDTTPD polymers were synthesized with branch side chains on donor unit and varying space-filling demands on TPD acceptor. Compare PRO2T2TPD polymers with PBDTTPD polymers, the UV-Vis absorption spectra were red-shifted (more than 120 nm) as the smaller Eg (energy gap). The reason is that stronger electron-donating ability of the RO2T2 unit from alkoxy side chains, destabilize the EHOMO values of the resulted polymers. The optical properties of PBDTTPD polymers were not sensitive to size and position of bulky alkoxy side chains on the rigid BDT units. However, the optical properties of PRO2T2TPD polymers were sensitive to size and position of bulky alkoyl side chains on the "swivel" (bithiophene, RO2T2) donor units. The absorption maxima of PRO2T2TPD polymer with β-branch side chains on RO2T2 and small methyl-substituted on TPD unit is red-shifted about 35 nm in solution relative to other PRO2T2TPD polymers, indicating enhanced intermolecular

interactions and a higher degree of ordering. The WAXD result shows that all the PBDTTPD polymers show π-π stacking regardless of branch position and the size of substituent on the acceptor. For PRO2T2TPD polymers, higher degree of order and better π-π stacking could formed only if proper local free spacing exists for side-chain interdigitation.

Chapter 4: 3,3'-dialkoxy-Bithiophene Based Homo-polymers and Donor-Donor Co-polymers

4.1 Introduction

Continuing with the theme of this dissertation, which is to evaluate the effect of bulky branched alkoxy side chains on the optoelectronic properties and self-assembly of conjugated polymers, a further logical step is to consider what happens when "strong" acceptors are not included to drive self-assembly (nor modify FMO energies). The studies here include simple homopolymers of the RO2T2 units employed in previous chapters, as well as their copolymers with unsubstituted thiophene derivatives as "spacers" between the bulky substituents along the backbone. These unsubstituted thiophene derivatives are typically considered to be donor units in typical D-A polymers containing "strong" acceptor units, but relative to the "very shallow" EHOMO of RO2T2 units, the unsubstituted thiophene units may as well be considered acceptors here.

With the exception of poly(3,4-alkylenedioxythiophene)s, e.g. PEDOT Figure 4.1, there is a surprising dearth of published conjugated polymers based on alkoxythiophenes. Poly(3,4-ethylenedioxythiophene), abbreviated as PEDOT, was developed by scientists at the Bayer AG research laboratories in 1980s.[173] PEDOT shows high conductivity, lower oxidation potential and better stability in the oxidized state, compared to alkyl substituted polythiophenes.[174] Together with good film-forming properties and high visible light transmissivity, PEDOT successfully used as hole injection layers in OLEDs and as anode to replace standard ITO anode.[175]

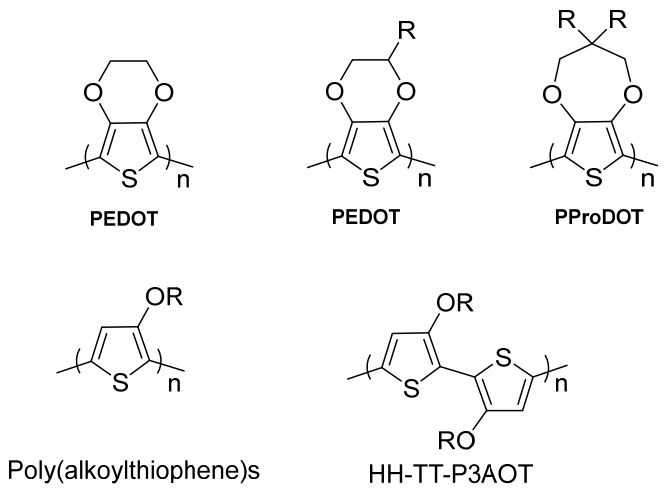

Figure 4.1: The structure of poly(alkoylthiophene)s.

By appending side chains to the alkylenedioxy bridge of PEDOT to improve solubility, solution-processable PEDOT derivatives have been synthesized and applied as electrochromic materials by Havinga[176] and Reynolds.[177] PProDOTs, with the longer 3-carbon bridge, has been the subject of systematic study of the structure-property relationships by Reynolds and coworkers.[16] The electron-donating ability changed as the insertion of an extra methylene, which lowers the polymer HOMO level (~0.1-0.3 eV), so the stability of the subsequent polymers was enhanced under atmospheric conditions.[16]

For mono-alkoxy substituted polythiophenes, Leclerc synthesized these polymers through chemical oxidation of monomers with anhydrous $FeCl_3$ in 1991.[178] Iraqi synthesized head-to-tail poly(alkoylthiophene)s with McCullough cross-coupling methods.[179] These polymers have low molecular weight and poor solubility, possibly as a result of the short side chains. Verbiest and coworkers synthesized poly(alkoxythiophene)s through three different methods and compared their properties.[180] The result shows us that chemical oxidized poly(alkoxythiophene)s significantly blue-shifted (about 50 nm) compare to

poly(alkoxythiophene)s synthesized from McCullough cross-coupling or GRIM (Grignard Metathesis method). The blue-shifted is attribute to the differences in the regioregularity, which was also supported by the NMR spectroscopy result.[180] By introducing branched side chains, Fujiki also got poly(alkoxythiophene)s and successfully Soxhlet different molecular weight fraction. The test shows that UV-vis absorption and photoluminescence depends on the molecular weight, and the spectrum red-shifted with the increase of molecular weight.[181] Through introducing butyl side chain, Leclerc synthesized 3,3'-dibutoxy-2,2'-bithiophene monomer first and then chemical oxidation of the monomer to get HH-TT-P3AOTs.[182] Koeckelberghs prepared HH-TT P3AOT through introducing longer side chain, the maximum absorption (583 nm) is significantly higher than the oxidatively prepared HH-TT P3AOT (545 nm) by Leclerc. The polymer backbone is planar according to the paper, which was attributed by the authors to intermolecular S-O interactions, described in chapter 3.[183] Kunugi also synthesized HH-TT-P3AOTs through chemical oxidation and applied as hole-injection layers of OLED.[184] Guo prepared the HH-TT-P3AOTs through Stille coupling and the DFT calculation result show that the 3,3′-dimethoxy-2,2′-bithiophene leads to coplanar geometries as the S-O interaction. These result show that HH-TT-P3AOTs with linear side chains could keep the planar structure as the S-O interaction.

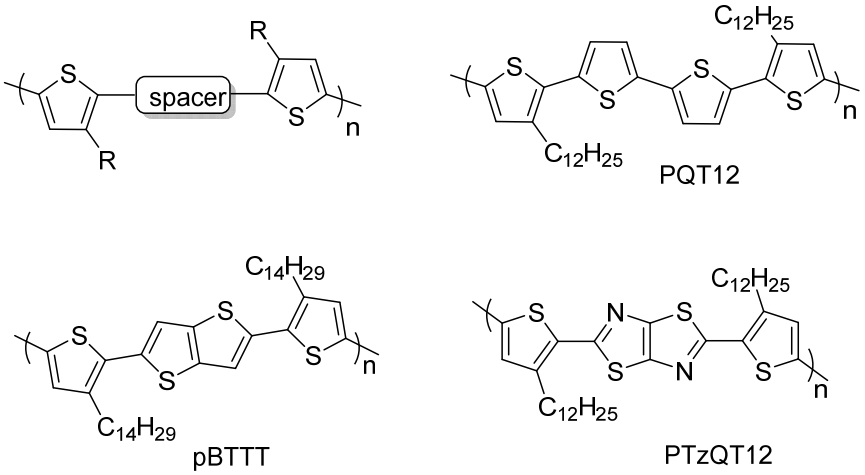

Figure 4.2: Design strategies for conjugated polymer using unsubstituted "spacers".

This design strategy of introducing spacers has been widely used during materials design as which could enhance planarity and self-assembly, therefore higher charge-carrier mobility.[185] Ong reported regioregular polythiophenes PQT12, which has long alkyl side-chains on thiophene for solution processability and bithiophene as spacer. The result shows that sufficiently long side chains has enabled PQT12 to undergo self-assembly under annealing to achieve long-range intermolecular side-chain interdigitations, leading to 3-D lamellar structures and good mobility (0.14 cm^2 $V^{-}1$ $s^{-}1$).[186] The lowing LUMO level from rotational freedom backbone improved the stability (only slight decrease in device performance after being stored under ambient conditions for one month) compare with regioregular P3HT devices in the same condition. McCulloch introduced thieno[3,2-b]thiophene as spacer and synthesized pBTTT polymers, liquid-crystalline phase could form as larger local free-volume between adjacent alkyl chains. The mobility of these materials is about 0.6 cm^2 $V^{-}1$ $s^{-}1$ under nitrogen, equivalent to that of a-Si TFTs used in commercial display.[187] Some other rigid fused-ring spacers such as dithienothiophene

(DTT),[188] thiazolothiazole (TzTz)[189] and naphthodithiophene (NDT)[190] were also used and formed polymer with substantial hole mobility.

There are several examples showing that the D-A copolymer based on dialkoxybithiophene did not preclude backbone planarization and π-stacking. Using RO2T2 units described in previous chapters, here we want to investigate homo-polymer of RO2T2 with bulky branch side chains to see if they can still keep the planar structure without D-A interactions. Based the research on chapter 3, D-A kind of RO2T2 polymers with bulk branch side chains could form π-π stacking if proper local free spacing exists for side-chain interdigitation. Here we also want to introduce spacers between the RO2T2 units to form PRO2T2-Ar copolymers. Different size of spacer, such as thiophene, thieno[3,2-b]thiophene and bithiophene were introduced to see the effect of spacer size to (opto)-electronic properties and self-assembly of PRO2T2-Ar copolymers.

So the project reported in this chapter focused on 3,3'-dialkoxy-2,2'-bithiophene (RO2T2) homo-polymers and their copolymers with unsubstituted thiophene derivatives as spacers. The hypotheses to be tested include:

1. How the bulky side-chains and branching position effect the optical and electronic properties, solubility, and self-assembly of RO2T2 homo-polymers.
2. How different spacer size modify the results observed from the above.

4.2 Synthesis of Monomers and RO2T2 Homo-polymers and Their Properties

4.2.1 Synthesis of Monomers and RO2T2 Homo-polymers

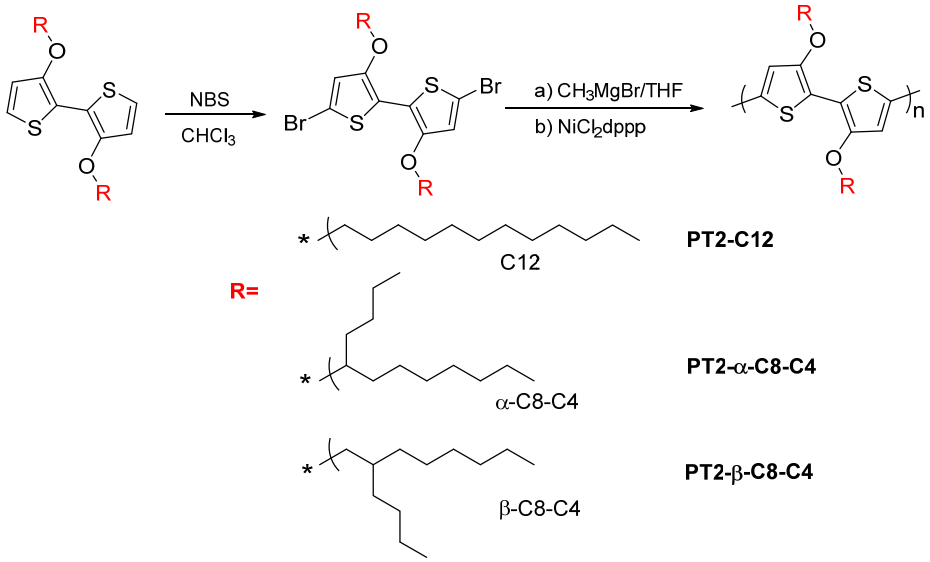

Scheme 4.1: Synthesis scheme of RO2T2 homopolymers.

Synthesis of RO2T2 units was described in chapter 3. Because of the electron-donating alkoxy substituents, electrophilic bromination reaction is very fast (about 20 mins) under -30 ^{O}C with NBS. The product can be easily purified using column chromatography to give a yellow oil with 90% yield. The dibrominated monomers were easily converted to the homopolymers using the Grignard metathesis method. The polymers were fractionated by Soxhlet extraction using acetone, methyl ethyl ketone, hexane and DCM (depends on the solubility). The properties can be found from table 4.1. We were surprised by our first observation of the phenomenon known as "super elution" during GPC characterization of the polymers in chapters 3. Given that the polymers reported in chapter 4 are not composed of alternating D-A units with "strong" acceptors that can enhance intermolecular interaction and therefore extensive aggregation in solution, it is much more surprising to observe "super elution" for all the polymers reported here. Therefore, we cannot report M_n values, and the extensive aggregation in solution prevented characterization by solution NMR.

Table 4.1: Properties of RO2T2 homo-polymers

Polymer	λ_{max}(abs) (nm)[a]	λ_{max}(film) (nm) [b]	λ_{onset} (film) (nm) [b]
PRO2T2-α-C8-C4	583	592	685
PRO2T2-β-C8-C4	580	599	702
PRO2T2-C12	560	581	720

a: $1x10^{-5}$ M in $CHCl_3$.

b: Pristine film spun-cast from 1 mg/ml $CHCl_3$ solution.

Synthesis of RO2T2 Homo-polymers with DHAP Method

Other than the Grignard metathesis method, the DHAP method was also tried to synthesis RO2T2 homo-polymers. DHAP method combines the C-H activation and oxidative coupling process together, so it is quite useful considering reduce the synthesis steps (scheme 4.2). Through control of the stoichiometry, it is relatively simple to monobrominate RO2T2 units.

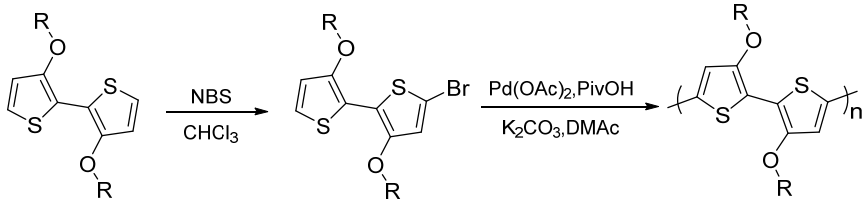

Scheme 4.2: Synthesis scheme of RO2T2 homo-polymers with DHAP methods.

Using 2-bromo- 3-hexylthiophene as starting material, Ozawa and coworkers prepared head-to-tail regioregular poly(3-hexylthio-phene) (HT-P3HT) with high molecular weight (M_n up to 30 600) and high regioregularity (up to 98%) through DHAP methods.[191] Here, monobrominated 3,3'-dialkoxy-2,2'-bithiophene (RO2T2) was synthesized and used for polymerization with DHAP methods. The condition for this reaction can be seen from scheme 4.2, using $Pd(OAc)_2$ as catalysts and a bulky proton source and K_2CO_3 as base, following the reported reference.[192,193,194] The polymerization works but the Mw is not as

high as the Grignard metathesis method probably because the decomposition of catalysts during reaction. It is possible to give higher Mw by DHAP methods with other condition, such as using Herrmann's catalyst[191] which was stable at high temperature and different ligand.

4.2.2 Optical Properties of PRO2T2 Homo-polymers

UV-Vis absorption spectra of the PRO2T2 polymers (1.0 x 10^{-5} M) in chloroform are shown in figure 4.3. The absorption of film was also tested; the film was spun-cast from 1 mg/ml chloroform solution.

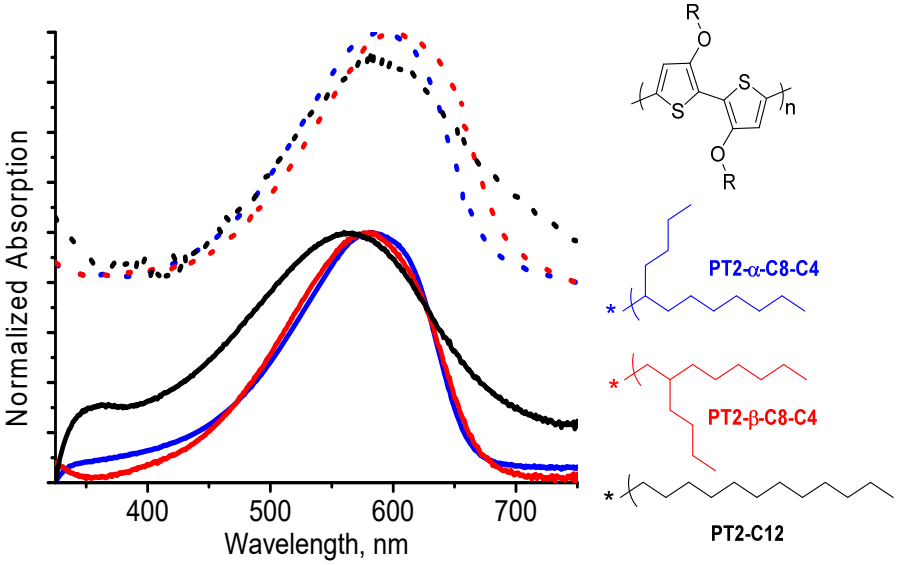

Figure 4.3: Normalized absorption spectra of PRO2T2 homo-polymers at RT in solution (1.0 x 10^{-5} M, $CHCl_3$) (solid line), and film (spun-cast from 1 mg/ml $CHCl_3$) (dash line).

The maximum absorption (about 580 nm) is comparable to the reported reference, possibly implies the planar polymer backbone even with bulk branch side chains. The film absorption of PRO2T2 polymers with α-branch side chain has very small red-shifted

compare with solution absorption, the β-branch side chain polymers red-shifted is obvious from solution to film absorption. However, none of these polymers has the fine structure, possibly because the quite weak pi-pi stacking for these polymers.

Different molecular weight fraction of PRO2T2 homo-polymers with α-branch side chain was separated through careful Soxhlet with different solvent. UV-Vis absorption spectra of the different Mw (molecular weight) fraction of PRO2T2 polymers (1.0×10^{-5} M) in chloroform could be seen from figure 4.4. It is quite clear that the absorption spectra red-shifted from the MEK to hexane fraction. No further shift is seen on going from hexane to $CHCl_3$ fraction. Though not conclusive, this suggests the effective conjugation length (ECL) was reached. Perhaps if more careful Soxhlet extraction using the Soxhlet extraction device specially designed in our lab for this purpose had been used, more intermediate fractions would have been collected and could better support the conclusion that the ECL was reached.

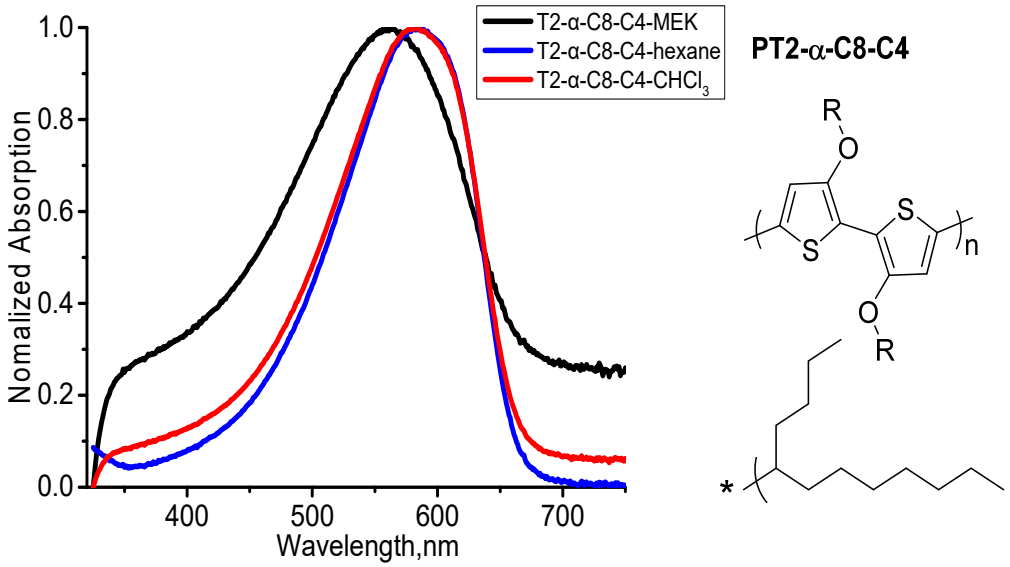

Figure 4.4: Normalized absorption of RO2T2 polymers at RT in solution (different Soxhlet fraction,1.0 x 10^{-5} M, $CHCl_3$)

4.2.3 Self Assembly of PRO2T2 Homo-polymers

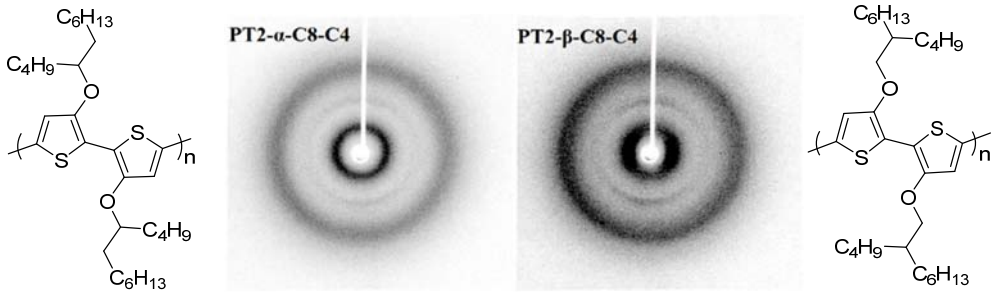

Figure 4.5: Fiber WAXD diffractograms for RO2T2 homopolymers.

According to the WAXD images depicted in figure 4.5, for homopolymers, there are just two radially symmetric reflections corresponding to the average distances separating disordered main and side chains. Therefore, the homopolymers were completely amorphous, at least with the thermal history of these samples. This is in agreement with the structureless UV-Vis absorption spectra.

4.3 Effect of Spacer on Polymer Optical, Electronic Properties and Self Assembly

4.3.1 Synthesis of PRO2T2-Ar Copolymers with Different Spacer and Their Properties

The dibrominated RO2T2 (3,3'-dialkoxy-2,2'-bithiophene) monomers were used directly from above section. All other monomers, such as 2,5-bis(trimethylstannyl)thieno[3,2-b]thiophene, 5,5'-bis(trimethylstannyl)-2,2'-thiophene and 5,5'-bis(trimethylstannyl)- 2,2'-bithiophene were commercially available and used directly without purification.

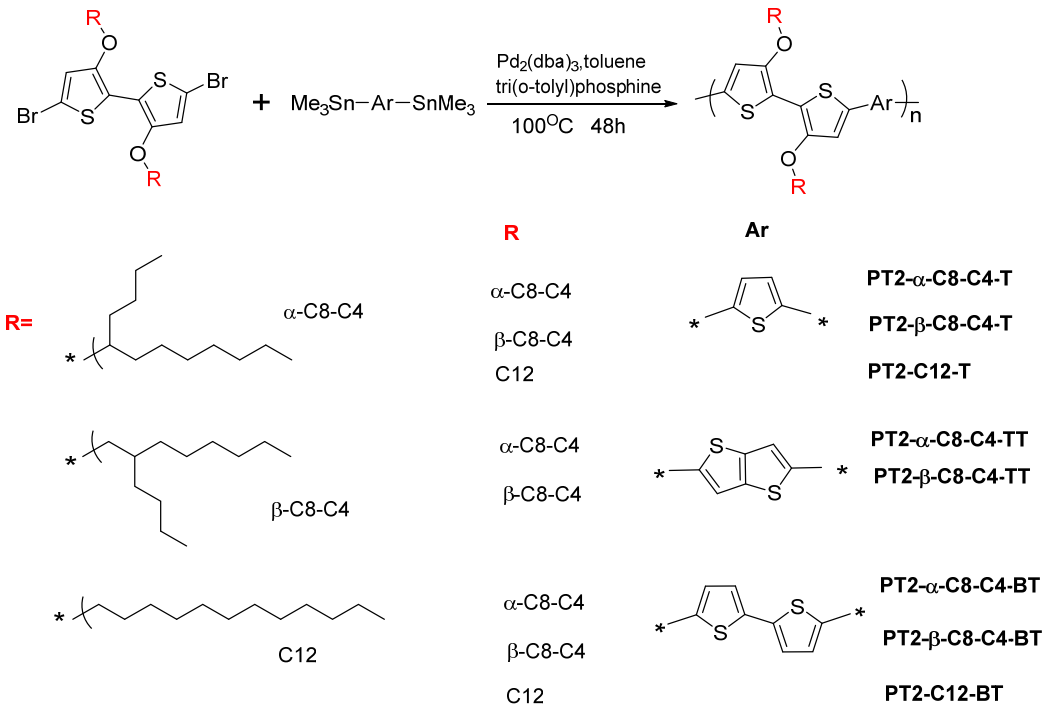

Scheme 4.3: Synthesis scheme of PRO2T2-Ar copolymers.

The PRO2T2Ar copolymers (scheme 4.3) were prepared by Stille polymerization in toluene. After polymerization, the resulting polymers were precipitated in methanol and collected. During the Soxhlet of PRO2T2Ar copolymers, we found that the Soxhlet solvent is close related to the branch position and the spacer. Somewhat surprisingly, despite an expected

lack of intermolecular donor-acceptor interactions, the solubilities were in some cases low for these polymers.

Except for the polymer with a single thiophene as spacer, all the polymers with β branch side chains need $CHCl_3$ to Soxhlet the highest Mw fractionindicating lower solubility comparing to their α branch analogues. This result is similar to the result from chapter 2 and chapter 3, shows that the solubility could improve if branches are closer to the backbone.

Table 4.2: Molecular weight and Soxhlet solvent for PRO2T2-Ar copolymers

Polymer	Solvent [a]	solvent	solvent
PRO2T2-α-C8-C4-T	hexane	rtDCM	
PRO2T2-β-C8-C4-T	hexane	rtDCM	
PRO2T2-C12-T	rtDCM	htDCM	
PRO2T2-α-C8-C4-TT	hexane	rtDCM	htDCM
PRO2T2-β-C8-C4-TT	hexane	DCM	$CHCl_3$ [b]
PRO2T2-α-C8-C4-BT	rtDCM	htDCM	
PRO2T2-β-C8-C4-BT	rtDCM	htDCM	$CHCl_3$ [b]
PRO2T2-C12-BT	htDCM	$CHCl_3$ [c]	

a: rt: room temperature, ht: high temperature.

b: After Soxhlet with $CHCl_3$, there is still some sample left there as poor soubility in $CHCl_3$.

The copolymers with the thiophene spacer were quite soluble; the highest Mw fraction can be Soxhlet with DCM, probably as a result of relatively higher volume-fraction of flexible side chains. For the reference PRO2T2-C12-T polymer, high temperature DCM was used to Soxhlet the highest Mw fraction; indicated the relative lower solubility as a result of the linear side chain. When switched to copolymer with thieno[3,2-b]thiophene as spacer, the solubility was decreased. For PRO2T2-β-C8-C4-TT polymer, there is even polymer fraction that cannot Soxhlet out with $CHCl_3$. The copolymer with bithiophene spacer with the lowest volume-fraction of flexible side chains, the DCM was used to Soxhlet the lower Mw

fraction. For the polymer PRO2T2-β-C8-C4-BT, some polymer fraction cannot Soxhlet out with $CHCl_3$. All these results together show us that the solubility was close relative to the volume-fraction of flexible side chains, the solubility was decreased with the decrease of volume-fraction of flexible side chains.

The summary of PRO2T2-Ar polymers is in table 4.3 (here the data is for the highest molecular weight fraction for each polymer).

Table 4.3: Properties of PRO2T2-Ar copolymers

Polymer	λ_{max}(abs) (nm) [a]	λ_{max}(film) (nm) [b]	λ_{onset} (film) (nm) [b]
PRO2T2-α-C8-C4-T	565	574	670
PRO2T2-β-C8-C4-T	575	593	704
PRO2T2-C12-T	595	649	720
PRO2T2-α-C8-C4-TT	579	585	706
PRO2T2-β-C8-C4-TT	592	617	712
PRO2T2-α-C8-C4-BT	556	580	683
PRO2T2-β-C8-C4-BT	574	593	707
PRO2T2-C12-BT	644	636	723

a $1x10^{-5}$ M in $CHCl_3$.

b: Pristine film spun-cast from 1 mg/ml $CHCl_3$ solution.

4.3.2 Optical Properties of PRO2T2-Ar Copolymers

After introducing the different spacer to form PRO2T2-Ar polymers, UV-Vis absorption spectra of these polymers (1.0×10^{-5} M) in chloroform could be seen from figure 4.6. The absorption of film was also tested; the film was spun-cast from 1 mg/ml chloroform solution. As we can see from figure 4.6, the absorption maxima α-branch polymers were 670, 706, 683 nm for thiophene, thieno[3,2-b]thiophene and bithiophene spacers. However, absorption maxima β-branch analogies were 704, 712, 707 nm respectively. The absorption

maxima of PRO2T2-Ar polymers with β-branch side chains are red-shifted in solution and thin films relative to those of polymers with α-branch side chains. In the case of polymers with β-branch side chains, the side chain branching position is further away from the polymer backbone, which allows stronger intermolecular interaction and/or better planarity of the backbone, leading to decreased solubility and enhanced molecular aggregation in solution. For polymers with α-branch side chains, the proximity of the side chain branching position to the RO2T2 core possibly hinders the intermolecular interaction and lead to greater aggregation in solution. For polymers with thiophene as spacer, which has the better solubility as the highest volume fraction of side chains，lead to the relatively smaller red-shifted comparing with other polymers. However, compared with D-A kind of RO2T2TPD polymers with observable shoulders at lower wavelengths, the absorption band of PRO2T2-Ar polymers shows a far less pronounced structure.

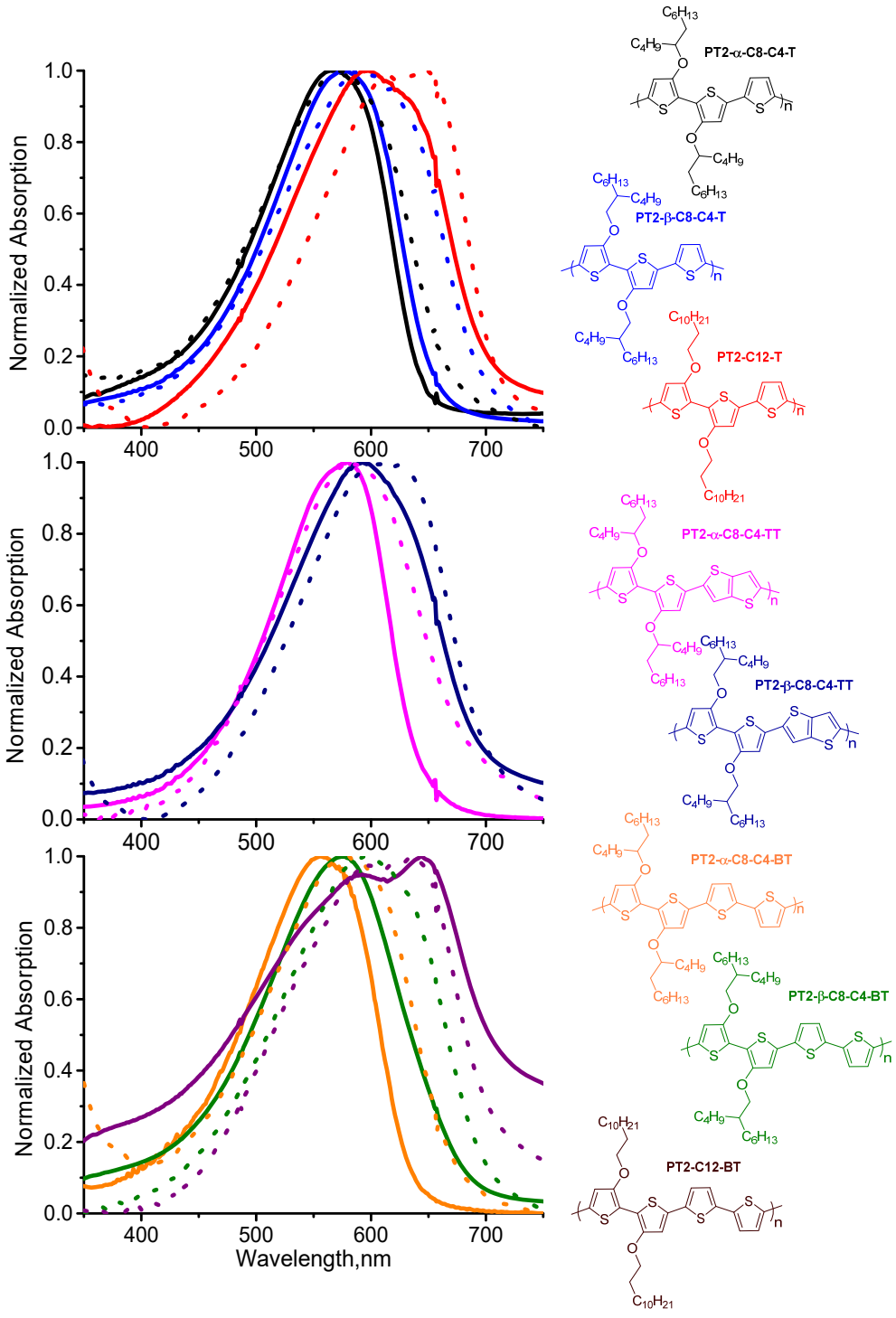

Figure 4.6: Normalized absorption of PRO2T2-Ar polymers at RT in solution (1.0×10^{-5} M, $CHCl_3$) (solid line), and film (spun-cast from 1 mg/ml $CHCl_3$) (dash line).

Different molecular weight fraction of PRO2T2-Ar polymers were separated through carefully Soxhlet with different solvent. UV-Vis absorption spectra of the different Mw

(molecular weight) fraction of PRO2T2-Ar polymers (1.0 x 10^{-5} M) in chloroform could be seen from figure 4.7. It is quite clear that the absorption spectra red-shifted with the increase of Mw for low Mw fraction part. However, to a certain Mw, the absorption spectra red-shifted is not obvious.

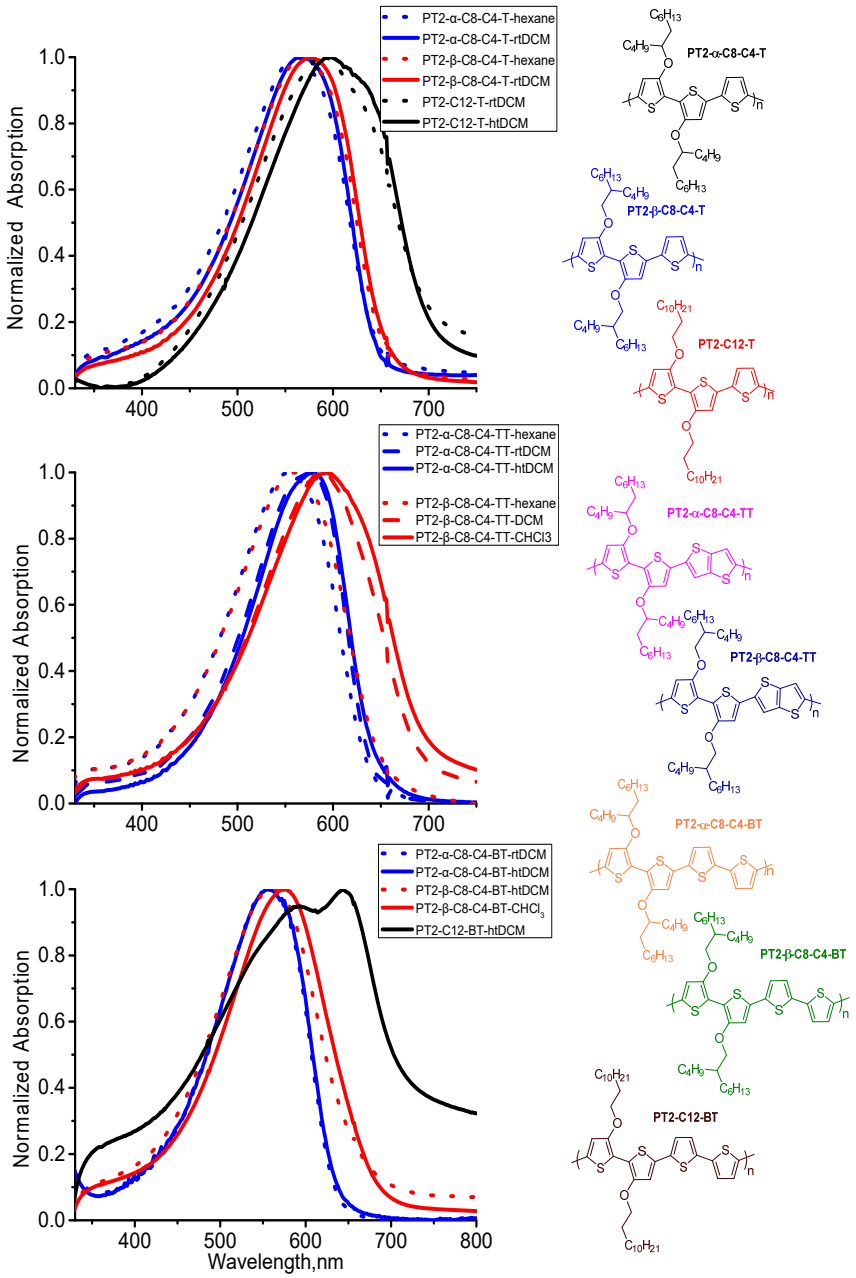

Figure 4.7: Normalized absorption of PRO2T2 polymers (different Soxhlet fraction). Here the ht: high temperaute, rt: room temperature.

4.3.3 Self Assembly of PRO2T2-Ar Copolymers

According to the WAXD images depicted in figure 4.8, for the copolymers with spacer, polymers with different branch position of side chains show very distinct diffraction patterns.

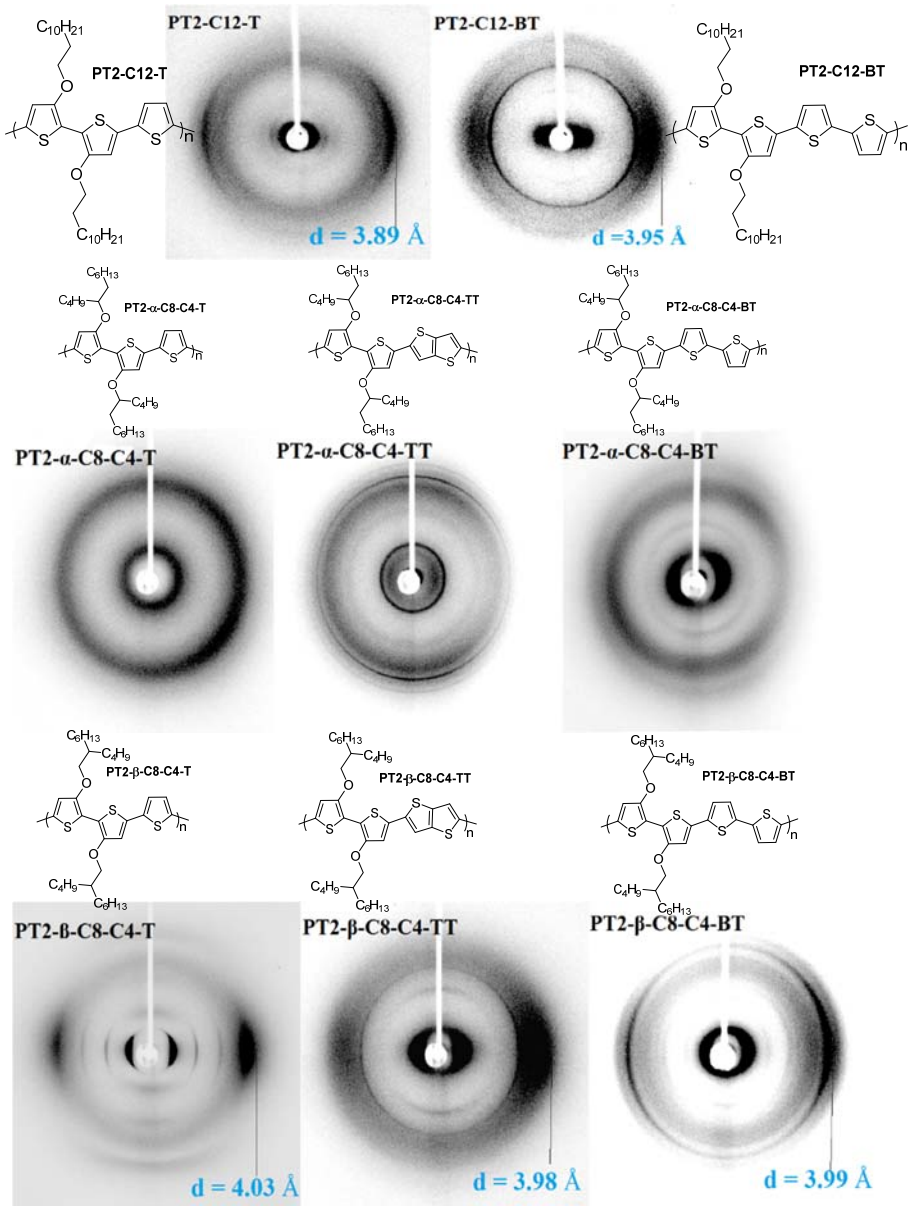

Figure 4.8: Fiber WAXD diffractograms for RO2T2 homopolymers and co-polymers.

The polymers with β-branch side chains show π-π stacking, however, there is no π-π stacking for all the copolymers with α-branch side chains no matter the size of

spacer. This clearly indicate the α-branch side chains are too disruptive; their space-filling demands overcome any forces that would lead to nano-phase separation into lamellar π-stacks. Actually, the copolymers with α-branch side chains and spacer were completely amorphous even with different free volume of spacers. For PRO2T2-β-C8-C4-T polymer, the diffraction patterns along the equatorial direction show relatively narrow arcs and more distinct diffraction patterns at smaller angles with relative d-spacings of L, L/2, L/3, and regularly decreasing intensities. These indicate parallel zones of alternating electron density corresponding to repeating pattern of polymer backbones separated by alkyl side chains (lamellar packing, with repeating distance L). The reason for these observations (well distinguished diffraction patterns in WAXD) may be due to the higher interdigitation tendency as the introducing of local free spacing.

4.3.4 Electrochemistry of PRO2T2-Ar Copolymers

Differential Pulse Voltammetry (DPV) measurements were obtained using polymer films cast on a Pt button electrode to get HOMO energy levels. All the measurements were carried under N2 atmosphere using 0.1 M $(n\text{-}Bu)_4N.PF_6$ as the supporting electrolyte in anhydrous acetronitrile solution. All the results are summarized in table 4.4. As estimated from the oxidation potentials, the HOMO energies of the most polymers are pretty stable, which is around 4.80 eV no matter what kind of spacers were chosen. The only exception is the homopolymer with linear side chains, the HOMO level is even lower, possibly indicated the stronger electron donating ability. In order to get ambient stable p-type material, we should have much deeper HOMO level (-5.1 eV with respect to the vacuum energy level),[195]

so electron-poor spacer might introduced to lower the HOMO level which has proved in chapter 3. Also it seems PRO2T2-Ar polymers with the linear side have slightly lower HOMO level, this means we were able to improve the stability of polymer with branch side chains respect to the polymer with linear side chains on the donor unit.

Table 4.4: Electrochemical and optical data for polymers

Polymer	E_{ox} (V) [a]	E_{HOMO} (eV) [b]	E_{LUMO} (eV) [c]	E_g^{opt} (eV) [d]
PRO2T2-α-C8-C4	-0.05∓0.03	-4.75∓0.03	-2.94∓0.03	1.81
PRO2T2-β-C8-C4	0.00∓0.05	-4.80∓0.05	-3.04∓0.05	1.76
PRO2T2-C12	-0.23∓0.05	-4.57∓0.05	-2.85∓0.05	1.72
PRO2T2-α-C8-C4-T	0.04∓0.03	-4.84∓0.03	-2.99∓0.05	1.85
PRO2T2-β-C8-C4-T	0.05∓0.03	-4.85∓0.03	-3.09∓0.03	1.76
PRO2T2-C12-T	-0.05∓0.04	-4.75∓0.04	-2.99∓0.04	1.76
PRO2T2-α-C8-C4-TT	0.04∓0.05	-4.84∓0.05	-3.08∓0.05	1.76
PRO2T2-β-C8-C4-TT	-0.01∓0.03	-4.79∓0.03	-3.05∓0.03	1.74
PRO2T2-α-C8-C4-BT	0.03∓0.05	-4.83∓0.05	-3.01∓0.05	1.82
PRO2T2-β-C8-C4-BT	0.09∓0.03	-4.89∓0.03	-3.17∓0.03	1.72
PRO2T2-C12-BT	-0.02∓0.03	-4.78∓0.03	-3.06∓0.03	1.72

Experimental conditions: 0.1 M $(n\text{-}Bu)_4N.PF_6$ in anhydrous acetonitrile as supporting electrolyte, platinum disc as working electrode, platinum wire as counter electrode, silver wire as reference electrode and Fe/Fe+ (-4.8 eV vs vacuum) as reference, scanning rate: 50 mV/s; All measurements conducted on solution-cast thin films under nitrogen. [a]Corrected E_{ox} value respect to Fc/Fc+. [b]E_{HOMO} = -[4.8+(E_{ox}-Fc/Fc+)], E_{ox} calculated using onset of DPV measurements (Oxidation peak). [c]$E_{LUMO} = Eg^{opt} + E_{HOMO}$. [d] Eg^{opt} Optical band gap estimated from the absorption edge of the film. Each of the sample run 3 times. We test Fc before each polymer test and polish the electrode then test Fc again, each time the difference is less than 20 mV.

4.4 Thermal Analysis of Polymers

Thermogravimetric analyses (TGA) shows that PRO2T2-Ar polymers are stable up to ~200 ºC. PRO2T2-Ar polymers with β branch side chain (thiophene or bithiophene) are stable even up to ~330 ºC (PRO2T2-β-C8-C4-TT was an exception).

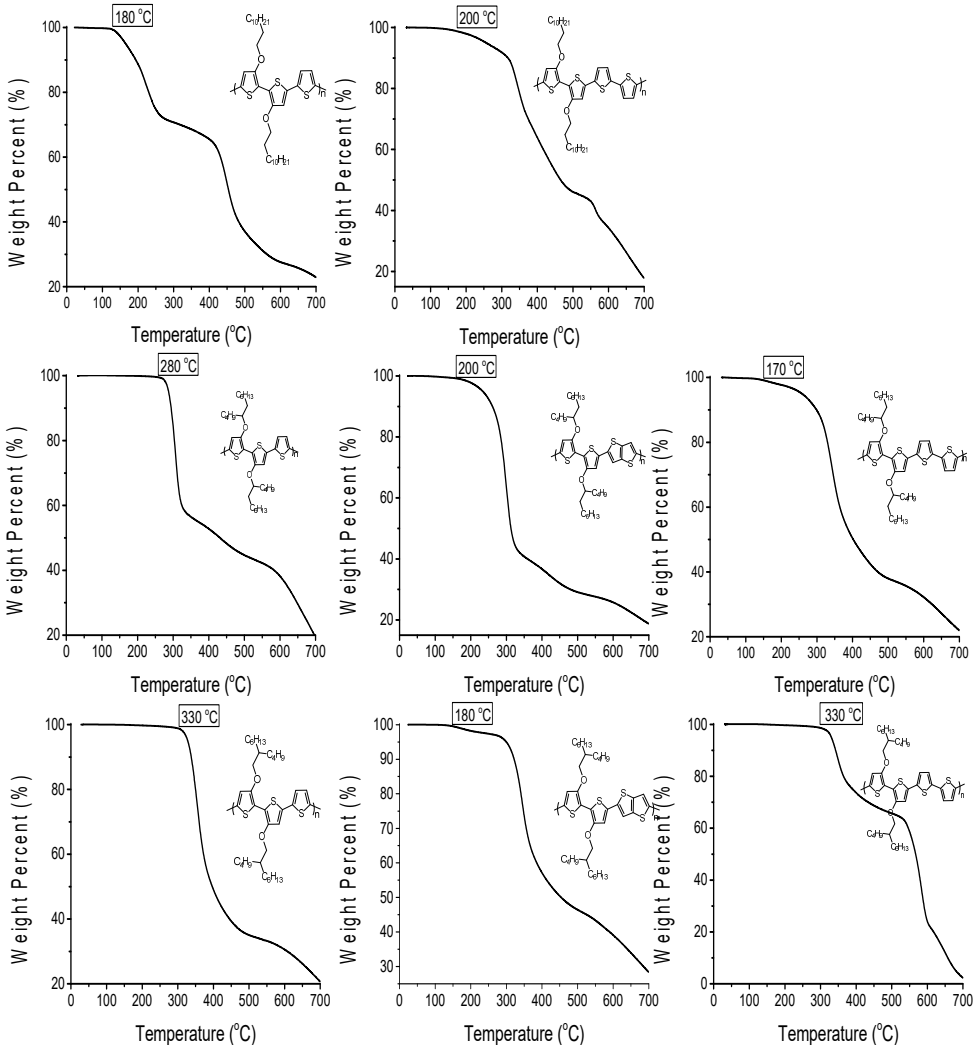

Figure 4.9: Thermogravimetic analyses of PRO2T2-Ar polymers.

None of the polymers showed any melting transition up to 180 °C or any transitions in the cooling scans during differential scanning calorimetry study (DSC).

4.5 Conclusions

The spectroscopic studies suggest these polymers with bulky side chains exhibit some varying level of backbone conjugation. Somewhat surprisingly, despite an expected lack of intermolecular donor-acceptor interactions, the solubilities were in some cases low, but

varied with volume fraction of side chains, the solubility was decreased with the decrease of volume-fraction of flexible side chains.

WAXD results show us that there is no π-π stacking for PRO2T2 home-polymers. After introducing some spacer for interdigitation, the polymers with β-branch side chains show π-π stacking. However, there is no π-π stacking for all the copolymers with α-branch side chains no matter the size of spacer. Oxidation potentials seem essentially insensitive to any of the structural variables (governed mostly by the backbone RO2RO2T2 units).

Chapter 5: Outlook and Future Plans

There are many interesting areas to explore except the projects which I have discussed in this dissertation. Up to now we were able to improve the solubility of D-A co-polymers by introducing bulky branches to the polymer backbone at the same time keeping the solid state packing. In this chapter we want to design a new donor 2-(3-alkoxythiophen-2-yl)thiazole and explore its application in D-A co-polymers, also introducing some new spacer to the 3,3'-dialkoxy-2,2'bithiophene (RO2T2) units .

5.1 New Donor Unit Based on 2-(3-alkoxythiophen-2-yl)thiazole and D-A co-polymers

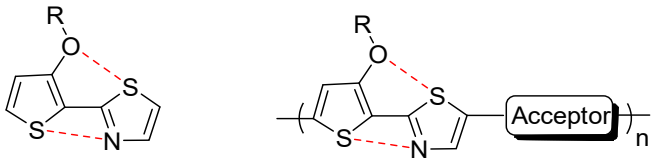

Figure 5.1: Proposed acceptor and related polymers.

Based on the study before, these results show that the 3,3'-dialkoxy-2,2'bithiophene (RO2T2) unit could keep certain planar structure even with bulky branch side chains. However, the DPV results indicated the low oxidation potential for polymers containing RO2T2 unit, which may not be stable in ambient air during the long time operation. It is well known that the device stability was closely related to oxidation potential of the materials. Increasing the oxidation potential could improve the material stability. Thiazole is an electron-deficient unit from electron-withdrawing imine groups (C=N),[196,197,198] which has been successfully used in conjugated polymer. Compared with thiophene analogues, thiazole-based polymers show lower HOMOs and improved device stability.[199,200,201,202] Through combining electron-poor thiazoles with the electron-rich 3-alkoxy-thiophene

would increase their oxidation potential, also keep better planar structure through the O---S and S---N interaction which limited the rotation of the single bond (see figure 5.1 left), the alkoxy side chains can be used to adjust the solubility. So the future plan is to prepare the copolymer with 2-(3-alkoxythiophen-2-yl)thiazole donor with acceptor (figure 5.1) and study their structure-property relations and possible application in solar cells or OFET device.

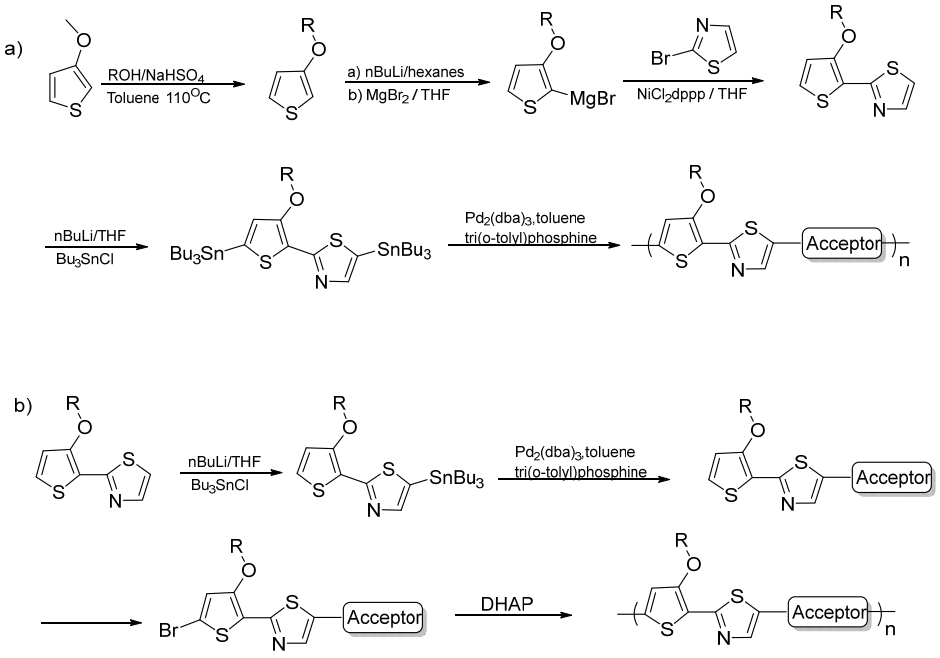

Scheme 5.1: Proposed scheme for synthesis of thiazole monomers and polymers.

If the 2-(3-alkoxythiophen-2-yl)thiazole could get through Kumada coupling (see scheme 5.1a), then tributyltin group could be introduced. The resulting donor unit may be copolymerized with a variety of acceptor units through Stille coupling, the formed polymers could be used for the fabrication of solar cells or OFET devices. However, the asymmetry of 2-(3-alkoxythiophen-2-yl)thiazole unit could lead to unrepeated polymer backbones. This can be overcome by introducing acceptor first, then running polymerization through DHAP methods (see scheme 5.1b).

5.2 PRO2T2-Ar Copolymers with New Spacer

PRO2T2-Ar copolymers were synthesized in chapter 4, some of the polymers can keep the pi-pi stacking even there is no intramolecular interaction between these spacers and the RO2T2 unit. Here we want to introduce some new spacers, such as thiazole, EDOT and thieno[3,4-b]pyrazine,[203,204] which could form the "inner lock" as the intramolecular interaction from O---S and/or S---N interaction. Thus, we could compare the H-H link of 3,3'-dialkoxy-2,2'bithiophene (RO2T2) to T-T link of T2, to study their structure-property relations (see figure 5.2).

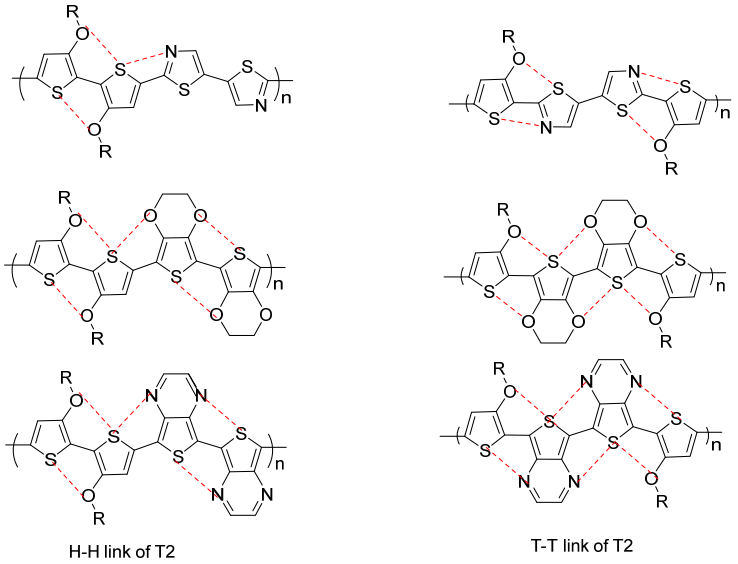

Figure 5.2: Proposed chemical structure of the PRO2T2-Ar Copolymers with conformational locking.

The proposed H-H link of RO2T2 copolymers could be synthesized by Stille coupling as we used before, following the scheme 5.2.

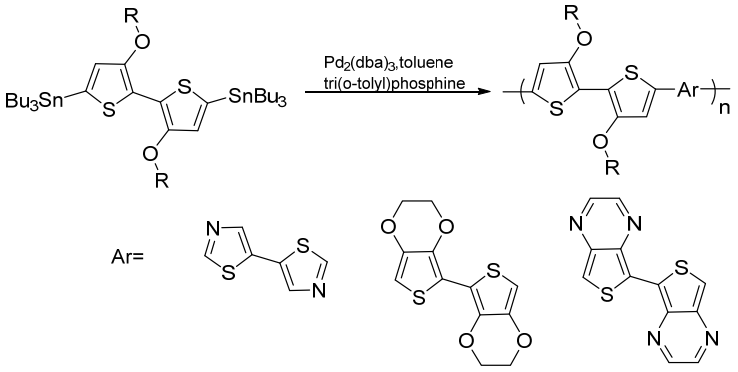

Scheme 5.2: Proposed scheme for synthesis of PRO2T2-Ar (H-H) copolymers.

The scheme for T-T link of RO2T2 copolymers was much more complicated, needing to get the monomer (see scheme 5.3) through several steps, then get the final copolymers through DHAP methods.

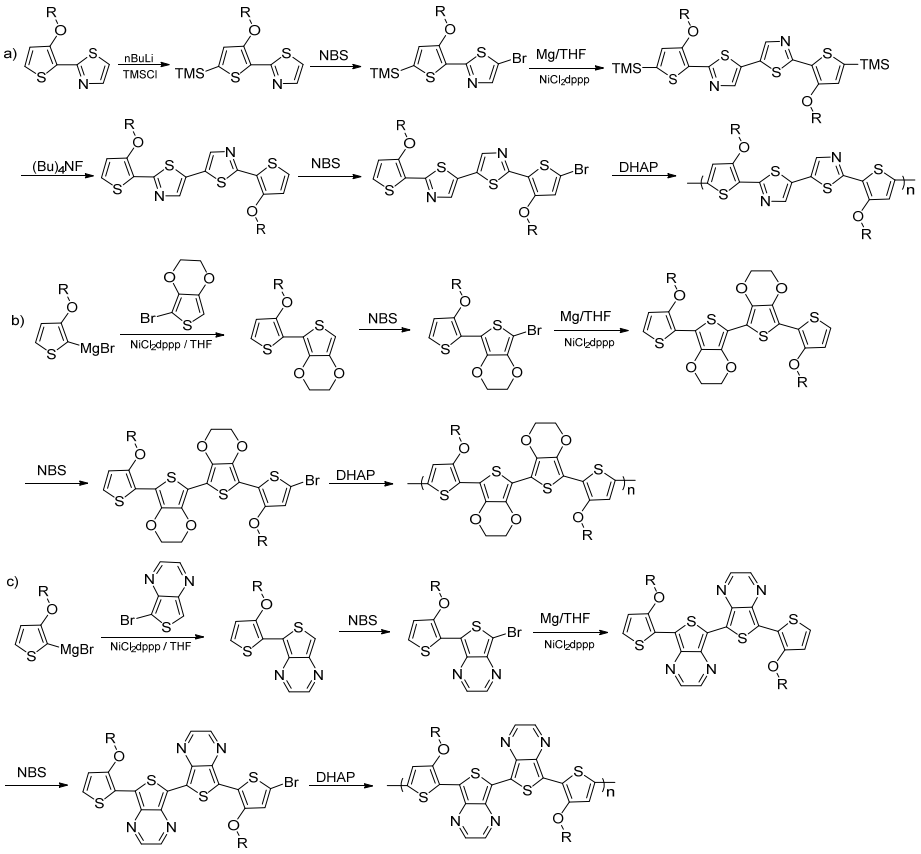

Scheme 5.3: Proposed scheme for synthesis of PRO2T2-Ar (T-T) copolymers.

Chapter 6: Experimental Section and Spectra

6.1 Materials and Method

Tetrahydrofuran (THF), acetonitrile and toluene were distilled from appropriate drying agents and stored over molecular sieves under argon or nitrogen. Acetaldehyde, butyraldehyde, valeraldehyde, hexanal, heptaldehyde, octanal, nonanol were purchased from Fisher chemicals and used without further purification. Unless otherwise stated all other materials were used as purchased. All manipulations and reactions were carried under nitrogen using standard Schlenk techniques. ^{1}H, ^{13}C and ^{19}F spectra were recorded using Varian INOVA 400 MHz spectrometer (purchased under the CRIF Program of the National Science Foundation, grant CHE-9974810). Chemical shifts were recorded relative to the referenced residual protio-solvent signals. GC-MS data were collected from an Agilent technologies 6890N GC with 5973 MSD using two different temperature programs (70 ºC →275 ºC, Helium 1.0 mL/min or 70 ºC→ 350 ºC, Helium 2.0 mL/min) depending on the analyte. Polymer relative molecular weights were measured using a Waters 600 E HPLC system, driven by waters Empower Software and equipped with two linear mixed-bed GPC columns (American Polymer Standards Corporation, AM Gel Linear/15) in series. Polymer elutants were measured using both refractive index and photodiode array detectors and the system was calibrated with 11 narrow PDI polystyrene samples in the range 580 to 2 x 10^6 Da with $CHCl_3$ at a flow rate of 1mL/min and column temperature 50 ºC. Endothermic maxima of 1 st order transitions detected by differential scanning calorimetry (Mettler 822e, heating rate = 10 ºC / min, nitrogen purge). TGA curves were recorded on a TA Instrument Model No. TGA Q500. UV-Vis absorption data were measured using Varian Cary 1

UV-Visible spectrophotometer. Differential pulse voltammetry (DPV) measurements were carried under nitrogen atmosphere using a BAS-100 A voltammetric analyzer with 0.1 M tetra-n-butylammonium hexafluorophosphate in anhydrous acetonitrile as supporting electrolyte. Fc/ Fc+ was used as external reference for all the measurements. As electrodes, used platinum disk working electrode, a platinum wire counter electrode and silver wire reference electrode. Scan rate was 50 mV/S. All DPV measurements were done under inert conditions. Polymer films were produced by drop casting from chloroform solutions (1 mg/ml). WAXD data of polymers were collected on Bruker-Nonius X8 Proteum using an area detector and extruded, oriented fibers, mounted perpendicular to the incoming beam.

6.2 **Synthesis Section of Chapter 2**

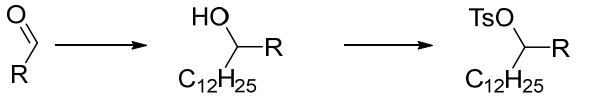

2.0a	$R:C_8H_{17}$	**2.1a**	$R:C_8H_{17}$
2.0b	$R:C_7H_{15}$	**2.1b**	$R:C_7H_{15}$
2.0c	$R:C_6H_{13}$	**2.1c**	$R:C_6H_{13}$
2.0d	$R:C_5H_{11}$	**2.1d**	$R:C_5H_{11}$
2.0e	$R:C_4H_9$	**2.1e**	$R:C_4H_9$
2.0f	$R:C_3H_7$	**2.1f**	$R:C_3H_7$
2.0g	$R:CH_3$	**2.1g**	$R:CH_3$

General synthesis of secondary alcohols:

Magnesium (1.83g, 75.0 mmol) was put into well-dried flask with addition funnel under inert atmosphere.1-Bromododecane (18.7g, 75.0 mmol) in 50 mL dry THF was added dropwise to the bottle, begin heating the flask (use the 1-2 setting), and allow the mixture to reflux gently. After added all the reagents drop by drop in about 30 mins, reflux the solution for about 2 hours. Upon cooling to 0 ºC, aldehyde (70.0 mmol) in 30 mL dry THF was added dropwise to the solution and stirred at room temperature for overnight. Water (50 mL) was added and the product was extracted into hexane, dried over Na_2SO_4 and the solvent

removed by rotary evaporation to afford the product as a white solid, which was purified by column to give product 2.0 as white solid.

Compound 2.0a: the procedure is same as general procedure, using nonanal as starting reactant. Purification over column chromatography (hexane/DCM: 15/1 to 10/1) produced white solid with 86% yield. ^{1}H NMR (400 MHz, $CDCl_3$) δ 3.58 (s, 1H), 1.51 – 1.16 (m, 37H), 0.87 (d, J = 6.8 Hz, 6H).^{13}C NMR (101 MHz, $CDCl_3$) δ 71.99, 37.48, 31.91, 31.88, 29.71, 29.67, 29.66, 29.64, 29.61, 29.59, 29.35, 29.28, 25.65, 22.68, 22.66, 14.10, 14.09. (**Note**: some peaks in ^{13}C NMR spectrum overlap). GC-MS: m/z: 294 ($C_{21}H_{42}^{+}$).

Compound 2.0b: the procedure is same as before, using octanal as starting reactant. Purification over column chromatography (hexane/DCM: 15/1 to 10/1) produced white solid with 89% yield. ^{1}H NMR (400 MHz, $CDCl_3$) δ 3.58 (s, 1H), 1.51 – 1.16 (m, 35H), 0.87 (t, J = 6.8 Hz, 6H).^{13}C NMR (101 MHz, $CDCl_3$) δ71.99, 37.47, 37.47, 31.90, 31.82, 29.70, 29.66, 29.64, 29.62, 29.60, 29.33, 29.28, 25.64, 22.66, 22.63, 14.07, 14.0. (**Note**: some peaks in ^{13}C NMR spectrum overlap). GC-MS: m/z: 280 ($C_{20}H_{40}^{+}$).

Compound 2.0c: the procedure is same as before, using heptaldehyde as starting reactant. Purification over column chromatography (hexane/DCM: 15/1 to 10/1) produced white solid with 81% yield. ^{1}H NMR (400 MHz, $CDCl_3$) δ 3.58 (s, 1H), 1.51 – 1.16 (m, 32H), 0.87 (t, J = 6.8 Hz, 6H).^{13}C NMR (101 MHz, $CDCl_3$) δ 71.83, 37.34, 31.76, 31.69, 29.57, 29.52, 29.51, 29.49, 29.46, 29.23, 29.20, 25.50, 25.47, 22.53, 22.46, 13.94, 13.91. (**Note**: some peaks in ^{13}C NMR spectrum overlap). GC-MS: m/z: 266 ($C_{19}H_{38}^{+}$).

Compound 2.0d: the procedure is same as before, using hexanal as starting reactant. Purification over column chromatography (hexane/DCM: 15/1 to 8/1) produced white solid

with 83% yield. ^{1}H NMR (400 MHz, $CDCl_3$) δ 3.58 (m, 1H), 1.51 – 1.16 (m, 30H), 0.87 (m, 6H). NMR (101 MHz, $CDCl_3$) δ 72.01, 37.44, 31.89, 29.68, 29.65, 29.63, 29.62, 29.60, 29.59, 29.32, 25.63, 25.30, 22.64, 14.09, 14.02. (**Note**: some peaks in ^{13}C NMR spectrum overlap). GC-MS: m/z: 252 ($C_{18}H_{36}^{+}$).

Compound 2.0e: the procedure is same as before, using valeraldehyde as starting reactant. Purification over column chromatography (hexane/DCM: 15/1to8/1) produced white solid with 78% yield. ^{1}H NMR (400 MHz, $CDCl_3$) δ 3.58 (m, 1H), 1.51 – 1.16 (m, 27H), 0.87 (m, 6H).^{13}C NMR (101 MHz, $CDCl_3$) δ 69.40, 34.91, 34.59, 29.33, 27.14, 27.09, 27.08, 27.06, 27.04, 26.77, 25.26, 23.08, 20.18, 20.10, 11.51, 11.48. (**Note**: some peaks in ^{13}C NMR spectrum overlap). GC-MS: m/z: 238 ($C_{17}H_{34}^{+}$).

Compound 2.0f: the procedure is same as before, using butyraldehyde as starting reactant. Purification over column chromatography (hexane/DCM: 15/1 to 6/1) produced white solid with 76% yield. ^{1}H NMR (400 MHz, $CDCl_3$) δ 3.58 (m, 1H), 1.51 – 1.16 (m, 25H), 0.87 (m, 6H).^{13}C NMR (101 MHz, $CDCl_3$) δ 71.64, 39.65, 37.49, 31.88, 29.70, 29.64, 29.63, 29.61, 29.59, 29.32, 25.63, 22.64, 18.79, 14.06. (**Note**: some peaks in ^{13}C NMR spectrum overlap). GC-MS: m/z: 224 ($C_{16}H_{32}^{+}$).

Compound 2.0g: the procedure is same as before, using acetaldehyde as starting reactant. Purification over column chromatography (hexane/DCM: 15/1 to 5/1) produced white solid with 66% yield. ^{1}H NMR (400 MHz, $CDCl_3$) δ 3.58 (m, 1H), 1.51 – 1.16 (m, 22H), 1.19 (d, J = 5.0, 3H), 0.87 (t, J = 8.1, 3H). ^{13}C NMR (101 MHz, $CDCl_3$) δ 67.96, 39.33, 31.88, 29.63, 29.60, 29.58, 29.32, 25.75, 23.37, 22.64, 14.03. (**Note**: some peaks in ^{13}C NMR spectrum overlap). GC-MS: m/z: 196 ($C_{14}H_{28}^{+}$).

General procedure for synthesis of secondary alkyl tosylates.

In a 250 mL flame-dried two neck round bottom flask, compound 2.0 (18 mmol), Et_3N (4.3 g, 22.5 mmol), and $Me_3N.HC1$ (1.73 g, 18.0 mmol) were mixed in 80 mL of CH_2Cl_2 and then cooled to 0ºC. A solution of p-toluenesulfonyl chloride (4.30 g, 22.5 mmol) in CH_2Cl_2 (70 mL) was added dropwise over 30 min and kept the reaction at room temperature. The solution was stirred at room temperature for overnight, water was added and the crude compound was extracted with CH_2Cl_2. The organic fraction was washed with water and brine, dried over Na_2SO_4 and concentrated by rotary evaporation. Subsequently, the crude product was purified by column chromatography to yield a colorless liquid.

Compound 2.1a: the procedure is same as general procedure, using 2.0a as starting reactant. Purification over column chromatography (hexane/DCM: 5/1 to 3/1) produced colorless oil with 66% yield. ^{1}H NMR (400 MHz, $CDCl_3$) δ 7.87 – 7.72 (m, 2H), 7.37 – 7.27 (m, 2H), 4.66 – 4.42 (m, J = 6.0 Hz, 1H), 2.43 (s, 3H), 1.64 – 1.47 (m, 4H), 1.36 – 1.10 (m, 33H), 0.88 (td, J = 6.9, 1.6 Hz, 6H). ^{13}C NMR (101 MHz, $CDCl_3$) δ 144.26, 134.74, 129.58, 127.63, 84.26, 76.77, 36.26, 34.05, 31.84, 29.42, 29.37, 29.26, 29.24, 24.63, 22.64, 21.53, 17.98, 14.07, 13.74.

Compound 2.1b: the procedure is same as before, using 2.0b as starting reactant. Purification over column chromatography (hexane/DCM: 5/1to3/1) produced colorless oil with 71% yield. ^{1}H NMR (400 MHz, $CDCl_3$) δ 7.87 – 7.72 (m, 2H), 7.34 – 7.29 (m, 2H), 4.56 – 4.5 (m, J = 6.0 Hz, 1H), 2.43 (s, 3H), 1.64 – 1.47 (m, 4H), 1.36 – 1.10 (m, 30H), 0.88 (td, J = 6.9, 1.6 Hz, 6H).^{13}C NMR (101 MHz, $CDCl_3$) δ 144.14, 134.85, 129.52, 127.63,

84.38, 34.10, 31.88, 31.65, 29.63, 29.61, 29.59, 29.46, 29.36, 29.32, 29.24, 29.19, 29.02, 24.63, 22.64, 22.56, 21.44, 14.04, 13.99. (**Note**: some peaks in ^{13}C NMR spectrum overlap).

Compound 2.1c: the procedure is same as before, using 2.0c as starting reactant. Purification over column chromatography (hexane/DCM: 5/1to3/1) produced colorless oil with 72% yield. ^{1}H NMR (400 MHz, $CDCl_3$) δ 7.84 – 7.75 (m, 2H), 7.36 – 7.28 (m, 2H), 4.57 – 4.49 (m, J = 6.0 Hz, 1H), 2.44 (s, 3H), 1.63 – 1.48 (m, 4H), 1.39 – 1.10 (m, 28H), 0.93 – 0.81 (m, 6H).^{13}C NMR (101 MHz, $CDCl_3$) δ 144.18, 134.83, 129.53, 127.63, 84.39, 34.11, 31.89, 31.56, 29.64, 29.62, 29.60, 29.47, 29.37, 29.33, 29.25, 28.90, 24.64, 24.60, 22.65, 22.44, 21.45, 14.05, 13.96. (**Note**: some peaks in ^{13}C NMR spectrum overlap).

Compound 2.1d: the procedure is same as before, using 2.0d as starting reactant. Purification over column chromatography (hexane/DCM: 5/1 to 3/1) produced colorless oil with 76% yield. ^{1}H NMR (400 MHz, $CDCl_3$) δ 7.82 – 7.79 (m, 2H), 7.34 – 7.29 (m, 2H), 4.58 – 4.50 (m, J = 6.0 Hz, 1H), 2.44 (s, 3H), 1.63 – 1.48 (m, 4H), 1.39 – 1.10 (m, 25H), 0.93 – 0.77 (m, 6H).^{13}C NMR (101 MHz, $CDCl_3$) δ 144.19, 134.79, 129.54, 127.64, 84.42, 34.10, 34.07, 31.89, 31.41, 29.64, 29.62, 29.60, 29.47, 29.37, 29.33, 29.25, 24.64, 24.31, 22.65, 22.40, 21.46, 14.06, 13.84. (**Note**: some peaks in ^{13}C NMR spectrum overlap).

Compound 2.1e: the procedure is same as before, using 2.0e as starting reactant. Purification over column chromatography (hexane/DCM: 5/1to3/1) produced colorless oil with 68% yield. ^{1}H NMR (400 MHz, $CDCl_3$) δ 7.82 – 7.79 (m, 2H), 7.34 – 7.29 (d, J =8.0 Hz, 2H), 4.58 – 4.50 (m, J = 6.0 Hz, 1H), 2.44 (s, 3H), 1.63 – 1.48 (m, 4H), 1.39 – 1.10 (m, 22H), 0.93 – 0.77 (m, 6H).^{13}C NMR (101 MHz, $CDCl_3$) δ 141.66, 132.23, 127.00, 125.10,

81.95, 31.50, 31.25, 29.33, 27.07, 27.05, 27.04, 26.90, 26.80, 26.76, 26.69, 24.22, 22.09, 20.09, 19.78, 18.96, 11.51, 11.23. (**Note**: some peaks in ^{13}C NMR spectrum overlap).

Compound 2.1f: the procedure is same as before, using 2.0f as starting reactant. Purification over column chromatography (hexane/DCM: 5/1 to 3/1) produced colorless oil with 80% yield. ^{1}H NMR (400 MHz, $CDCl_3$) δ 7.83 – 7.75 (m, 2H), 7.34 – 7.29 (d, J =8.0 Hz, 2H), 4.58 – 4.50 (m, J = 6.0 Hz, 1H), 2.44 (s, 3H), 1.63 – 1.48 (m, 4H), 1.39 – 1.10 (m, 20H), 0.90 – 0.80 (m, 6H).^{13}C NMR (101 MHz, $CDCl_3$) δ 144.22, 134.78, 129.72, 127.63, 84.24, 36.27, 34.06, 31.88, 29.63, 29.61, 29.59, 29.46, 29.36, 29.32, 29.24, 24.63, 22.65, 21.52, 17.98, 14.07, 13.73. (**Note**: some peaks in ^{13}C NMR spectrum overlap).

Compound 2.1g: the procedure is same as before, using 2.0g as starting reactant. Purification over column chromatography (hexane/DCM: 5/1 to 2/1) produced colorless oil with 78% yield. ^{1}H NMR (400 MHz, $CDCl_3$) δ 7.83 – 7.75 (m, 2H), 7.34 – 7.29 (d, J =8.0 Hz, 2H), 4.58 – 4.50 (m, J = 6.0 Hz, 1H), 2.44 (s, 3H), 1.63 – 1.48 (m, 2H), 1.39 – 1.10 (m, 23H), 0.88 (t, J = 6.9 Hz, 3H). 13C NMR (101 MHz, $CDCl_3$) δ 144.19, 134.82, 129.49, 127.71, 84.52, 34.11, 31.90, 31.66, 29.63, 29.47, 29.37, 29.33, 29.26, 29.21, 29.03, 24.66, 22.62, 21.51, 14.03. (**Note**: some peaks in ^{13}C NMR spectrum overlap).

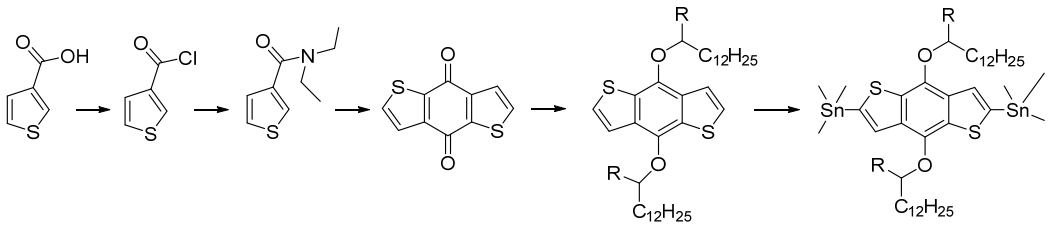

2.2 **2.3** **2.4**

2.5a R:C_8H_{17}
2.5b R:C_7H_{15}
2.5c R:C_6H_{13}
2.5d R:C_5H_{11}
2.5e R:C_4H_9
2.5f R:C_3H_7
2.5g R:CH_3

2.6a R:C_8H_{17}
2.6b R:C_7H_{15}
2.6c R:C_6H_{13}
2.6d R:C_5H_{11}
2.6e R:C_4H_9
2.6f R:C_3H_7
2.6g R:CH_3

Thiophene-3-carbonyl Chloride 2.2: Thiophene-3-carboxylic acid (30.11 g, 0.235 mol) and 100 mL of methylene chloride were put into a 250 mL flask. The mixture was cooled by ice-water bath, and then oxalyl chloride (59.7 g, 0.47 mol) was added in one portion. The reactant was stirred overnight at ambient temperature, and a clear solution was obtained. After removing the solvent and unreacted oxalyl chloride by rotary evaporation, compound 2.2 was obtained as colorless solid. It was dissolved into 100 mL of dichloromethane and used for the next step without further purification.

N, N-Diethylthiophene-3-carboxamide 2.3: In a 500 mL flask in ice-water bath, diethylamine (34.4 g, 0.47 mol) and 100 mL of dichloromethane were mixed, and the solution of thiophene-3-carbonyl chloride was added into the flask slowly. After all of the solution was added, the ice bath was removed, and the reactant was stirred at ambient temperature for overnight. Then, the reactant was washed by water several times, and the organic layer was dried over Na_2SO_4. After removing solvent, the crude product was purified by distillation under vacuum, and 35 g of compound 2.3 (0.191 mol, yield 81.4%) was obtained as a pale yellow oil. ^{1}H NMR ($CDCl_3$, 400 MHz), δ (ppm): 7.48 (s, 1H), 7.32 (d, 1H), 7.20 (d, 1H), 3.41 (m, 4H), 1.19 (t, 6H).

Benzo[1,2-b:4,5-b']dithiophene-4,8-dione 2.4: Compound 2.3 (0.148 mol, 27.2 g) was put into a well-dried flask with 150 mL of THF under an inert atmosphere. The solution was cooled down by an ice-water bath, 59.4 mL of n-butyllithium (0.148 mol, 2.5 mol/L) was added into the flask dropwise within 30 min. Then, the reactant was stirred at ambient temperature for overnight. The reactant was poured into 500 g of ice water and stirred for 1 hour. The mixture was filtrated, and the yellow precipitate was washed by 200 mL of water, 50 mL of methanol, and 50 mL of hexane successively. 14.0 g of compound 2.4 was obtained as a yellow powder (63.6mmol, yield 85.6%). ^{1}H NMR ($CDCl_3$, 400 MHz), δ (ppm): 7.75 (d, 2 H), 7.95 (d, 2 H).

General procedure for the alkylation of Benzo[1,2-b:4,5-b']dithiophene-4,8-dione: Compound 2.4 (880 mg, 4 mmol) was suspended in 40 mL of water into a 100 mL flask equipped with a condenser. Zinc powder (590 mg, 9 mmol) was added under vigorous stirring, followed by 2.4 g of NaOH. As the temperature was raised from room temperature to reflux, the color of the mixture changed from yellow, to dark red, and then to orange. After 1 h, a catalytic amount of tetrabutylammonium bromide were added to the reaction mixture (Note: an excess amount of zinc powder (0.32 g, 5 mmol) can be added if the color doesn't turn to yellow within two hours). After run overnight to two days, the reaction mixture was poured into iced water, and extracted with hexane. The organic layers were combined, washed with brine, dried over anhydrous Na_2SO_4, and concentrated under vacuum. The crude product was finally purified by column chromatography to afford the desired compound.

Compound 2.5a: follow the general produre using 1 as starting reactant. Reaction was refluxed at 110 ºC over 2 days. Purification over column chromatography (hexane/DCM: 15/1) produced yellow oil with 42% yield. ^{1}H NMR (400 MHz, $CDCl_3$) δ 7.46 (d, J = 5.6 Hz, 2H), 7.32 (d, J = 5.6 Hz, 2H), 4.57 (p, J = 5.8 Hz, 2H), 1.70 (m, 8H), 1.53 – 1.39 (m, 8H), 1.35 – 1.18 (m, J = 20.8 Hz, 58H), 0.87 (q, J = 6.8 Hz, 12H).^{13}C NMR (101 MHz, $CDCl_3$) δ 142.93, 132.24, 130.27, 125.32, 120.57, 82.39, 34.16, 31.79, 31.72, 29.72, 29.54, 29.52, 29.46, 29.42, 29.23, 29.12, 25.23, 22.56, 22.52, 13.97. (**Note**: some peaks in ^{13}C NMR spectrum overlap). HRMS: 810.6376 (M+). Calcd for $C_{52}H_{90}O_2S_2$: 810.6382.

Compound 2.5b: follow the procedure using 1 as starting reactant. Purification over column chromatography (hexane/DCM: 15/1) produced yellow oil with 46% yield. ^{1}H NMR (400 MHz, $CDCl_3$) δ 7.46 (d, J = 5.6 Hz, 2H), 7.32 (d, J = 5.6 Hz, 2H), 4.57 (p, J = 5.8 Hz, 2H), 1.70 (m, 8H), 1.53 – 1.39 (m, 8H), 1.35 – 1.18 (m, J = 20.8 Hz, 52H), 0.87 (q, J = 6.8 Hz, 12H).^{13}C NMR (101 MHz, $CDCl_3$) δ 143.06, 132.37, 130.40, 125.45, 120.70, 101.94, 82.52, 34.30, 31.92, 31.80, 29.85, 29.82, 29.65, 29.59, 29.36, 29.26, 25.37, 22.69, 22.63, 14.00. (**Note**: some peaks in ^{13}C NMR spectrum overlap).

Compound 2.5c: follow the procedure using 1 as starting reactant. Reaction was refluxed at 110 ºC over 2 days. Purification over column chromatography (hexane/DCM: 15/1) produced yellow oil with 51% yield. ^{1}H NMR (400 MHz, $CDCl_3$) δ 7.46 (d, J = 5.6 Hz, 2H), 7.32 (d, J = 5.6 Hz, 2H), 4.57 (p, J = 5.8 Hz, 2H), 1.70 (m, 8H), 1.53 – 1.39 (m, 8H), 1.35 – 1.20 (m, J = 20.8 Hz, 49H), 0.87 (q, J = 6.8 Hz, 12H).^{13}C NMR (101 MHz, $CDCl_3$) δ 143.11, 132.42, 130.38, 125.44, 120.72, 82.47, 34.36, 31.97, 31.86, 29.90, 29.72, 29.70, 29.69,

29.63, 29.57, 29.41, 25.41, 25.38, 22.73, 22.63, 14.13, 14.09. (**Note**: some peaks in ^{13}C NMR spectrum overlap). HRMS: 754.5739 (M+). Calcd for $C_{48}H_{82}O_2S_2$: 754.5765.

Compound 2.5d: follow the procedure using 1 as starting reactant. Reaction was refluxed at 110 ºC over 2 days. Purification over column chromatography (hexane/DCM: 15/1) produced yellow oil with 48% yield. ^1H NMR (400 MHz, $CDCl_3$) δ 7.46 (d, J = 5.6 Hz, 2H), 7.32 (d, J = 5.6 Hz, 2H), 4.57 (p, J = 5.8 Hz, 2H), 1.70 (m, 8H), 1.53 – 1.39 (br, 8H), 1.35 – 1.20 (m, J = 20.8 Hz, 44H), 0.87 (m, 12H).^{13}C NMR (101 MHz, $CDCl_3$) δ 143.10, 132.43, 130.42, 125.46, 120.73, 82.51, 34.36, 34.33, 32.12, 31.98, 29.91, 29.73, 29.71, 29.70, 29.64, 29.42, 25.42, 25.09, 22.74, 22.67, 14.15, 14.07. (**Note**: some peaks in ^{13}C NMR spectrum overlap).

Compound 2.5e: follow the procedure using 1 as starting reactant. Reaction was refluxed at 110 ºC over 2 days. Purification over column chromatography (hexane/DCM: 10/1) produced yellow oil with 52% yield. ^1H NMR (400 MHz, $CDCl_3$) δ 7.46 (d, J = 5.6 Hz, 2H), 7.32 (d, J = 5.6 Hz, 2H), 4.57 (p, J = 5.8 Hz, 2H), 1.70 (m, 8H), 1.53 – 1.39 (br, 8H), 1.35 – 1.20 (m, J = 20.8 Hz, 40H), 0.87 (m, 12H).^{13}C NMR (101 MHz, $CDCl_3$) δ 143.07, 132.42, 130.43, 125.48, 120.72, 82.52, 34.33, 34.03, 31.96, 29.89, 29.71, 29.69, 29.68, 29.63, 29.40, 27.57, 25.40, 22.98, 22.73, 14.14, 14.09. (**Note**: some peaks in ^{13}C NMR spectrum overlap).

Compound 2.5f: follow the procedure using 1 as starting reactant. Reaction was refluxed at 110 ºC over 2 days. Purification over column chromatography (hexane/DCM: 10/1) produced yellow oil with 56% yield. ^1H NMR (400 MHz, $CDCl_3$) δ 7.46 (d, J = 5.6 Hz, 2H), 7.32 (d, J = 5.6 Hz, 2H), 4.57 (p, J = 5.8 Hz, 2H), 1.70 (m, 8H), 1.53 – 1.39 (br, 8H), 1.35 – 1.20 (m, J = 20.8 Hz, 36H), 0.87 (m, 12H). 13C NMR (101 MHz, $CDCl_3$) δ 143.06, 132.37,

130.40, 125.45, 120.70, 101.94, 82.52, 34.30, 31.93, 31.80, 29.86, 29.82, 29.65, 29.59, 29.36, 29.26, 25.37, 22.98, 22.63, 14.13, 14.09. (**Note**: some peaks in ^{13}C NMR spectrum overlap).

Compound 2.5g: follow the procedure using 1 as starting reactant. Reaction was refluxed at 110 ^{o}C over 2 days. Purification over column chromatography (hexane/DCM: 15/1) produced yellow oil with 65% yield. ^{1}H NMR (400 MHz, $CDCl_3$) δ 7.86 – 7.69 (m, 2H), 7.39 – 7.29 (m, 2H), 4.69 – 4.37 (m, 2H), 2.44 (s, 6H), 1.77 – 1.39 (m, 4H), 1.36 – 1.05 (m, 42H), 0.88 (t, J = 6.9 Hz, 6H). 13C NMR (101 MHz, $CDCl_3$) δ 143.06, 132.37, 130.40, 125.45, 120.70, 101.94, 82.52, 34.30, 31.96, 29.89, 29.71, 29.69, 29.68, 29.63, 29.40, 27.57, 25.40, 22.69, 22.63, 14.14, 14.09. (**Note**: some peaks in ^{13}C NMR spectrum overlap).

General procedure for the stanyllation of 4,8-bis(alkyloxy)benzo[1,2-b:4,5-b']dithiophene (BDT):

Compound 2.5 (1.45 mmol) was solubilized in 15 mL of dry THF under inert atmosphere. The mixture was cooled down to -78 °C using a dry ice-acetone bath, and 1.3 mL of n-butyllithium (3.2 mmol, 2.5 M in n-hexane) was added dropwise. After being stirred at -78 °C for 1 h, the solution was slowly warmed up to room temperature and stirred for 30 min. The mixture was cooled in the dry ice-acetone bath, and 3.6 mL of trimethyltin chloride (3.63 mmol, 1.0 M in THF) was added in one portion. The reaction mixture was stirred overnight at room temperature, then poured into 100 mL of cool water, and was extracted with hexane. The organic layers were combined, washed with brine, dried over anhydrous Na_2SO_4 and concentrated under vacuum, which was used for next step.

Compound 2.6a: See the general procedure using 2.5a as starting reactant with 95% yield.

^{1}H NMR (400 MHz, $CDCl_3$) δ 7.67 – 7.40 (m, 2H), 4.80 – 4.52 (m, 2H), 1.80 – 1.61 (m, 8H), 1.60 – 1.41 (m, 8H), 1.35 – 1.12 (m, 58H), 0.96 – 0.78 (m, 12H), 0.62 – 0.23 (m, 18H).^{13}C NMR (101 MHz, $CDCl_3$) δ 141.82, 139.66, 134.34, 133.75, 128.58, 82.11, 34.34, 31.92, 30.01, 29.99, 29.76, 29.71, 29.69, 29.42, 29.36, 29.33, 25.35, 22.72, 14.16, -8.36. (**Note**: some peaks in ^{13}C NMR spectrum overlap). HRMS: 1138.5663 (M^+). Calcd for $C_{58}H_{106}O_2S_2Sn_2$: 1138.5678.

Compound 2.6b: See the general procedure using 2.5b as starting reactant with 90% yield. ^{1}H NMR (400 MHz, $CDCl_3$) δ 7.67 – 7.40 (m, 2H), 4.80 – 4.52 (m, 2H), 1.80 – 1.61 (m, 8H), 1.60 – 1.41 (m, 8H), 1.35 – 1.12 (m, 52H), 0.96 – 0.78 (m, 12H), 0.62 – 0.23 (m, 18H).^{13}C NMR (101 MHz, $CDCl_3$) δ 142.04, 139.66, 134.28, 133.69, 128.53, 82.09, 34.25, 31.91, 31.84, 29.95, 29.87, 29.69, 29.66, 29.35, 29.32, 25.36, 22.67, 14.08, -8.39. (**Note**: some peaks in ^{13}C NMR spectrum overlap). HRMS: 1110.7071 (M^+). Calcd for $C_{56}H_{102}O_2S_2Sn_2$: 1110.5365.

Compound 2.6c: See the general procedure using 2.5c as starting reactant with 93% yield. ^{1}H NMR (400 MHz, $CDCl_3$) δ 7.56 – 7.46 (m, 2H), 4.67 – 4.55 (m, 2H), 1.75 – 1.62 (m, 8H), 1.57 – 1.42 (m, 8H), 1.36 – 1.16 (m, 52H), 0.92 – 0.82 (m, 12H), 0.59 – 0.25 (m, 18H).^{13}C NMR (101 MHz, $CDCl_3$) δ 141.83, 139.65, 134.35, 133.65, 128.50, 82.02, 34.32, 31.97, 31.94, 29.98, 29.75, 29.71, 29.67, 29.63, 29.41, 25.43, 25.35, 22.73, 22.68, 22.66, 16.72, -8.38. (**Note**: some peaks in ^{13}C NMR spectrum overlap).

Compound 2.6d: See the general procedure using 2.5d as starting reactant with 92% yield. ^{1}H NMR (400 MHz, $CDCl_3$) δ 7.56 – 7.46 (m, 2H), 4.65 – 4.55 (m, 2H), 1.75 – 1.62 (m, 8H), 1.57 – 1.42 (m, 8H), 1.36 – 1.16 (m, 44H), 0.92 – 0.82 (m, 12H), 0.59 – 0.25 (m,

18H).^{13}C NMR (101 MHz, $CDCl_3$) δ 141.82, 139.68, 134.34, 133.74, 128.57, 82.13, 34.32, 34.27, 32.18, 31.97, 30.01, 29.75, 29.71, 29.41, 25.43, 25.08, 22.74, 14.16, 14.12, 14.10, -8.37. (**Note**: some peaks in ^{13}C NMR spectrum overlap). HRMS: 1054.6405 (M^+). Calcd for $C_{52}H_{94}O_2S_2Sn_2$: 1054.4739.

Compound 2.6e: See the general procedure using 2.5e as starting reactant with 94% yield. ^{1}H NMR (400 MHz, $CDCl_3$) δ 7.57 – 7.45 (m, 2H), 4.73 – 4.52 (m, 2H), 1.78 – 1.62 (m, 8H), 1.56 – 1.40 (m, 8H), 1.37 – 1.13 (m, 40H), 0.91 – 0.78 (m, 12H), 0.63 – 0.22 (m, 18H). ^{13}C NMR (101 MHz, $CDCl_3$) δ 141.79, 139.67, 134.19, 133.72, 128.55, 82.05, 34.31, 33.97, 31.93, 29.97, 29.71, 29.67, 29.36, 27.68, 25.88, 22.99, 22.69, 14.09. HRMS: 1026.4588 (M^+). Calcd for $C_{50}H_{90}O_2S_2Sn_2$: 1026.4426.

Compound 2.6f: See the general procedure using 2.5f as starting reactant with 95% yield. ^{1}H NMR (400 MHz, $CDCl_3$) δ 7.56 – 7.46 (m, 2H), 4.65 – 4.55 (m, 2H), 1.75 – 1.62 (m, 8H), 1.57 – 1.42 (m, 8H), 1.36 – 1.16 (m, 36H), 0.92 – 0.82 (m, 12H), 0.59 – 0.25 (m, 18H). ^{13}C NMR (101 MHz, $CDCl_3$) δ 139.73, 134.57, 133.78, 128.83, 81.87, 36.52, 34.30, 31.97, 30.00, 29.74, 29.70, 29.41, 25.74, 22.73, 18.65, 14.41, 14.15, -8.39. HRMS: 998.5777 (M^+). Calcd for $C_{48}H_{86}O_2S_2Sn_2$: 998.4113.

Compound 2.6g: See the general procedure using 2.5g as starting reactant with 95% yield. ^{1}H NMR (400 MHz, $CDCl_3$) δ 7.55 – 7.43 (m, 2H), 4.74 – 4.61 (m, 2H), 1.90 (dt, J = 15.4, 7.2 Hz, 2H), 1.77 – 1.65 (m, 2H), 1.62 – 1.51 (m, 4H), 1.43 – 1.20 (m, 44H), 0.89 (t, J = 6.8 Hz, 6H), 0.65 – 0.23 (m, 16H). ^{13}C NMR (101 MHz, $CDCl_3$) δ 141.59, 139.57, 134.13, 133.57, 128.38, 81.79, 36.28, 34.08, 31.77, 29.81, 29.53, 29.21, 25.21, 22.54, 18.46, 14.23, 13.98, -8.50.

Synthesis β-branch alcohols, tosylation and monomers:

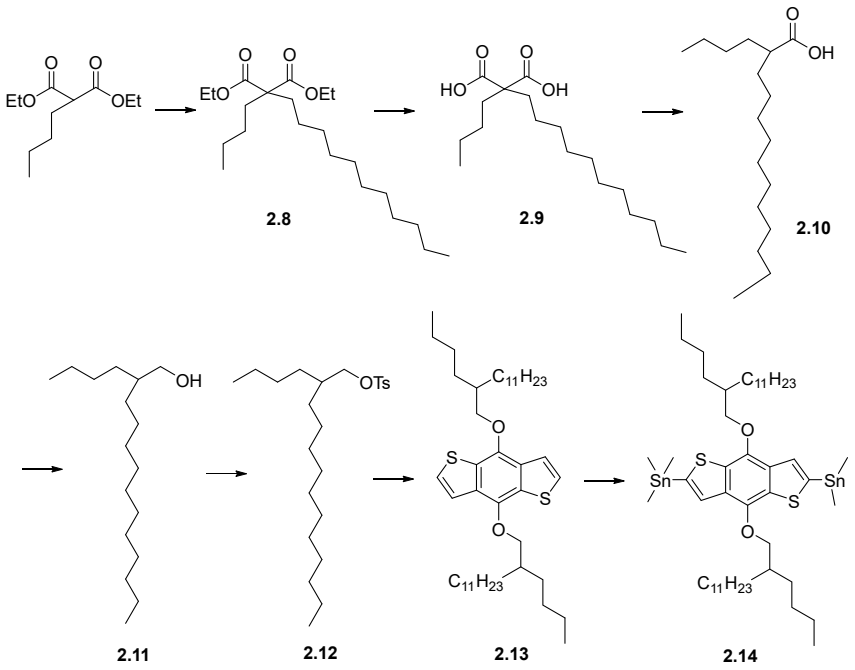

Synthesis of diethyl 2-butyl-2-undecylmalonate 2.8: Diethyl 2-butylmalonate (21.6 g, 0.1 mol) was added to a stirring solution of NaH (4.8 g, 0.12 mol, 60% in oil) in DMSO (100 ml). 1-Bromoundecane (25.9 g, 0.11 mol) was added dropwise to the resulting solution and was stirred at room temperature for overnight. Water was added (200 mL) and the product was extracted into EtOAc, dried over Na_2SO_4 and the solvent was removed by rotary evaporation to afford the product as a yellow oil, which was purified by column (hexane: DCM=10:1 to DCM) to give product as colorless oil (28.4 g, 76.7%).^{1}H NMR (400 MHz, $CDCl_3$) δ 4.22 – 4.13 (t, J = 6.0 Hz, 4H), 1.86 (m, 4H), 1.41 – 1.08 (m, 28H), 0.95 – 0.84 (t, 6H).

Synthesis of 2-butyl-2-undecylmalonic acid 2.9: The obtained diethyl 2-butyl-2-undecylmalonate (19.0 g, 50.0 mmol) was added to a mixture of aqueous KOH (22.4 g in 100 mL water) and iPrOH (200 mL). The mixture was heated at 80°C for overnight and then diluted with water giving a slurry. After separate the organic layer,

which was neutralized with 3M HCl (200 mL). The water phase was extracted by hexane, removed the solvent by rotary evaporation to afford compound 2.9 (15.0 g, 95.5%), which was used for next step without further purification. This acid was almost insoluble in dichloromethane at room temperature.

Synthesis of 2-butyltridecanoic acid 2.10: 2-butyl-2-undecylmalonic acid 2.9 was decarboxylated by heated the sample directly to 175 ^{o}C under inert atmosphere for 2 hours, yielding the desired 2-butyltridecanoic acid 2.10, which was used for next step without further purification.

Synthesis of 2-butyltridecan-1-ol 2.11: 2-butyltridecanoic acid 2.10 (11.0g, 47.0 mmol) in THF (50 mL) was added dropwise to the solution of $LiAlH_4$ (1.7g, 44.8 mmol) in 20 mL dry THF at 0 ^{o}C. The resulting solution was stirred at room temperature for overnight. The solution was poured carefully onto iced 1M HCl (200 mL). The organic layer was separated, dried over Na_2SO_4 and the solvent removed by rotary evaporation before being passed through column (hexane: DCM=10:1 to hexane: DCM=1:2) affording the title compound as a colorless oil (8.5 g, 81%, two steps). ^{1}H NMR (400 MHz, $CDCl_3$) δ 3.54 (d, J = 5.0 Hz, 3H), 1.51 – 1.20 (m, 28H), 1.09 – 0.69 (m, 6H).

Synthesis of 2-butyltridecyl 4-methylbenzenesulfonate 2.12: In a 250 mL flame-dried two neck round bottom flask, compound 2.11 (8.5 g, 33 mmol), Et_3N (8.33 g, 82.5 mmol), and Me_3N.HC1 (3.15 g, 33.0 mmol) were mixed in 50 mL of CH_2Cl_2 and then cooled to 0^{o}C. A solution of p-toluenesulfonyl chloride (7.86 g, 22.5 mmol) in CH_2Cl_2 (50 mL) was added dropwise over 30 min. The solution was stirred at room temperature for overnight, water was added and the crude compound was extracted with CH_2Cl_2. The organic fraction was

washed with water and brine, dried over Na_2SO_4, and concentrated by rotary evaporation. Subsequently, the crude product was purified by column chromatography (hexane: DCM=5:1 to 2:1) to yield a colorless liquid (12.2 g, 90.2%). ^{1}H NMR (400 MHz, $CDCl_3$) δ 7.83 – 7.72 (m, 2H), 7.41 – 7.32 (m, 2H), 3.91 (d, J = 5.3 Hz, 2H), 2.44 (s, 3H), 1.64 – 1.49 (m, 1H), 1.34 – 1.09 (m, 26H), 0.86 (m, 6H).^{13}C NMR (101 MHz, $CDCl_3$) δ 144.53, 133.11, 129.71, 127.86, 72.74, 37.55, 31.89, 30.56, 30.26, 29.76, 29.64, 29.61, 29.59, 29.51, 29.33, 29.33, 28.61, 26.43, 22.80, 22.66, 21.53, 14.08, 13.92. (**Note**: some peaks in ^{13}C NMR spectrum overlap).

Compound 2.13: the procedure follows the general procedure for the alkylation of Benzo[1,2-b:4,5-b']dithiophene-4,8-dione with 85% yield. ^{1}H NMR (400 MHz, $CDCl_3$) δ 7.47 (m, 2H), 7.36 (m, 2H), 4.17 (d, J = 5.4 Hz, 4H), 1.84 (dt, J = 12.2, 5.9 Hz, 2H), 1.64 (m, 4H), 1.53 – 1.17 (m, 48H), 1.04 – 0.74 (m, 12H).^{13}C NMR (101 MHz, $CDCl_3$) δ 144.69, 131.52, 129.95, 125.85, 120.26, 76.33, 39.27, 32.02, 31.39, 31.09, 30.16, 29.79, 29.78, 29.77, 29.76, 29.47, 29.29, 27.07, 23.20, 22.78, 14.21, 14.19. (**Note**: some peaks in ^{13}C NMR spectrum overlap).

Compound 2.14: the procedure follows general procedure for the stanyllation of 4,8-bis(alkyloxy)benzo[1,2-b:4,5-b']dithiophene (BDT) with 94% yield. ^{1}H NMR (400 MHz, $CDCl_3$) δ 7.69 – 7.41 (m, 2H), 4.18 (t, J = 4.9 Hz, 4H), 1.89 – 1.74 (m, 2H), 1.66 (m, 4H), 1.47 – 1.18 (m, 48H), 0.90 (m, 12H), 0.67 – 0.24 (m, 18H).^{13}C NMR (101 MHz, $CDCl_3$) δ 143.27, 140.32, 133.91, 132.84, 127.99, 75.78, 39.24, 31.98, 31.47, 31.16, 30.24, 29.83, 29.81, 29.79, 29.72, 29.43, 29.30, 27.14, 23.78, 22.56, 14.95. (**Note**: some peaks in ^{13}C NMR spectrum overlap).

Attempted synthesis of the β-branch alcohols:

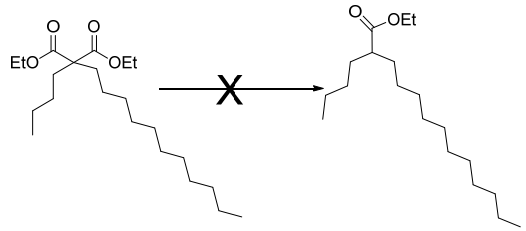

a: NaCl,DMSO,160^{O}C,overnight

b: NaBr,DMSO,160^{O}C,overnight

c: LiBr,DMSO,160^{O}C,overnight

For the alcohols synthesis, several methods were tried, the ester group is not easy to removed after several experiment (see conditions).

Condition a: A solution of diethyl 2-butyl-2-undecylmalonate (3g, 8.1 mmol), NaCl (1.89 g, 32.4 mmol) and water (0.73 mL, 40.5 mmol) in DMSO (50 mL) was heated with stirring at 160°C for overnight. The reaction was checked by TLC; messy product was formed.

Condition b: A solution of diethyl 2-butyl-2-undecylmalonate (3g, 8.1 mmol), NaBr (3.33 g, 32.4 mmol) and water (0.73 mL, 40.5 mmol) in DMSO (50 mL) was heated with stirring at 160°C for overnight. The reaction was checked by TLC; messy product was formed.

Condition c: A solution of diethyl 2-butyl-2-undecylmalonate (3g, 8.1 mmol), LiBr (2.81 g, 32.4 mmol) and water (0.73 mL, 40.5 mmol) in DMSO (50 mL) was heated with stirring at 160°C for overnight. The reaction was checked by TLC; messy product was formed.

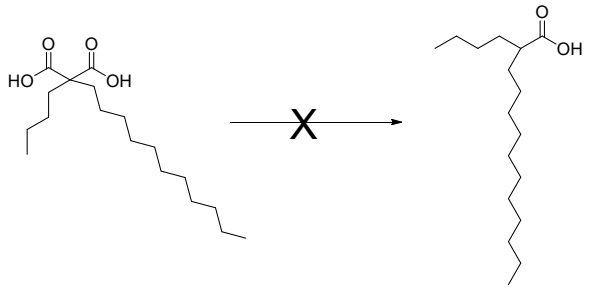

a: concentrated HCl,reflux,overnight

b: CH_3COOH,H_2SO_4,reflux,overnight

Then I have tried remove one acid group under acid conditions, sees it did not work.

Condition a: A solution of diethyl 2-butyl-2-undecylmalonic acid (2 g, 6.4 mmol), in concentrated HCl (50 mL) was heated to reflux for overnight. The reaction was checked by TLC; no desired compound was detected.

Condition b: A solution of diethyl 2-butyl-2-undecylmalonic acid (2 g, 6.4 mmol), in acetic acid (50 mL) and concentrated H_2SO_4(20 mL) was heated to reflux for overnight. The reaction was checked by TLC; no desired compound was detected.

General procedure for the polymerization:

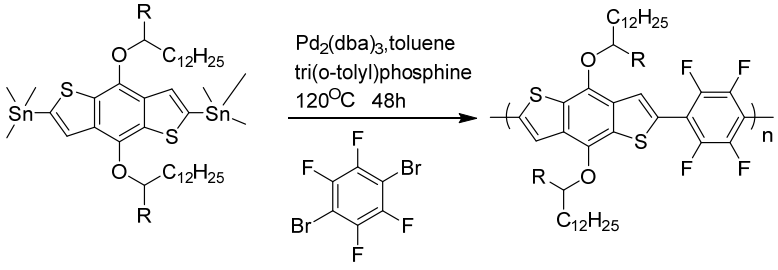

PBDTTFB-αC8 R: C_8H_{17}
PBDTTFB-αC7 R: C_7H_{15}
PBDTTFB-αC6 R: C_6H_{13}
PBDTTFB-αC5 R: C_5H_{11}
PBDTTFB-αC4 R: C_4H_9
PBDTTFB-αC3 R: C_3H_7
PBDTTFB-αC1 R: CH_3

To an air free flask containing the two monomers (0.2 mmol each) was added a mixture of $Pd_2(dba)_3$ and tri(o-tolyl)-phosphine (1:8 molar ratio between $Pd_2(dba)_3$ and tri(o-tolyl)-phosphine: 0.03% Pd loading) under inert atmosphere. After 3 pump/purge cycles of reduced pressure and refilling with N_2, anhydrous, degassed Toluene (4 ml) was added via syringe and the vessel was sealed and its contents stirred vigorously in a 120 °C oil bath for 48 hours. After polymerization, the reaction mixture was dripped into 100 ml vigorously solvent (MeOH: HCl=100ml: 5ml) to give precipitate, which is then collected by thimble and Soxhlet extraction with acetone, 3-pentantone, pentane (hexane) and $CHCl_3$ (depends

on the solubility). For polymer molecular weight determination, polymer samples were dissolved in HPLC grade $CHCl_3$ at a concentration of 0.5 mg/ml, filtering through a 0.2 μm PVDF filter. Gel permeation chromatography (GPC) was performed with HPLC grade $CHCl_3$ eluant at 1.0 mL/min. The apparent molecular weights and polydispersities (M_w/M_n) were determined with a calibration based on linear polystyrene standards using Empower software from Waters.

PBDTTFB-αC8: Yield 74%. This was prepared following the general procedure for polymerization. Due to very easy solubility in Soxhlet extraction only used methanol and acetone. Then purified polymer using pentane recrystallization. After dried in vacuum polymer PBDTTFB-αC8 obtained as purple solid. M_n: 16.9 kDa, PDI: 1.31.

PBDTTFB-αC7: Yield 72%. This was prepared following the general procedure for polymerization. Due to very easy solubility in Soxhlet extraction only used methanol and acetone. Then purified polymer using pentane recrystallization. After dried in vacuum polymer PBDTTFB-αC7 obtained as purple solid. M_n: 26.9 kDa, PDI: 1.35.

PBDTTFB-αC6: Yield 64%. This was prepared following the general procedure for polymerization. Due to very easy solubility in Soxhlet extraction only used methanol and acetone. Then purified polymer using pentane recrystallization. After dried in vacuum polymer PBDTTFB-αC6 obtained as purple solid. M_n: 5.4 kDa, PDI: 1.92.

PBDTTFB-αC5: Yield 74%. This was prepared following the general procedure for polymerization. Due to very easy solubility in Soxhlet extraction only used methanol and acetone. Then purified polymer using pentane recrystallization. After dried in vacuum polymer PBDTTFB-αC5 obtained as purple solid. M_n: 17.8 kDa, PDI: 1.61.

PBDTTFB-αC4: Yield 60%. This was prepared following the general procedure for polymerization. Due to very easy solubility in Soxhlet extraction only used methanol and acetone. Then purified polymer using pentane recrystallization. After dried in vacuum polymer PBDTTFB-αC4 obtained as red solid. M_n: 11.1 kDa, PDI: 1.51.

PBDTTFB-αC3: Yield 78%. This was prepared following the general procedure for polymerization and purified by sequential Soxhlet extraction using methanol, acetone, hexane and chloroform as the solvents. After dried in vacuum polymer PBDTTFB-αC3 obtained as red solid. Molecular weight was not available due to the low solubility in $CHCl_3$.

PBDTTFB-αC1: Yield 84%. This was prepared following the general procedure for polymerization and purified by sequential Soxhlet extraction using methanol, acetone, hexane and chloroform as the solvents. After dried in vacuum polymer PBDTTFB-αC1 obtained as red solid. Molecular weight was not available due to the low solubility in $CHCl_3$.

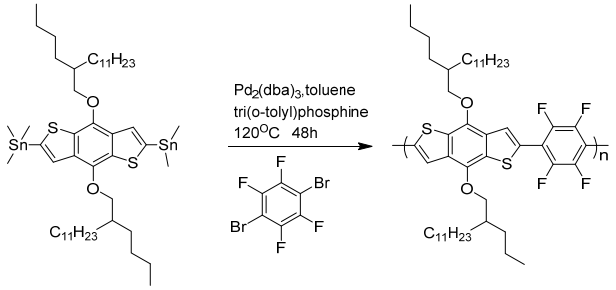

PBDTTFB - βC4

PBDTTFB-βC4: Yield 70%. This was prepared following the general procedure for polymerization and purified by sequential Soxhlet extraction using methanol, acetone, hexane and chloroform as the solvents. After dried in vacuum polymer PBDTTFB-βC4

obtained as red solid. Molecular weight was not available due to the low solubility in $CHCl_3$.

6.3 Synthesis Section of Chapter 3

Synthesis of N-alkyl derivatives of thieno[3,4-c]pyrrole- 4,6-dione

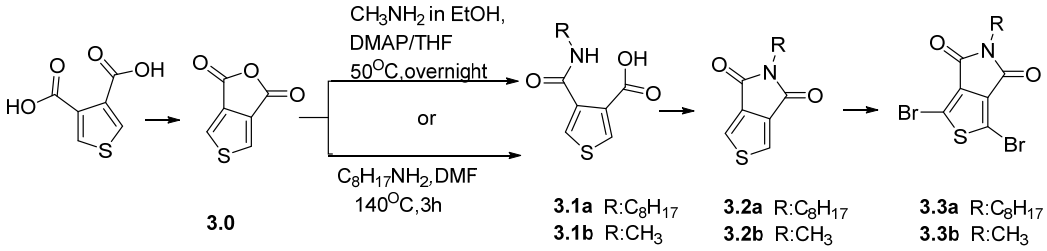

Thiophene 3,4-dicarboxylic acid was purchased from Ark Pharm. 5-methylthieno[3,4-c]pyrrole-4,6-dione and 1,3-dibromo-5-methylthieno[3, 4-c]pyrrole-4, 6-dione (3.3b) were prepared according to modified literature procedures (see below).

Synthesis of thiophene 3,4-dicarboxylic acid anhydride 3.0: A solution of thiophene-3,4-dicarboxylic acid (1.99g, 11.6 mmol) in acetic anhydride (50 mL) was stirred at 140 ºC overnight. The solvent was removed by distillation under vacuum and the crude product was used for the next step without any purification.

Synthesis of 3.1a. The brown solid (assuming 11.6 mmol) was dissolved in DMF (20 mL) then 1.2 equiv of n-octylamine (1.8 g, 13.92 mmol) was added and the mixture was heated to 140 ºC for 3 h. The reaction mixture was cooled down and the solution was poured in to ice water, filtered to get the brown soild and washed by water, which is used for next step without further purification.

Synthesis of 3.1b. A solution of thiophene-3,4-dicarboxylic acid (1.99g, 11.6 mmol) in acetic anhydride (50 mL) was stirred at 140 ºC overnight. The solvent was removed and the crude product was used for the next step without any purification. The brown solid (assuming 11.6 mmol) was dissolved in THF (40 mL) then 1.2 equiv of n-methylamine in ethnol(13.92 mmol, 1.75ml, 33%weight), DMAP (283mg, 2.32 mmol) was added and the mixture was heated to 50 ºC for overnight. The solvent was removed and get the brown solid, which is used for next step without further purification.

General procedure for synthesis of 3.2:

The crude solid was dissolved in thionyl chloride (40 mL) and the mixture was refluxed at 80 ºC for 4 h. After the removal of the volatiles, the crude product was purified by column chromatography.

Synthesis of 5-octylthieno[3, 4-c]pyrrole-4, 6-dione 3.2a: Follow the general procedure, the crude product was purified by column chromatography using (hexane/DCM: 1/1 to 1/2) as the eluent to afford the title product as a white solid (1.3g, 42.3%, 3 steps). ^{1}H NMR (400 MHz, $CDCl_3$) δ 7.80 (d, J = 0.9 Hz, 2H), 3.73 – 3.45 (m, 2H), 1.77 – 1.52 (m, 2H), 1.29 (m, 10H), 0.95 – 0.80 (m,3H). ^{13}C NMR (101 MHz, $CDCl_3$) δ 157.72, 132.23, 110.26, 36.23, 29.15, 26.48, 25.64, 24.18, 19.99, 11.45. (**Note**: some peaks in ^{13}C NMR spectrum overlap).

Synthesis of 5-methylthieno[3, 4-c]pyrrole-4, 6-dione 3.2b: Follow the general procedure, the crude product was purified by column chromatography (hexane/DCM: 1/1 to DCM) as the eluent to afford the title product as a white solid (980mg, 50.6%, 3 steps). ^{1}H NMR (400 MHz, CDCl3) δ 7.80 (d, J = 0.8 Hz, 1H), 3.11 (s, 1H). ^{13}C NMR (101 MHz, CDCl3) δ 174.07, 147.98, 136.94, 35.75.

Synthesis of 1,3-dibromo-5-octylthieno[3,4-c]pyrrole-4,6-dione 3.3a:

5-octylthieno[3,4-c]pyrrole-4,6-dione (1.01g, 3.8mmmol) was used as starting materials, dissolved in a mixture of sulfuric acid (7.0mL) and trifluoroacetic acid (20 mL). While stirring, NBS (2.35 g, 13.2 mmol) was added in five portions to the solution and the reaction mixture was stirred at room temperature overnight. The brown-red solution was diluted with water (50 mL). The mixture was extracted with dichloromethane. The organic phase was dried over Na_2SO_4 and the solvent was evaporated under reduced pressure. The crude product was purified by column chromatography (hexane/DCM: 1/1 to DCM) as the eluent to afford the title product as white solid (1.31 g, 82%). ^{1}H NMR (400 MHz, $CDCl_3$) δ 3.68 – 3.51 (m, 2H), 1.69 – 1.55 (m, 2H), 1.41 – 1.11 (m, 10H), 0.98 – 0.64 (m, 3H). ^{13}C NMR (101 MHz, $CDCl_3$) δ 160.19, 134.78, 112.78, 38.77, 31.71, 29.04, 28.18, 26.66, 22.56, 14.02. (**Note**: some peaks in ^{13}C NMR spectrum overlap).

Synthesis of 1, 3-dibromo-5-methylthieno[3,4-c]pyrrole-4,6-dione 3.3b:

Follow the same procedure of synthesis 3.3a, using 5-methylthieno[3,4-c]pyrrole-4,6-dione (735mg, 4.4 mmol) as staring materials. The crude product was purified by column chromatography (hexane/DCM: 1/1 to DCM) to afford the title product as white needles (1.16 g, 80%). ^{1}H NMR (400 MHz, $CDCl_3$) δ 3.09 (s, 3H). ^{13}C NMR (101 MHz, $CDCl_3$) δ 160.33, 134.74, 113.03, 24.67.

General procedure for the polymerization:

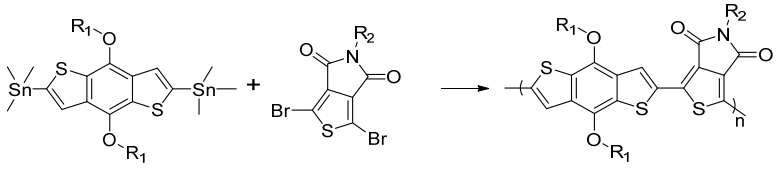

4,8-bis(alkyloxy)benzo[1,2-b:4,5-b']dithiophene-2,6-diyl)bis(trimethylstannane), (0.2 mmol), N-alkyl derivatives of thieno[3,4-c]pyrrole- 4,6-dione (0.2 mmol), tris(dibenzylideneacetone)dipalladium (2.75 mg, 3.0 μmol) and tri-o-tolylphosphine (7.30 mg, 24.0 μmol) were combined in a 10 mL reactor. Then, 4.0 mL of dry toluene was added to the reaction flask and the reaction mixture was stirred for 48 h at 120 °C. The mixture was then slowly precipitated into the mixture of methanol (100 mL) and concentrated HCl (5 mL). The precipitate was filtered through a Soxhlet thimble and purified via Soxhlet extraction with methanol, acetone, room temperature MEK (methyl ethyl ketone), high temperature MEK, 3-pentanone and hexane (depends on solubility).

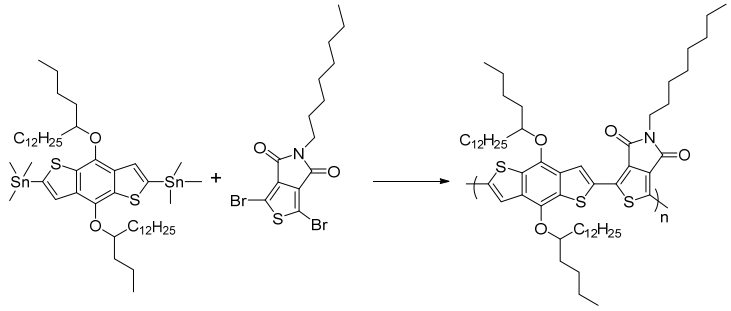

PBDTTPD-αC8: Yield 85%. This was prepared following the general procedure for polymerization and purified by sequential Soxhlet extraction using methanol, acetone, MEK (methyl ethyl ketone) and 3-pentanone as the solvents. After dried in vacuum polymer obtained as blue solid.

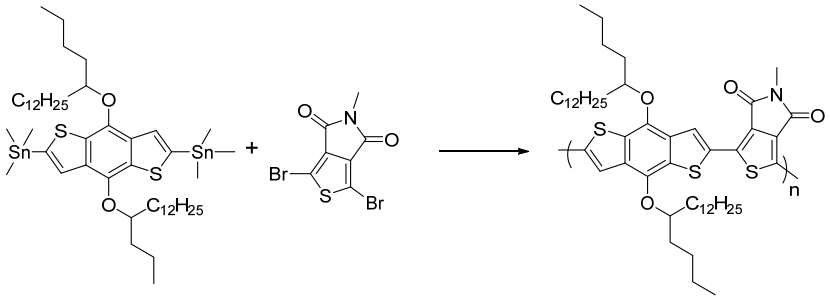

PBDTTPD-αC1: Yield 70%. This was prepared following the general procedure for polymerization and purified by sequential Soxhlet extraction using methanol, acetone, MEK (methyl ethyl ketone) as the solvents. After dried in vacuum polymer obtained as blue solid.

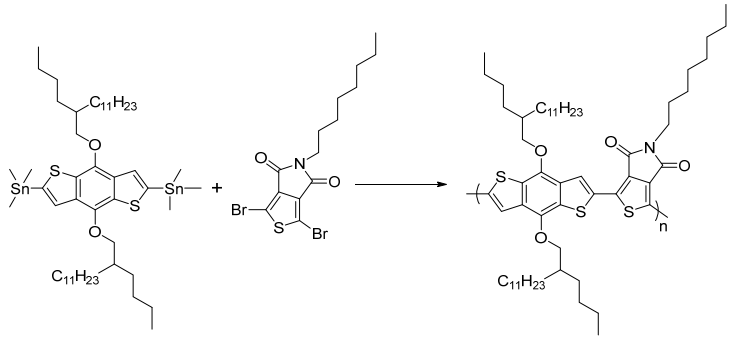

PBDTTPD-βC8: Yield 95%. This was prepared following the general procedure for polymerization and purified by sequential Soxhlet extraction using methanol, acetone, MEK (methyl ethyl ketone) and hexane as the solvents. After dried in vacuum polymer obtained as blue solid.

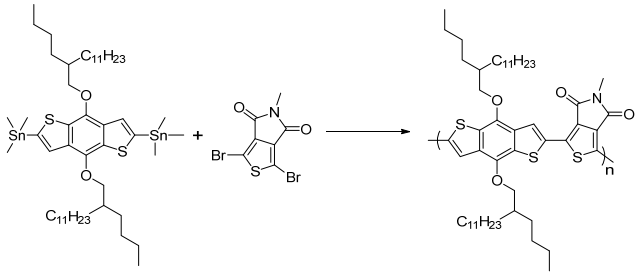

PBDTTPD-βC1: Yield 88%. This was prepared following the general procedure for polymerization and purified by sequential Soxhlet extraction using methanol, acetone, MEK (methyl ethyl ketone), 3-pentanone and hexane as the solvents. After dried in vacuum polymer obtained as blue solid.

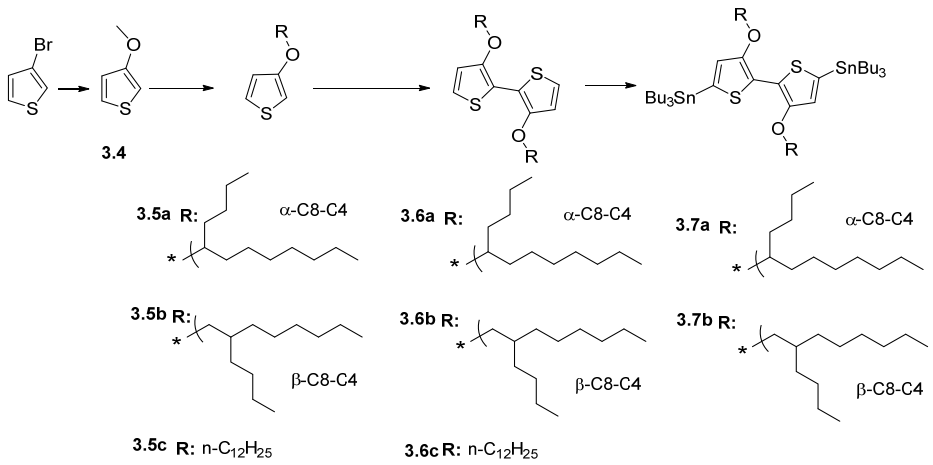

3-methoxythiophene 3.4: Approximately (65.2g, 0.4 mol) of 3-bromothiophene was added 100 mL of methanol were added to 200 mL of NMP, and cooling to 0 °C. Then sodium methoxide (25.9 g, 0.48 mmol) and CuBr (7.6 g, 0.04 mmol) were added to the solution. This solution was stirred at 110 °C for 24 hrs. Water (2.5 L) was added to the reaction mixture, then adjust the pH to 7 with HCl solution. The product was extracted into hexane, dried over Na_2SO_4 and the solvent was removed by rotary evaporation to afford the product as a yellow oil, distill under vacuum to give colorless oil about 35.0g (yield 76.7%). ^{1}H NMR (DMSO-d6, 400 MHz), δ(ppm): 6.94 (s, 1H), 6.32 (d, 1H), 6.09 (d, 1H), 3.29 (s, 3H).

General procedure for synthesis of 3-alkoxy-thiophene 3.5: About (3.42 g, 30 mmol) of 3-methoxythiophene and (60 mmol, 2.0 eq) of alcohol were added to 50 mL of toluene containing (0.36 g, 3 mmol) of $NaHSO_4$. The solution was refluxed at 115 °C for overnight, and then mixed with 100 mL of hexane. Afterward, the organic phase was collected and washed with saturated brine. The hexane was removed under vacuum, and the product was purified by silica gel column chromatography using hexane as the eluent to obtain product.

Compound 3.5a: Synthesis follow the general procedure, the crude product was purified to obtain product as colorless oil (6.44 g, 80.4%). ^{1}H NMR (400 MHz, $CDCl_3$) δ 7.14 (d, J =

2.9 Hz, 1H), 6.73 (d, *J* = 3.6 Hz, 1H), 6.20 (s, 1H), 3.99 (t, *J* = 26.1 Hz, 1H), 2.14 (d, *J* = 25.0 Hz, 2H), 1.80 – 1.08 (m, 23H).

Compound 3.5b: Synthesis follow the general procedure, the crude product was purified to obtain product as colorless oil (6.0 g, 74.5%). ^{1}H NMR (400 MHz, $CDCl_3$) δ 7.20 – 7.11 (dd, J = 5.6, 3.2 Hz,1H), 6.80 – 6.67 (dd, J = 5.6, 1.5 Hz ,1H), 6.21 (dd, J = 3.2, 1.5 Hz, 1H), 3.81 (d, J = 5.7 Hz, 2H), 1.74 (dq, J = 12.0, 5.7 Hz, 1H), 1.45 – 1.21 (m, 16H), 0.95 – 0.82 (m, 6H). ^{13}C NMR (101 MHz, $CDCl_3$) δ 158.35, 124.33, 119.65, 96.74, 73.11, 38.05, 31.97, 31.44, 31.13, 29.76, 29.14, 26.90, 23.12, 22.74, 14.13.

Compound 3.5c: Synthesis follow the general procedure, the crude product was purified to obtain product as white solid (7.0 g, 87.1%). ^{1}H NMR (400 MHz, $CDCl_3$) δ 7.18 – 7.09 (m, 1H), 6.78 – 6.66 (m, 1H), 6.20 (dd, *J* = 3.1, 1.6 Hz, 1H), 3.92 (t, *J* = 6.6 Hz, 2H), 1.85 – 1.67 (m, 2H), 1.48 – 1.17 (m, 18H), 0.86 (dd, *J* = 8.1, 5.7 Hz, 3H). ^{13}C NMR (101 MHz, $CDCl_3$) δ 158.11, 124.39, 119.51, 96.85, 77.39, 77.07, 76.76, 70.19, 32.02, 29.75, 29.71, 29.69, 29.51, 29.47, 29.38, 26.97, 26.15, 22.78, 14.16.

General procedure for synthesis of 3,3'-dialkoxy-2,2'-bithiophene 3.6:

n-BuLi (11.0 mmol, 2.5M, 1.1 eq.) was added dropwise into a solution of 3-(R-oxy)thiophene (1.0 eq. 10 mmol) in hexanes(30 mL) at -20 °C and was stirred for another 1 h at room temperature under nitrogen. This solution was added directly to freshly made $MgBr_2$ (2.0 eq.) solution in one portion at -20 °C (see details down). After that, the mixture solution was heated to reflux for 2h, then cooling down to room temperature. Upon stirring for an additional 1h, 1, 2-dibromoethane (1.0 eq.) and $NiCl_2$dppp (5 mol%) were added sequentially into the resulting suspension. Then the solution was stirred for overnight

at room temperature, the reaction was quenched by water, and extracted by hexanes. The organic layer was dried over Na_2SO_4. The hexane was removed under vacuum; the residue was purified by column chromatography (hexanes) to obtain product.

$MgBr_2$ synthesis: A solution of 1, 2-dibromoethane (2.2 eq 2.2 mmol) in anhydrous THF (50 ml) was added drop by drop to a flask with Mg powder (3.0 eq. 3.0 mmol) and a stir bar under nitrogen. This reaction generated a lot of bubbles. Upon completion of addition, the resulted suspension was stirred for another 2 h under reflux. Then lower the reaction temperature to room temperature, generated a lot of precipitation.

Compound 3.6a: Synthesis follow the general procedure, the crude product was purified to obtain product as colorless oil (60.4%). ^{1}H NMR (400 MHz, $CDCl_3$) δ 7.04 (d, J = 5.6 Hz, 2H), 6.78 (d, J = 5.6 Hz, 2H), 4.21 (p, J = 5.8 Hz, 2H), 1.81 – 1.59 (m, 8H), 1.50 – 1.18 (m, 28H), 0.88 (q, J = 7.1 Hz, 12H). ^{13}C NMR (101 MHz, $CDCl_3$) δ 148.55, 118.66, 113.46, 112.03, 79.38, 31.59, 31.34, 29.22, 27.10, 26.63, 25.03, 22.85, 20.22, 20.06, 11.50, 11.46.

Compound 3.6b: Synthesis follow the general procedure, the crude product was purified to obtain product as colorless oil (59.2%). ^{1}H NMR (400 MHz, $CDCl_3$) δ 7.07 (d, J = 5.5 Hz, 2H), 6.84 (d, J = 5.6 Hz, 2H), 4.00 (d, J = 5.4 Hz, 4H), 1.90 – 1.73 (m, 2H), 1.63 – 1.19 (m, 32H), 0.91 – 0.80 (m, 12H). ^{13}C NMR (101 MHz, $CDCl_3$) δ 152.06, 121.35, 115.52, 113.58, 74.29, 38.50, 31.95, 31.37, 31.07, 29.76, 29.19, 26.93, 23.14, 22.76, 14.17.

Compound 3.6c: Synthesis follow the general procedure, the crude product was purified to obtain product as colorless oil (63.2%). ^{1}H NMR (400 MHz, $CDCl_3$) δ 7.07 (d, *J* = 5.6 Hz, 2H), 6.83 (d, *J* = 5.6 Hz, 2H), 4.09 (s, 4H), 1.84 (dd, *J* = 8.3, 6.8 Hz, 4H), 1.55 – 1.46 (m, 4H), 1.28 (d, *J* = 14.8 Hz, 32H), 0.88 (t, *J* = 6.9 Hz, 6H). ^{13}C NMR (101 MHz, $CDCl_3$) δ

151.90, 121.55, 116.01, 114.08, 71.96, 31.89, 29.67, 29.64, 29.62, 29.58, 29.53, 29.33, 26.02, 22.66, 14.09.

General procedure for the stanyllation of 3,3'-dialkoxy-2,2'-bithiophene:

Compound 3.6 (1.45 mmol) was solubilized in 15 mL of dry THF under inert atmosphere. The mixture was cooled down to -78 °C using a dry ice-acetone bath, and 1.3 mL of n-butyllithium (3.2 mmol, 2.5 M in n-hexane) was added dropwise. After being stirred at -78 °C for 1 h, the solution was slowly warmed up to room temperature and stirred for 30 min. The mixture was cooled in the dry ice-acetone bath, and tributyltin chloride (3.63 mmol) was added in one portion. The reaction mixture was stirred overnight at room temperature, then poured into 100 mL of cool water, and was extracted with hexane. The organic layers were combined, washed with brine, dried over anhydrous Na_2SO_4 and concentrated under vacuum, which was purified by column chromatography (aluminum B was basic with NEt_3, hexanes as eluent) to give product as yellow oil.

Compound 3.7a: Synthesis follow the general procedure, the crude product was purified to obtain product as colorless oil about 1.32g (81.6%). ^{1}H NMR (400 MHz, $CDCl_3$) δ 6.89 – 6.56 (m, 2H), 4.33 – 4.03 (m, 2H), 1.82 – 1.51 (m, 20H), 1.49 – 1.17 (m, 44H), 1.11 – 1.03 (m, 10H), 0.92 – 0.81 (m, 30H). ^{13}C NMR (101 MHz, $CDCl_3$) δ 152.86, 131.78, 123.83, 120.66, 81.55, 34.22, 33.88, 31.84, 30.83, 29.78, 29.25, 29.17, 27.79, 26.92, 25.44, 22.81, 22.61, 14.03, 13.99, 13.63, 10.71.

Compound 3.7b: Synthesis follow the general procedure, the crude product was purified to obtain product as colorless oil 1.44g (89.3%). ^{1}H NMR (400 MHz, $CDCl_3$) δ 6.93 – 6.62 (m,

2H), 3.99 (d, J = 5.2 Hz, 4H), 1.90 – 1.70 (m, 2H), 1.66 – 1.39 (m, 22H), 1.38-1.22 (m, 36H), 1.11 – 1.04 (m, 10H), 0.93 – 0.81 (m, 30H). ^{13}C NMR (101 MHz, $CDCl_3$) δ 151.21, 129.59, 120.39, 116.97, 71.46, 35.98, 29.34, 28.80, 28.50, 28.27, 27.17, 26.42, 25.02 – 24.53, 24.37, 20.51, 20.09, 11.53, 11.48, 11.04, 8.11.

General procedure for the polymerization:

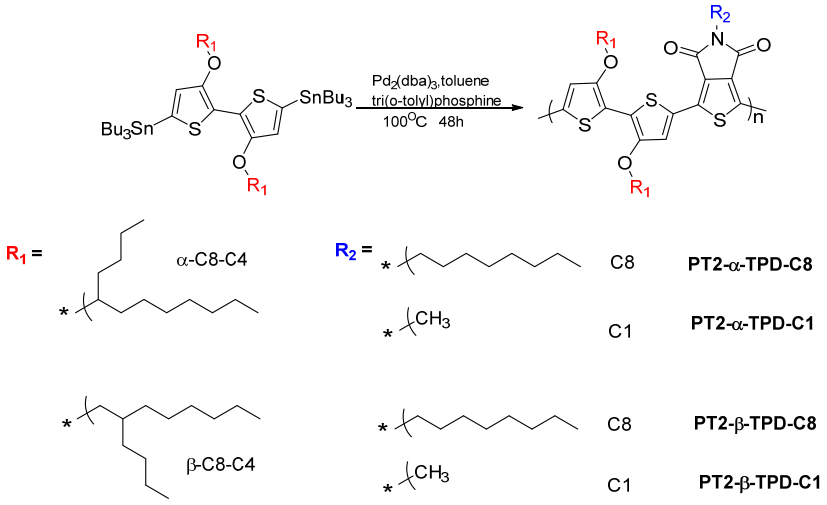

(3,3'-dialkoxy-[2,2'-bithiophene]-5,5'-diyl)bis(tributylstannane), (0.2 mmol), N-alkyl of thieno[3,4-c]pyrrole- 4,6-dione (0.2 mmol), tris(dibenzylideneacetone)dipalladium (2.75 mg, 3.0 µmol) and tri-o-tolylphosphine (7.30 mg, 24.0 µmol) were combined in a 10 mL reactor. Then, 4.0 mL of dry toluene was added to the reaction flask and the reaction mixture was stirred for 48 h at 120 °C. The mixture was then slowly precipitated into the mixture of methanol (100 mL) and concentrated HCl (5 mL). The precipitate was filtered through a Soxhlet thimble and purified via Soxhlet extraction with acetone, hexane and DCM (depends on solubility).

PT2TPD-αC1 Yield 75%. This was prepared following the general procedure for polymerization and purified by sequential Soxhlet extraction using acetone, hexane and DCM as the solvents. After dried in vacuum polymer obtained as dark blue solid.

PT2TPD-αC8 Yield 89%. This was prepared following the general procedure for polymerization and purified by sequential Soxhlet extraction using acetone, hexane (room temperature and high temperature) and DCM as the solvents. After dried in vacuum polymer obtained as dark blue solid.

PT2TPD-βC1 Yield 85%. This was prepared following the general procedure for polymerization and purified by sequential Soxhlet extraction using acetone, hexane (room temperature and high temperature) as the solvents. After dried in vacuum polymer obtained as dark blue solid.

PT2TPD-βC8 Yield 83%. This was prepared following the general procedure for polymerization and purified by sequential Soxhlet extraction using acetone, hexane (room temperature and high temperature) as the solvents. After dried in vacuum polymer obtained as dark blue solid.

6.4 Synthesis Section of Chapter 4

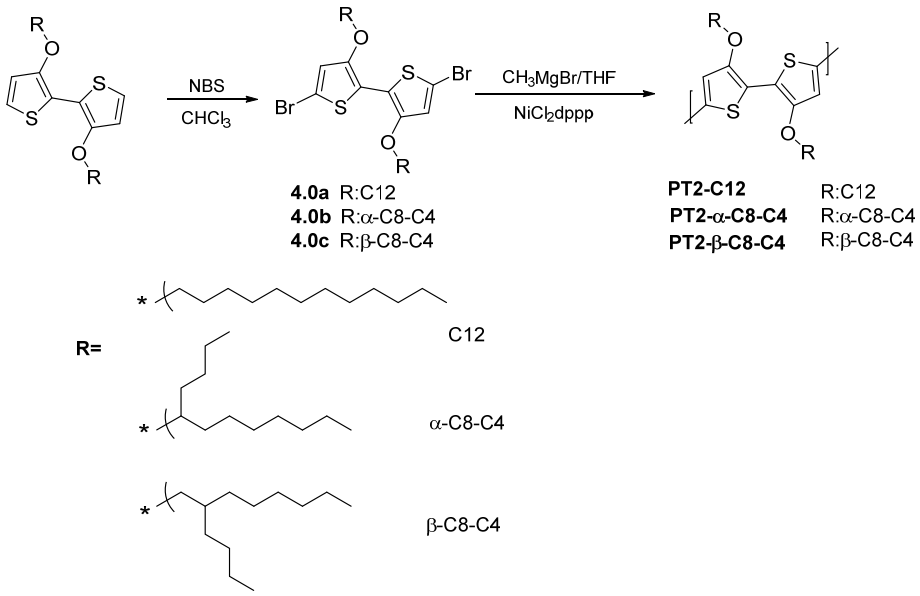

General procedure synthesis of 5,5'-dibromo-3,3'-dialkoxy-2,2'-bithiophene.

3,3'-dialkoxy-2,2'-bithiophene (2.5 mmol) was dissolved in a chloroform (20 mL) and cooling to -50 °C. While stirring, NBS (0.89 g, 5.0 mmol) was added in one portions to the solution and the reaction mixture was stirred for 0.5 hour, then raise to room temperature for 0.5 hour. The solution was diluted with water (50 mL). The mixture was extracted with dichloromethane. The organic phase was dried over Na_2SO_4 and the solvent was evaporated under reduced pressure. The crude product was purified by column chromatography (hexane to hexane/DCM: 10/1) to afford the title product as yellow oil.

Compound 4.0a: Synthesis follow the general procedure, the crude product was purified by column chromatography to afford the title product as yellow solid (81%).^{1}H NMR (400 MHz, $CDCl_3$) δ 6.81 (s, 2H), 4.03 (t, J = 6.6 Hz, 4H), 1.87 – 1.76 (m, 4H), 1.53 – 1.18 (m, 36H), 0.88 (t, J = 6.9 Hz, 6H). ^{13}C NMR (101 MHz, $CDCl_3$) δ 150.27, 118.99, 115.07, 109.88, 72.33, 31.90, 29.64, 29.61, 29.55, 29.50,

29.47, 29.33, 29.24, 25.89, 22.67, 14.10. HRMS: 690.1749 (M^+). Calcd for $C_{32}H_{52}O_2S_2Br_2$: 690.1775.

Compound 4.0b: Synthesis follow the general procedure, the crude product was purified to obtain product as colorless oil (90.4%). ^{1}H NMR (400 MHz, $CDCl_3$) δ 6.75 (s, 1H), 4.12 (m, 2H), 1.80 – 1.57 (m, 8H), 1.45 – 1.12 (m, 28H), 0.94 – 0.80 (m, 12H). ^{13}C NMR (101 MHz, $CDCl_3$) δ 149.58, 119.02, 115.60, 109.61, 82.79, 34.15, 33.85, 31.77, 29.59, 29.17, 27.58, 25.31, 22.73, 22.65, 14.09, 14.02. HRMS: 690.1749 (M^+). Calcd for $C_{32}H_{52}O_2S_2Br_2$: 690.1775.

Compound 4.0c: Synthesis follow the general procedure, the crude product was purified to obtain product as colorless oil (88.7%). ^{1}H NMR (400 MHz, $CDCl_3$) δ 6.82 (s, 2H), 3.93 (d, J = 4.3 Hz, 4H), 1.81 (dt, J = 11.9, 5.9 Hz, 2H), 1.61 – 1.18 (m, 32H), 1.00 – 0.71 (m, 12H). ^{13}C NMR (101 MHz, $CDCl_3$) δ 150.42, 118.70, 114.52, 109.61, 74.85, 38.27, 31.84, 31.21, 30.89, 29.64, 29.03, 26.77, 23.02, 22.68, 14.10. HRMS: 690.1749 (M^+). Calcd for $C_{32}H_{52}O_2S_2Br_2$: 690.1775.

General procedure for 3,3'-dialkoxy-2,2'-bithiophene homo-polymer synthesis:

The homopolymer under Grignard metathesis method. The process as follows: compound 4.0 treated with 1 eq. of methyl grignard reagent in THF under N_2, after reacted at room temperature for 0.5h, then raise to 70 ^{O}C for 2 hrs. After that, added Ni(dppp)Cl_2 as catalysts, heated to 70 ^{O}C for 24 hours. The polymers fractionated by Soxhlet extraction using acetone, methyl ethyl ketone, hexane and DCM (depends on the solubility).

PT2-α-C8-C4 Yield 75%. This was prepared following the general procedure for polymerization and purified by sequential Soxhlet extraction using acetone, MEK (methyl

ethyl ketone), hexane and DCM as the solvents. After dried in vacuum polymer obtained as dark blue solid.

PT2-β-C8-C4 Yield 65%. This was prepared following the general procedure for polymerization and purified by sequential Soxhlet extraction using acetone, MEK (methyl ethyl ketone) and hexane as the solvents. After dried in vacuum polymer obtained as dark blue solid.

PT2-C12 Yield 70%. This was prepared following the general procedure for polymerization and purified by sequential Soxhlet extraction using acetone, MEK (methyl ethyl ketone) and hexane as the solvents. After dried in vacuum polymer obtained as dark blue solid.

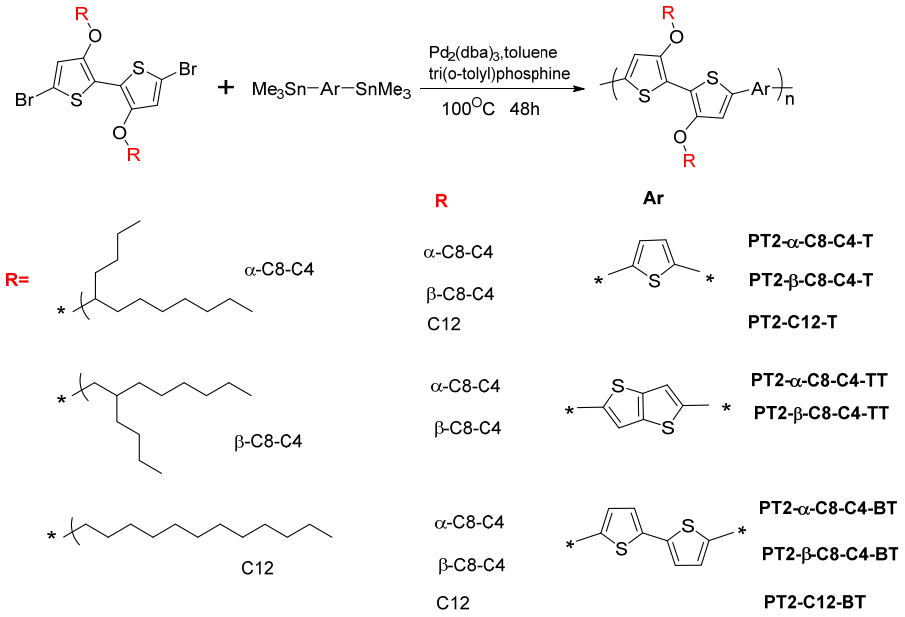

General procedure for polymer synthesis

5,5'-dibromo-3,3'-bis(R-oxy)-2,2'-bithiophene (0.2mmol), Ar-bis(trimethylstannane) (0.2 mmol), tris(dibenzyliden-eacetone)dipalladium (2.75 mg, 3.0 μmol) and tri-o-tolylphosphine (7.30 mg, 24.0 μmol) were combined in a 10 mL reactor. Then, 4.0 mL of dry toluene was added to the reaction flask and the reaction mixture was

stirred for 48 h at 100 °C. After polymerization, the resulting polymer was then slowly precipitated into the mixture of methanol (100 mL) and concentrated HCl (5 mL) to give precipitate. The precipitate was filtered through a Soxhlet thimble and purified via Soxhlet extraction with acetone, hexane, dichloromethane and chloroform (depends on soubility).

PT2-α-C8-C4-T Yield 95%. This was prepared following the general procedure for polymerization and purified by sequential Soxhlet extraction using acetone, hexane and DCM as the solvents. After dried in vacuum polymer obtained as dark blue solid.

PT2-β-C8-C4-T Yield 93%. This was prepared following the general procedure for polymerization and purified by sequential Soxhlet extraction using acetone, hexane and DCM as the solvents. After dried in vacuum polymer obtained as dark blue solid.

PT2-C12-T Yield 88%. This was prepared following the general procedure for polymerization and purified by sequential Soxhlet extraction using acetone, hexane and DCM (room temperature and high temperature) as the solvents. After dried in vacuum polymer obtained as dark blue solid.

PT2-α-C8-C4-TT Yield 85%. This was prepared following the general procedure for polymerization and purified by sequential Soxhlet extraction using acetone, hexane and DCM (room temperature and high temperature) as the solvents. After dried in vacuum polymer obtained as dark blue solid.

PT2-β-C8-C4-TT Yield 91%. This was prepared following the general procedure for polymerization and purified by sequential Soxhlet extraction using acetone, hexane, DCM and chloroform as the solvents. After dried in vacuum polymer obtained as dark blue solid.

PT2-α-C8-C4-BT Yield 95%. This was prepared following the general procedure for polymerization and purified by sequential Soxhlet extraction using acetone, hexane and DCM (room temperature and high temperature) as the solvents. After dried in vacuum polymer obtained as dark blue solid.

PT2-β-C8-C4-BT Yield 91%. This was prepared following the general procedure for polymerization and purified by sequential Soxhlet extraction using acetone, hexane, DCM and chloroform as the solvents. After dried in vacuum polymer obtained as dark blue solid.

PT2-C12-BT Yield 93%. This was prepared following the general procedure for polymerization and purified by sequential Soxhlet extraction using acetone, hexane, DCM and chloroform as the solvents. After dried in vacuum polymer obtained as dark blue solid.

For polymer molecular weight determination, polymer samples were dissolved in HPLC grade $CHCl_3$ at a concentration of 0.5 mg/ml, filtering through a 0.2 μm PVDF filter. Gel permeation chromatography (GPC) was performed with HPLC grade $CHCl_3$ eluant at 1.0 mL/min. The apparent molecular weights and polydispersities (M_w/M_n) were determined with a calibration based on linear polystyrene standards using Empower software from Waters.

6.5 Electrochemistry Measurements

DPV curves for Chapter 2: Polymer films (1mg/ml in $CHCl_3$) in tetra-n-butylammonium hexafluorophosphate solution (0.1 M in dry acetonitrile), 295 K, Scan rate = 50 mV. s^{-1} Corrected for Fc/Fc+.

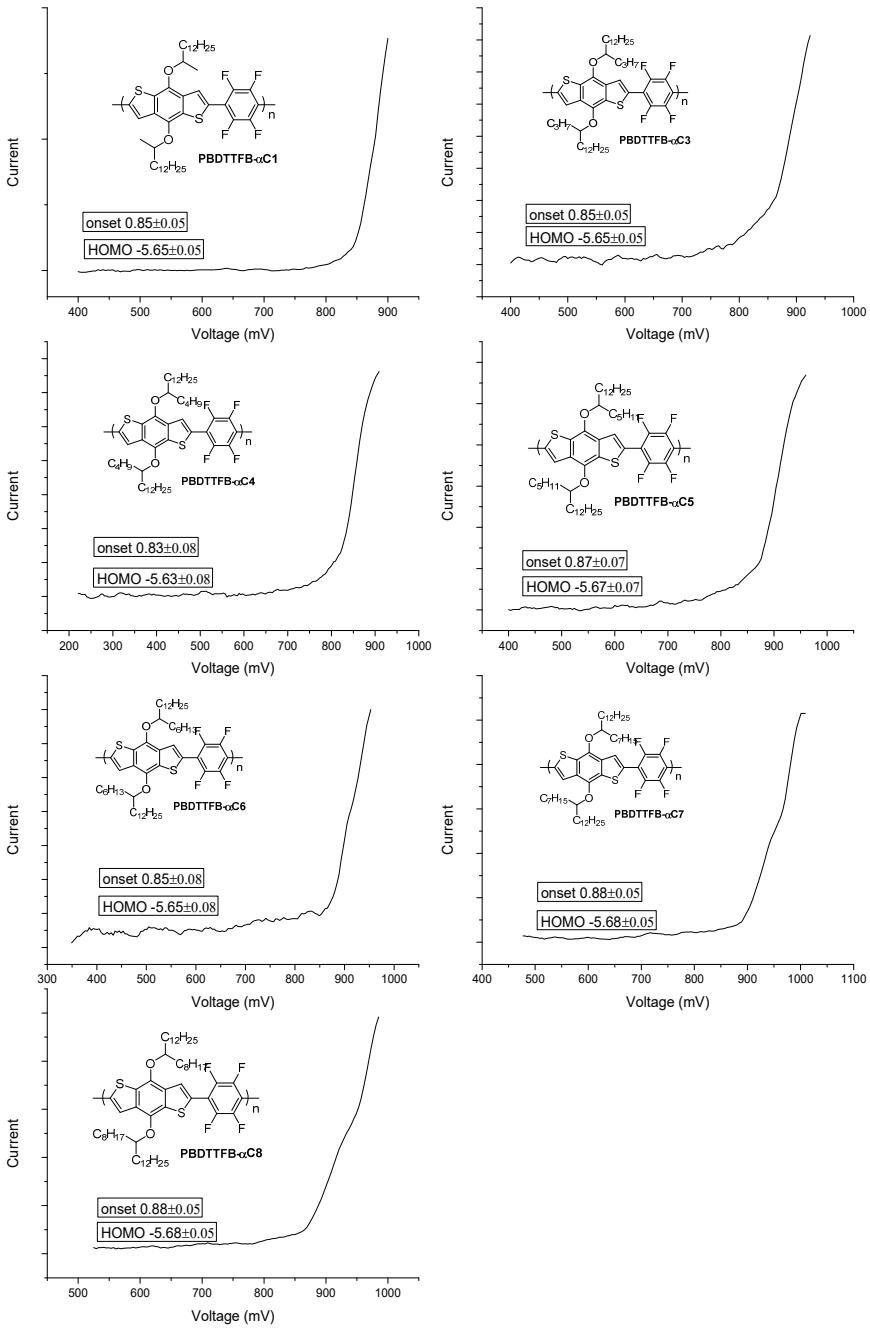

DPV curves for Chapter 3: Polymer films (1mg/ml in $CHCl_3$) in tetra-n-butylammonium hexafluorophosphate solution (0.1 M in dry acetonitrile), 295 K, Scan rate = 50 mV. s^{-1} Corrected for Fc/Fc+.

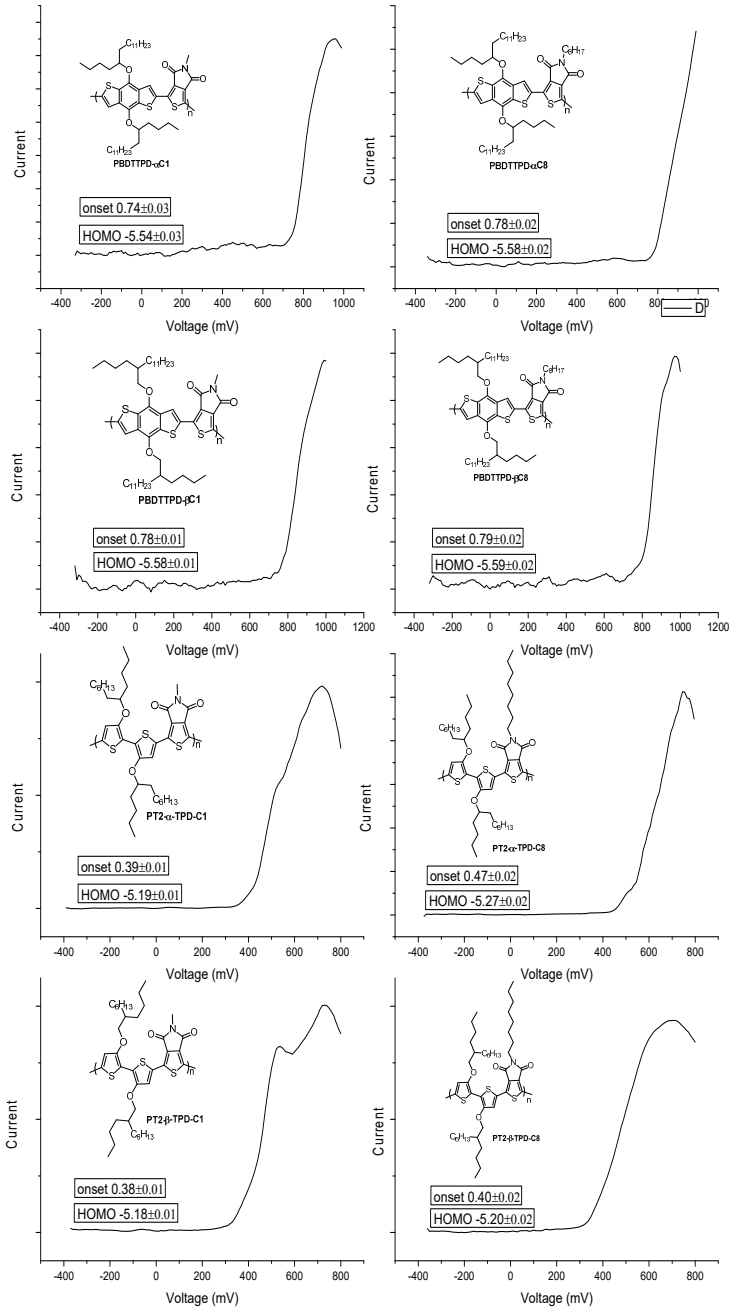

DPV curves for Chapter 4: Polymer films (1mg/ml in $CHCl_3$) in tetra-n-butylammonium hexafluorophosphate solution (0.1 M in dry acetonitrile), 295 K, Scan rate = 50 mV. s^{-1} Corrected for Fc/Fc+.

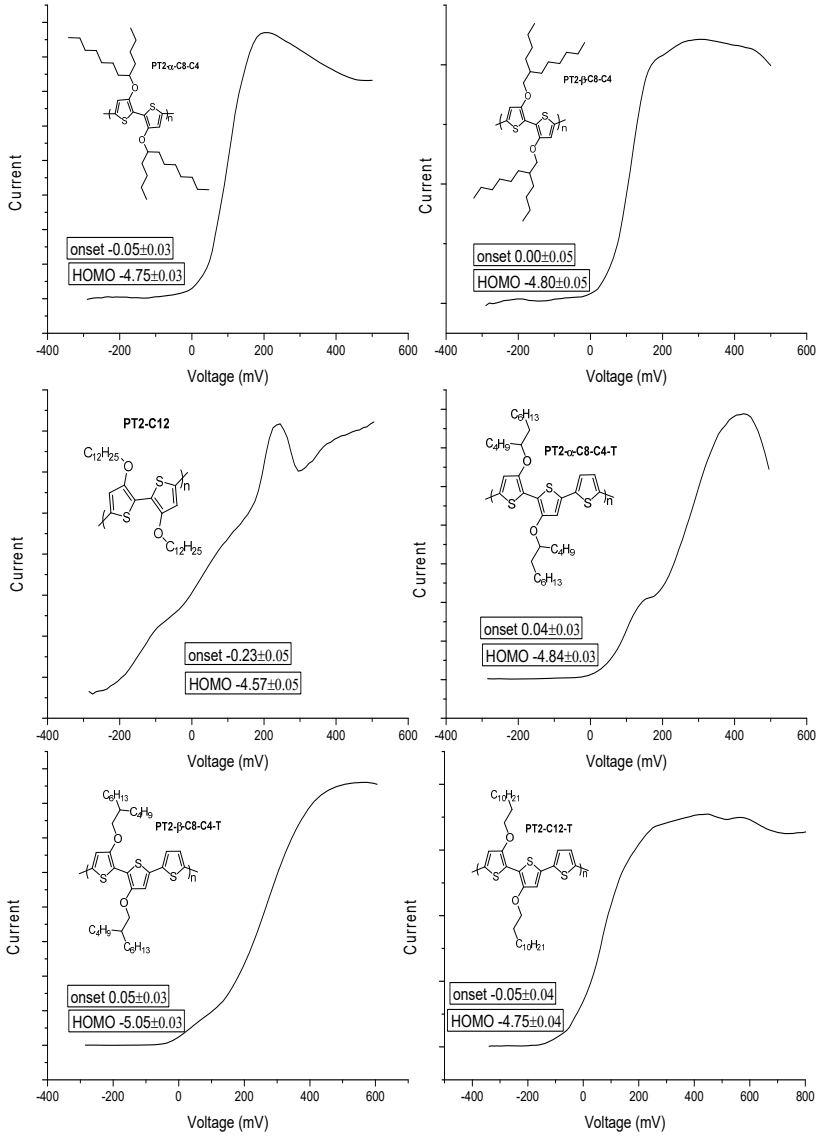

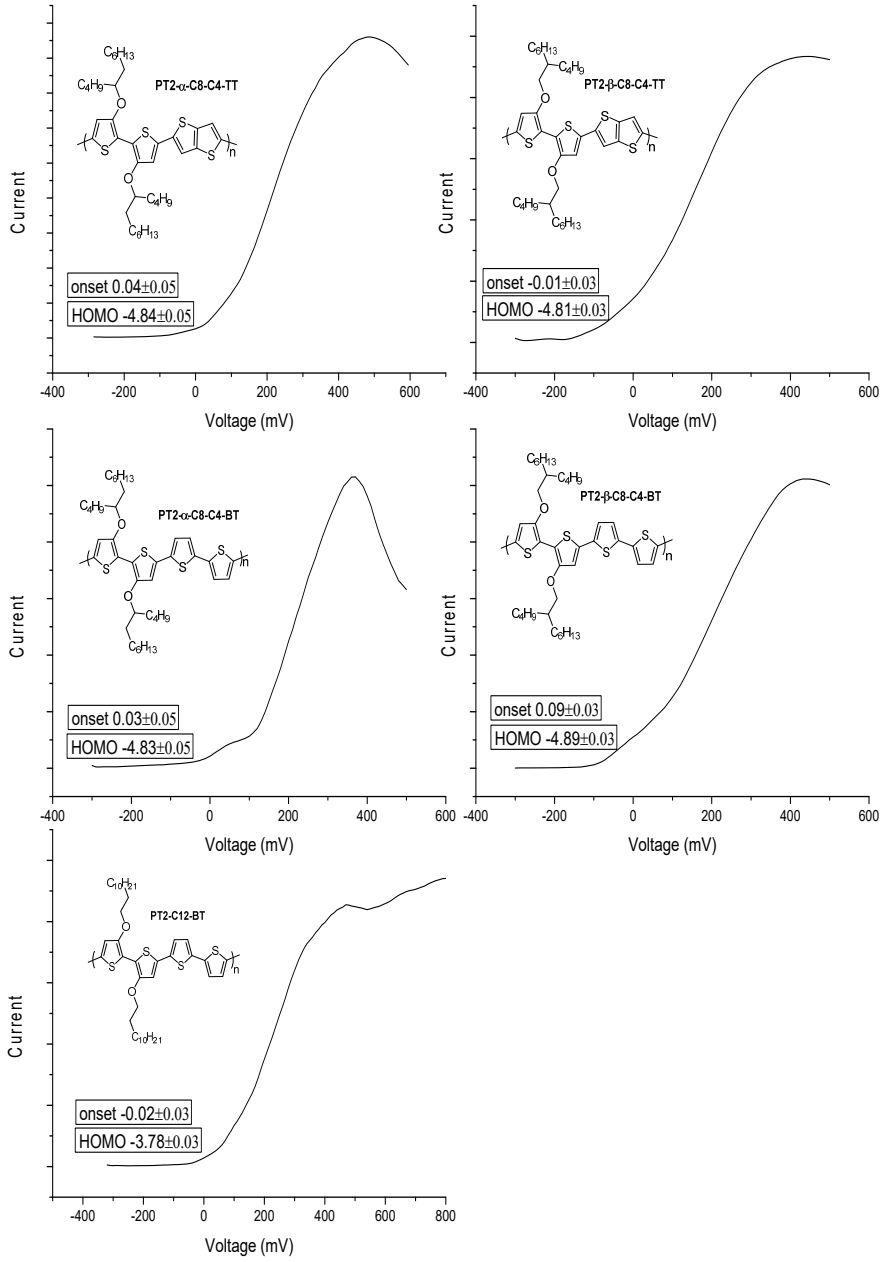
PT2-α-C8-C4-TT
onset 0.04±0.05
HOMO -4.84±0.05
PT2-β-C8-C4-TT
onset -0.01±0.03
HOMO -4.81±0.03
PT2-α-C8-C4-BT
onset 0.03±0.05
HOMO -4.83±0.05
PT2-β-C8-C4-BT
onset 0.09±0.03
HOMO -4.89±0.03
PT2-C12-BT
onset -0.02±0.03
HOMO -3.78±0.03
Current
Voltage (mV)

6.6 DSC Measurements

DSC curves for Chapter 2: test by DSC Q20 (heating rate = 10 ºC/ min, cooling rate = 5 ºC/ min, nitrogen purge). Here the small peak (C4, C6, C8) near 80 ºC (heating process) and 60 ºC (cooling process) came from instrument (verified by blank test).

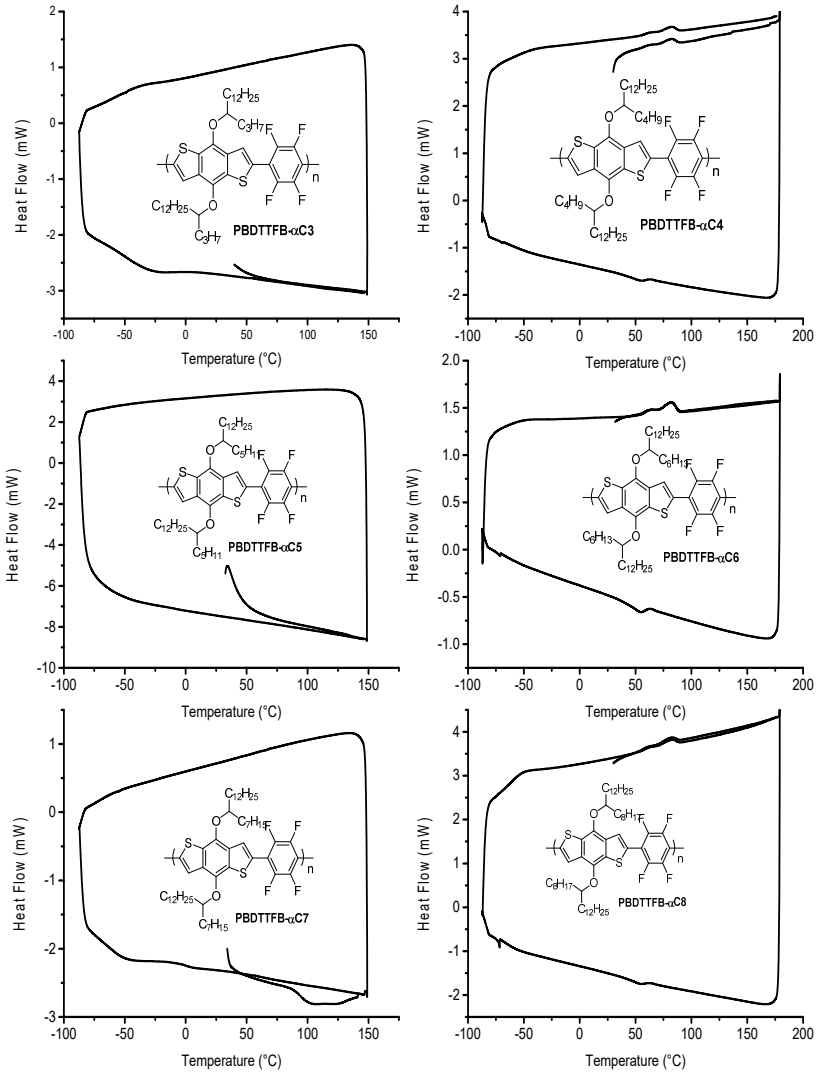

DSC curves for Chapter 3: test by DSC Q20 (heating rate = 10 ºC/ min, cooling rate = 5 ºC/ min, nitrogen purge). Here the small peak near 80 ºC (heating process) and 60 ºC (cooling process) came from instrument (verified by blank test).

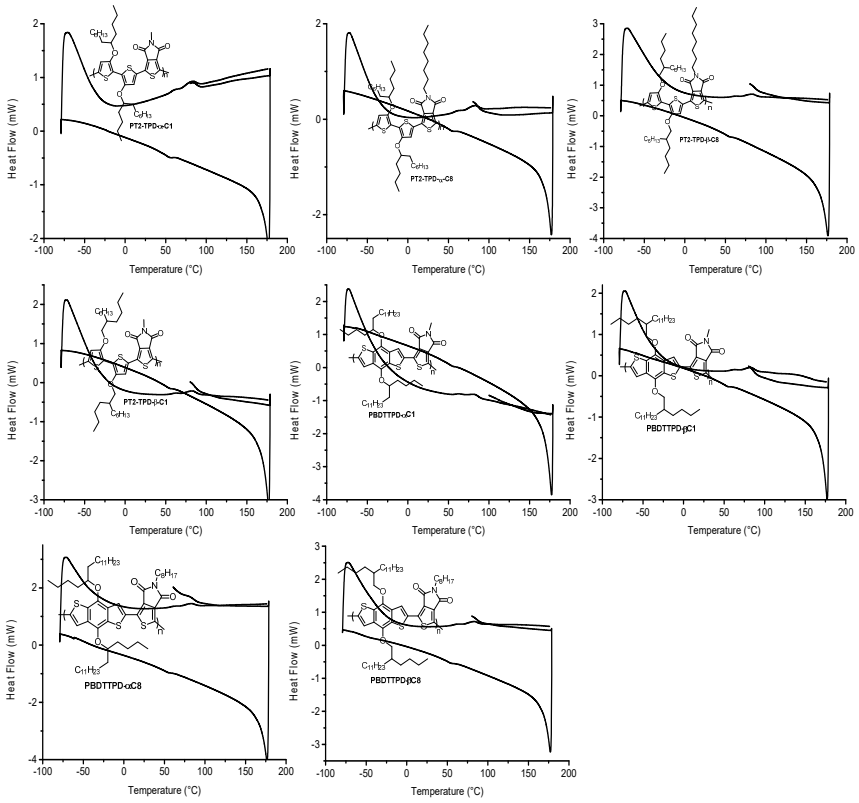

DSC curves for Chapter 4: test by DSC Q20 (heating rate = 10 ºC/ min, cooling rate = 5 ºC/ min, nitrogen purge). Here the small peak near 80 ºC (heating process) and 60 ºC (cooling process) came from instrument (verified by blank test).

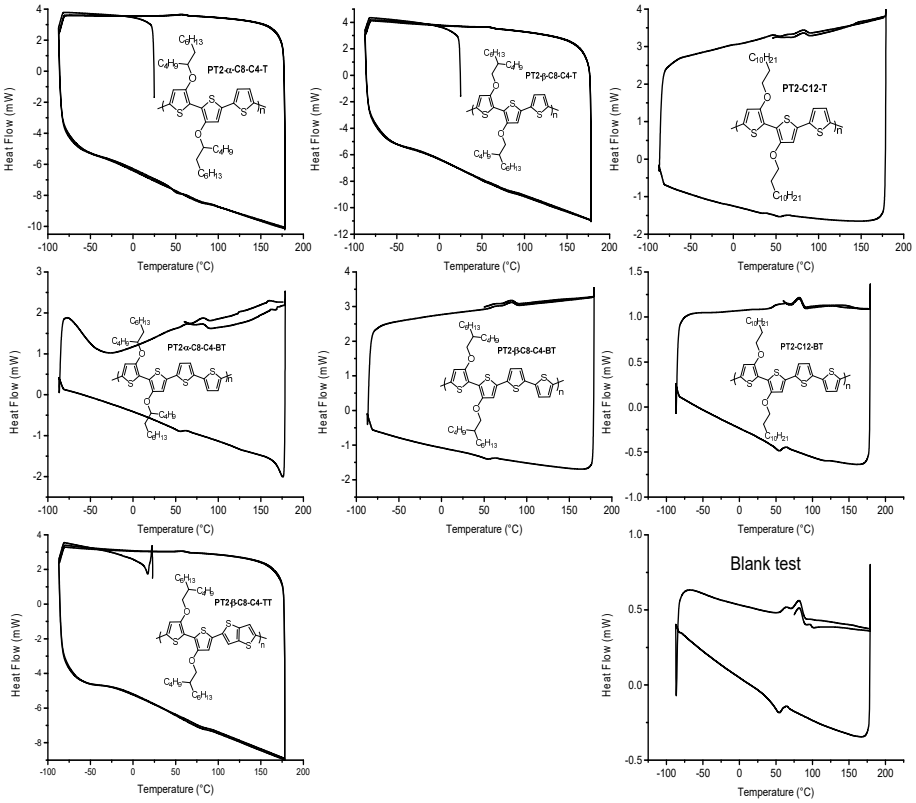

6.7 NMR Spectra

NMR Spectra for Chapter 2

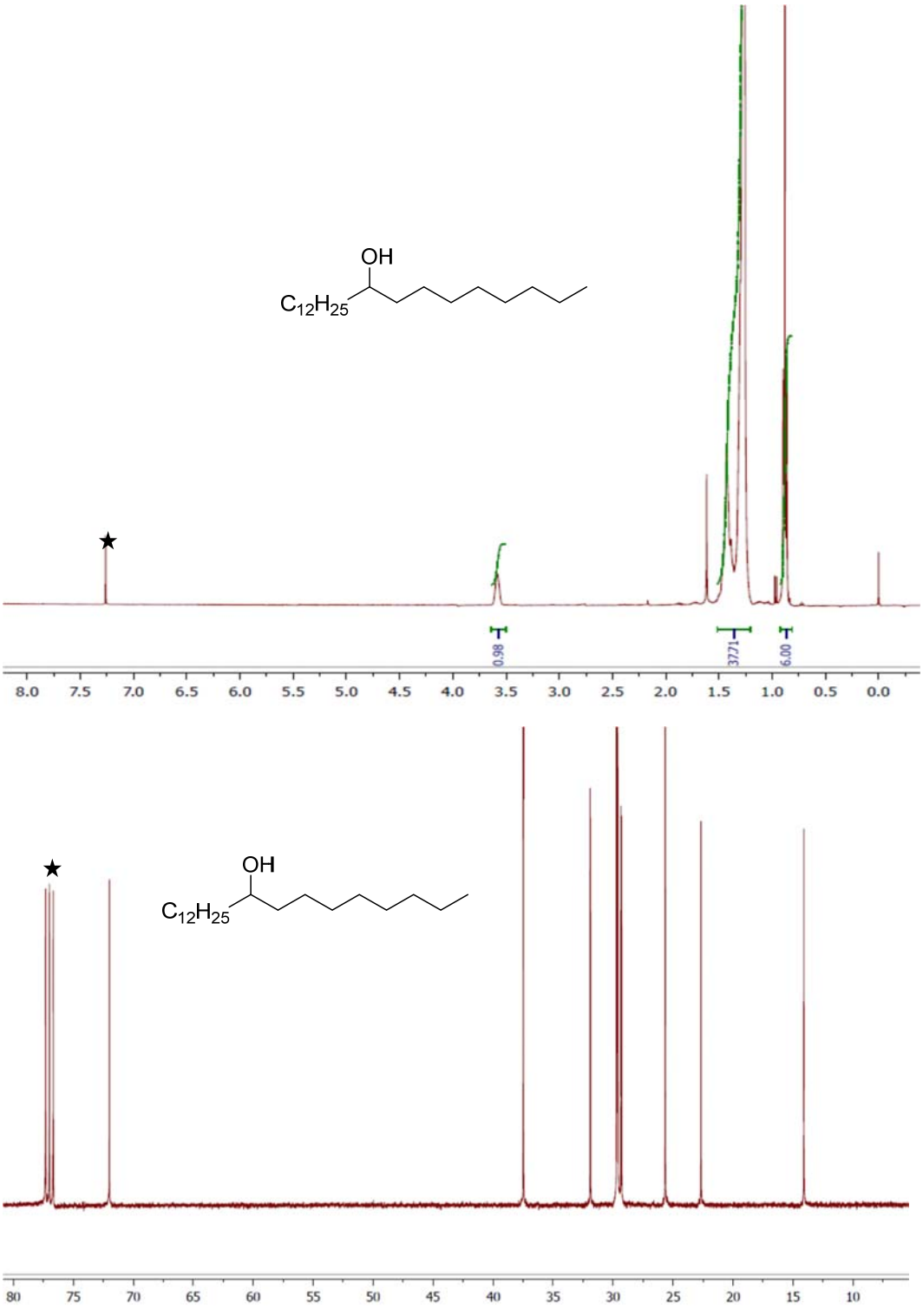

^{1}H (top) and ^{13}C (bottom) NMR spectra (CDCl3, r.t.) of 2.0a (★ solvent).

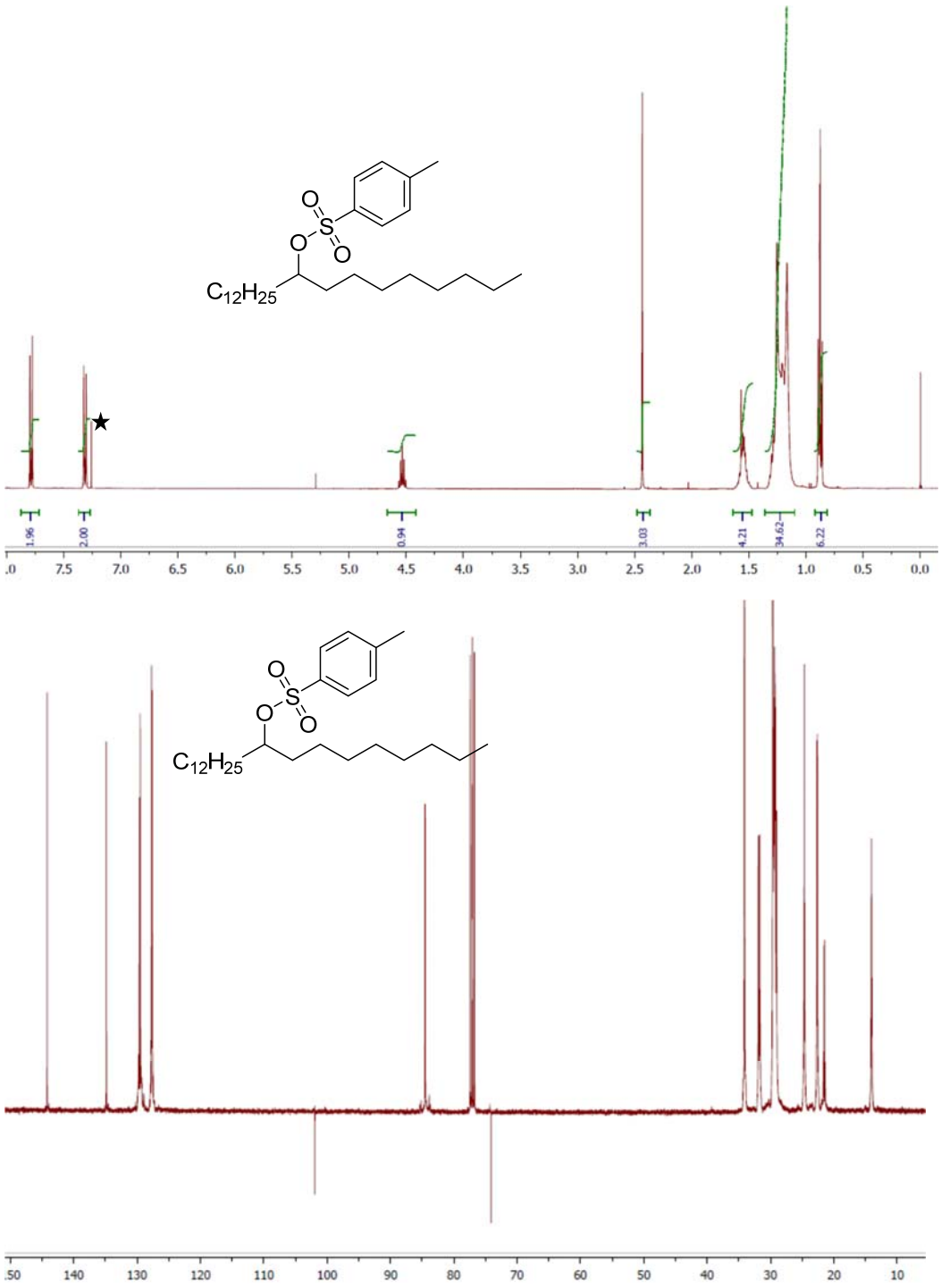

^{1}H (top) and ^{13}C (bottom) NMR spectra ($CDCl_3$, r.t.) of 2.1a (★ solvent).

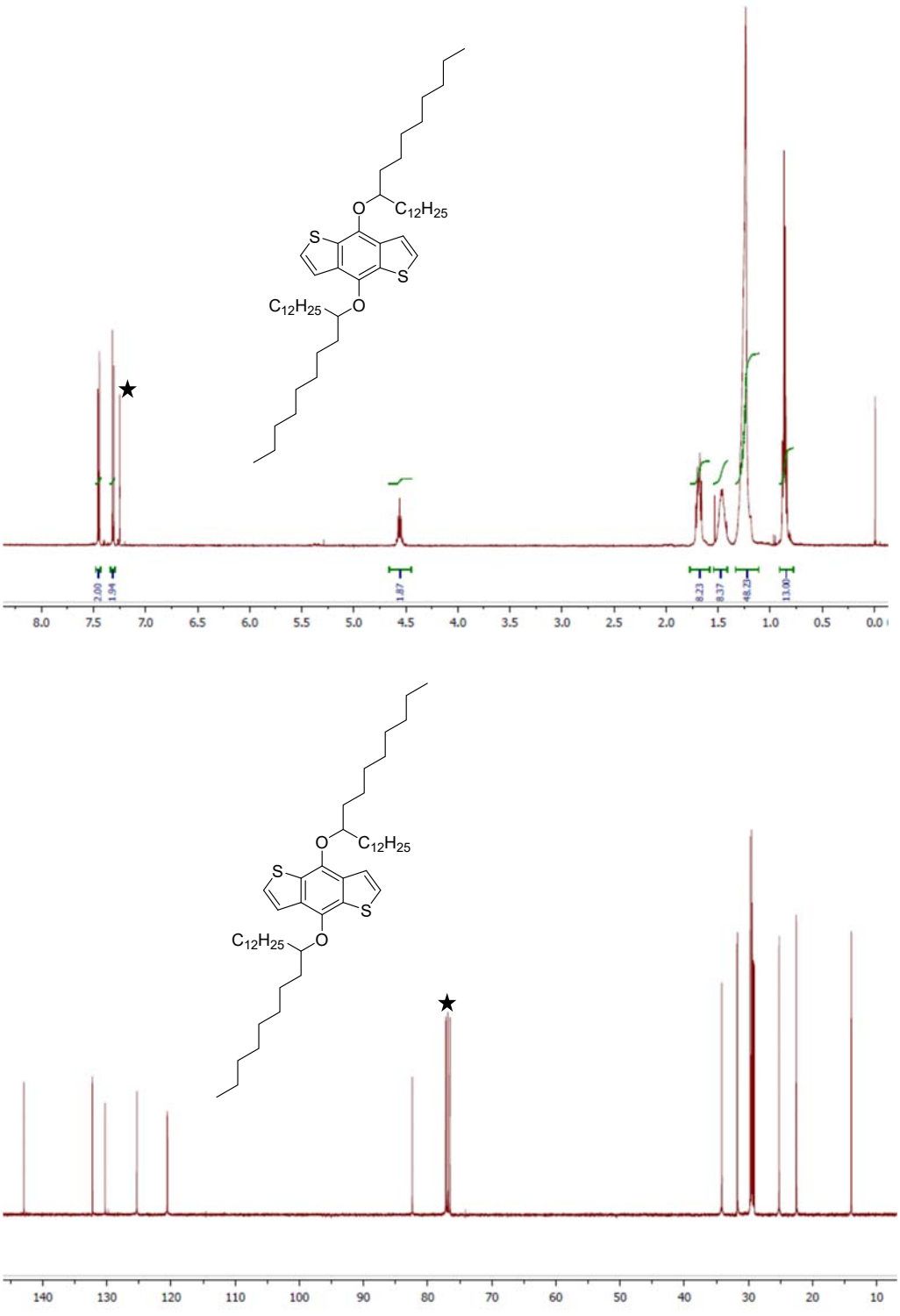

^{1}H (top) and ^{13}C (bottom) NMR spectra ($CDCl_3$, r.t.) of 2.5a (★ solvent).

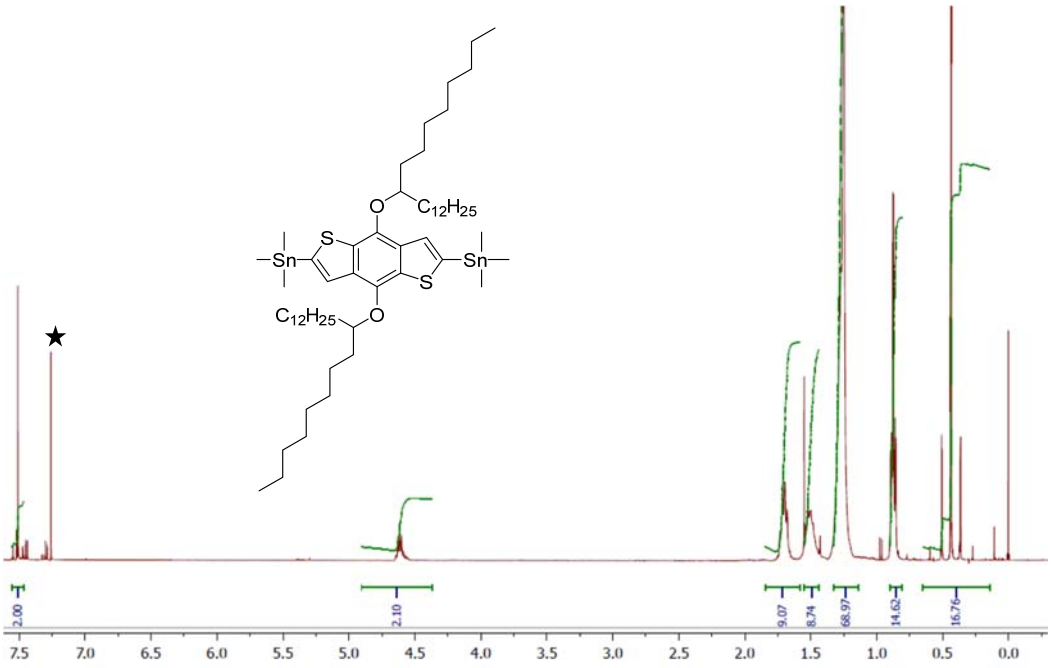

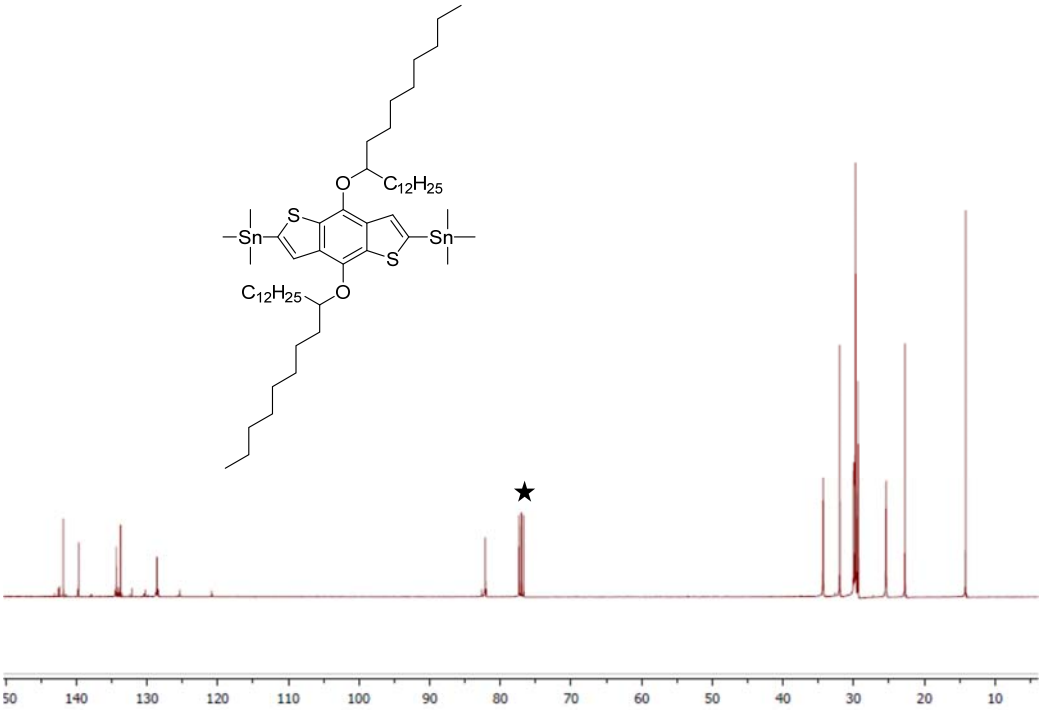

^{1}H (top) and ^{13}C (bottom) NMR spectra ($CDCl_3$, r.t.) of 2.6a (★solvent).

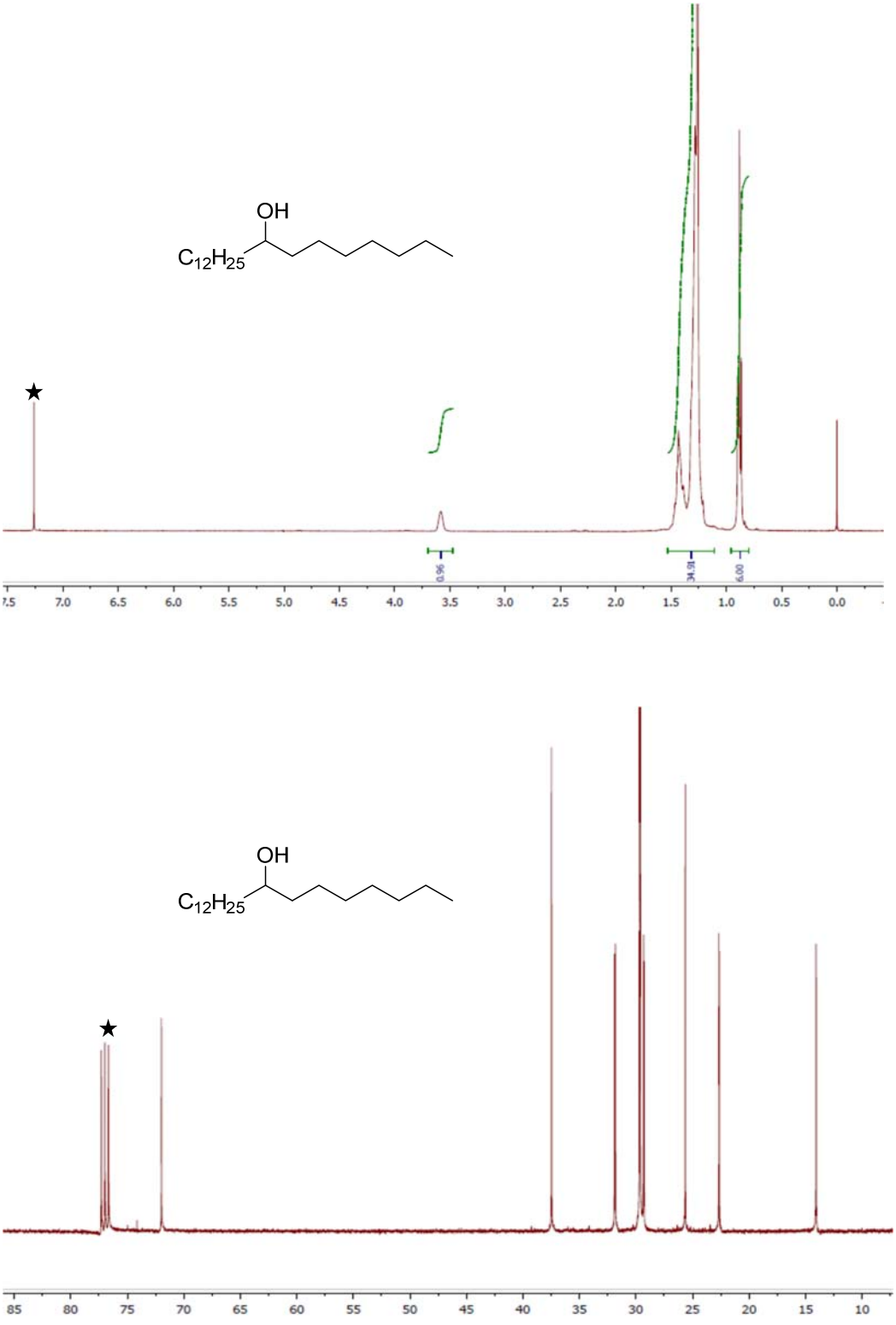

^{1}H (top) and ^{13}C (bottom) NMR spectra ($CDCl_3$, r.t.) of 2.0b (★ solvent).

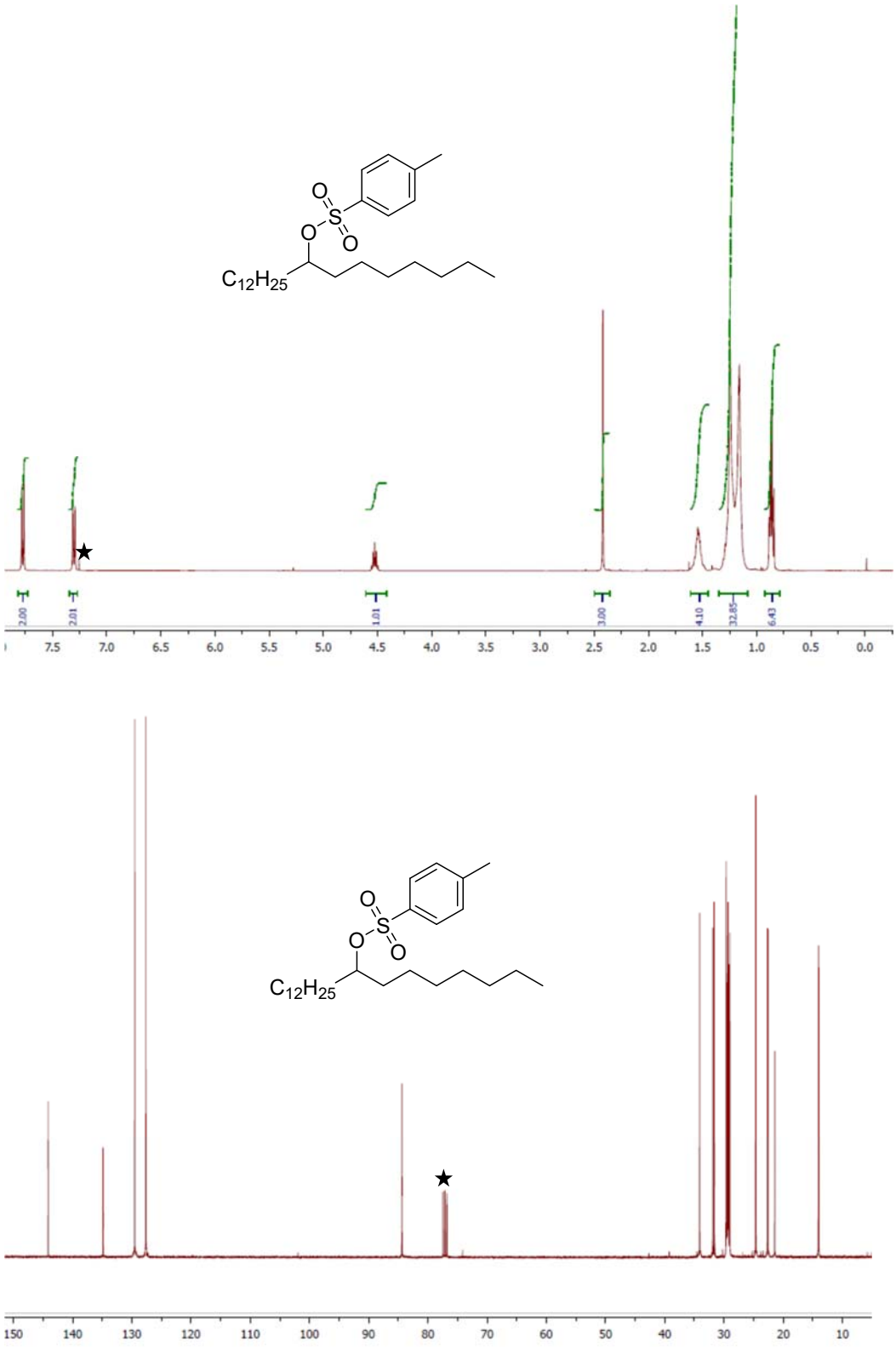

^{1}H (top) and ^{13}C (bottom) NMR spectra ($CDCl_3$, r.t.) of 2.1b (★ solvent).

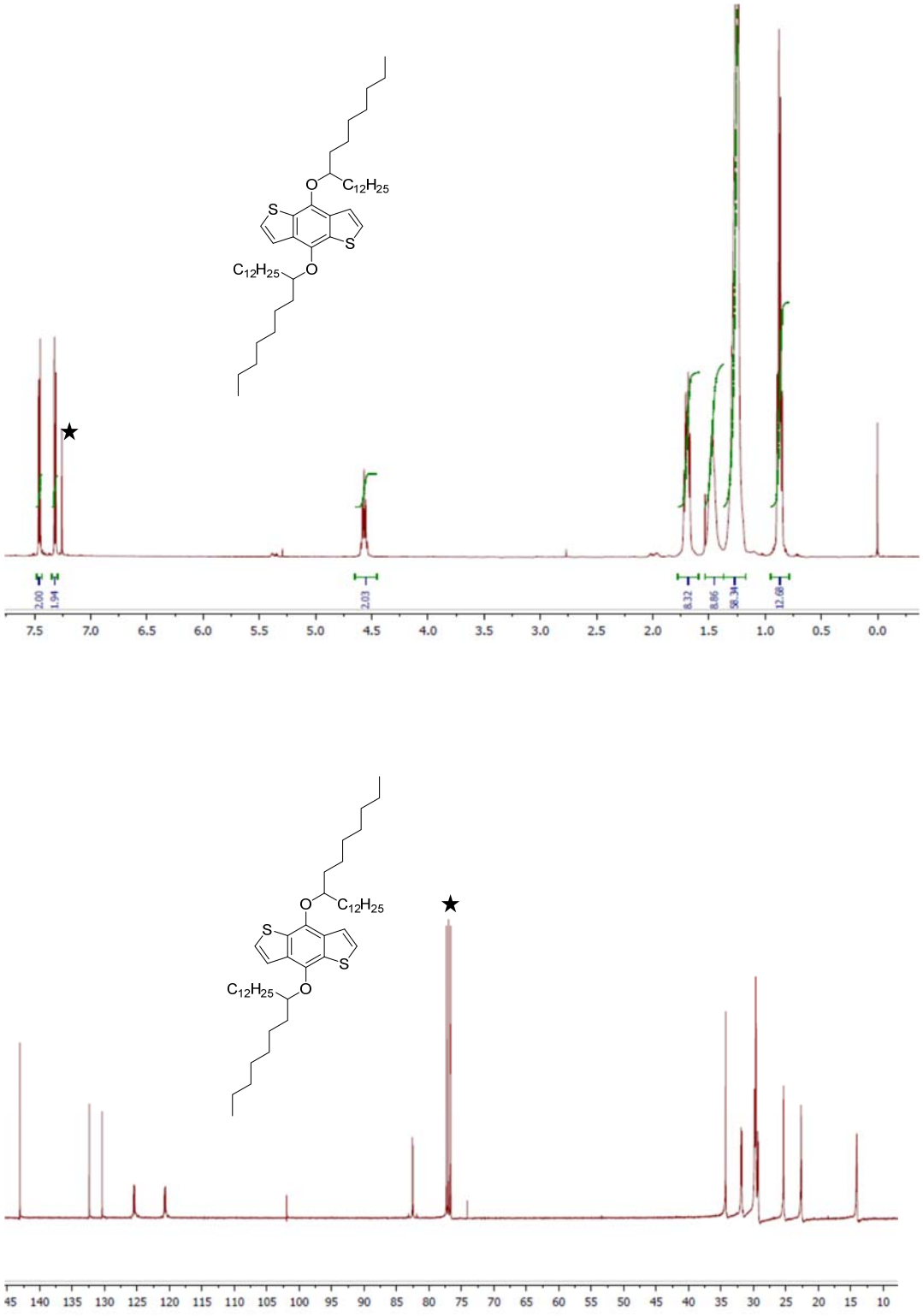

^{1}H (top) and ^{13}C (bottom) NMR spectra ($CDCl_3$, r.t.) of 2.5b (★ solvent).

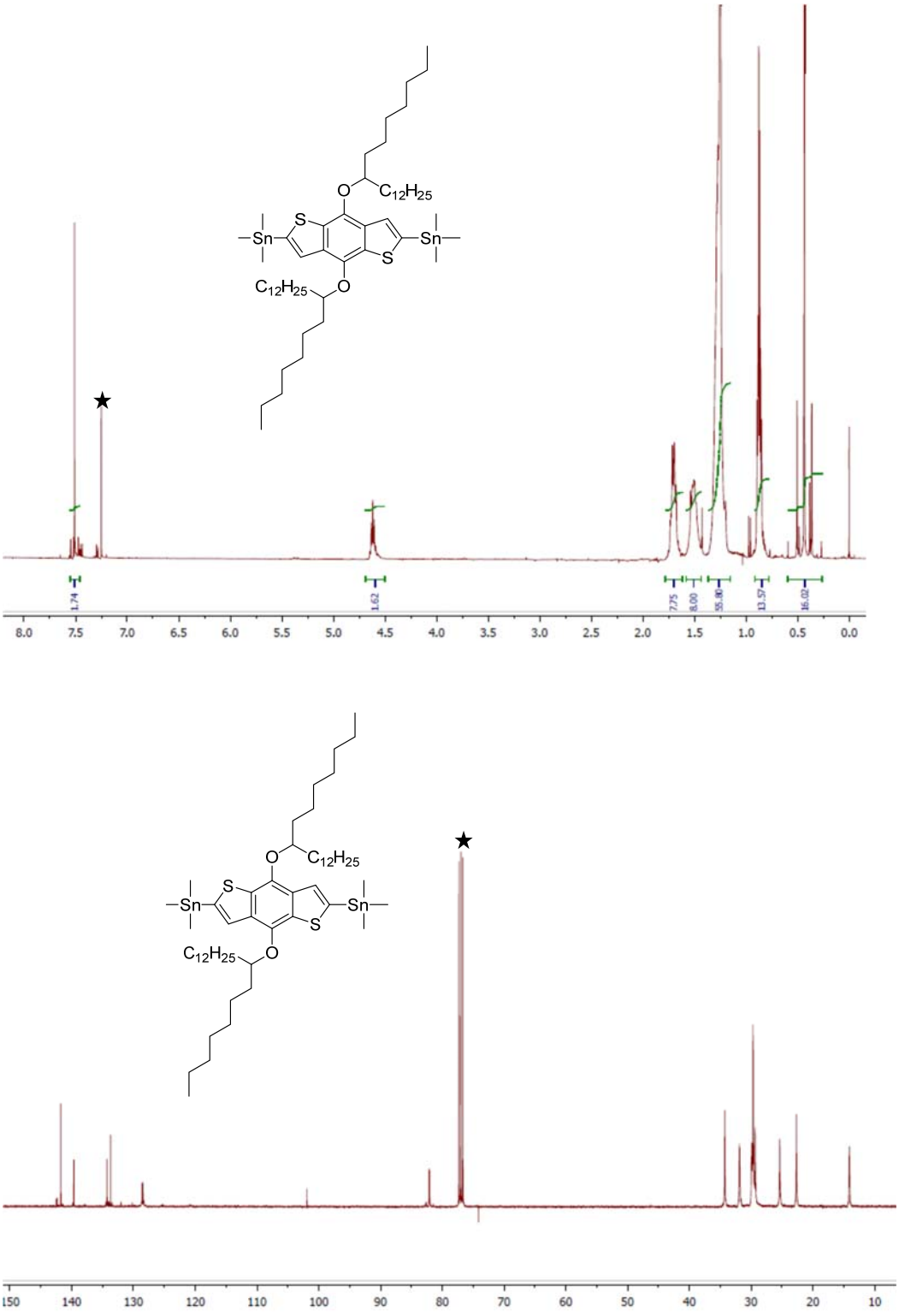

^{1}H (top) and ^{13}C (bottom) NMR spectra ($CDCl_3$, r.t.) of 2.6b (★ solvent).

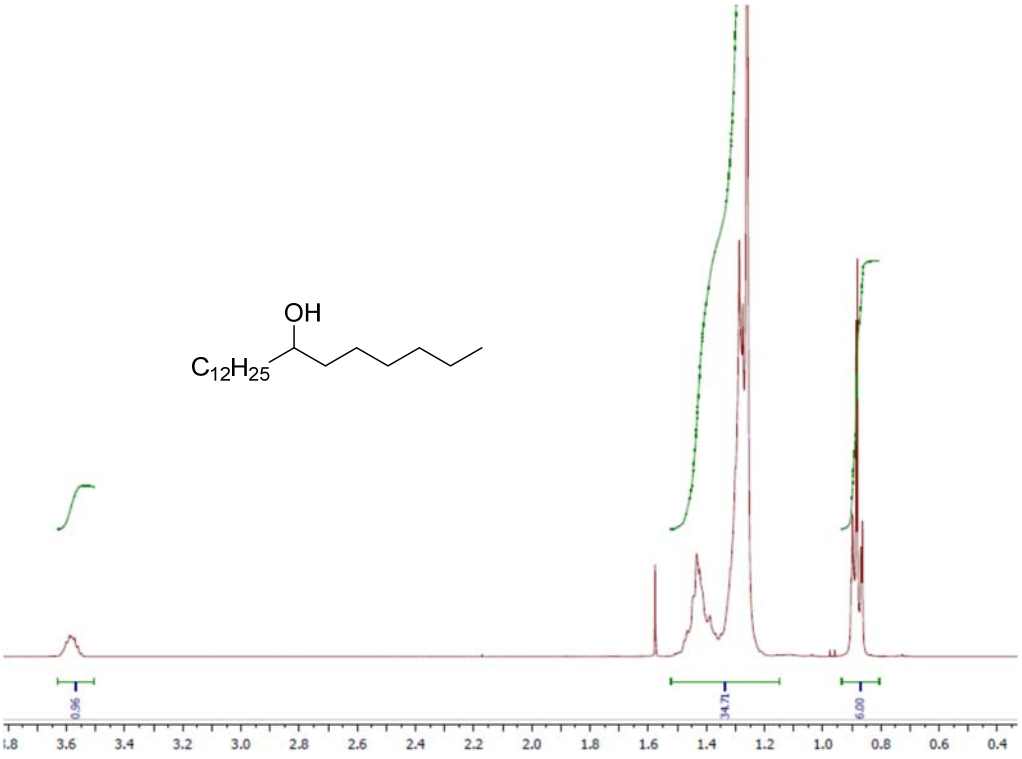

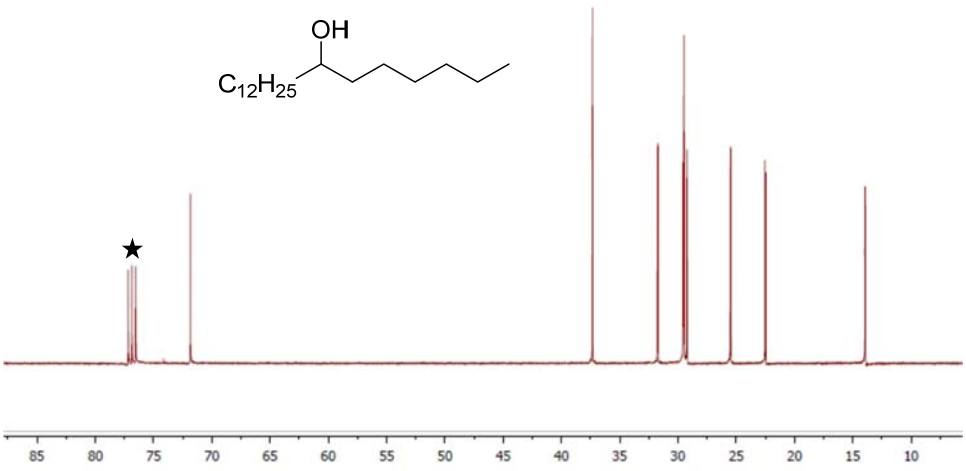

^{1}H (top) and ^{13}C (bottom) NMR spectra ($CDCl_3$, r.t.) of 2.0c (★solvent).

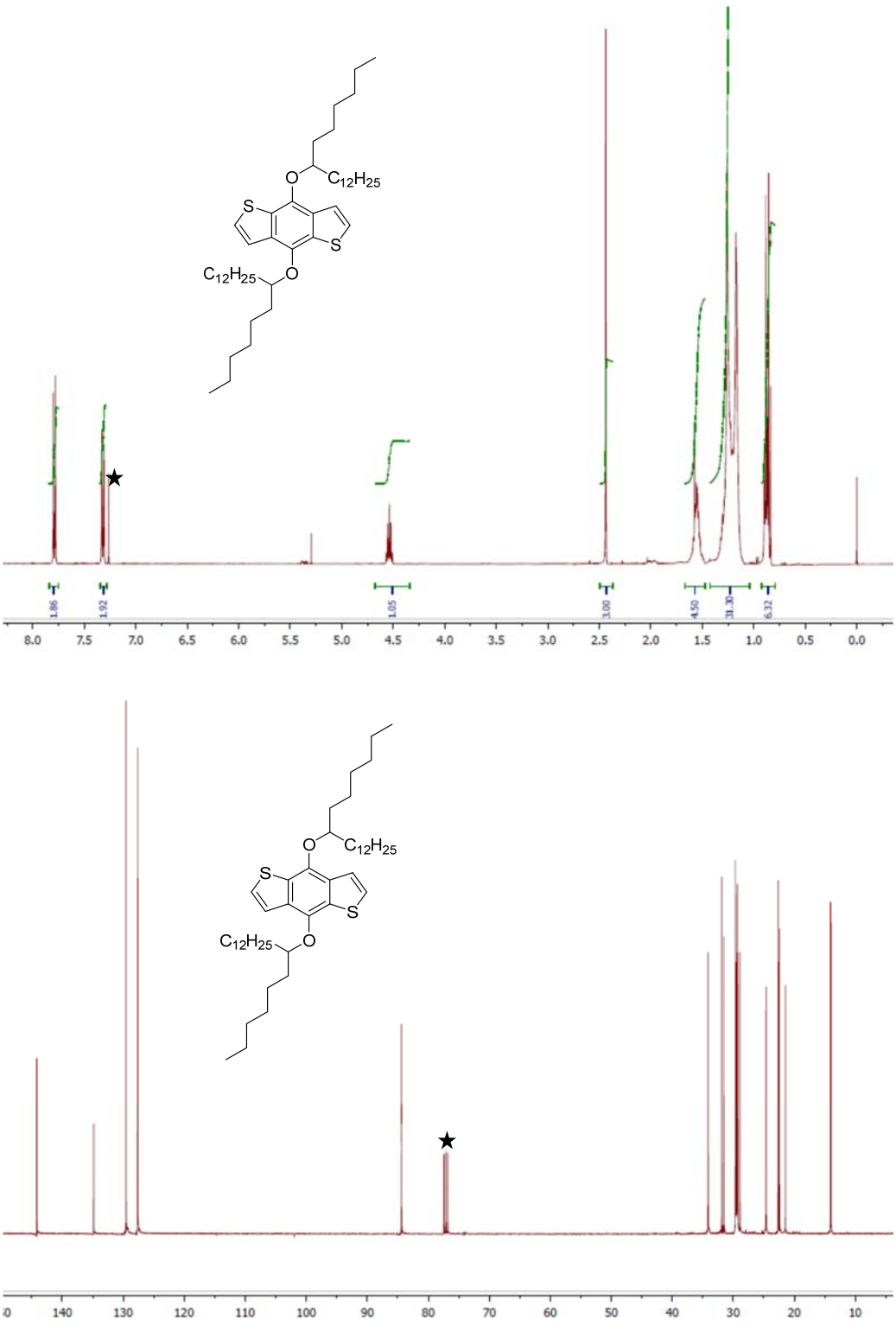

^{1}H (top) and ^{13}C (bottom) NMR spectra ($CDCl_3$, r.t.) of 2.5c (★ solvent).

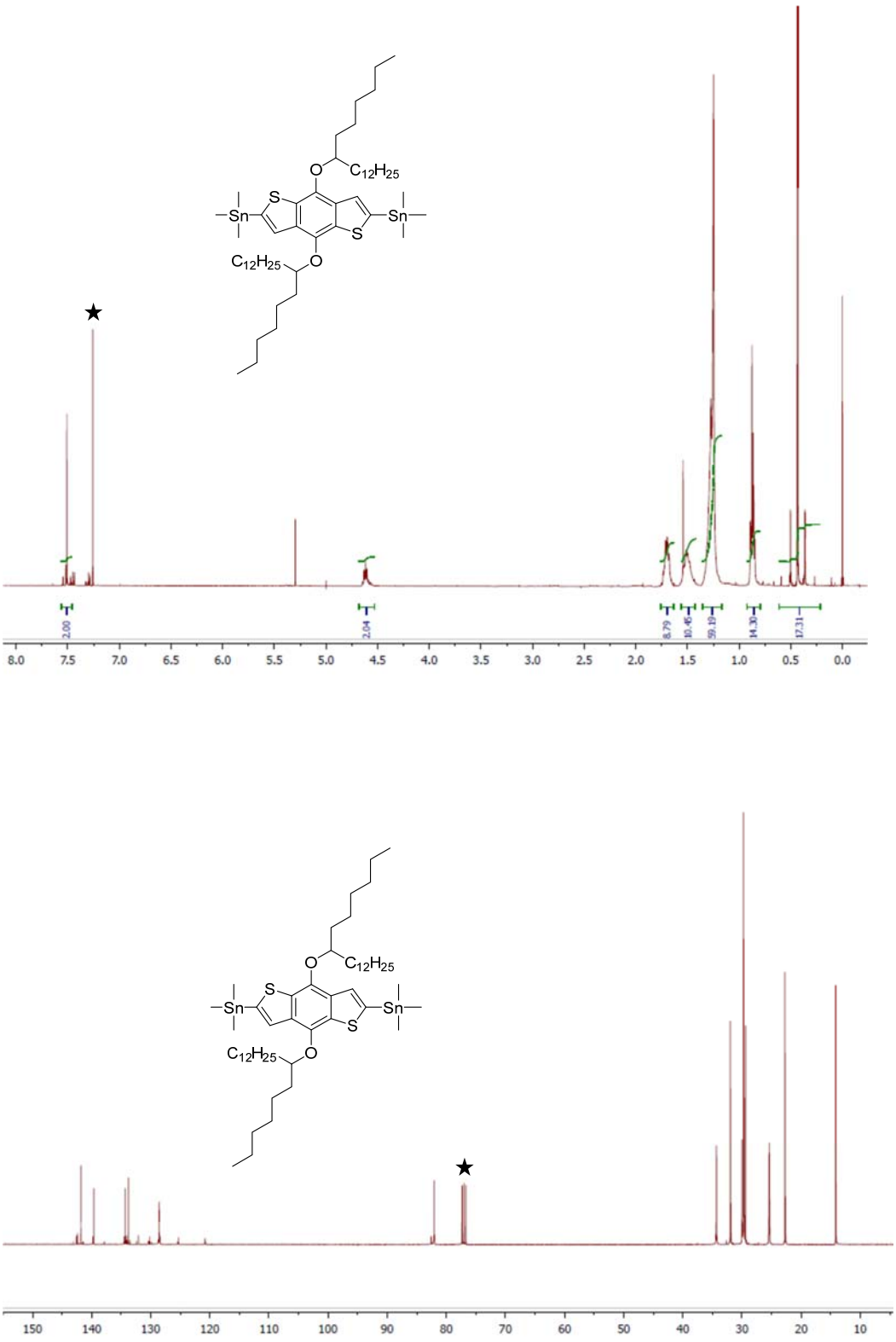

^{1}H (top) and ^{13}C (bottom) NMR spectra ($CDCl_3$, r.t.) of 2.6c (★ solvent).

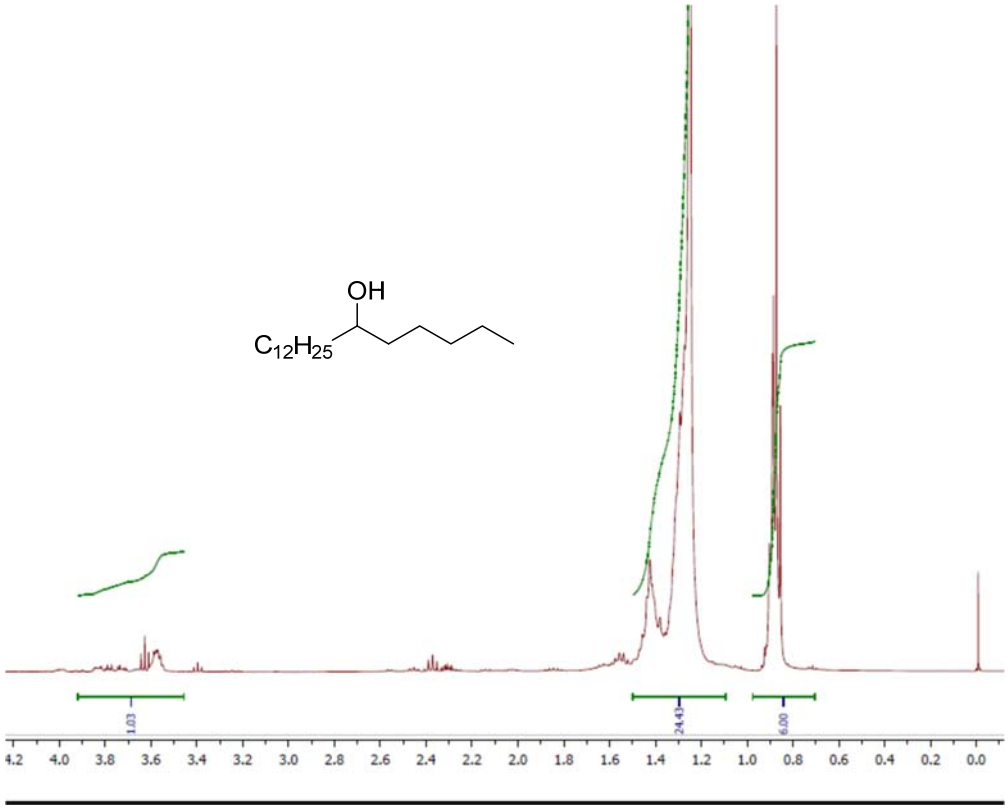

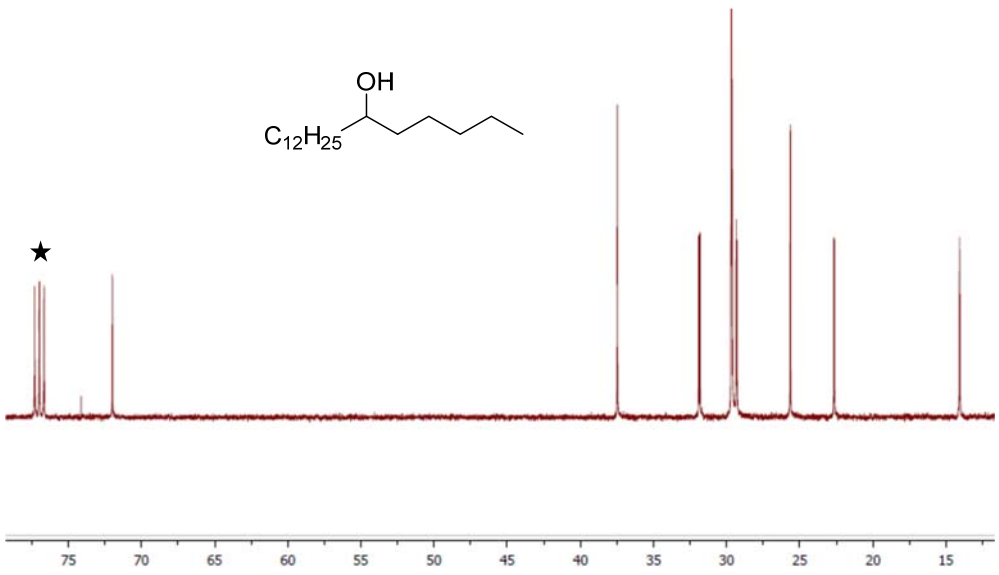

^{1}H (top) and ^{13}C (bottom) NMR spectra ($CDCl_3$, r.t.) of 2.0d (★ solvent).

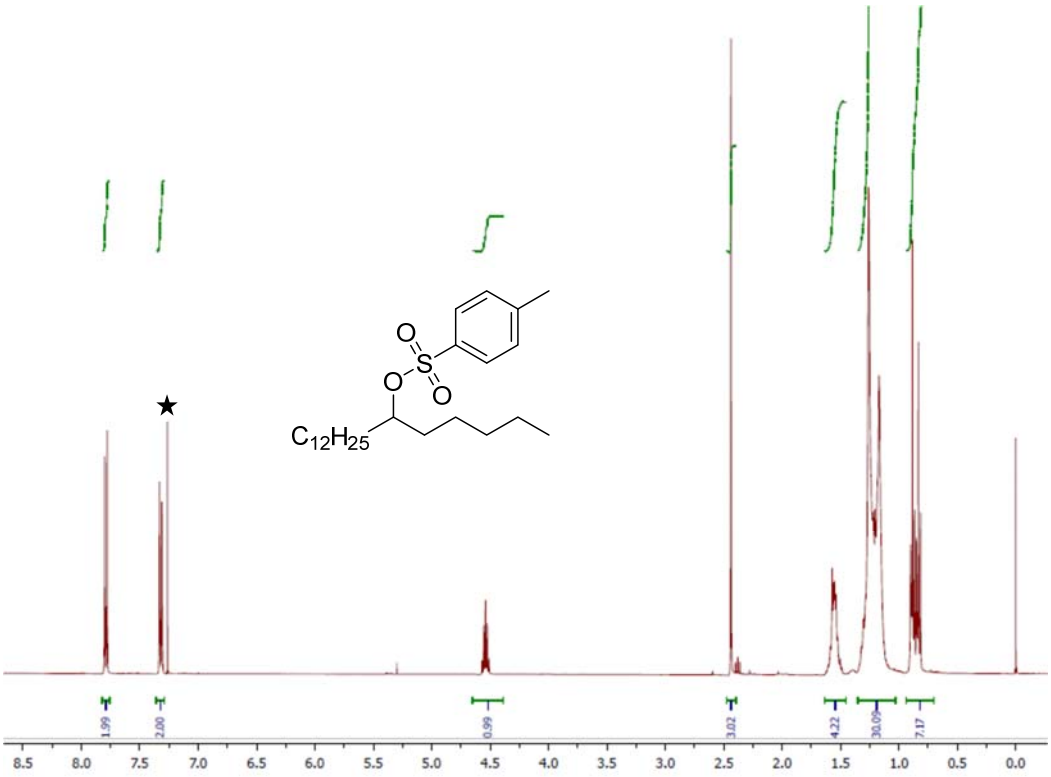

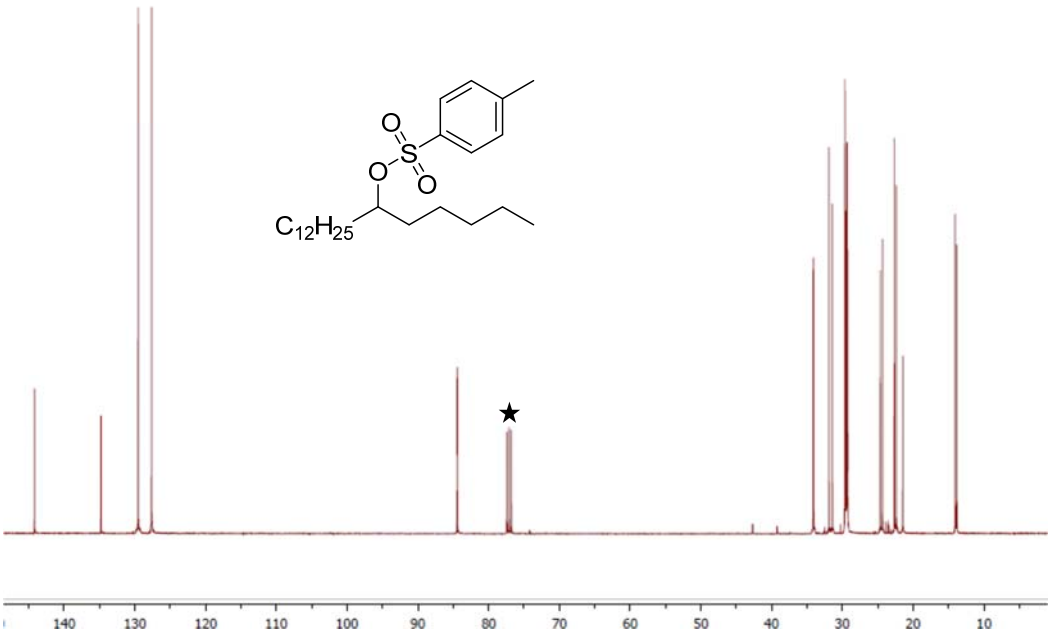

^{1}H (top) and ^{13}C (bottom) NMR spectra ($CDCl_3$, r.t.) of 2.1d (★solvent).

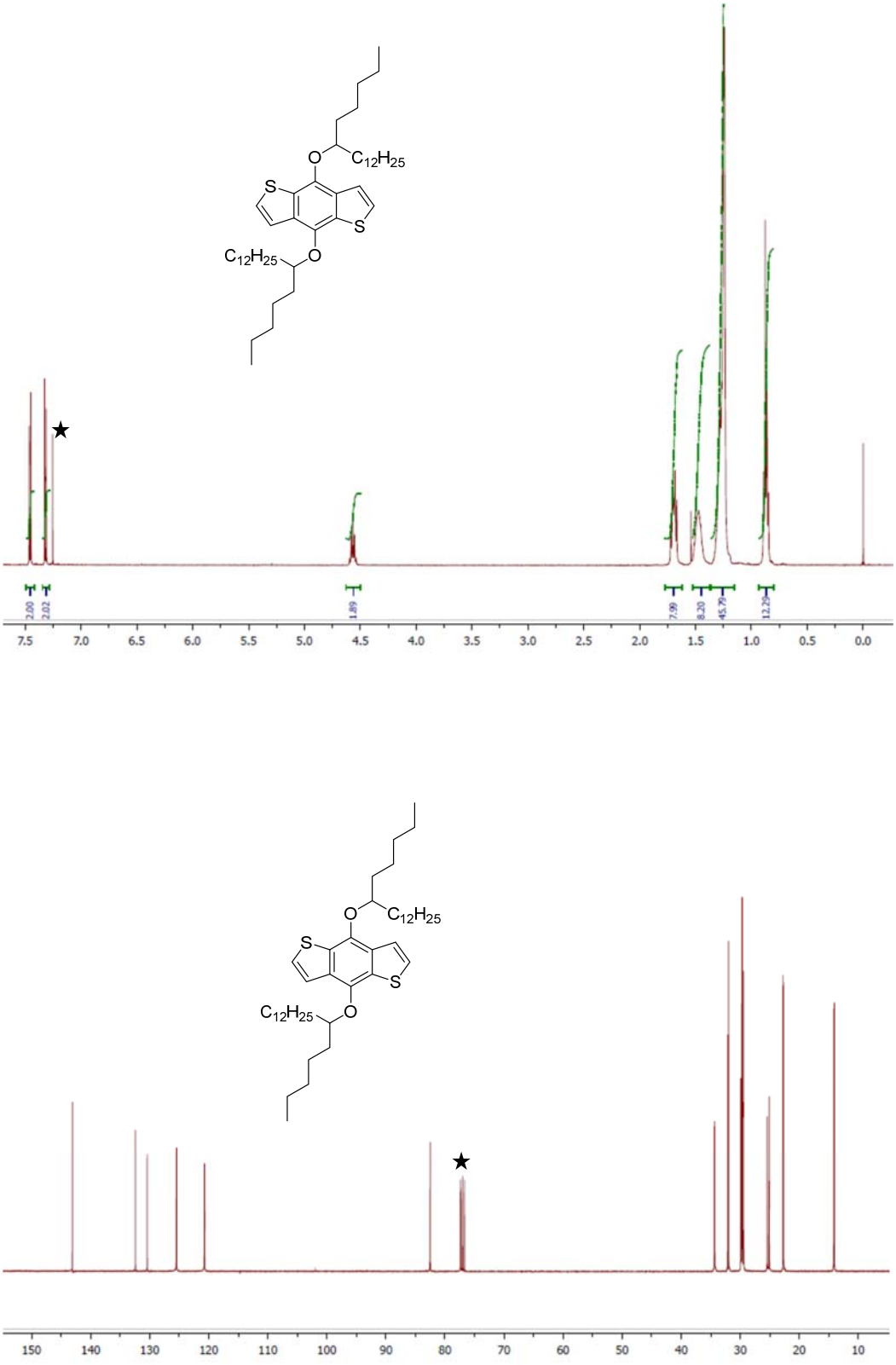

^{1}H (top) and ^{13}C (bottom) NMR spectra ($CDCl_3$, r.t.) of 2.5d (★ solvent).

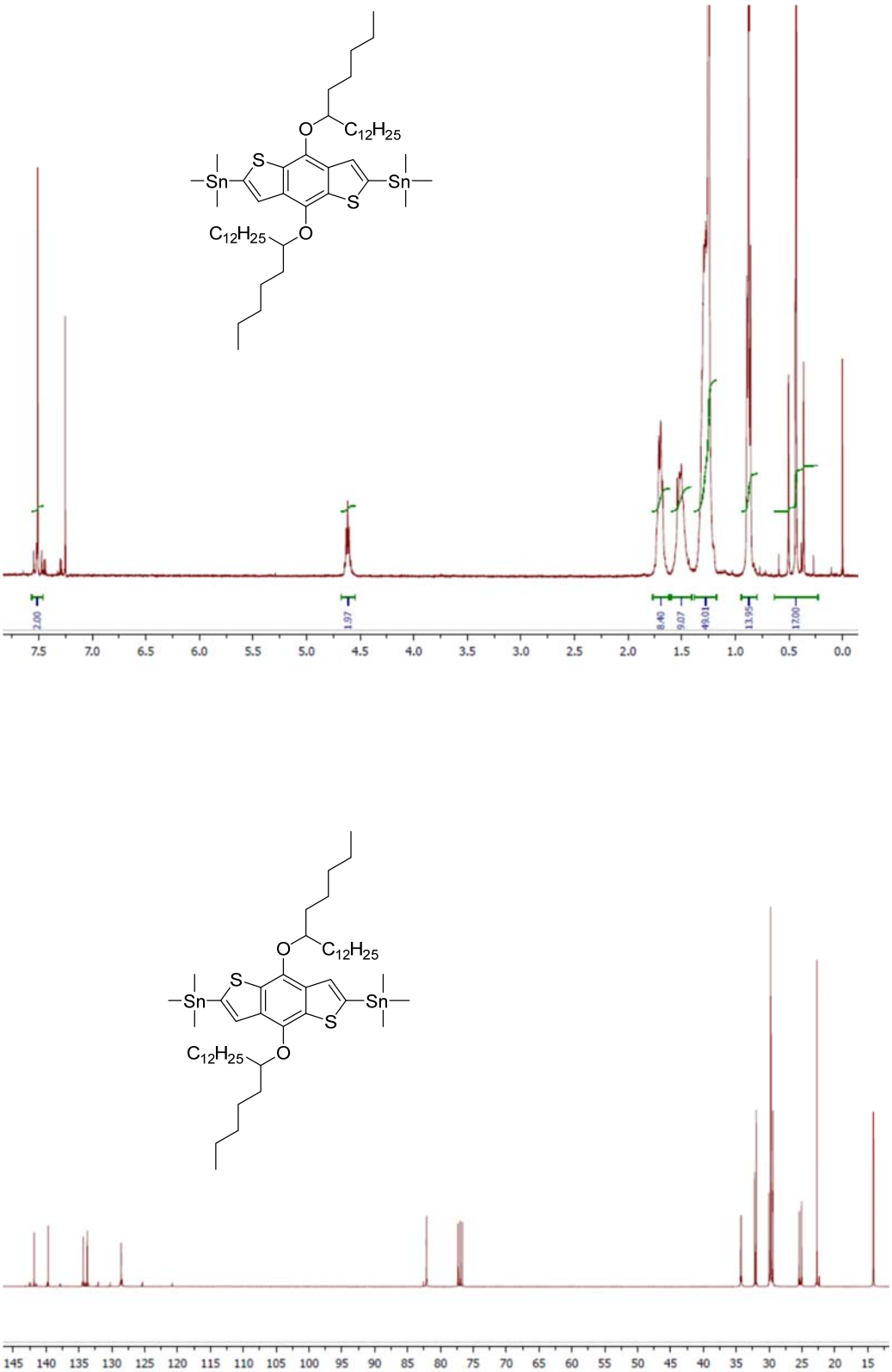

^{1}H (top) and ^{13}C (bottom) NMR spectra ($CDCl_3$, r.t.) of 2.6d (★ solvent).

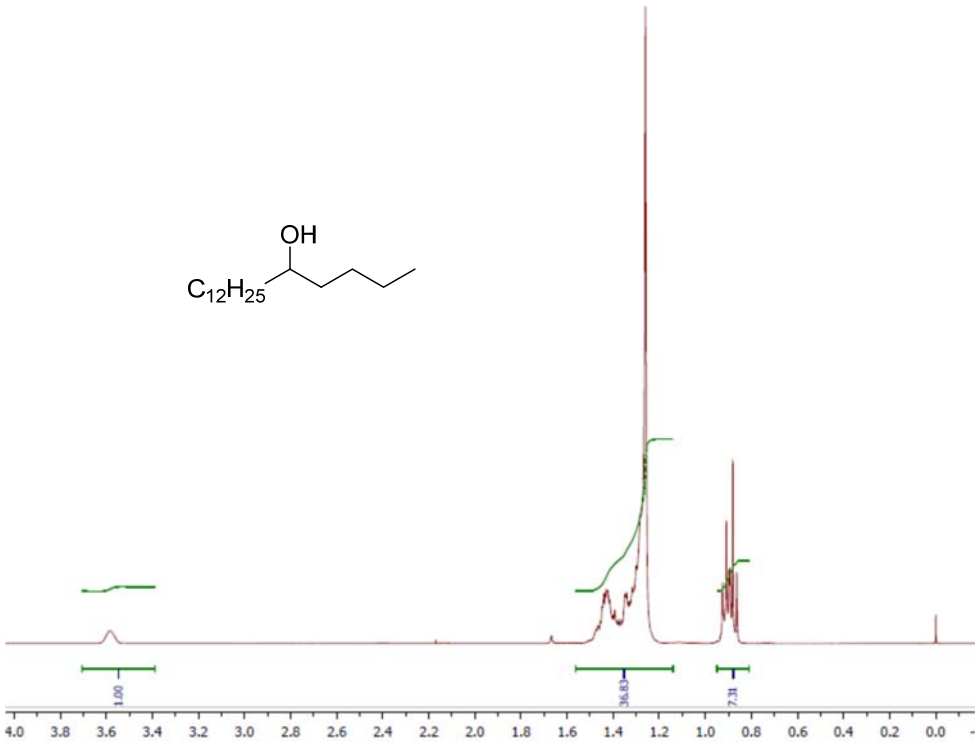

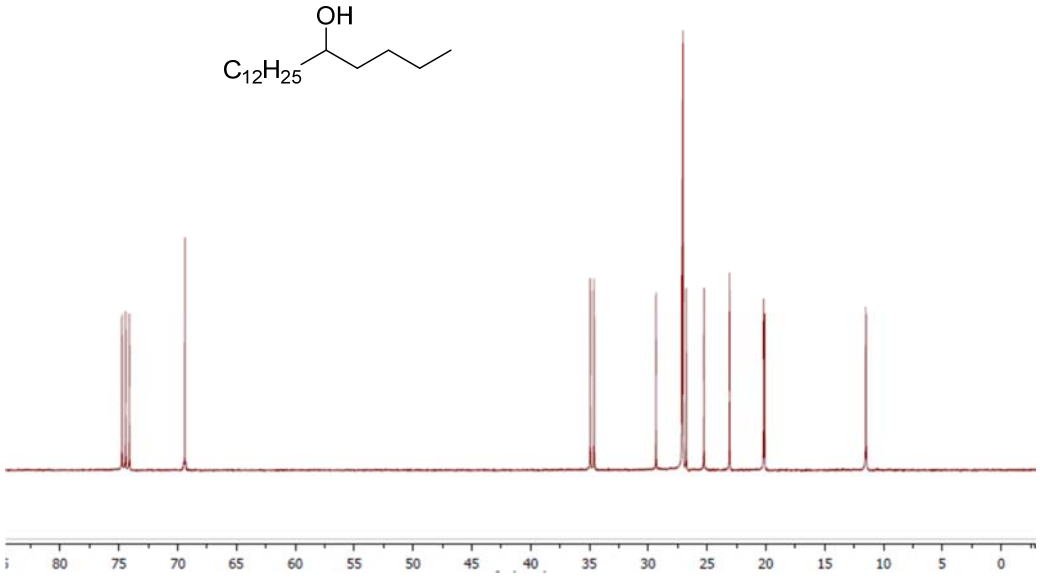

^{1}H (top) and ^{13}C (bottom) NMR spectra ($CDCl_3$, r.t.) of 2.0e (★ solvent).

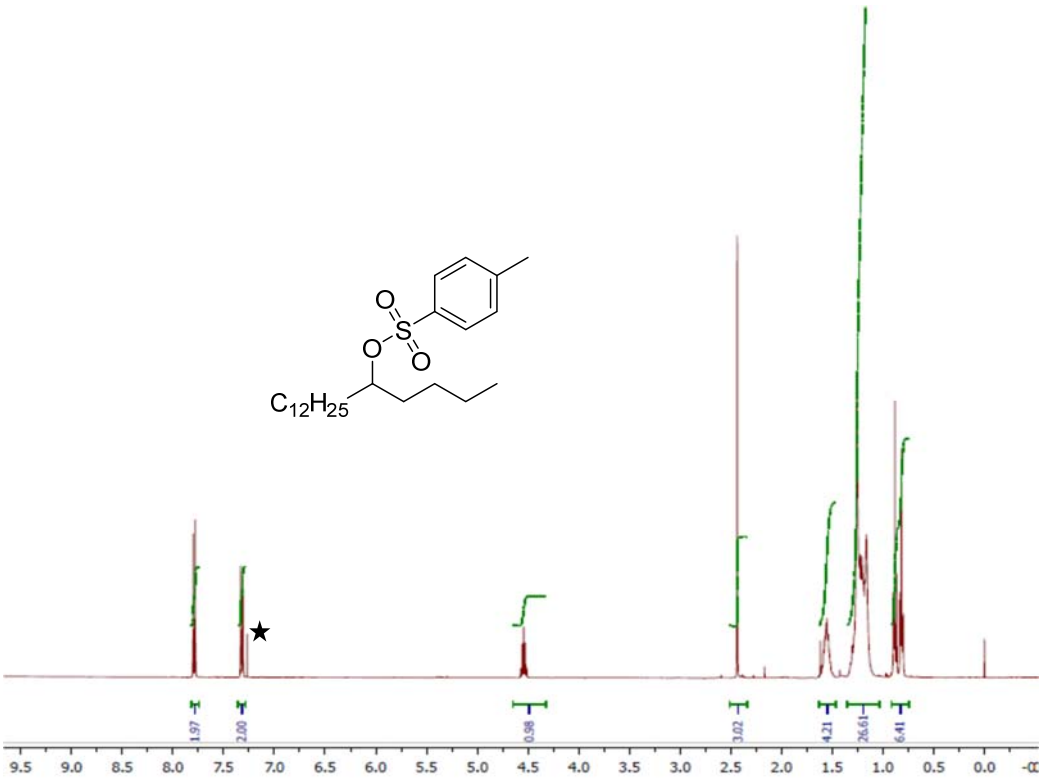

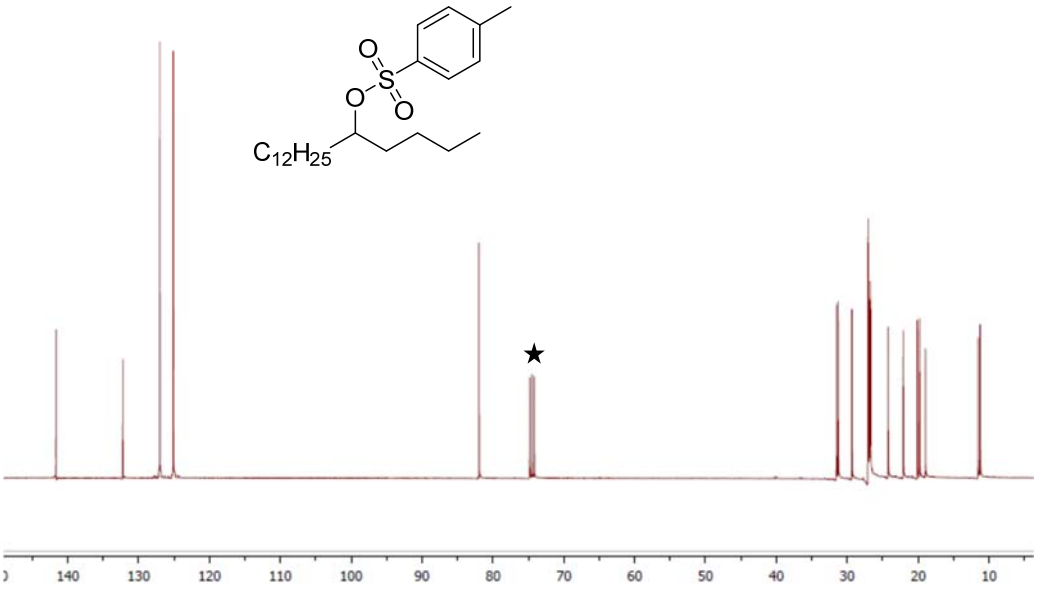

^{1}H (top) and ^{13}C (bottom) NMR spectra ($CDCl_3$, r.t.) of 2.1e (★ solvent).

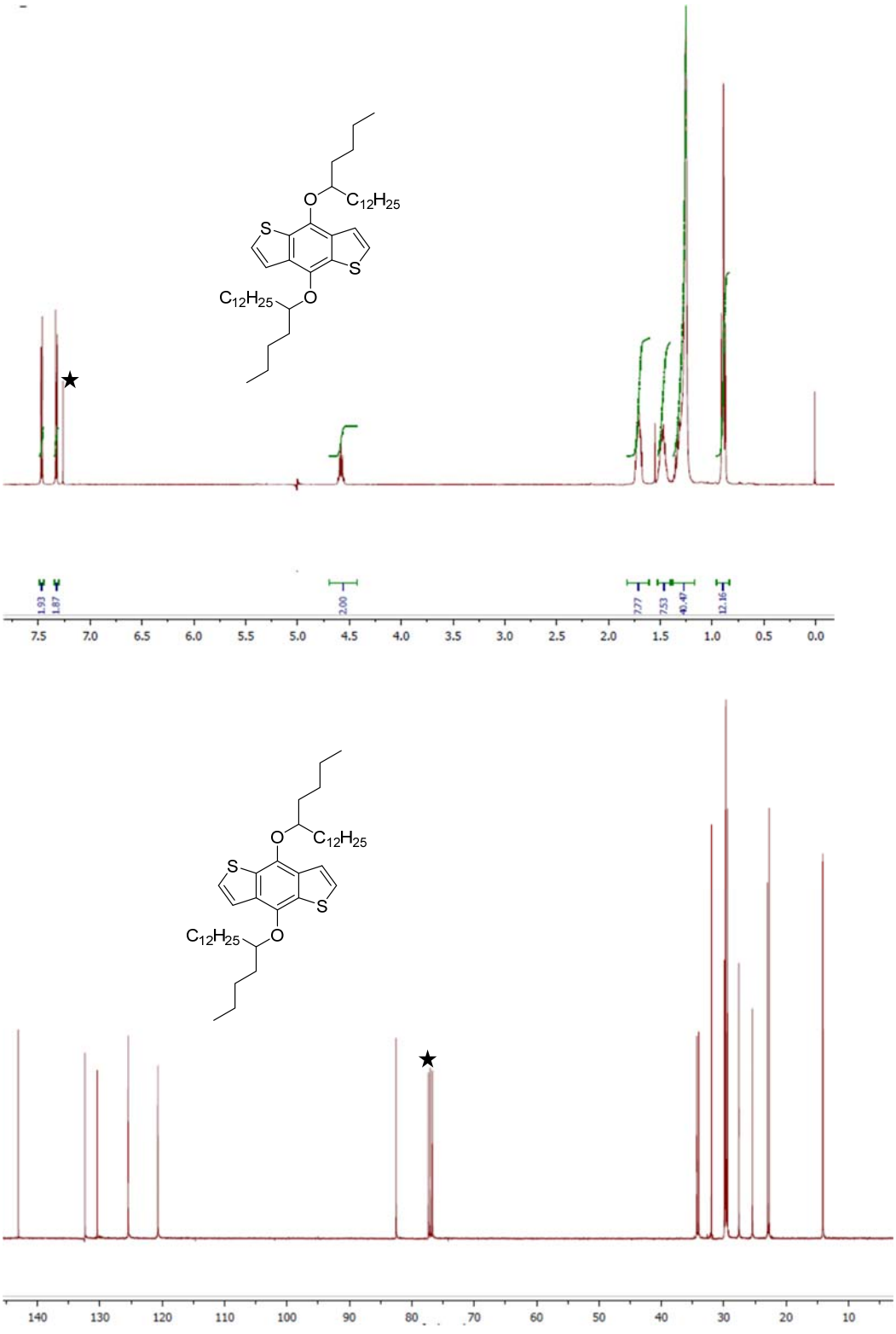

^{1}H (top) and ^{13}C (bottom) NMR spectra ($CDCl_3$, r.t.) of 2.5e (★ solvent).

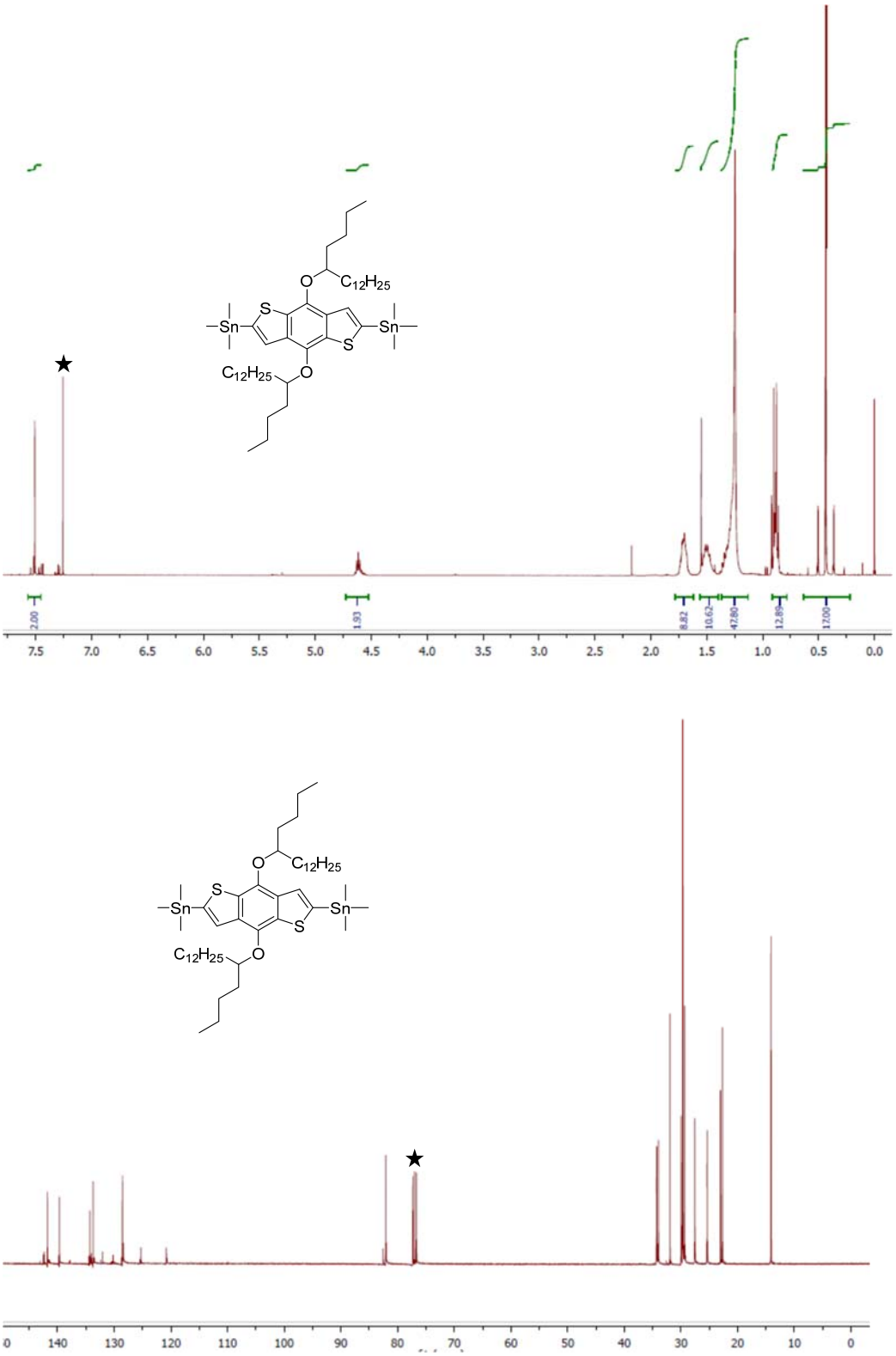

^{1}H (top) and ^{13}C (bottom) NMR spectra ($CDCl_3$, r.t.) of 2.6e (★ solvent).

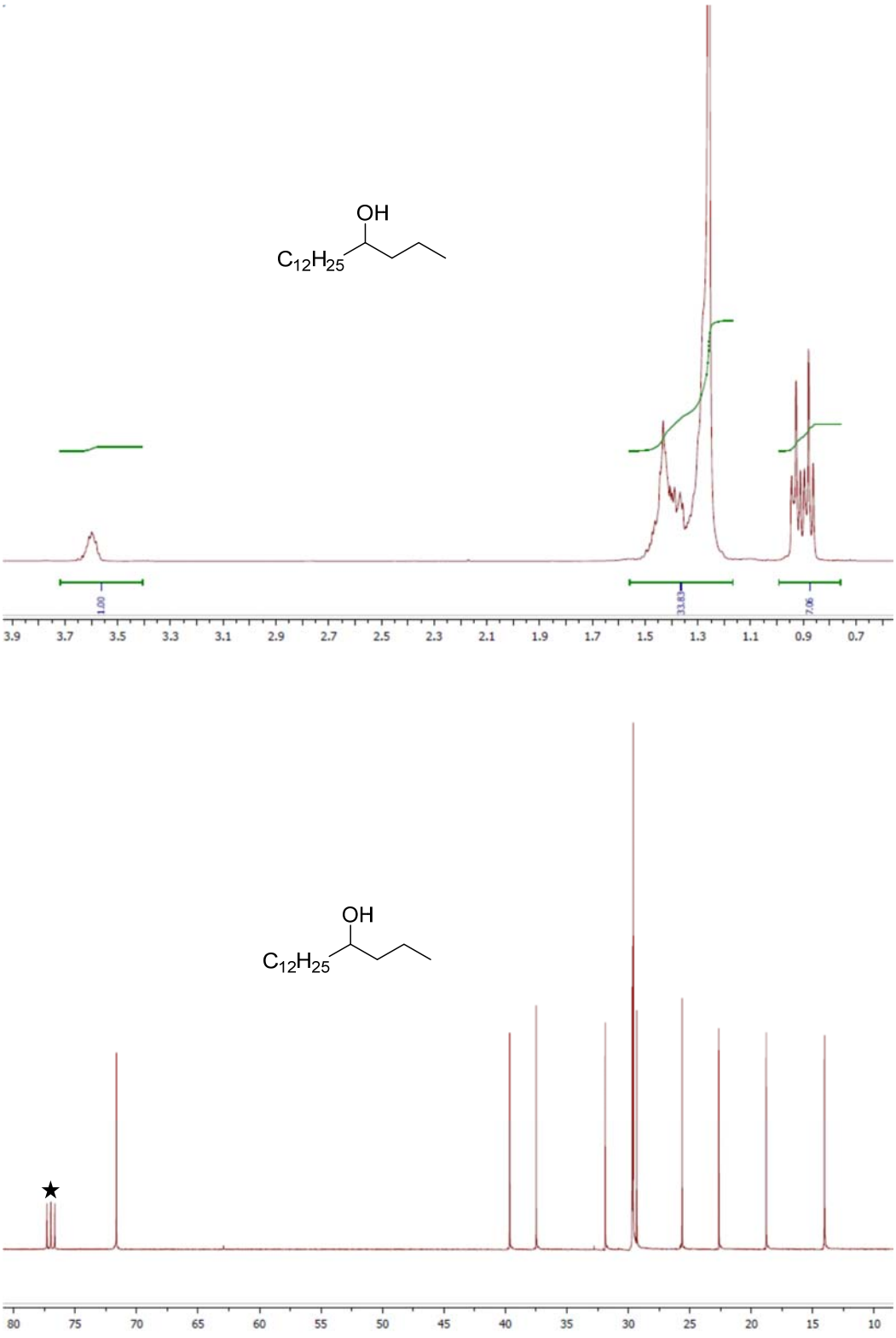

^{1}H (top) and ^{13}C (bottom) NMR spectra ($CDCl_3$, r.t.) of 2.0f (★solvent).

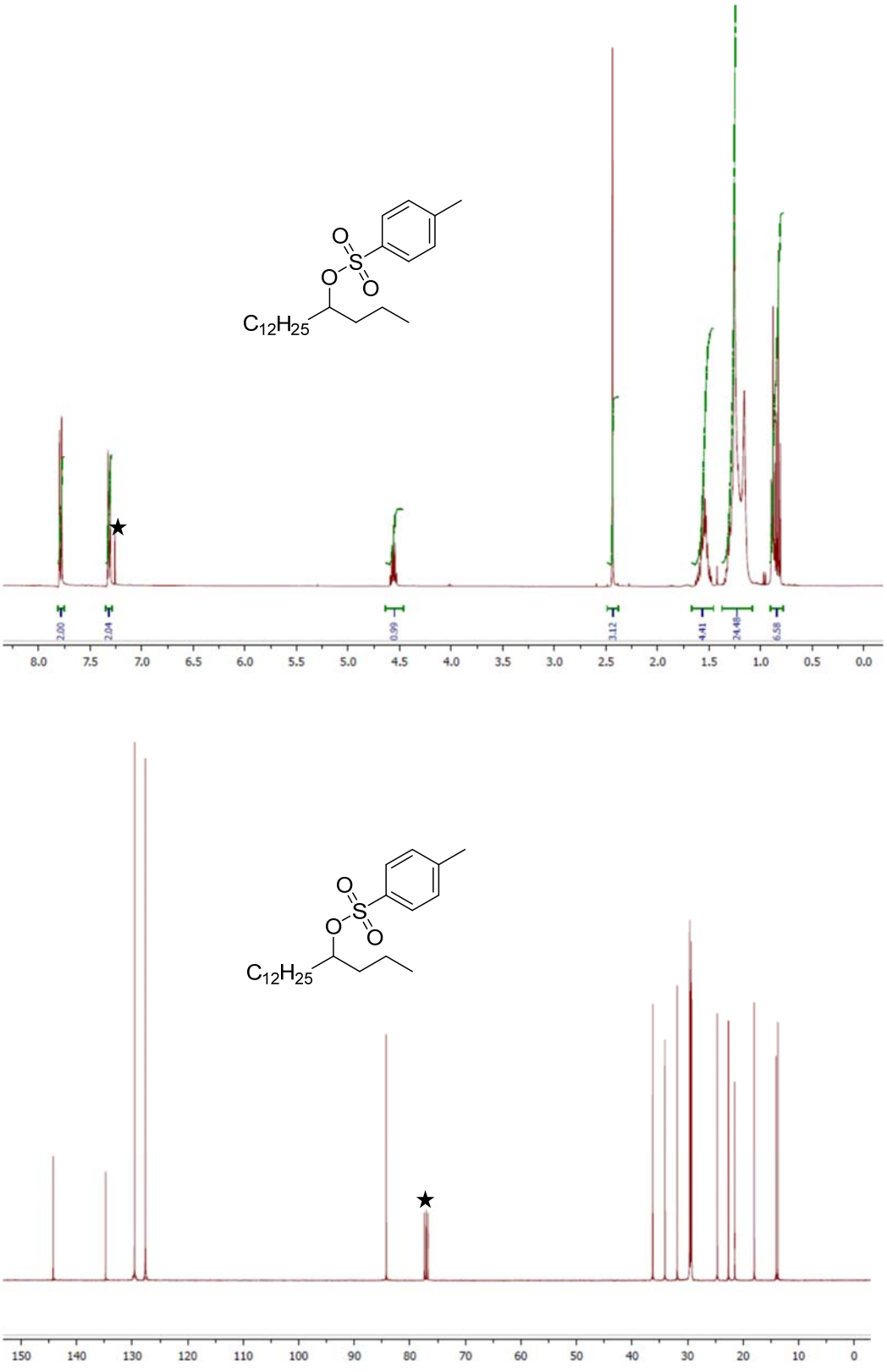

^{1}H (top) and ^{13}C (bottom) NMR spectra ($CDCl_3$, r.t.) of 2.1f (★solvent).

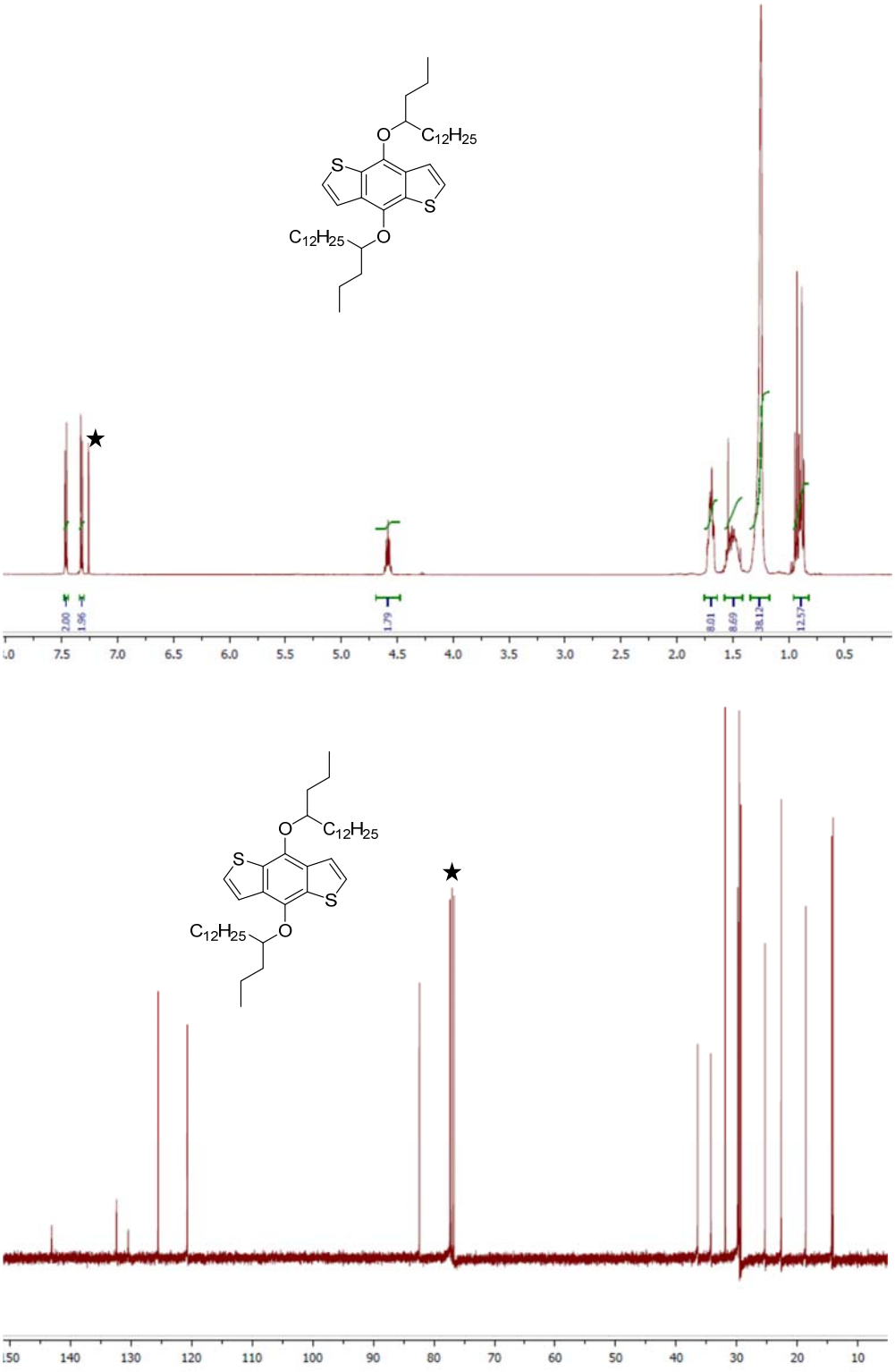

^{1}H (top) and ^{13}C (bottom) NMR spectra ($CDCl_3$, r.t.) of 2.5f (★ solvent).

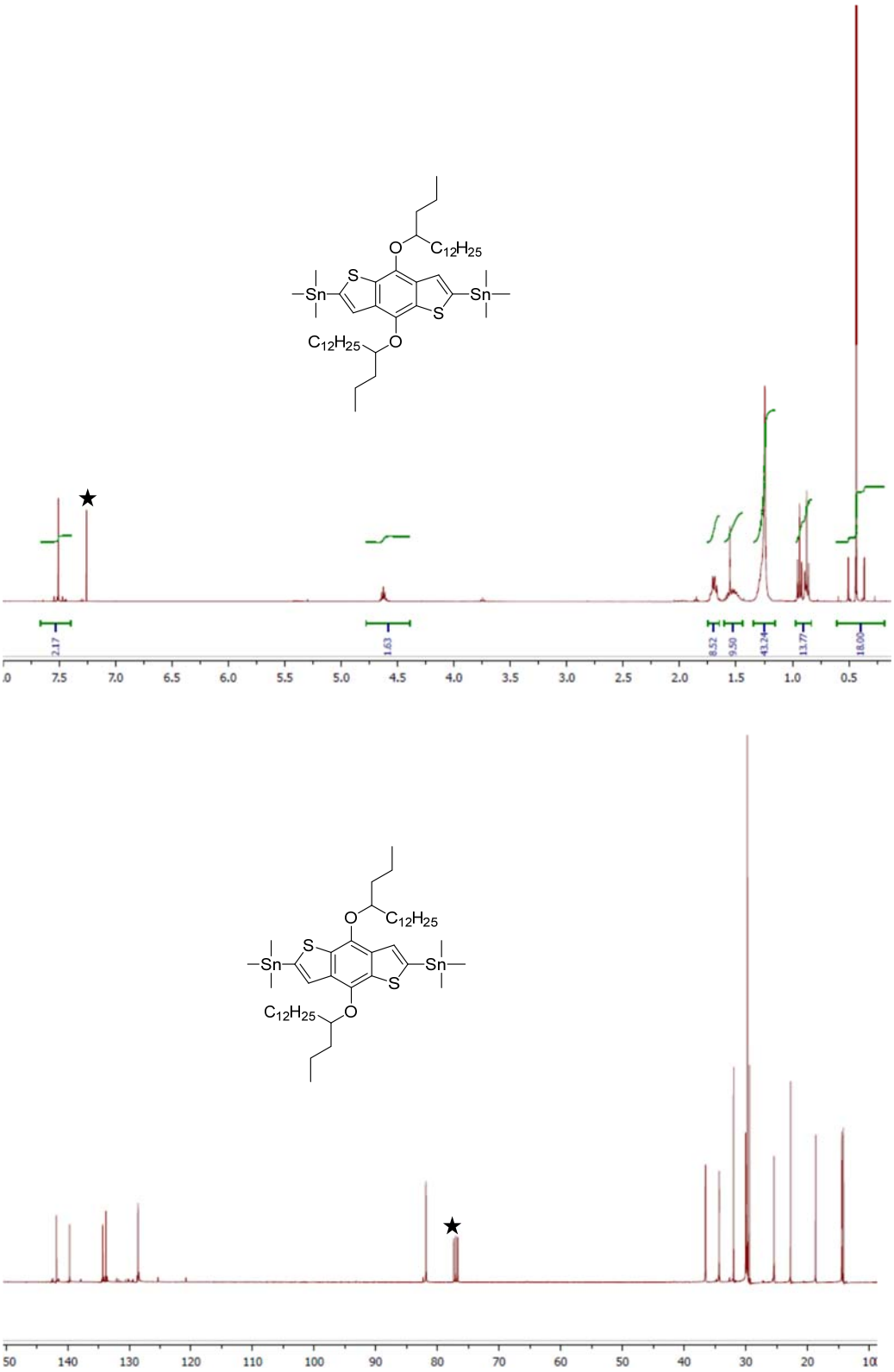

^{1}H (top) and ^{13}C (bottom) NMR spectra ($CDCl_3$, r.t.) of 2.6f (★solvent).

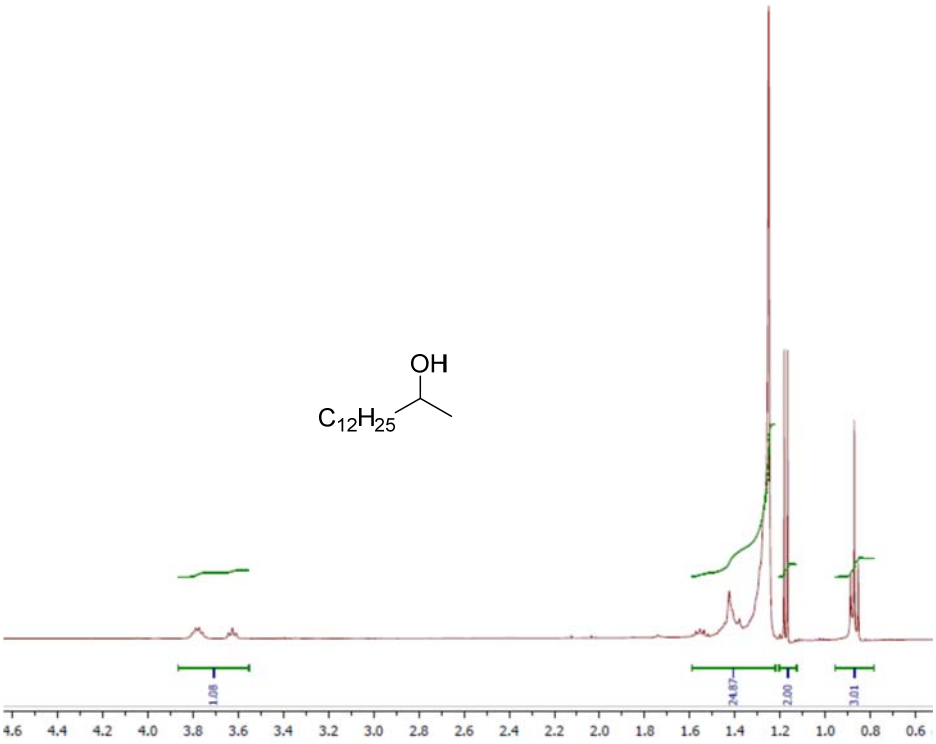

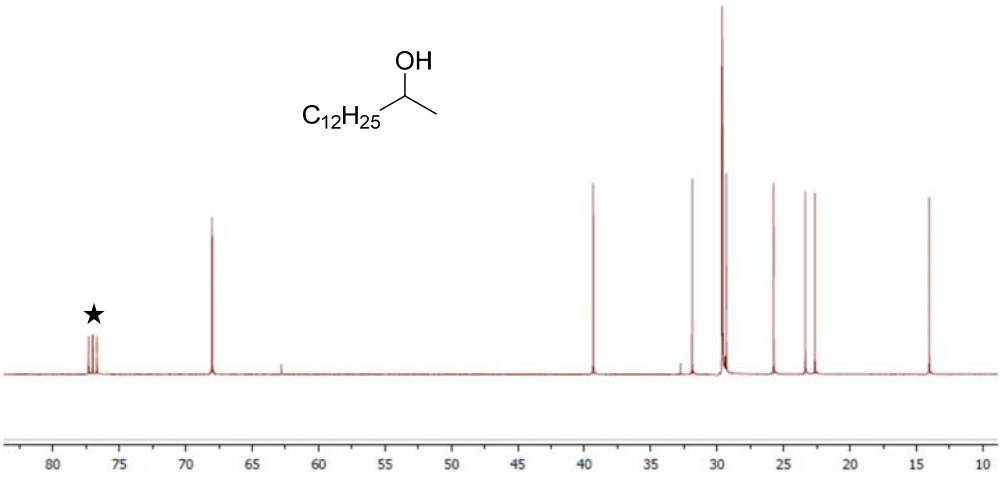

^{1}H (top) and ^{13}C (bottom) NMR spectra ($CDCl_3$, r.t.) of 2.0g (★ solvent).

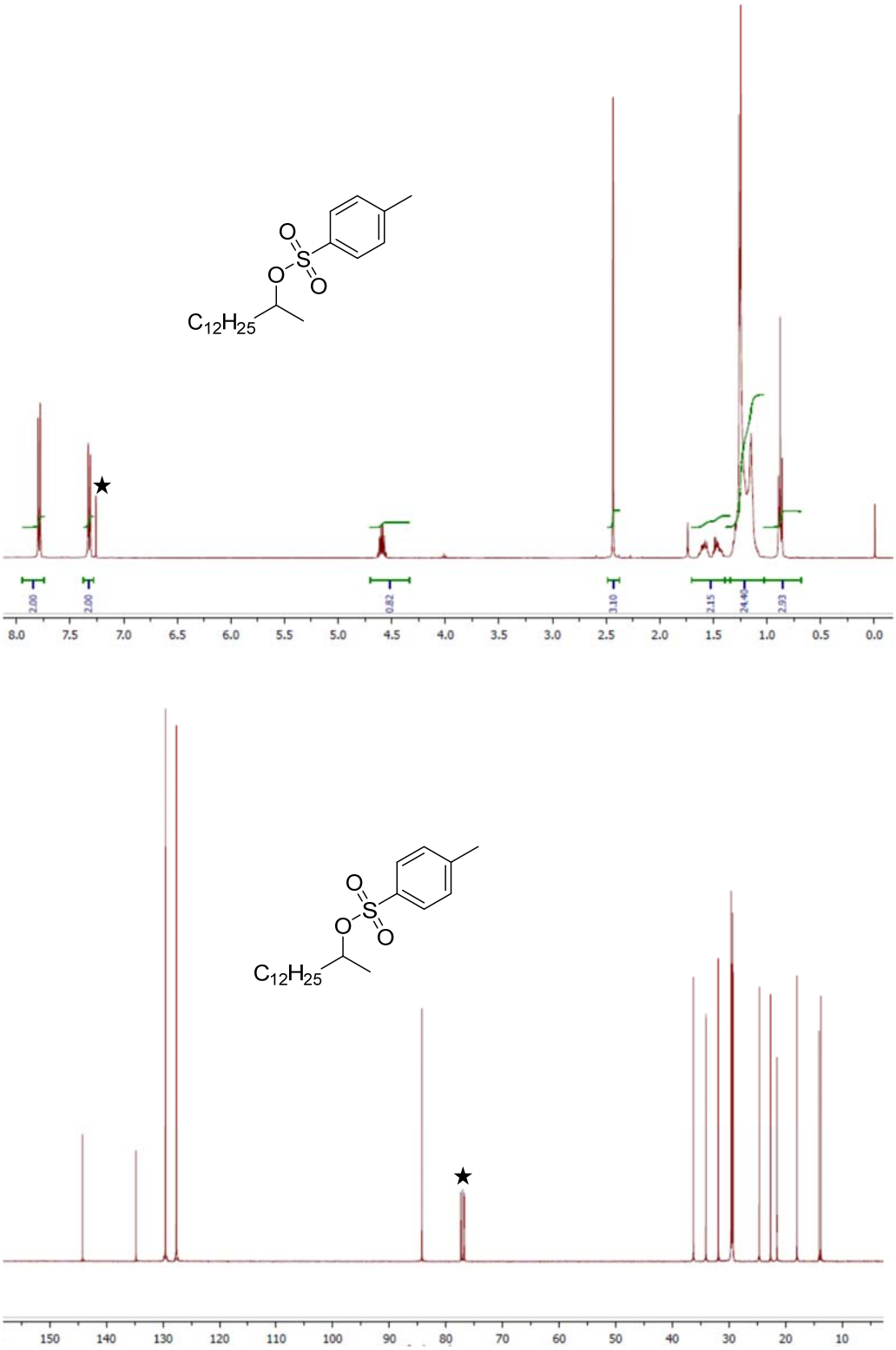

^{1}H (top) and ^{13}C (bottom) NMR spectra ($CDCl_3$, r.t.) of 2.1g (★ solvent).

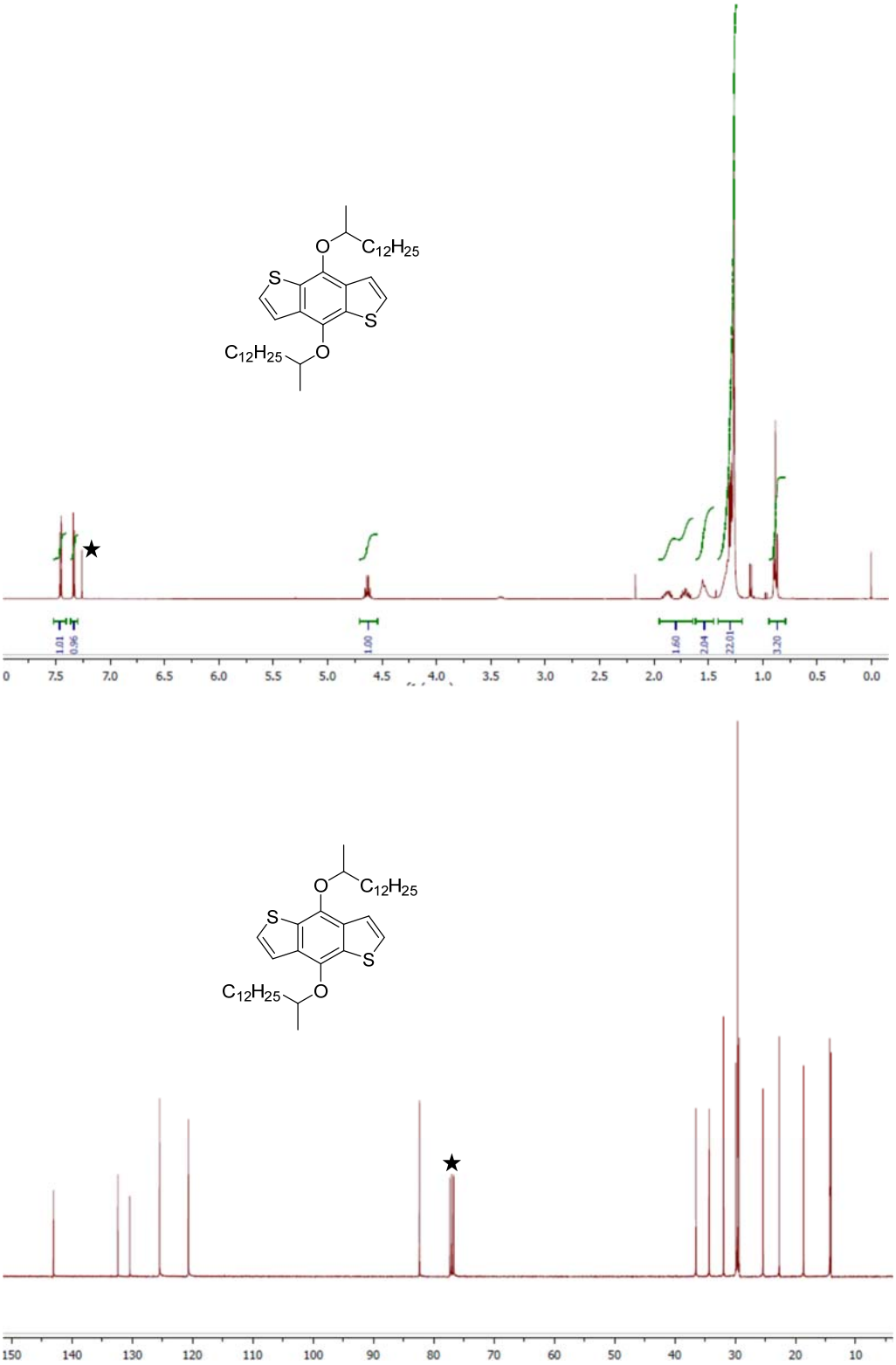

^{1}H (top) and ^{13}C (bottom) NMR spectra ($CDCl_3$, r.t.) of 2.5g (★ solvent).

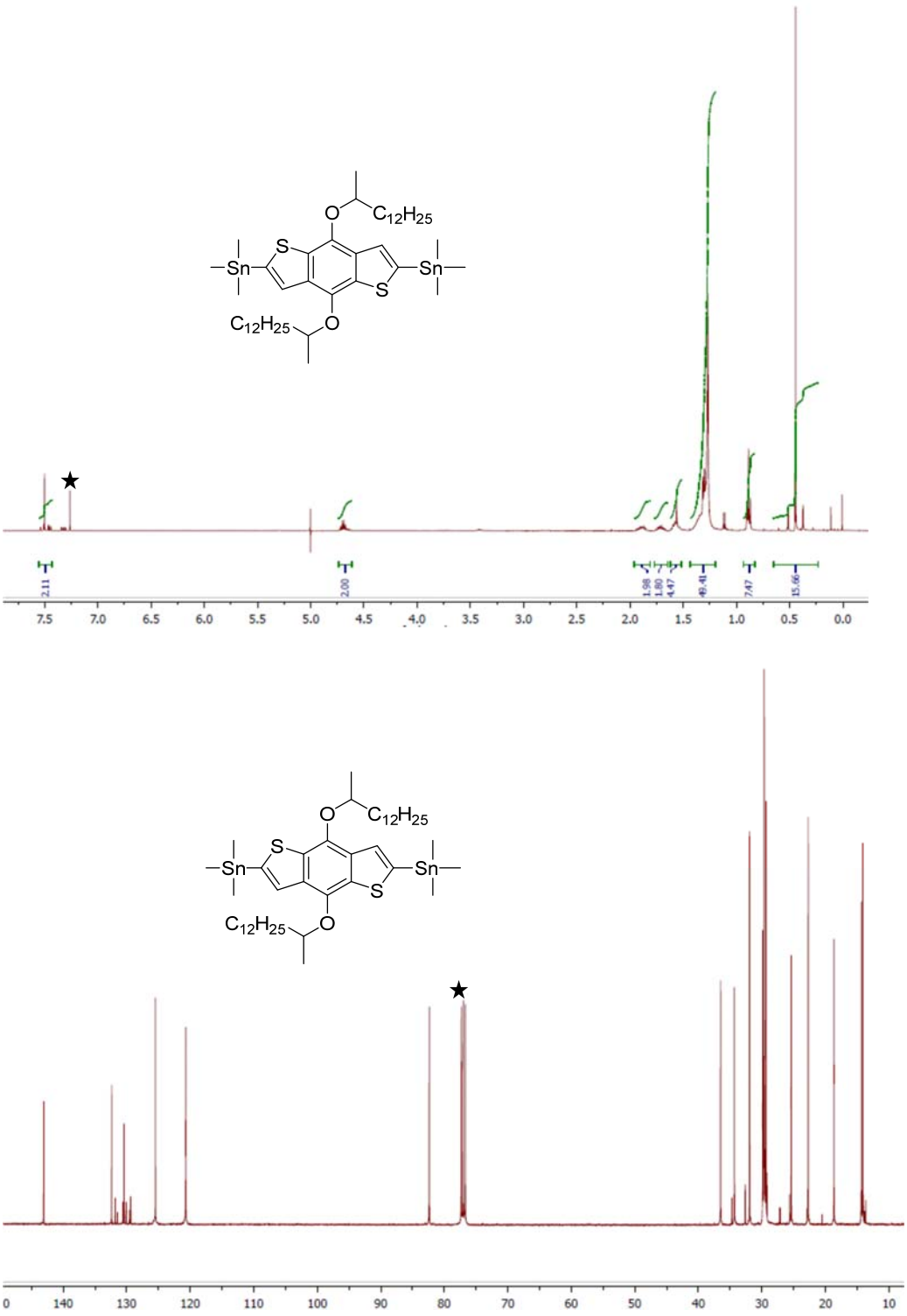

^{1}H (top) and ^{13}C (bottom) NMR spectra ($CDCl_3$, r.t.) of 2.6g (★ solvent).

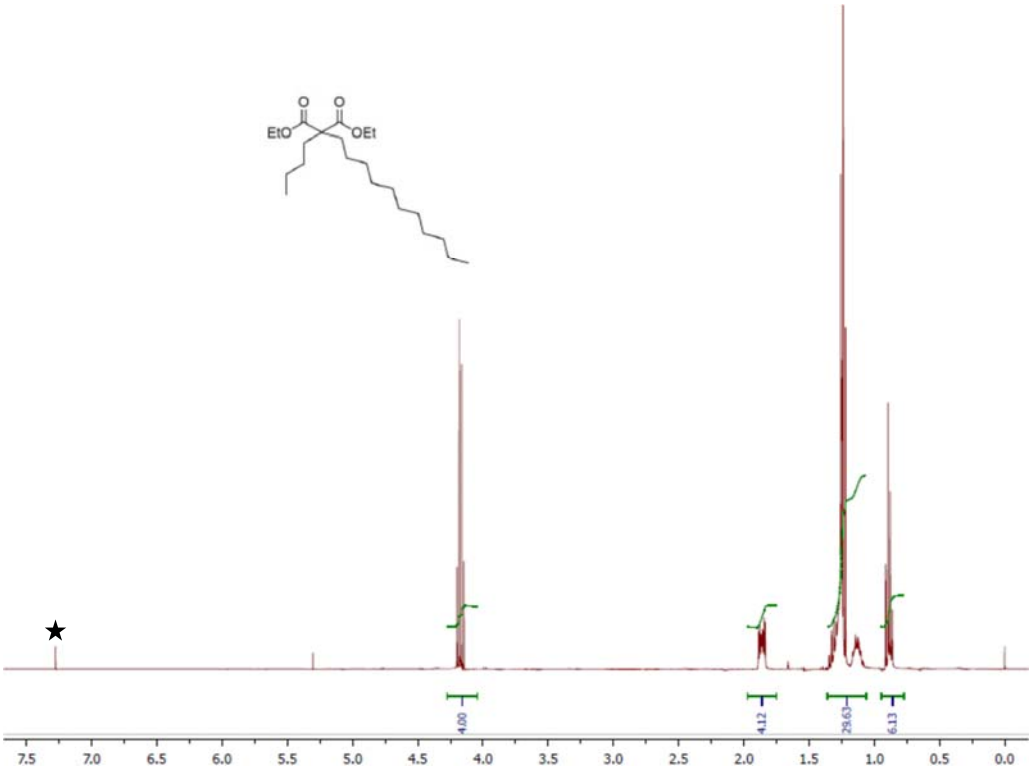

^{1}H NMR spectra ($CDCl_3$, r.t.) of 2.9 (★solvent).

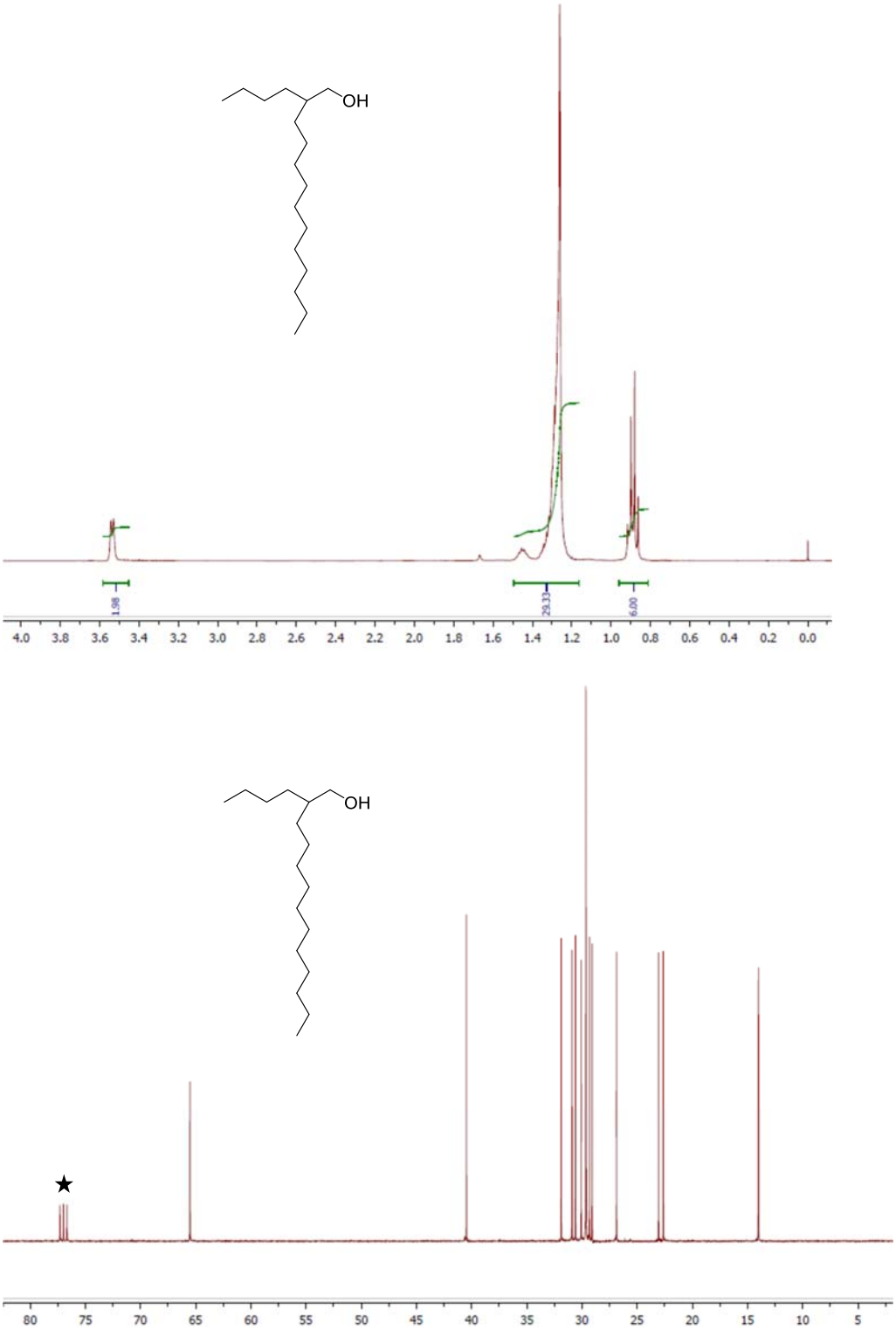

^{1}H (top) and ^{13}C (bottom) NMR spectra ($CDCl_3$, r.t.) of 2.11 (★ solvent).

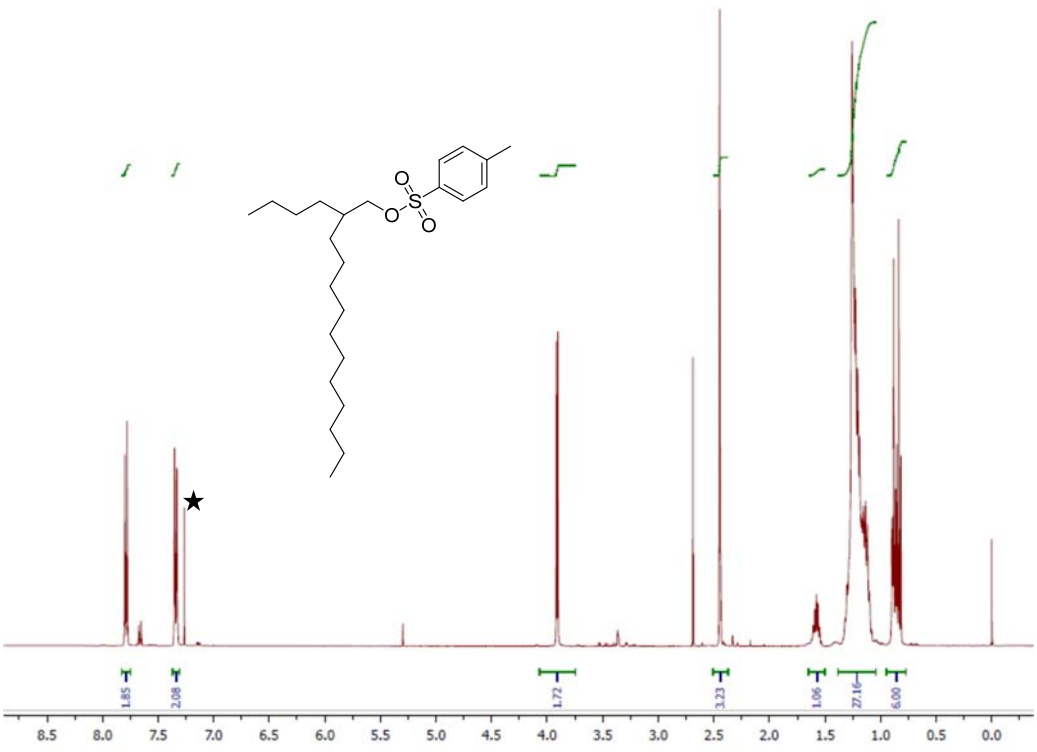

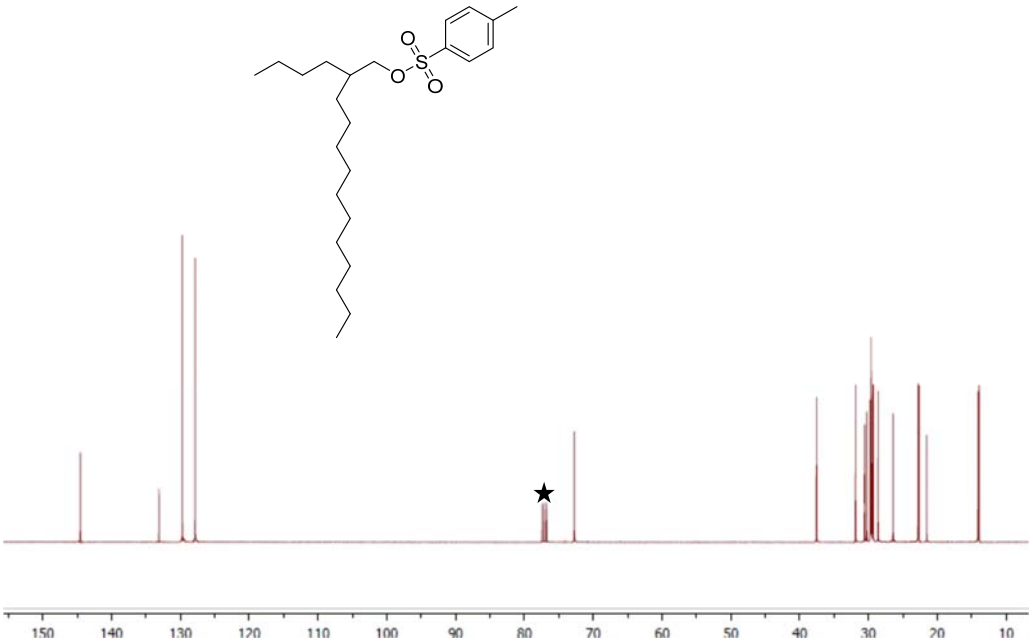

^{1}H (top) and ^{13}C (bottom) NMR spectra ($CDCl_3$, r.t.) of 2.12 (★ solvent).

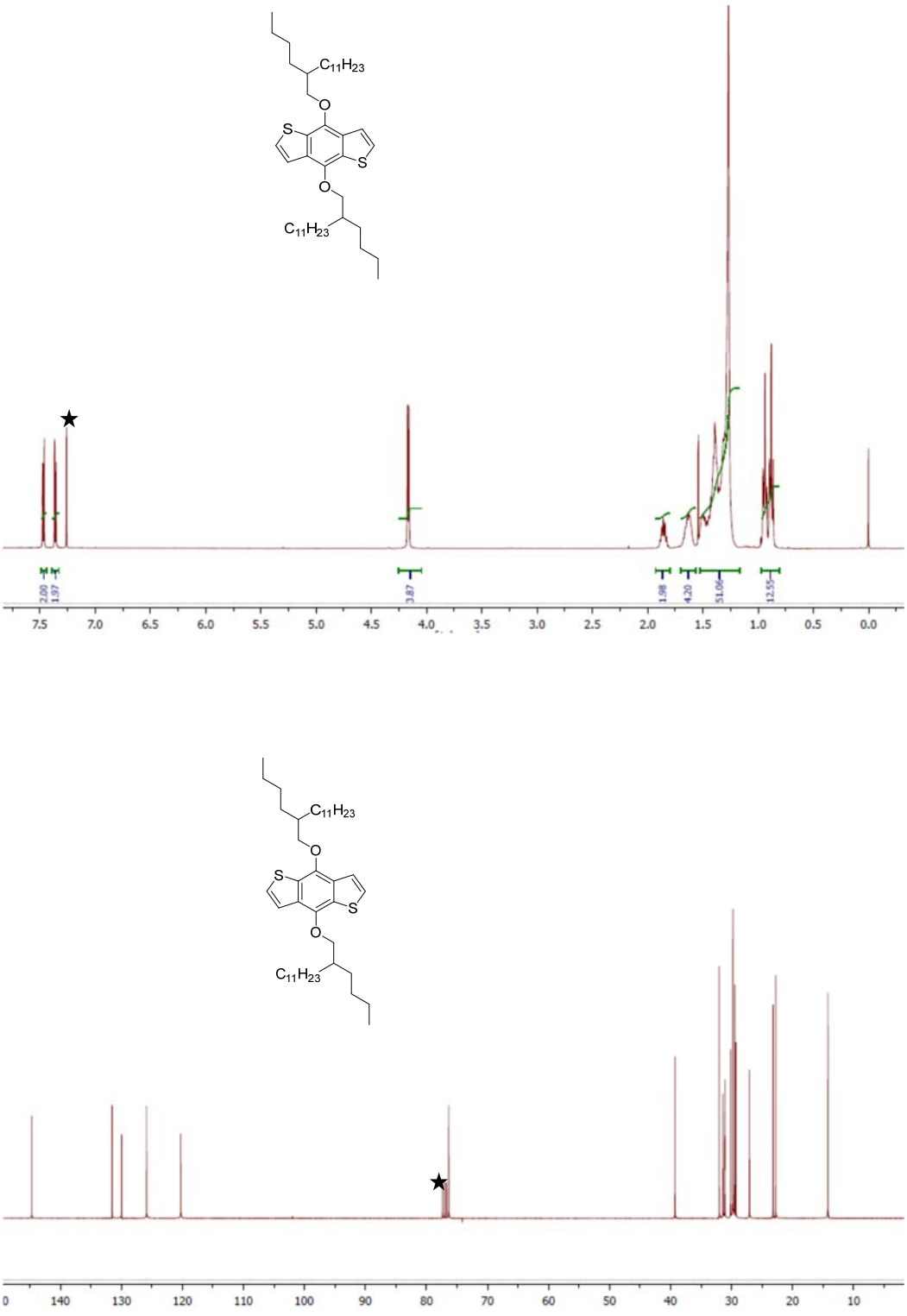

^{1}H (top) and ^{13}C (bottom) NMR spectra ($CDCl_3$, r.t.) of 2.13 (★ solvent).

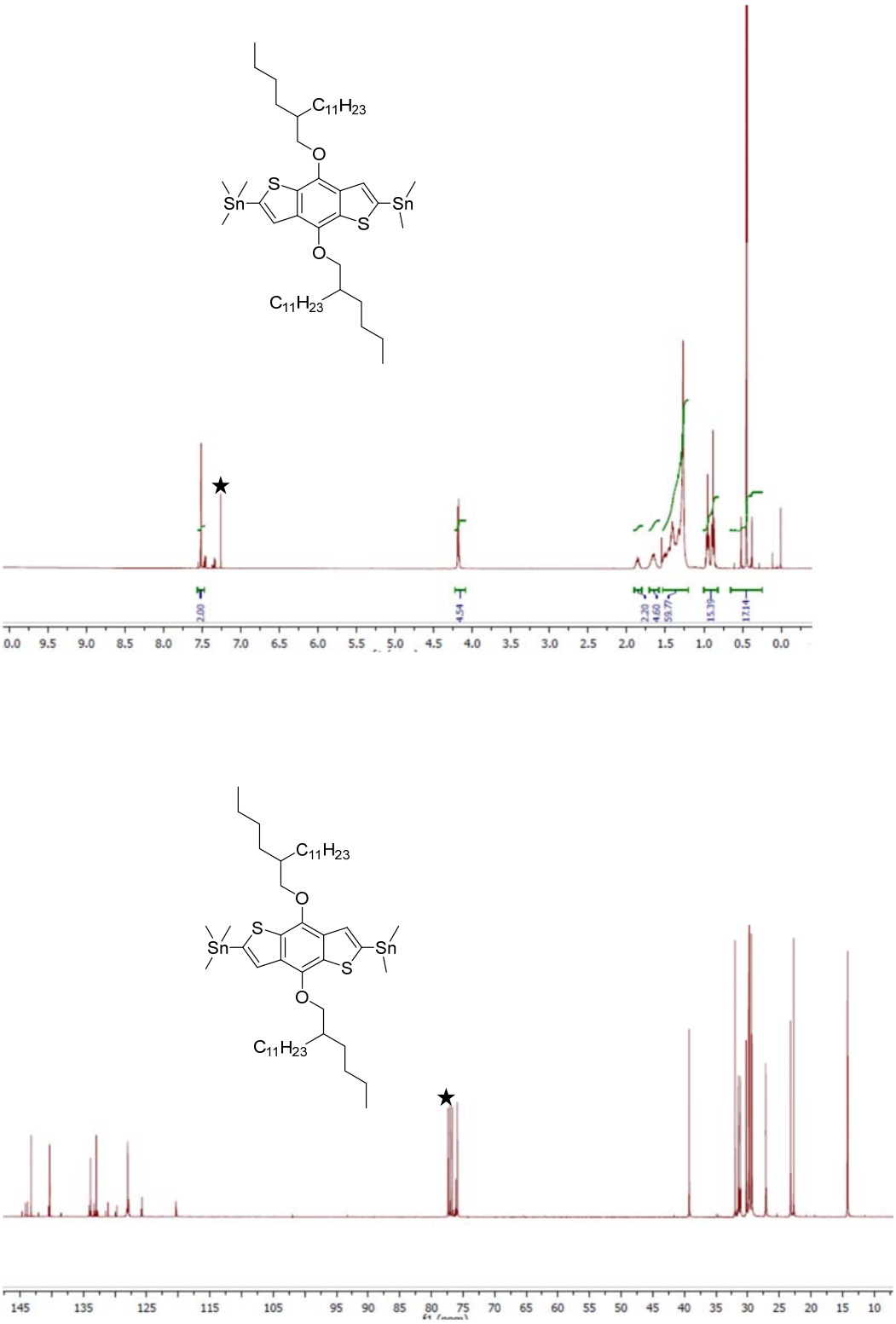

^{1}H (top) and ^{13}C (bottom) NMR spectra ($CDCl_3$, r.t.) of 2.14 (★ solvent).

NMR Spectra for Chapter 3

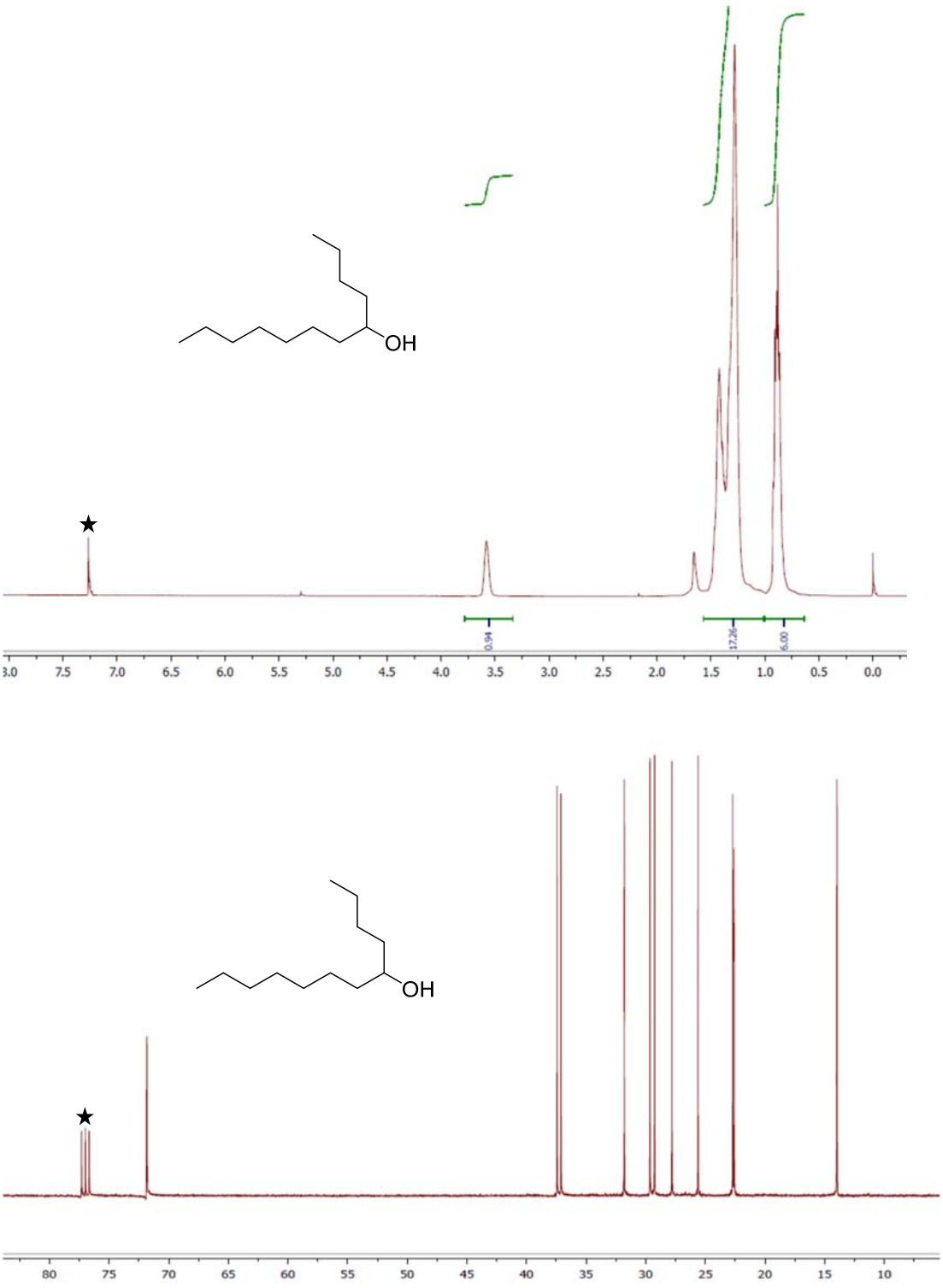

^{1}H (top) and ^{13}C (bottom) NMR spectra ($CDCl_3$, r.t.) of dodecan-5-ol (★ solvent).

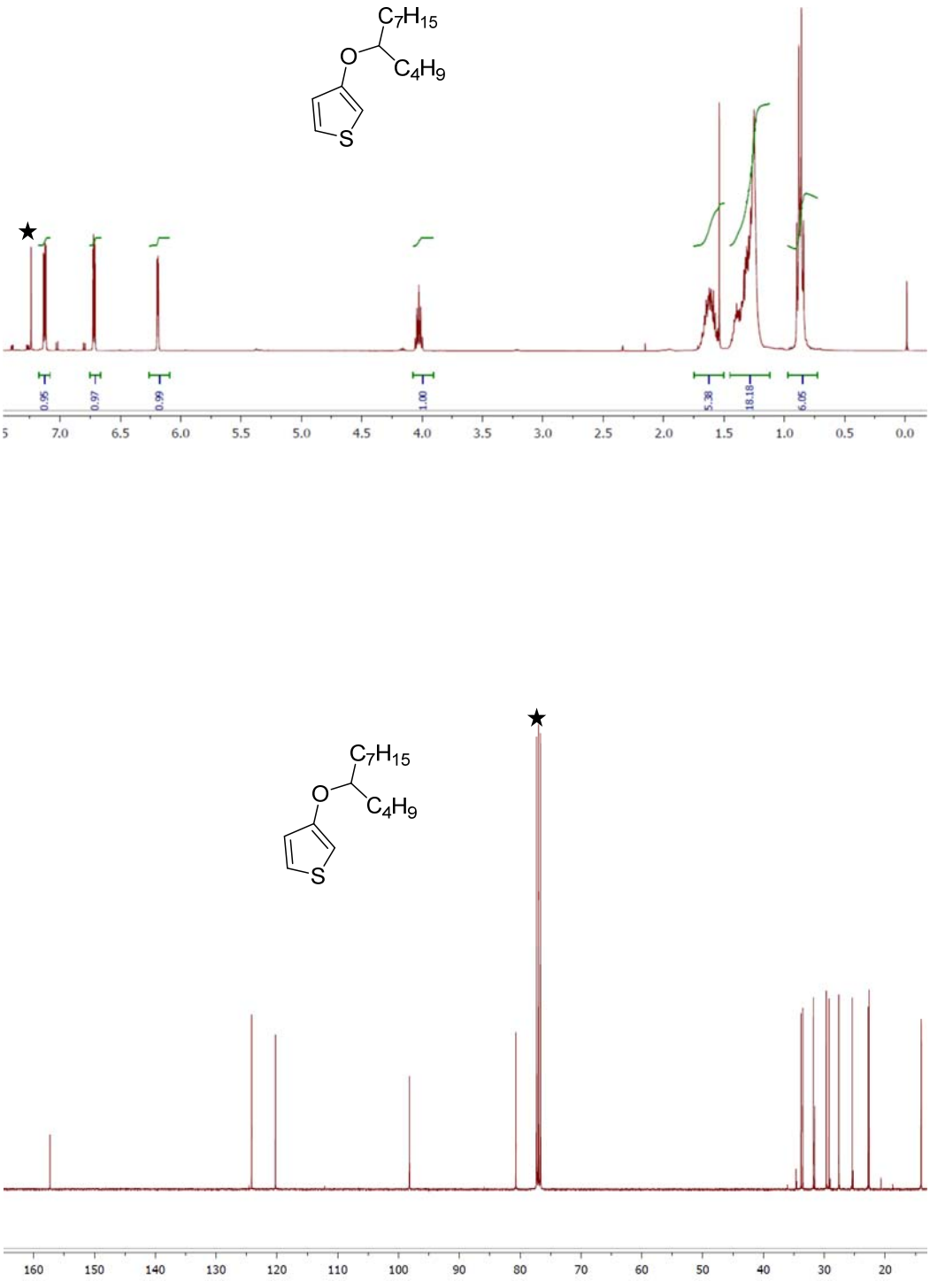

^{1}H (top) and ^{13}C (bottom) NMR spectra ($CDCl_3$, r.t.) of compound 3.5a (★solvent).

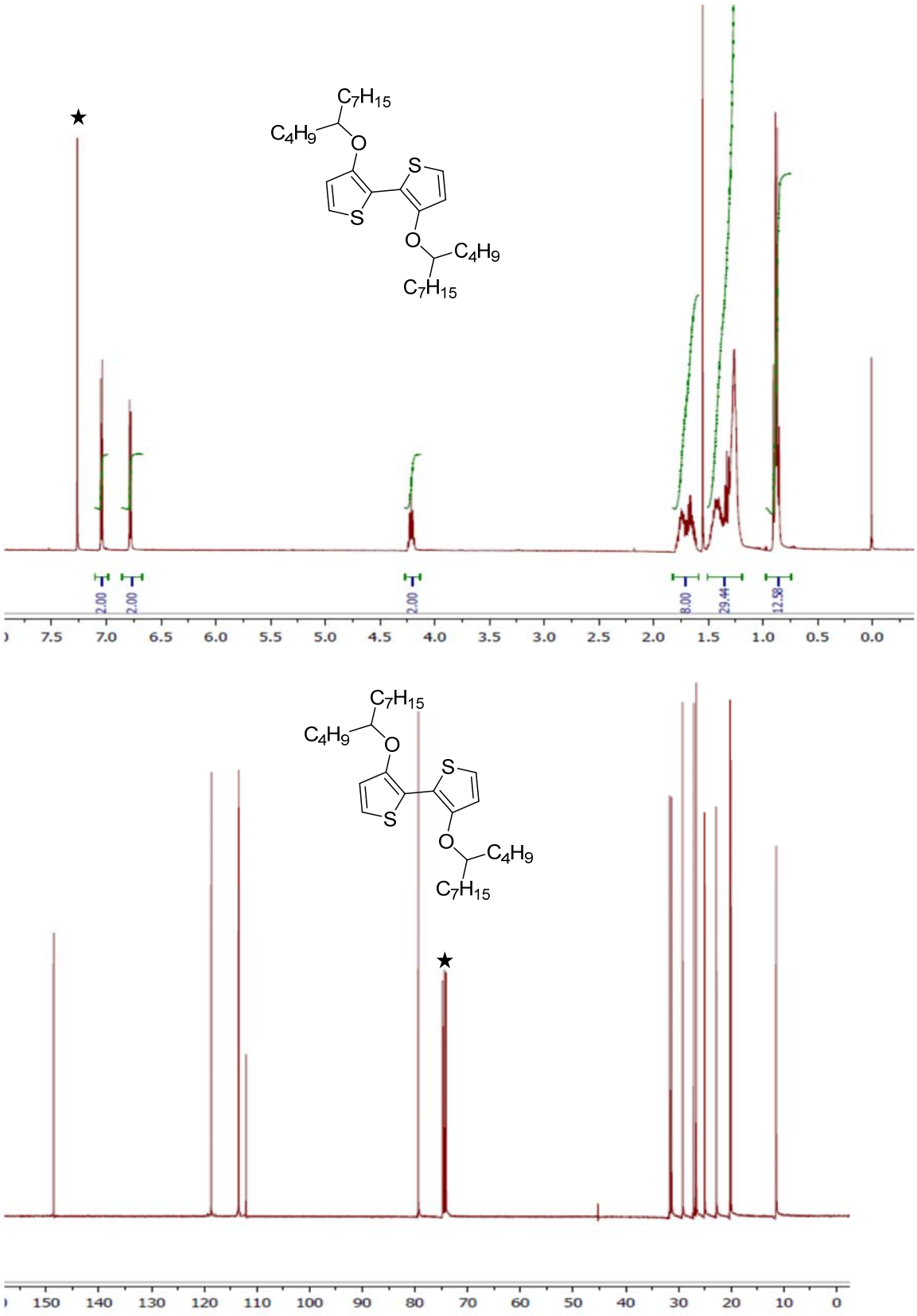

^{1}H (top) and ^{13}C (bottom) NMR spectra ($CDCl_3$, r.t.) of compound 3.6a (★solvent).

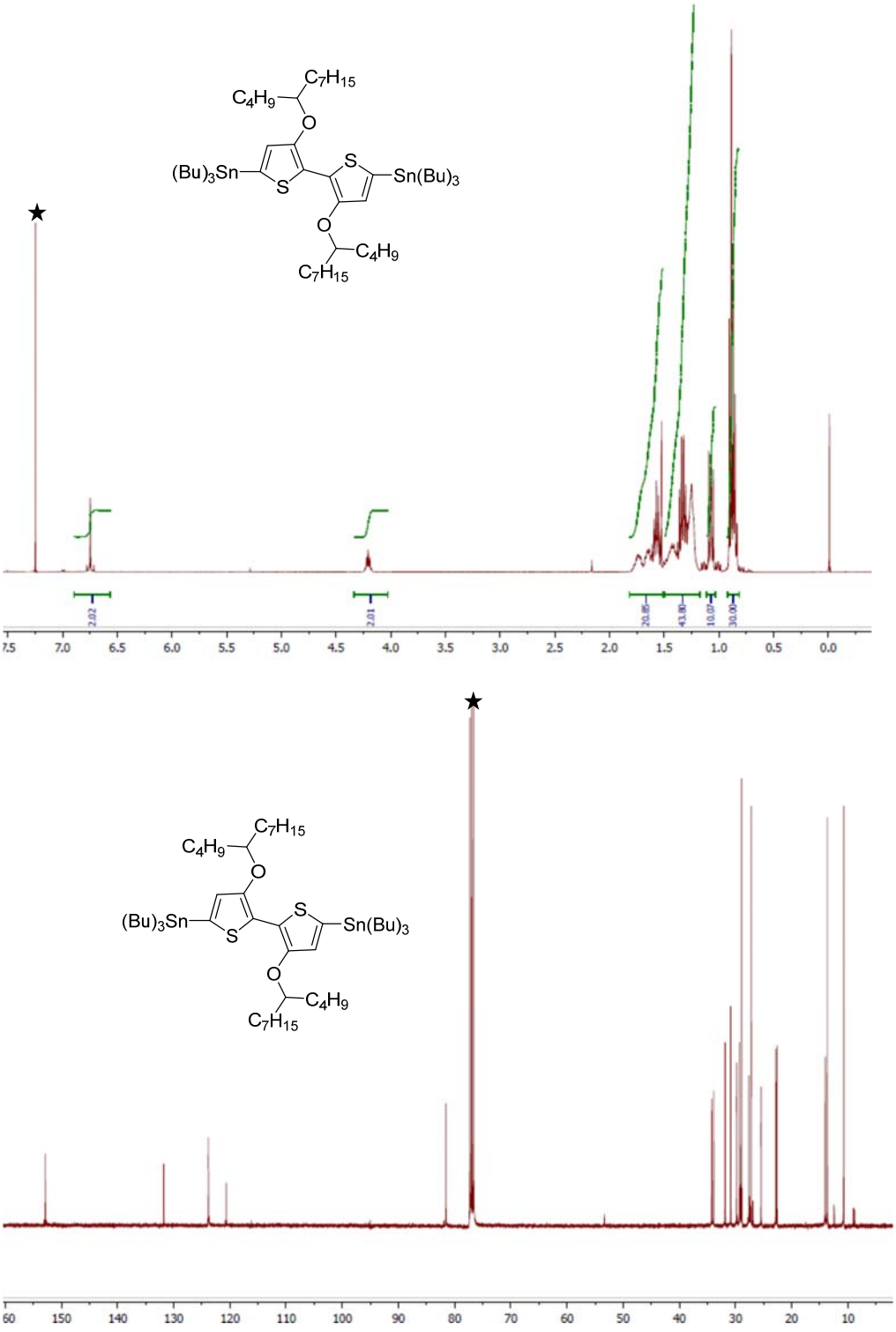

^{1}H (top) and ^{13}C (bottom) NMR spectra ($CDCl_3$, r.t.) of compound 3.7a (★solvent).

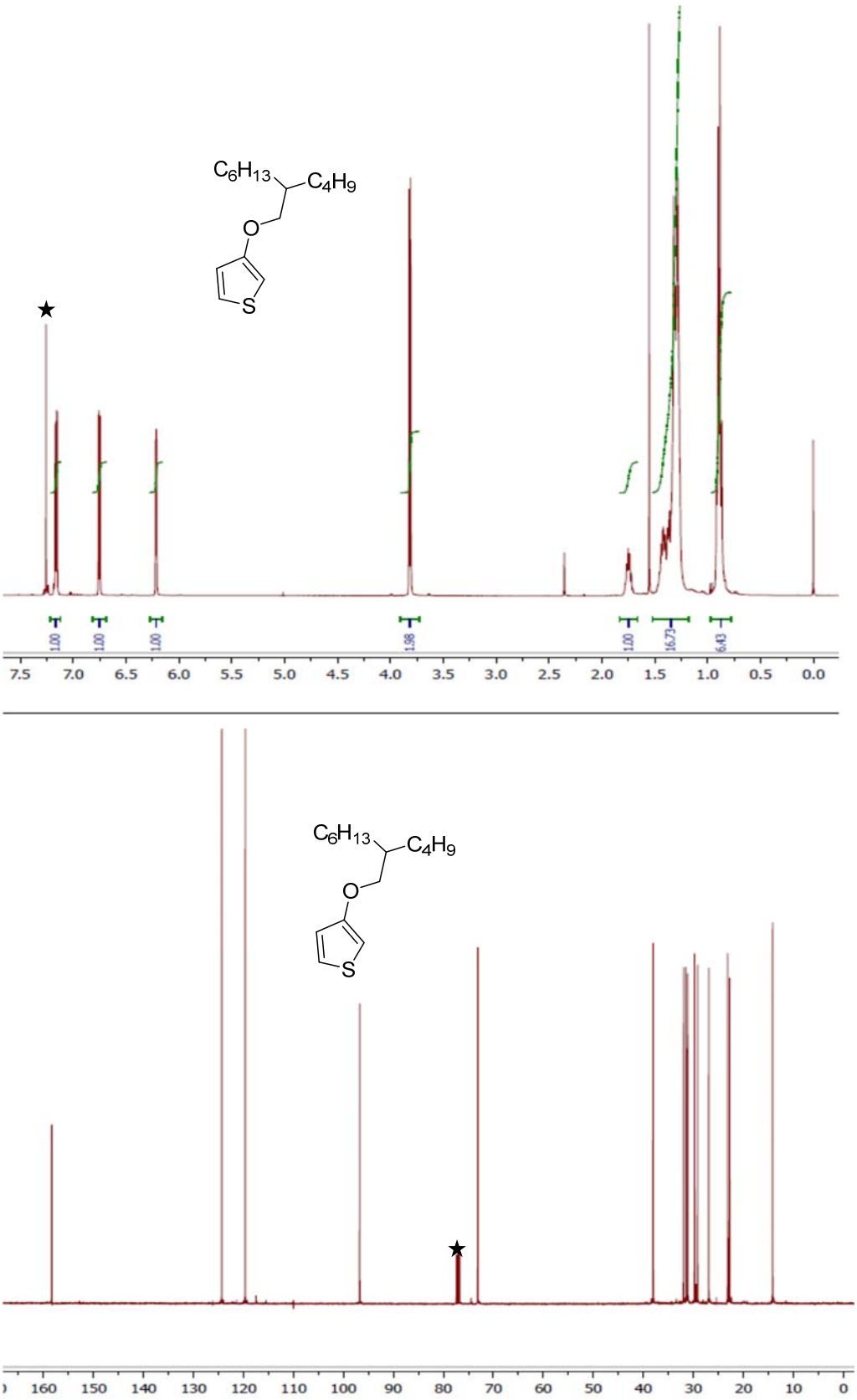

^{1}H (top) and ^{13}C (bottom) NMR spectra ($CDCl_3$, r.t.) of compound 3.5b (★solvent).

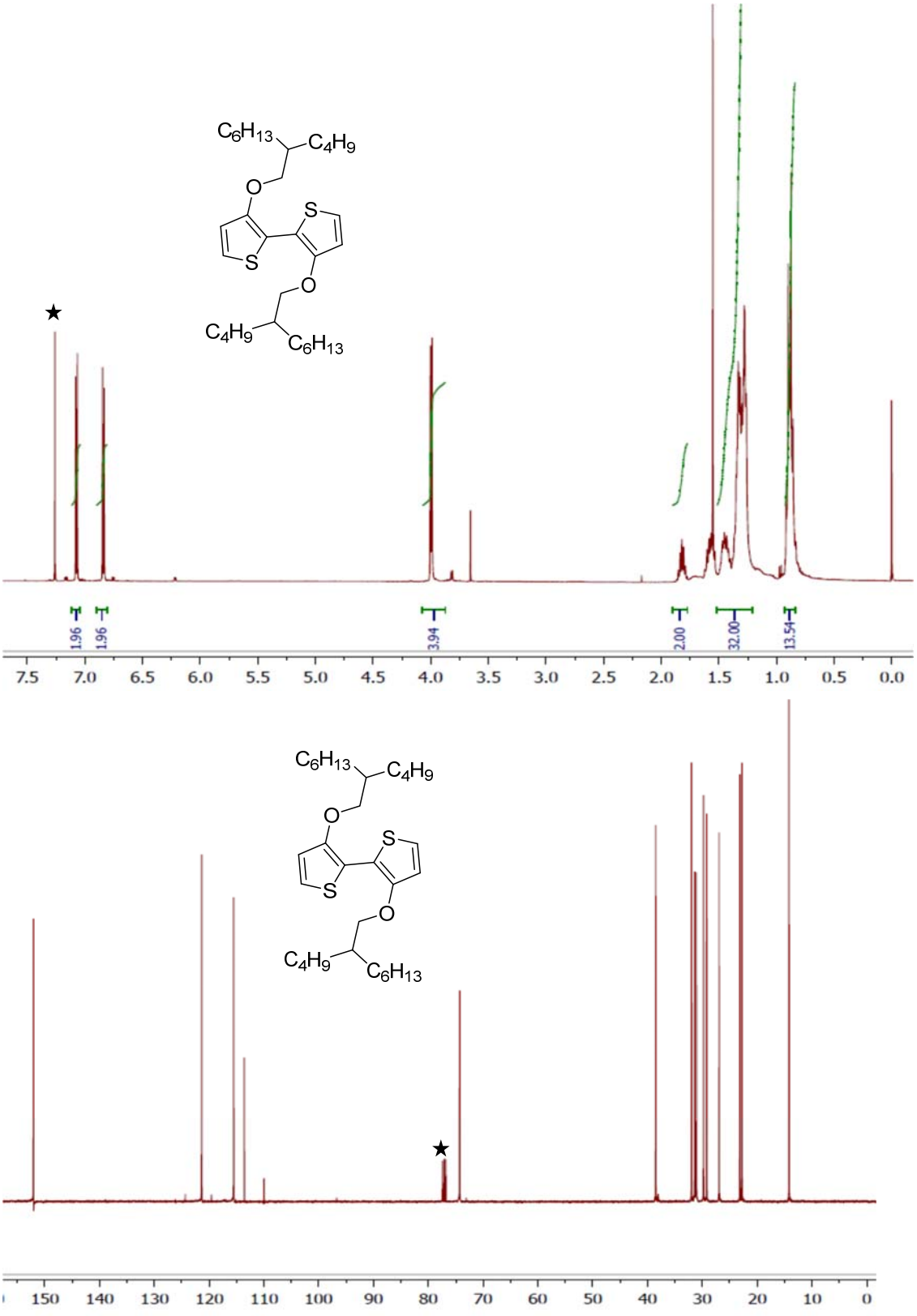

^{1}H (top) and ^{13}C (bottom) NMR spectra ($CDCl_3$, r.t.) of compound 3.6b (★solvent).

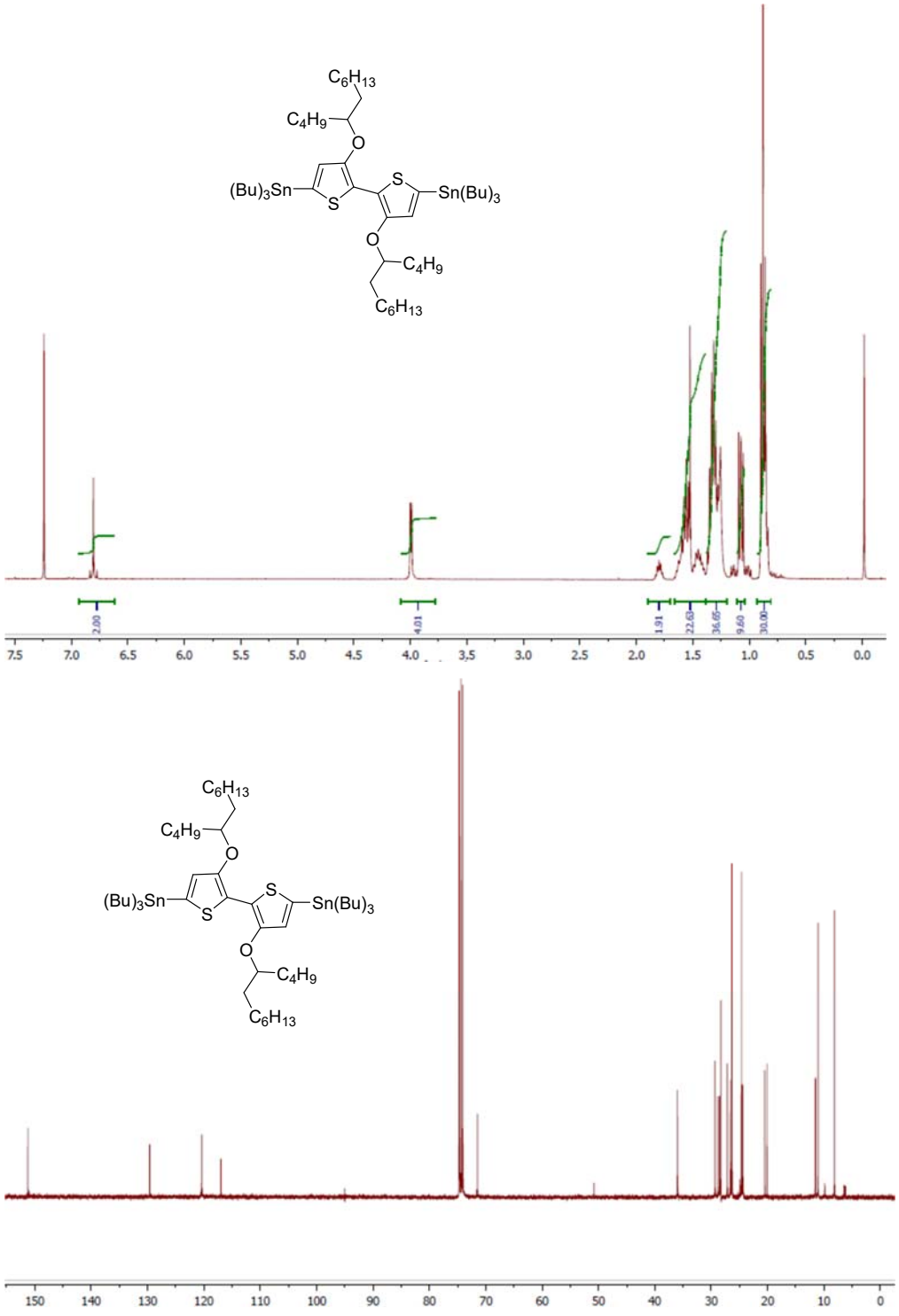

^{1}H (top) and ^{13}C (bottom) NMR spectra ($CDCl_3$, r.t.) of compound 3.7b (★solvent).

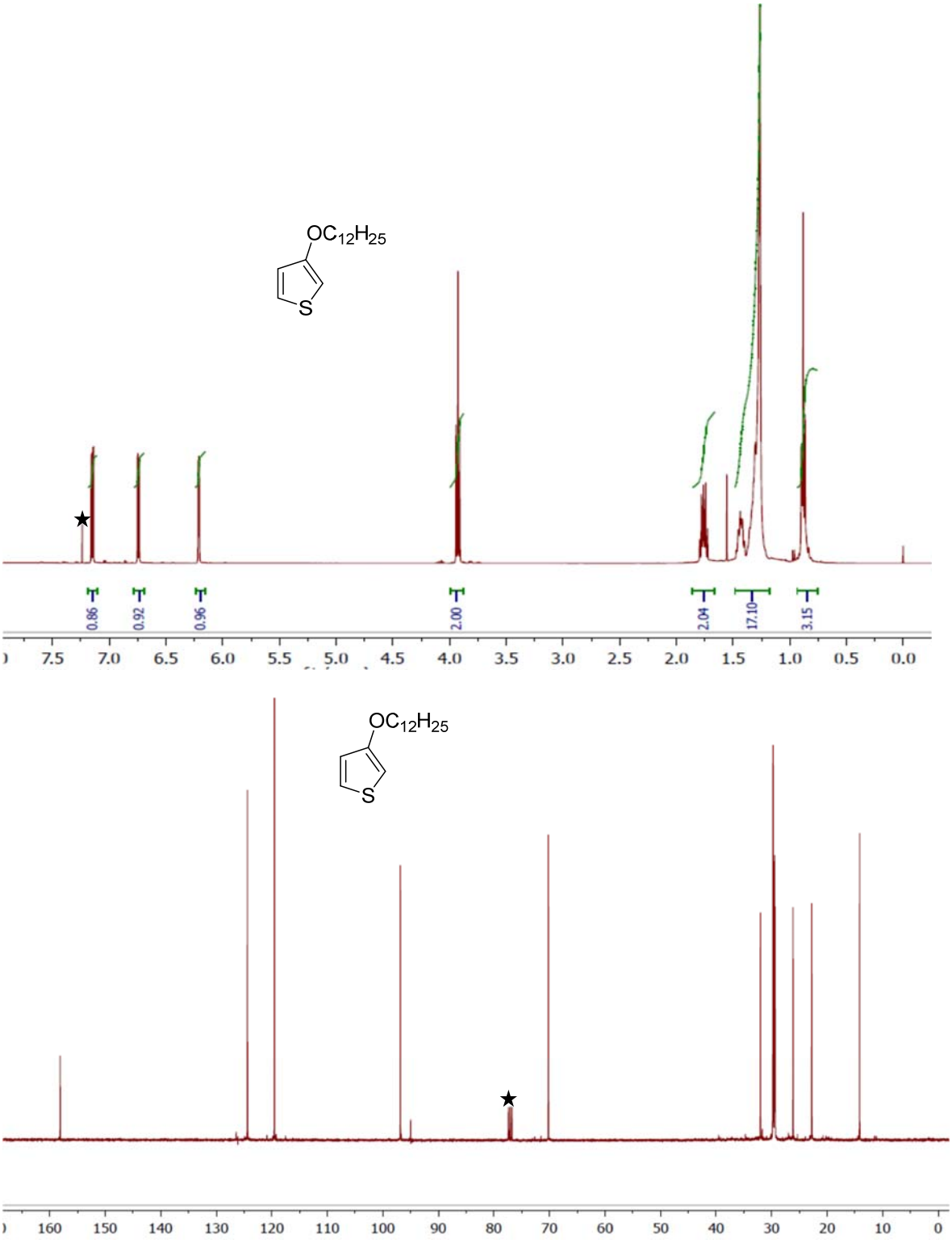

^{1}H (top) and ^{13}C (bottom) NMR spectra ($CDCl_3$, r.t.) of 3.5c (★solvent).

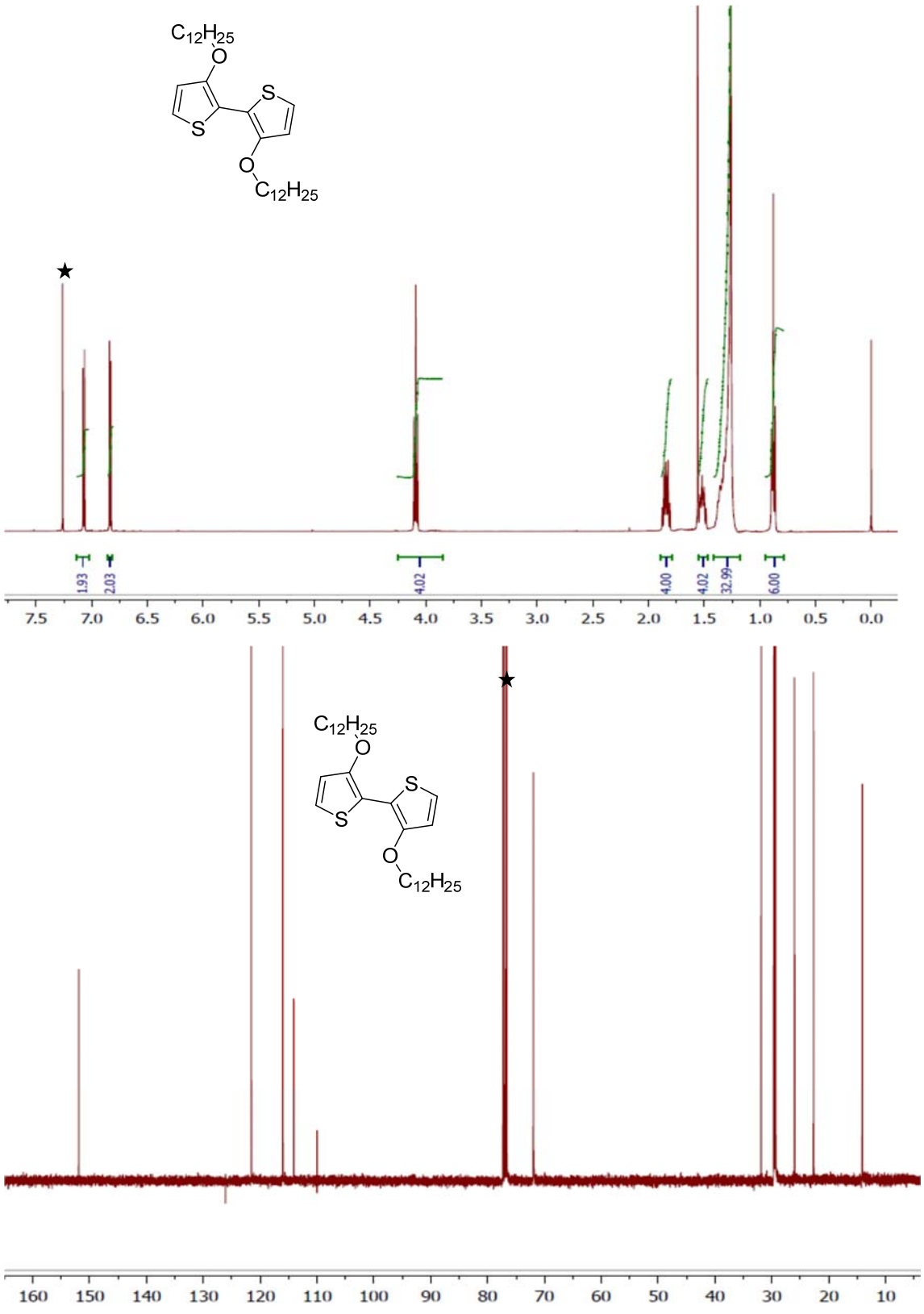

^{1}H (top) and ^{13}C (bottom) NMR spectra ($CDCl_3$, r.t.) of compound 3.6c (★ solvent).

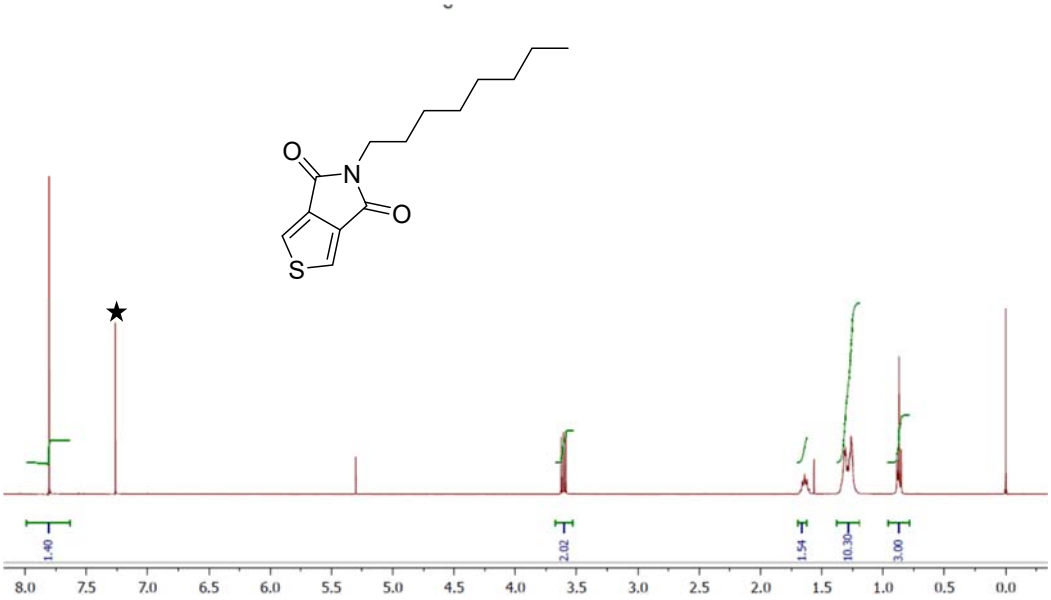

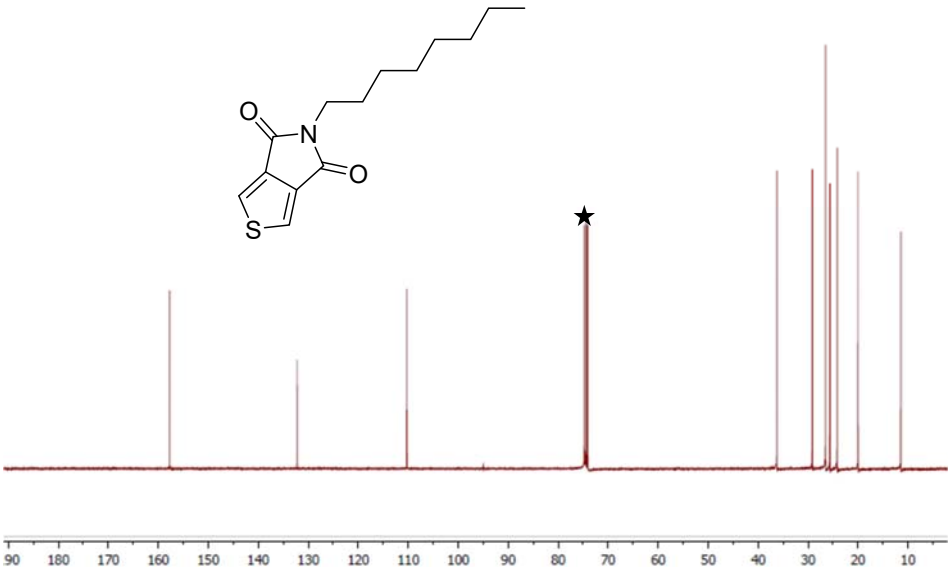

^{1}H (top) and ^{13}C (bottom) NMR spectra ($CDCl_3$, r.t.) of compound 3.2a (★ solvent).

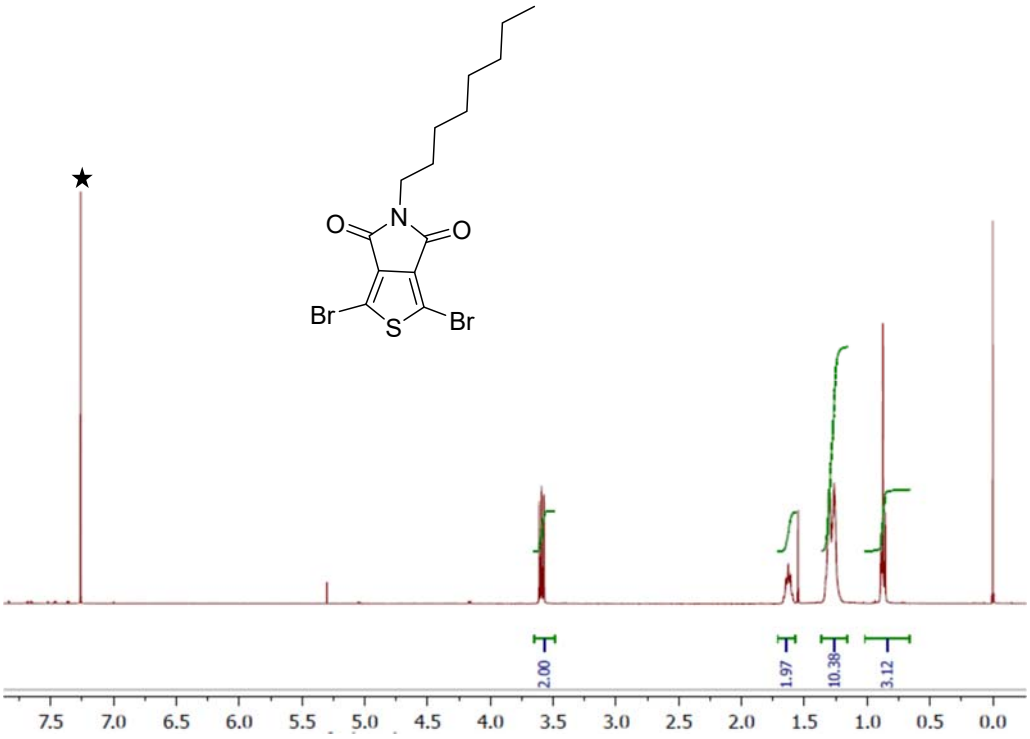

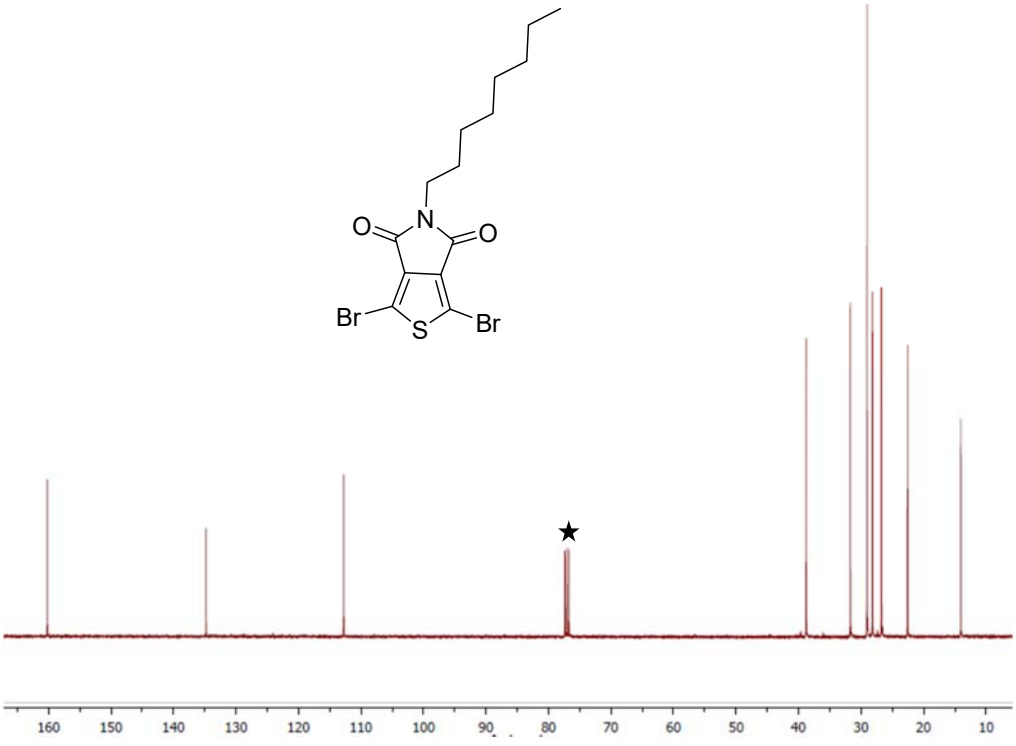

^{1}H (top) and ^{13}C (bottom) NMR spectra ($CDCl_3$, r.t.) of compound 3.3a (★ solvent).

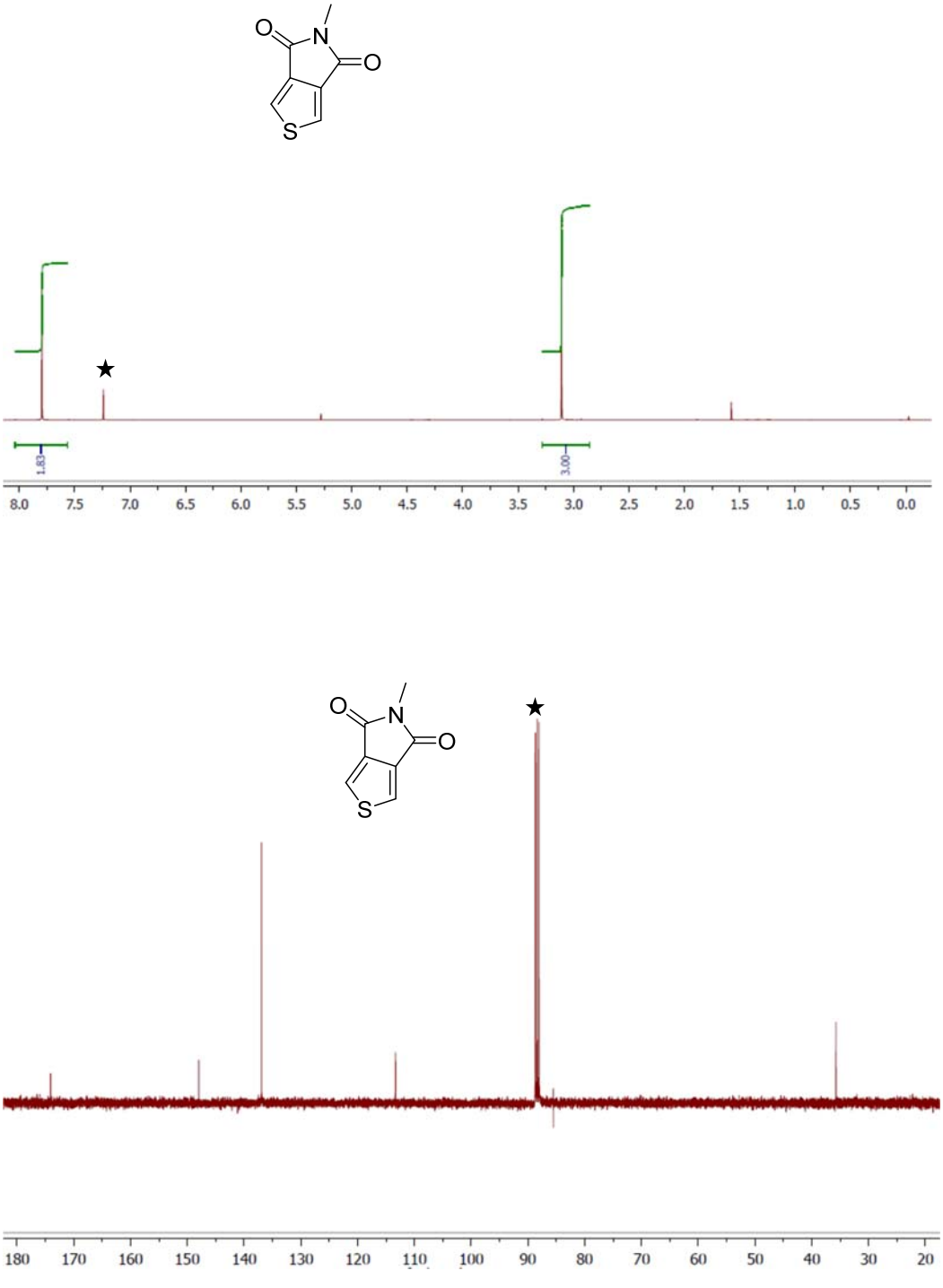

^{1}H (top) and ^{13}C (bottom) NMR spectra ($CDCl_3$, r.t.) of compound 3.2b (★ solvent).

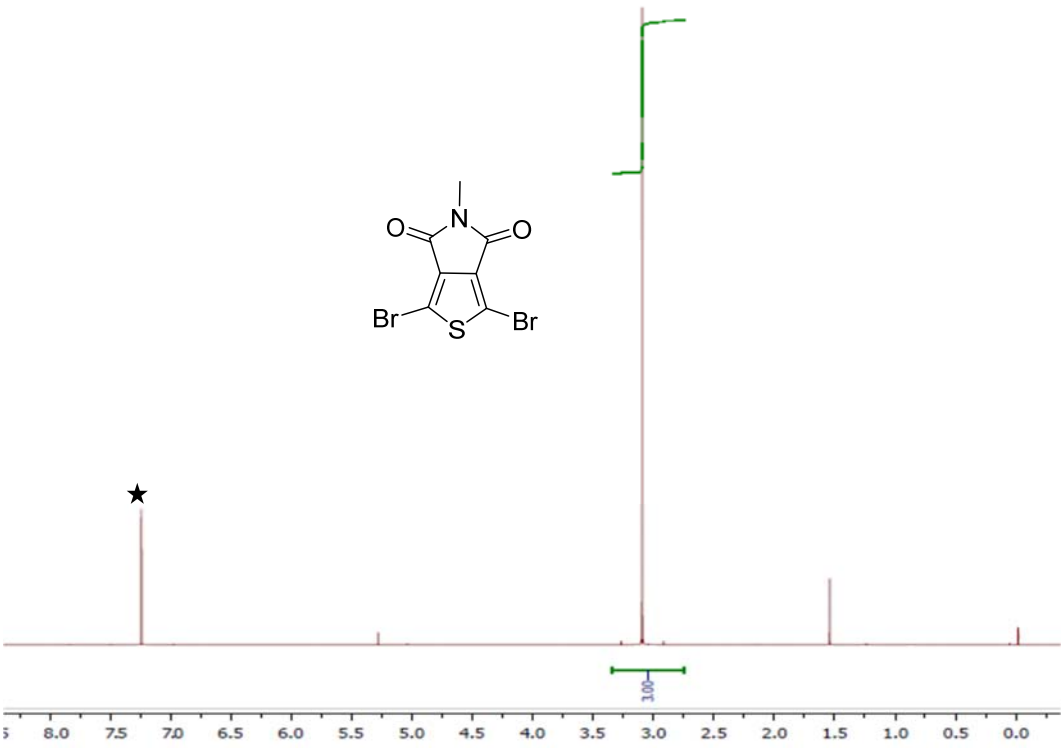

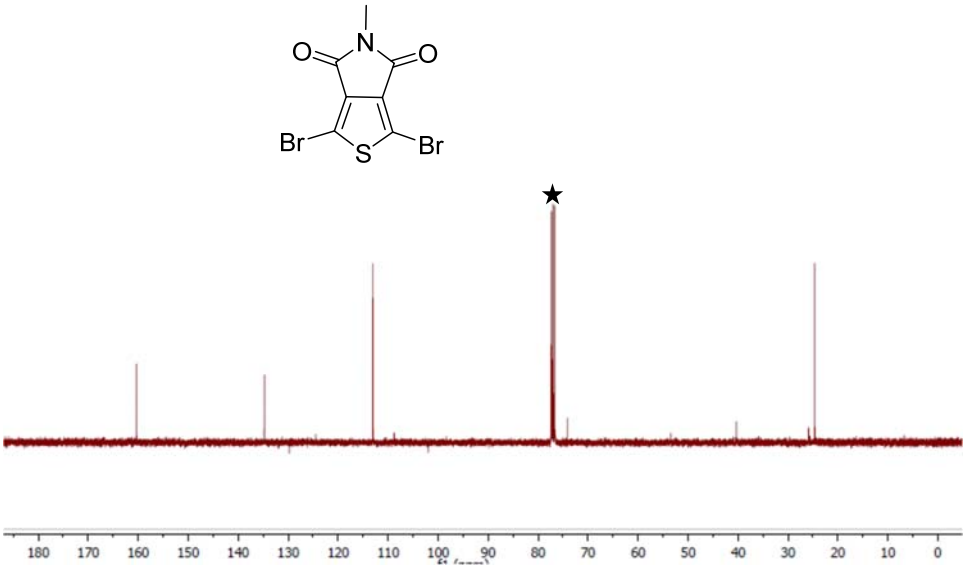

^{1}H (top) and ^{13}C (bottom) NMR spectra ($CDCl_3$, r.t.) of compound 3.3b (★solvent).

NMR Spectra for Chapter 4

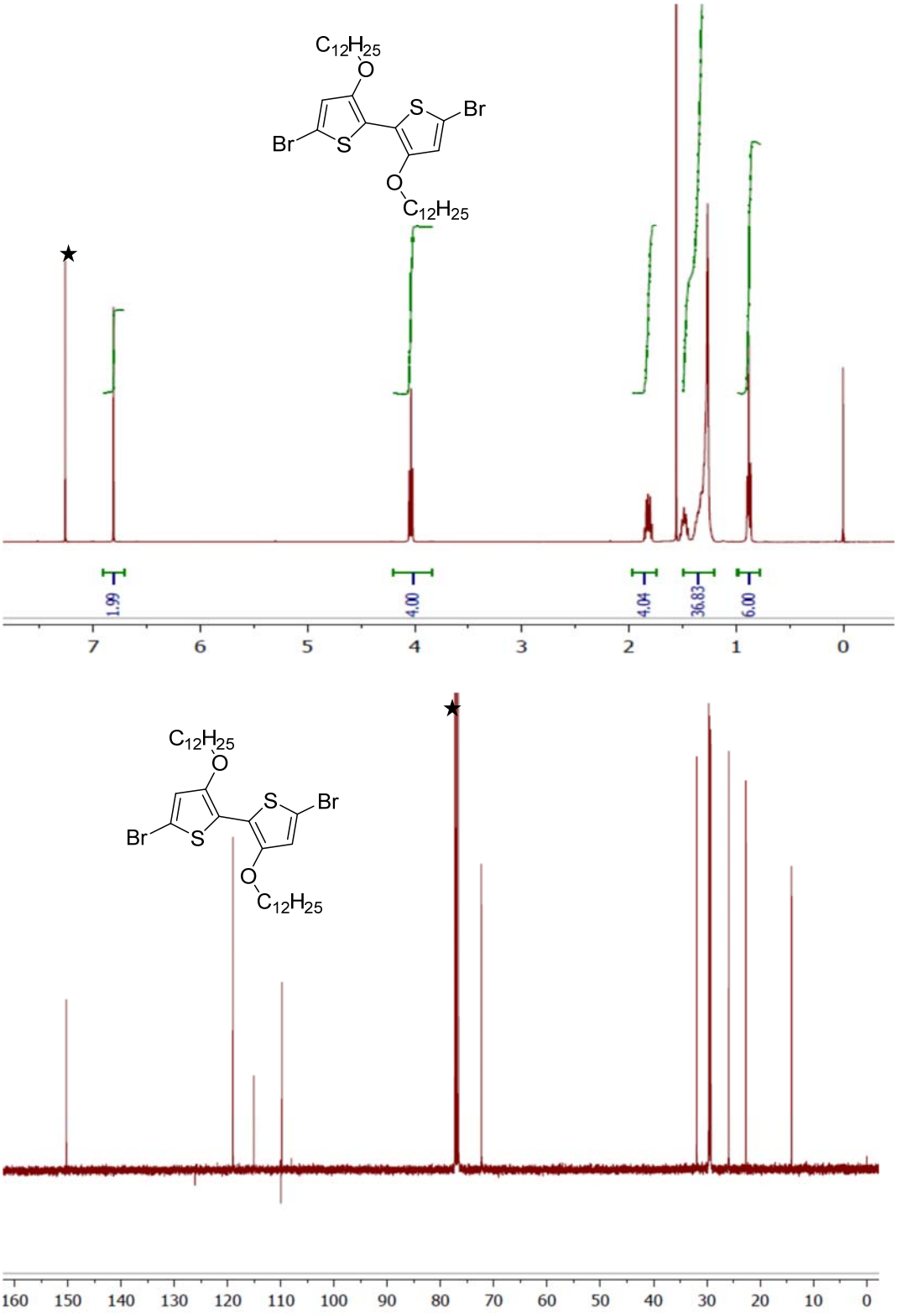

^{1}H (top) and ^{13}C (bottom) NMR spectra ($CDCl_3$, r.t.) of compound 4.0a (★solvent).

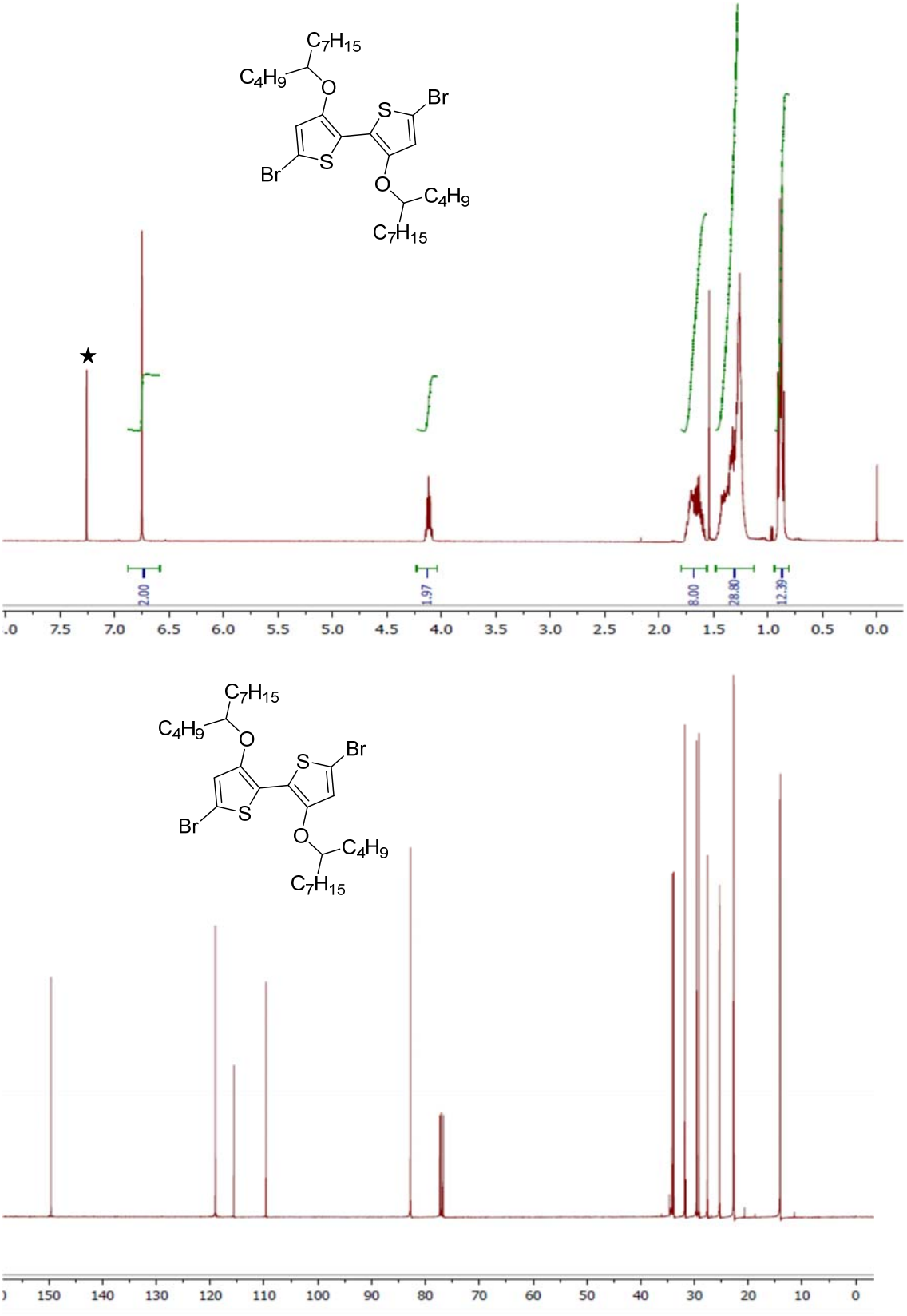

^{1}H (top) and ^{13}C (bottom) NMR spectra ($CDCl_3$, r.t.) of compound 4.0b (★ solvent).

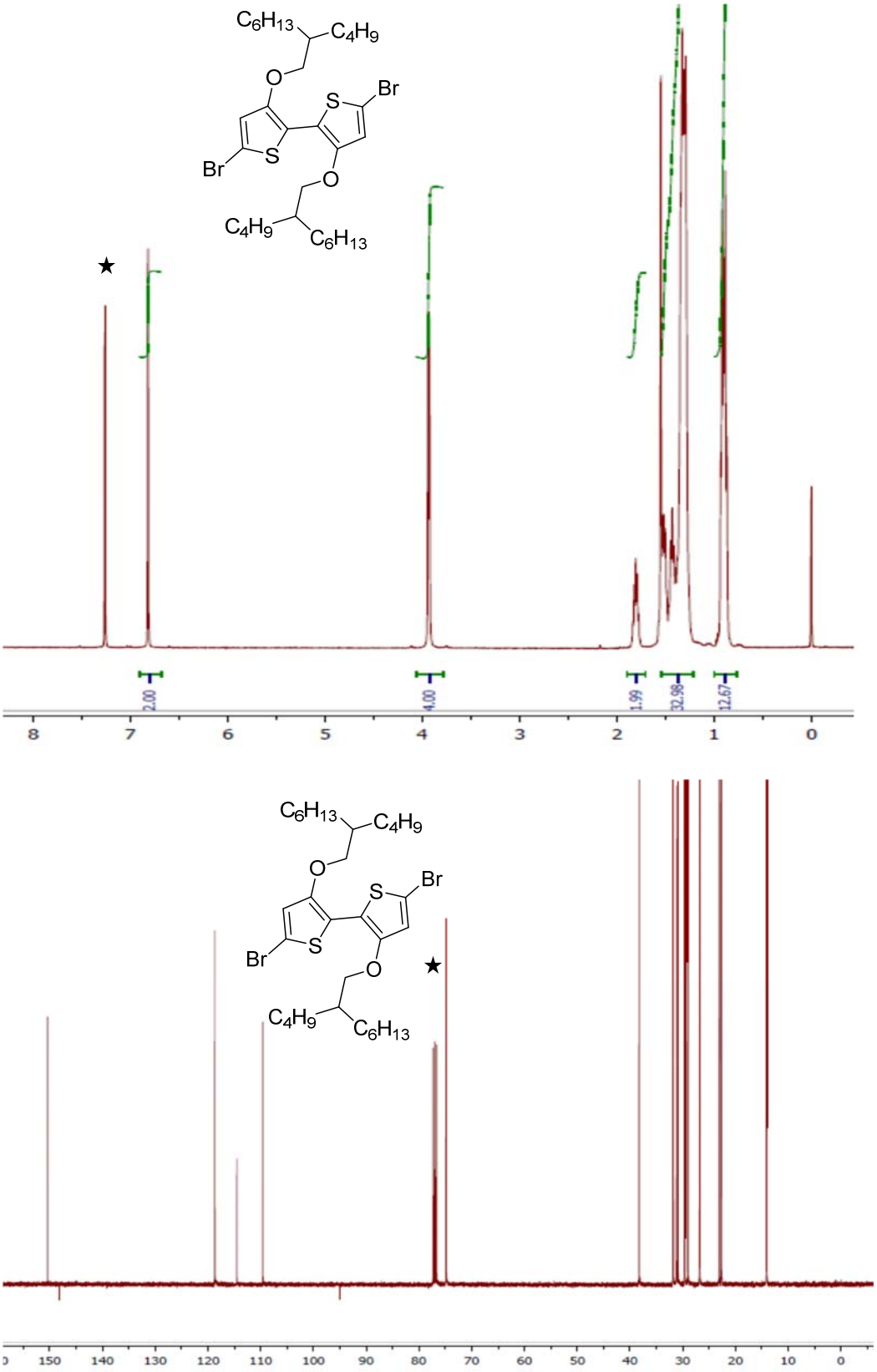

^{1}H (top) and ^{13}C (bottom) NMR spectra ($CDCl_3$, r.t.) of compound 4.0c (★ solvent).

References:

(1) Shirakawa, H.; Louis, E. J.; MacDiarmid, A. G.; Chiang, C. K.; Heeger, A. J. *Journal of the Chemical Society, Chemical Communications* **1977**, 578.

(2) Heeger, A. J. *Chemical Society Reviews* **2010**, *39*, 2354.

(3) Tourillon, G.; Garnier, F. *Journal of Electroanalytical Chemistry and Interfacial Electrochemistry* **1982**, *135*, 173.

(4) Diaz, A.; Kanazawa, K. K.; Gardini, G. P. *Journal of the Chemical Society, Chemical Communications* **1979**, 635.

(5) Diaz, A.; Logan, J. *Journal of Electroanalytical Chemistry and Interfacial Electrochemistry* **1980**, *111*, 111.

(6) Sato, M.-a.; Tanaka, S.; Kaeriyama, K. *Journal of the Chemical Society, Chemical Communications* **1986**, 873.

(7) Jen, K.-Y.; Miller, G.; Elsenbaumer, R. L. *Journal of the Chemical Society, Chemical Communications* **1986**, 1346.

(8) Hotta, S.; Rughooputh, S.; Heeger, A.; Wudl, F. *Macromolecules* **1987**, *20*, 212.

(9) McCullough, R. D.; Lowe, R. D. *Journal of the Chemical Society, Chemical Communications* **1992**, 70.

(10) Chen, T. A.; Rieke, R. D. *Journal of the American Chemical Society* **1992**, *114*, 10087.

(11) Zhang, Z. G.; Wang, J. *Journal of Materials Chemistry* **2012**, *22*, 4178.

(12) Forrest, S. R. *Nature* **2004**, *428*, 911.

(13) Grimsdale, A. C.; Leok Chan, K.; Martin, R. E.; Jokisz, P. G.; Holmes, A. B. *Chemical reviews* **2009**, *109*, 897.

(14) Sirringhaus, H. *Advanced materials* **2014**, *26*, 1319.

(15) Lu, L.; Zheng, T.; Wu, Q.; Schneider, A. M.; Zhao, D.; Yu, L. *Chemical reviews* **2015**, *115*, 12666.

(16) Beaujuge, P. M.; Reynolds, J. R. *Chemical reviews* **2010**, *110*, 268.

(17) McQuade, D. T.; Pullen, A. E.; Swager, T. M. *Chemical reviews* **2000**, *100*, 2537.

(18) Po, R.; Bianchi, G.; Carbonera, C.; Pellegrino, A. *Macromolecules* **2015**, *48*, 453.

(19) Swager, T. M. *Macromolecules* **2017**, *50*, 4867.

(20) DeLongchamp, D. M.; Kline, R. J.; Jung, Y.; Lin, E. K.; Fischer, D. A.; Gundlach, D. J.; Cotts, S. K.; Moad, A. J.; Richter, L. J.; Toney, M. F. *Macromolecules* **2008**, *41*, 5709.

(21) Hämäläinen, M.; Hari, R.; Ilmoniemi, R. J.; Knuutila, J.; Lounasmaa, O. V. *Reviews of modern Physics* **1993**, *65*, 413.

(22) Roncali, J. *Chemical reviews* **1997**, *97*, 173.

(23) Roncali, J. *Macromolecular Rapid Communications* **2007**, *28*, 1761.

(24) Liang, Y.; Feng, D.; Wu, Y.; Tsai, S.-T.; Li, G.; Ray, C.; Yu, L. *Journal of the American Chemical Society* **2009**, *131*, 7792.

(25) Liu, C.; Wang, K.; Gong, X.; Heeger, A. J. *Chemical Society reviews* **2016**, *45*, 4825.

(26) Huang, H.; Yang, L.; Facchetti, A.; Marks, T. J. *Chemical reviews* **2017**, *117*, 10291.

(27) Carsten, B.; Szarko, J. M.; Lu, L.; Son, H. J.; He, F.; Botros, Y. Y.; Chen, L. X.; Yu, L. *Macromolecules* **2012**, *45*, 6390.
(28) Rolczynski, B. S.; Szarko, J. M.; Son, H. J.; Liang, Y.; Yu, L.; Chen, L. X. *Journal of the American Chemical Society* **2012**, *134*, 4142.
(29) Perepichka, I. F.; Levillain, E.; Roncali, J. *Journal of Materials Chemistry* **2004**, *14*, 1679.
(30) Scharber, M. C.; Mühlbacher, D.; Koppe, M.; Denk, P.; Waldauf, C.; Heeger, A. J.; Brabec, C. J. *Advanced materials* **2006**, *18*, 789.
(31) Thompson, B. C.; Fréchet, J. M. *Angewandte chemie international edition* **2008**, *47*, 58.
(32) Zhou, H.; Yang, L.; Stoneking, S.; You, W. *ACS applied materials & interfaces* **2010**, *2*, 1377.
(33) Zhou, H.; Yang, L.; Price, S. C.; Knight, K. J.; You, W. *Angewandte Chemie* **2010**, *49*, 7992.
(34) Li, G.; Zhu, R.; Yang, Y. *Nature photonics* **2012**, *6*, 153.
(35) Günes, S.; Neugebauer, H.; Sariciftci, N. S. *Chemical reviews* **2007**, *107*, 1324.
(36) Yu, G.; Gao, J.; Hummelen, J. C.; Wudl, F.; Heeger, A. J. *Science* **1995**, *270*, 1789.
(37) Zhao, J.; Li, Y.; Yang, G.; Jiang, K.; Lin, H.; Ade, H.; Ma, W.; Yan, H. *Nature Energy* **2016**, *1*, 15027.
(38) Chen, S.; Liu, Y.; Zhang, L.; Chow, P. C. Y.; Wang, Z.; Zhang, G.; Ma, W.; Yan, H. *Journal of the American Chemical Society* **2017**, *139*, 6298.
(39) Li, Y. *Accounts of Chemical Research* **2012**, *45*, 723.
(40) Henson, Z. B.; Mullen, K.; Bazan, G. C. *Nature chemistry* **2012**, *4*, 699.
(41) Hummelen, J. C.; Knight, B. W.; LePeq, F.; Wudl, F.; Yao, J.; Wilkins, C. L. *The Journal of Organic Chemistry* **1995**, *60*, 532.
(42) Zhan, C.; Yao, J. *Chemistry of Materials* **2016**, *28*, 1948.
(43) Liang, N.; Jiang, W.; Hou, J.; Wang, Z. *Mater. Chem. Front.* **2017**, *1*, 1291.
(44) Mori, D.; Benten, H.; Okada, I.; Ohkita, H.; Ito, S. *Energy & Environmental Science* **2014**, *7*, 2939.
(45) Deshmukh, K. D.; Qin, T.; Gallaher, J. K.; Liu, A. C. Y.; Gann, E.; O'Donnell, K.; Thomsen, L.; Hodgkiss, J. M.; Watkins, S. E.; McNeill, C. R. *Energy Environ. Sci.* **2015**, *8*, 332.
(46) Zhao, J.; Li, Y.; Lin, H.; Liu, Y.; Jiang, K.; Mu, C.; Ma, T.; Lin Lai, J. Y.; Hu, H.; Yu, D.; Yan, H. *Energy Environ. Sci.* **2015**, *8*, 520.
(47) Kwon, O. K.; Uddin, M. A.; Park, J. H.; Park, S. K.; Nguyen, T. L.; Woo, H. Y.; Park, S. Y. *Advanced materials* **2016**, *28*, 910.
(48) Lin, Y.; Zhang, Z.-G.; Bai, H.; Wang, J.; Yao, Y.; Li, Y.; Zhu, D.; Zhan, X. *Energy Environ. Sci.* **2015**, *8*, 610.
(49) Li, S.; Ye, L.; Zhao, W.; Zhang, S.; Mukherjee, S.; Ade, H.; Hou, J. *Advanced materials* **2016**, *28*, 9423.
(50) Patil, Y.; Misra, R.; Keshtov, M. L.; Sharma, G. D. *The Journal of Physical Chemistry C* **2016**, *120*, 6324.
(51) Bin, H.; Zhang, Z. G.; Gao, L.; Chen, S.; Zhong, L.; Xue, L.; Yang, C.; Li, Y. *Journal of the American Chemical Society* **2016**, *138*, 4657.

(52) Huang, Y.; Kramer, E. J.; Heeger, A. J.; Bazan, G. C. *Chemical reviews* **2014**, *114*, 7006.
(53) Liu, F.; Wang, C.; Baral, J. K.; Zhang, L.; Watkins, J. J.; Briseno, A. L.; Russell, T. P. *Journal of the American Chemical Society* **2013**, *135*, 19248.
(54) Lee, J. K.; Ma, W. L.; Brabec, C. J.; Yuen, J.; Moon, J. S.; Kim, J. Y.; Lee, K.; Bazan, G. C.; Heeger, A. J. *Journal of the American Chemical Society* **2008**, *130*, 3619.
(55) Yao, Y.; Hou, J.; Xu, Z.; Li, G.; Yang, Y. *Advanced Functional Materials* **2008**, *18*, 1783.
(56) Dittmer, J. J.; Marseglia, E. A.; Friend, R. H. *Advanced materials* **2000**, *12*, 1270.
(57) Yang, X.; Loos, J.; Veenstra, S. C.; Verhees, W. J.; Wienk, M. M.; Kroon, J. M.; Michels, M. A.; Janssen, R. A. *Nano letters* **2005**, *5*, 579.
(58) Hwang, Y. J.; Courtright, B. A.; Ferreira, A. S.; Tolbert, S. H.; Jenekhe, S. A. *Advanced materials* **2015**, *27*, 4578.
(59) Pearson, A. J.; Wang, T.; Jones, R. A. L.; Lidzey, D. G.; Staniec, P. A.; Hopkinson, P. E.; Donald, A. M. *Macromolecules* **2012**, *45*, 1499.
(60) Lu, G. H.; Li, L. G.; Yang, X. N. *Advanced materials* **2007**, *19*, 3594.
(61) Bull, T. A.; Pingree, L. S.; Jenekhe, S. A.; Ginger, D. S.; Luscombe, C. K. *ACS nano* **2009**, *3*, 627.
(62) Chirvase, D.; Parisi, J.; Hummelen, J. C.; Dyakonov, V. *Nanotechnology* **2004**, *15*, 1317.
(63) Wang, E.; Hou, L.; Wang, Z.; Hellstrom, S.; Zhang, F.; Inganas, O.; Andersson, M. R. *Advanced materials* **2010**, *22*, 5240.
(64) Remmele, J.; Shen, D. E.; Mustonen, T.; Fruehauf, N. *ACS applied materials & interfaces* **2015**, *7*, 12001.
(65) Kondo, Y.; Tanabe, H.; Kudo, H.; Nakano, K.; Otake, T. *Materials* **2011**, *4*, 2171.
(66) Ma, C.; Taya, M.; Xu, C. *Polymer Engineering & Science* **2008**, *48*, 2224.
(67) Li, K.; Zhang, Q.; Wang, H.; Li, Y. *ACS applied materials & interfaces* **2014**, *6*, 13043.
(68) Murphy, A. R.; Fréchet, J. M. *Chemical reviews* **2007**, *107*, 1066.
(69) Mei, J.; Diao, Y.; Appleton, A. L.; Fang, L.; Bao, Z. *Journal of the American Chemical Society* **2013**, *135*, 6724.
(70) Dou, L.; Liu, Y.; Hong, Z.; Li, G.; Yang, Y. *Chemical reviews* **2015**, *115*, 12633.
(71) Carsten, B.; He, F.; Son, H. J.; Xu, T.; Yu, L. *Chemical reviews* **2011**, *111*, 1493.
(72) Azarian, D.; Dua, S. S.; Eaborn, C.; Walton, D. R. *Journal of Organometallic Chemistry* **1976**, *117*, C55.
(73) Stille, J. K. *Angewandte Chemie International Edition* **1986**, *25*, 508.
(74) Espinet, P.; Echavarren, A. M. *Angewandte Chemie International Edition* **2004**, *43*, 4704.
(75) Carsten, B.; He, F.; Son, H. J.; Xu, T.; Yu, L. *Chemical reviews* **2011**, *111*, 1493.
(76) Guo, X.; Watson, M. D. *Organic letters* **2008**, *10*, 5333.
(77) Guo, X.; Kim, F. S.; Jenekhe, S. A.; Watson, M. D. *Journal of the American Chemical Society* **2009**, *131*, 7206.

(78) Thilanga Liyanage, A. D.; Milián-Medina, B.; Zhang, B.; Gierschner, J.; Watson, M. D. *Macromolecular Chemistry and Physics* **2016**, *217*, 2068.
(79) Beaujuge, P. M.; Pisula, W.; Tsao, H. N.; Ellinger, S.; Müllen, K.; Reynolds, J. R. *Journal of the American Chemical Society* **2009**, *131*, 7514.
(80) Bao, Z.; Chan, W. K.; Yu, L. *Journal of the American Chemical Society* **1995**, *117*, 12426.
(81) Miyaura, N.; Suzuki, A. *Chemical reviews* **1995**, *95*, 2457.
(82) Li, J.; Ballmer, S. G.; Gillis, E. P.; Fujii, S.; Schmidt, M. J.; Palazzolo, A. M.; Lehmann, J. W.; Morehouse, G. F.; Burke, M. D. *Science* **2015**, *347*, 1221.
(83) Jacks, T. E.; Belmont, D. T.; Briggs, C. A.; Horne, N. M.; Kanter, G. D.; Karrick, G. L.; Krikke, J. J.; McCabe, R. J.; Mustakis, J. G.; Nanninga, T. N. *Organic process research & development* **2004**, *8*, 201.
(84) Huo, L.; Hou, J.; Zhang, S.; Chen, H. Y.; Yang, Y. *Angewandte Chemie* **2010**, *49*, 1500.
(85) (a) Orru, R. V.; de Greef, M. *Synthesis* **2003**, *2003*, 1471(b) Cox, P. A.; Leach, A. G.; Campbell, A. D.; Lloyd-Jones, G. C. *Journal of the American Chemical Society* **2016**, *138*, 9145.
(86) Ji, L.; Edkins, R. M.; Sewell, L. J.; Beeby, A.; Batsanov, A. S.; Fucke, K.; Drafz, M.; Howard, J. A.; Moutounet, O.; Ibersiene, F.; Boucekkine, A.; Furet, E.; Liu, Z.; Halet, J. F.; Katan, C.; Marder, T. B. *Chemistry* **2014**, *20*, 13618.
(87) Carrillo, J. A.; Turner, M. L.; Ingleson, M. J. *Journal of the American Chemical Society* **2016**, *138*, 13361.
(88) McCullough, R. D. *Advanced Materials* **1998**, *10*, 93.
(89) Osaka, I.; McCullough, R. D. *Accounts of chemical research* **2008**, *41*, 1202.
(90) Loewe, R. S.; Khersonsky, S. M.; McCullough, R. D. *Advanced materials* **1999**, *11*, 250.
(91) Loewe, R. S.; Ewbank, P. C.; Liu, J.; Zhai, L.; McCullough, R. D. *Macromolecules* **2001**, *34*, 4324.
(92) Sheina, E. E.; Liu, J.; Iovu, M. C.; Laird, D. W.; McCullough, R. D. *Macromolecules* **2004**, *37*, 3526.
(93) Mercier, L. G.; Leclerc, M. *Accounts of Chemical Research* **2013**, *46*, 1597.
(94) Bura, T.; Blaskovits, J. T.; Leclerc, M. *Journal of the American Chemical Society* **2016**, *138*, 10056.
(95) Pouliot, J. R.; Grenier, F.; Blaskovits, J. T.; Beaupre, S.; Leclerc, M. *Chemical reviews* **2016**, *116*, 14225.
(96) Dudnik, A. S.; Aldrich, T. J.; Eastham, N. D.; Chang, R. P.; Facchetti, A.; Marks, T. J. *Journal of the American Chemical Society* **2016**, *138*, 15699.
(97) Fujinami, Y.; Kuwabara, J.; Lu, W.; Hayashi, H.; Kanbara, T. *ACS Macro Letters* **2012**, *1*, 67.
(98) Seger, M. J. *Optimization of the optical and electrochemical properties of donor-acceptor copolymers through functional group and side chain modification*; University of Kentucky, 2013.

(99) Liyanage, A. D. T. *Fluorinated arene, imide and unsaturated pyrrolidinone based donor acceptor conjugated polymers: Synthesis, structure-property and device studies*; University of Kentucky, 2013.
(100) Greve, D. R.; Apperloo, J. J.; Janssen, R. A. *European Journal of Organic Chemistry* **2001**, *2001*, 3437.
(101) Morgado, J.; Cacialli, F.; Friend, R.; Chuah, B.; Rost, H.; Holmes, A. *Macromolecules* **2001**, *34*, 3094.
(102) Gray, G. W. *Liquid crystals* **1998**, *24*, 5.
(103) Cammidge, A. N. *Philosophical Transactions of the Royal Society of London A: Mathematical, Physical and Engineering Sciences* **2006**, *364*, 2697.
(104) Gray, G.-W. *Le Journal de Physique Colloques* **1975**, *36*, C1.
(105) Gray, G. *BDH monograph* **1978**.
(106) Lin, Y.-Y.; Gundlach, D.; Nelson, S. F.; Jackson, T. N. *IEEE Transactions on Electron Devices* **1997**, *44*, 1325.
(107) Anthony, J. E. *Chemical Reviews* **2006**, *106*, 5028.
(108) Adam, D.; Schuhmacher, P.; Simmerer, J.; Häussling, L.; Siemensmeyer, K.; Etzbachi, K.; Ringsdorf, H.; Haarer, D. *Nature* **1994**, *371*, 141.
(109) Voigt-Martin, I.; Garbella, R.; Schumacher, M. *Liquid Crystals* **1994**, *17*, 775.
(110) Wu, J.; Watson, M. D.; Zhang, L.; Wang, Z.; Müllen, K. *Journal of the American Chemical Society* **2004**, *126*, 177.
(111) Watson, M. D.; Wagener, K. B. *Macromolecules* **2000**, *33*, 8963.
(112) Few, C. S.; Wagener, K. B.; Thompson, D. L. *Macromolecular rapid communications* **2014**, *35*, 123.
(113) Mei, J.; Bao, Z. *Chemistry of Materials* **2014**, *26*, 604.
(114) Graham, K. R.; Cabanetos, C.; Jahnke, J. P.; Idso, M. N.; El Labban, A.; Ngongang Ndjawa, G. O.; Heumueller, T.; Vandewal, K.; Salleo, A.; Chmelka, B. F.; Amassian, A.; Beaujuge, P. M.; McGehee, M. D. *Journal of the American Chemical Society* **2014**, *136*, 9608.
(115) Zhang, Z.-G.; Li, Y. *Science China Chemistry* **2014**, *58*, 192.
(116) Zhang, Y.; Hau, S. K.; Yip, H.-L.; Sun, Y.; Acton, O.; Jen, A. K. Y. *Chemistry of Materials* **2010**, *22*, 2696.
(117) Zhang, G.; Fu, Y.; Zhang, Q.; Xie, Z. *Chemical communications* **2010**, *46*, 4997.
(118) Zou, Y.; Najari, A.; Berrouard, P.; Beaupré, S.; Réda Aïch, B.; Tao, Y.; Leclerc, M. *Journal of the American Chemical Society* **2010**, *132*, 5330.
(119) Piliego, C.; Holcombe, T. W.; Douglas, J. D.; Woo, C. H.; Beaujuge, P. M.; Fréchet, J. M. *Journal of the American Chemical Society* **2010**, *132*, 7595.
(120) Cabanetos, C.; El Labban, A.; Bartelt, J. A.; Douglas, J. D.; Mateker, W. R.; Frechet, J. M.; McGehee, M. D.; Beaujuge, P. M. *Journal of the American Chemical Society* **2013**, *135*, 4656.
(121) Yao, H.; Ye, L.; Zhang, H.; Li, S.; Zhang, S.; Hou, J. *Chemical reviews* **2016**, *116*, 7397.
(122) Beimling, P.; Koßmehl, G. *Chemische Berichte* **1986**, *119*, 3198.
(123) Laquindanum, J. G.; Katz, H. E.; Lovinger, A. J.; Dodabalapur, A. *Advanced materials* **1997**, *9*, 36.

(124) Pan, H.; Li, Y.; Wu, Y.; Liu, P.; Ong, B. S.; Zhu, S.; Xu, G. *Journal of the American Chemical Society* **2007**, *129*, 4112.
(125) Hou, J.; Park, M.-H.; Zhang, S.; Yao, Y.; Chen, L.-M.; Li, J.-H.; Yang, Y. *Macromolecules* **2008**, *41*, 6012.
(126) Huo, L.; Hou, J. *Polymer Chemistry* **2011**, *2*, 2453.
(127) Sista, P.; Biewer, M. C.; Stefan, M. C. *Macromolecular rapid communications* **2012**, *33*, 9.
(128) Huang, Y.; Liu, F.; Guo, X.; Zhang, W.; Gu, Y.; Zhang, J.; Han, C. C.; Russell, T. P.; Hou, J. *Advanced Energy Materials* **2013**, *3*, 930.
(129) Liao, S. H.; Jhuo, H. J.; Cheng, Y. S.; Chen, S. A. *Advanced materials* **2013**, *25*, 4766.
(130) Wan, Q.; Guo, X.; Wang, Z.; Li, W.; Guo, B.; Ma, W.; Zhang, M.; Li, Y. *Advanced Functional Materials* **2016**, *26*, 6635.
(131) Zhou, J.; Wan, X.; Liu, Y.; Zuo, Y.; Li, Z.; He, G.; Long, G.; Ni, W.; Li, C.; Su, X.; Chen, Y. *J Am Chem Soc* **2012**, *134*, 16345.
(132) Kan, B.; Zhang, Q.; Li, M.; Wan, X.; Ni, W.; Long, G.; Wang, Y.; Yang, X.; Feng, H.; Chen, Y. *J Am Chem Soc* **2014**, *136*, 15529.
(133) Sun, K.; Xiao, Z.; Lu, S.; Zajaczkowski, W.; Pisula, W.; Hanssen, E.; White, J. M.; Williamson, R. M.; Subbiah, J.; Ouyang, J.; Holmes, A. B.; Wong, W. W.; Jones, D. J. *Nature communications* **2015**, *6*, 6013.
(134) Nie, W.; MacNeill, C. M.; Li, Y.; Noftle, R. E.; Carroll, D. L.; Coffin, R. *Macromolecular rapid communications* **2011**, *32*, 1163.
(135) Coffin, R. C.; MacNeill, C. M.; Peterson, E. D.; Ward, J. W.; Owen, J. W.; McLellan, C. A.; Smith, G. M.; Noftle, R. E.; Jurchescu, O. D.; Carroll, D. L. *Journal of Nanotechnology* **2011**, *2011*, 1.
(136) Sainova, D.; Janietz, S.; Asawapirom, U.; Romaner, L.; Zojer, E.; Koch, N.; Vollmer, A. *Chemistry of materials* **2007**, *19*, 1472.
(137) Luzio, A.; Fazzi, D.; Nübling, F.; Matsidik, R.; Straub, A.; Komber, H.; Giussani, E.; Watkins, S. E.; Barbatti, M.; Thiel, W. *Chemistry of Materials* **2014**, *26*, 6233.
(138) Wang, Y.; Watson, M. D. *Macromolecules* **2008**, *41*, 8643.
(139) Lee, B.; Lo, C.-T.; Seifert, S.; Winans, R. E. *Journal of applied crystallography* **2006**, *39*, 749.
(140) Blanton, T.; Barnes, C.; Lelental, M. *Journal of applied crystallography* **2000**, *33*, 172.
(141) Knaapila, M.; Svensson, C.; Barauskas, J.; Zackrisson, M.; Nielsen, S. S.; Toft, K. N.; Vestergaard, B.; Arleth, L.; Olsson, U.; Pedersen, J. S. *Journal of synchrotron radiation* **2009**, *16*, 498.
(142) Tanaka, K.; Toda, F. *Chemical reviews* **2000**, *100*, 1025.
(143) Tellitu, I.; Beitia, I.; Díaz, M.; Alonso, A.; Moreno, I.; Domínguez, E. *Tetrahedron* **2015**, *71*, 8251.
(144) Cabrera-Rivera, F. A.; Hernández-Vázquez, L. G.; Flores-Sánchez, P.; Durán-Galván, M.; Escalante, J. *Green and Sustainable Chemistry* **2017**, *7*, 270.
(145) Liu, F.; Tang, C.; Chen, Q.-Q.; Shi, F.-F.; Wu, H.-B.; Xie, L.-H.; Peng, B.; Wei, W.; Cao, Y.; Huang, W. *The Journal of Physical Chemistry C* **2009**, *113*, 4641.

(146) Li, G.; Kang, C.; Gong, X.; Zhang, J.; Li, C.; Chen, Y.; Dong, H.; Hu, W.; Li, F.; Bo, Z. *Macromolecules* **2014**, *47*, 4645.
(147) Wang, C.; Chen, S.; Wang, K.; Zhao, S.; Zhang, J.; Wang, Y. *The Journal of Physical Chemistry C* **2012**, *116*, 17796.
(148) McDowell, J. J.; Schick, I.; Price, A.; Faulkner, D.; Ozin, G. *Macromolecules* **2013**, *46*, 6794.
(149) Xu, B.; Sheibani, E.; Liu, P.; Zhang, J.; Tian, H.; Vlachopoulos, N.; Boschloo, G.; Kloo, L.; Hagfeldt, A.; Sun, L. *Advanced materials* **2014**, *26*, 6629.
(150) Liang, Y.; Xu, Z.; Xia, J.; Tsai, S. T.; Wu, Y.; Li, G.; Ray, C.; Yu, L. *Advanced materials* **2010**, *22*, E135.
(151) Hu, Y.; Abate, A.; Cao, Y.; Ivaturi, A.; Zakeeruddin, S. M.; Grätzel, M.; Robertson, N. *The Journal of Physical Chemistry C* **2016**, *120*, 15027.
(152) Henson, Z. B.; Welch, G. C.; van der Poll, T.; Bazan, G. C. *J Am Chem Soc* **2012**, *134*, 3766.
(153) Small, C. E.; Chen, S.; Subbiah, J.; Amb, C. M.; Tsang, S.-W.; Lai, T.-H.; Reynolds, J. R.; So, F. *Nature Photonics* **2011**, *6*, 115.
(154) Frey, J.; Bond, A. D.; Holmes, A. B. *Chem. Commun.* **2002**, 2424.
(155) Raimundo, J.-M.; Blanchard, P.; Frère, P.; Mercier, N.; Ledoux-Rak, I.; Hierle, R.; Roncali, J. *Tetrahedron Letters* **2001**, *42*, 1507.
(156) Leriche, P.; Turbiez, M.; Monroche, V.; Frère, P.; Blanchard, P.; Skabara, P. J.; Roncali, J. *Tetrahedron letters* **2003**, *44*, 649.
(157) Kim, F. S.; Guo, X.; Watson, M. D.; Jenekhe, S. A. *Advanced materials* **2010**, *22*, 478.
(158) Guo, X.; Quinn, J.; Chen, Z.; Usta, H.; Zheng, Y.; Xia, Y.; Hennek, J. W.; Ortiz, R. P.; Marks, T. J.; Facchetti, A. *J Am Chem Soc* **2013**, *135*, 1986.
(159) Mateker, W. R.; Douglas, J. D.; Cabanetos, C.; Sachs-Quintana, I. T.; Bartelt, J. A.; Hoke, E. T.; El Labban, A.; Beaujuge, P. M.; Fréchet, J. M. J.; McGehee, M. D. *Energy & Environmental Science* **2013**, *6*, 2529.
(160) Amb, C. M.; Chen, S.; Graham, K. R.; Subbiah, J.; Small, C. E.; So, F.; Reynolds, J. R. *J Am Chem Soc* **2011**, *133*, 10062.
(161) Guo, X.; Zhou, N.; Lou, S. J.; Smith, J.; Tice, D. B.; Hennek, J. W.; Ortiz, R. P.; Navarrete, J. T. L.; Li, S.; Strzalka, J.; Chen, L. X.; Chang, R. P. H.; Facchetti, A.; Marks, T. J. *Nature Photonics* **2013**, *7*, 825.
(162) Guo, X.; Xin, H.; Kim, F. S.; Liyanage, A. D. T.; Jenekhe, S. A.; Watson, M. D. *Macromolecules* **2011**, *44*, 269.
(163) Nielsen, C. B.; Bjørnholm, T. *Organic letters* **2004**, *6*, 3381.
(164) Bao, X.; Hong, R.; Liu, P.; Deng, W. *Synthetic Metals* **2014**, *188*, 156.
(165) Hai, J.; Zhao, B.; Zhang, F.; Sheng, C.-X.; Yin, L.; Li, Y.; Zhu, E.; Bian, L.; Wu, H.; Tang, W. *Polymer* **2013**, *54*, 4930.
(166) Koeckelberghs, G.; Vangheluwe, M.; Persoons, A.; Verbiest, T. *Macromolecules* **2007**, *40*, 8142.
(167) Wagner, P.; Jolley, K. W.; Officer, D. L. *Australian Journal of Chemistry* **2011**, *64*, 335.

(168) Song, C. K.; Eckstein, B. J.; Tam, T. L. D.; Trahey, L.; Marks, T. J. *ACS applied materials & interfaces* **2014**, *6*, 19347.
(169) Nielsen, C. B.; Giovannitti, A.; Sbircea, D.-T.; Bandiello, E.; Niazi, M. R.; Hanifi, D. A.; Sessolo, M.; Amassian, A.; Malliaras, G. G.; Rivnay, J. *J. Am. Chem. Soc* **2016**, *138*, 10252.
(170) Gidh, A. V.; Decker, S. R.; Vinzant, T. B.; Himmel, M. E.; Williford, C. *Journal of Chromatography A* **2006**, *1114*, 102.
(171) Gidh, A. V.; Decker, S. R.; Vinzant, T. B.; Himmel, M. E.; Williford, C. W. *Chemical Engineering Communications* **2006**, *193*, 1546.
(172) Lei, T.; Dou, J. H.; Pei, J. *Advanced materials* **2012**, *24*, 6457.
(173) Groenendaal, L.; Jonas, F.; Freitag, D.; Pielartzik, H.; Reynolds, J. R. *Advanced materials* **2000**, *12*, 481.
(174) Heywang, G.; Jonas, F. *Advanced Materials* **1992**, *4*, 116.
(175) Kim, W.; Mäkinen, A.; Nikolov, N.; Shashidhar, R.; Kim, H.; Kafafi, Z. *Applied Physics Letters* **2002**, *80*, 3844.
(176) Havinga, E.; Mutsaers, C.; Jenneskens, L. *Chemistry of materials* **1996**, *8*, 769.
(177) Kumar, A.; Welsh, D. M.; Morvant, M. C.; Piroux, F.; Abboud, K. A.; Reynolds, J. R. *Chemistry of Materials* **1998**, *10*, 896.
(178) Daoust, G.; Leclerc, M. *Macromolecules* **1991**, *24*, 455.
(179) Iraqi, A.; Clark, D.; Jones, R.; Krier, A. *Synthetic metals* **1999**, *102*, 1220.
(180) Koeckelberghs, G.; Vangheluwe, M.; Doorsselaere, K. V.; Robijns, E.; Persoons, A.; Verbiest, T. *Macromolecular Rapid Communications* **2006**, *27*, 1920.
(181) Zhang, Z.-B.; Fujiki, M. *Polymer journal* **2001**, *33*, 597.
(182) Faid, K.; Cloutier, R.; Leclerc, M. *Macromolecules* **1993**, *26*, 2501.
(183) Vangheluwe, M.; Verbiest, T.; Koeckelberghs, G. *Macromolecules* **2008**, *41*, 1041.
(184) Ohshita, J.; Tada, Y.; Kunai, A.; Harima, Y.; Kunugi, Y. *Synthetic Metals* **2009**, *159*, 214.
(185) McCulloch, I.; Heeney, M.; Chabinyc, M. L.; DeLongchamp, D.; Kline, R. J.; Cölle, M.; Duffy, W.; Fischer, D.; Gundlach, D.; Hamadani, B.; Hamilton, R.; Richter, L.; Salleo, A.; Shkunov, M.; Sparrowe, D.; Tierney, S.; Zhang, W. *Advanced materials* **2009**, *21*, 1091.
(186) Ong, B. S.; Wu, Y.; Liu, P.; Gardner, S. *Journal of the American Chemical Society* **2004**, *126*, 3378.
(187) McCulloch, I.; Heeney, M.; Bailey, C.; Genevicius, K.; Macdonald, I.; Shkunov, M.; Sparrowe, D.; Tierney, S.; Wagner, R.; Zhang, W.; Chabinyc, M. L.; Kline, R. J.; McGehee, M. D.; Toney, M. F. *Nature materials* **2006**, *5*, 328.
(188) Li, J.; Qin, F.; Li, C. M.; Bao, Q.; Chan-Park, M. B.; Zhang, W.; Qin, J.; Ong, B. S. *Chemistry of Materials* **2008**, *20*, 2057.
(189) Osaka, I.; Zhang, R.; Sauvé, G. v.; Smilgies, D.-M.; Kowalewski, T.; McCullough, R. D. *Journal of the American Chemical Society* **2009**, *131*, 2521.
(190) Osaka, I.; Abe, T.; Shinamura, S.; Miyazaki, E.; Takimiya, K. *Journal of the American Chemical Society* **2010**, *132*, 5000.
(191) Wang, Q.; Takita, R.; Kikuzaki, Y.; Ozawa, F. *Journal of the American Chemical Society* **2010**, *132*, 11420.

(192) Rudenko, A. E.; Wiley, C. A.; Stone, S. M.; Tannaci, J. F.; Thompson, B. C. *Journal of Polymer Science Part A: Polymer Chemistry* **2012**, *50*, 3691.
(193) Kuwabara, J.; Nohara, Y.; Choi, S. J.; Fujinami, Y.; Lu, W.; Yoshimura, K.; Oguma, J.; Suenobu, K.; Kanbara, T. *Polymer Chemistry* **2013**, *4*, 947.
(194) Yamazaki, K.; Kuwabara, J.; Kanbara, T. *Macromolecular rapid communications* **2013**, *34*, 69.
(195) De Leeuw, D.; Simenon, M.; Brown, A.; Einerhand, R. *Synthetic Metals* **1997**, *87*, 53.
(196) Yamamoto, T.; Suganuma, H.; Maruyama, T.; Kubota, K. *Journal of the Chemical Society, Chemical Communications* **1995**, 1613.
(197) Yamamoto, T.; Suganuma, H.; Maruyama, T.; Inoue, T.; Muramatsu, Y.; Arai, M.; Komarudin, D.; Ooba, N.; Tomaru, S.; Sasaki, S. *Chemistry of materials* **1997**, *9*, 1217.
(198) Politis, J. K.; Curtis, M. D.; Gonzalez, L.; Martin, D. C.; He, Y.; Kanicki, J. *Chemistry of materials* **1998**, *10*, 1713.
(199) Osaka, I.; Zhang, R.; Liu, J.; Smilgies, D.-M.; Kowalewski, T.; McCullough, R. D. *Chemistry of Materials* **2010**, *22*, 4191.
(200) Kim, D. H.; Lee, B.-L.; Moon, H.; Kang, H. M.; Jeong, E. J.; Park, J.-I.; Han, K.-M.; Lee, S.; Yoo, B. W.; Koo, B. W. *Journal of the American Chemical Society* **2009**, *131*, 6124.
(201) Ortiz, R. P.; Yan, H.; Facchetti, A.; Marks, T. J. *Materials* **2010**, *3*, 1533.
(202) Guo, X.; Quinn, J.; Chen, Z.; Usta, H.; Zheng, Y.; Xia, Y.; Hennek, J. W.; Ortiz, R. P.; Marks, T. J.; Facchetti, A. *Journal of the American Chemical Society* **2013**, *135*, 1986.
(203) Wen, L.; Nietfeld, J. P.; Amb, C. M.; Rasmussen, S. C. *The Journal of organic chemistry* **2008**, *73*, 8529.
(204) Hachmann, J.; Olivares-Amaya, R.; Jinich, A.; Appleton, A. L.; Blood-Forsythe, M. A.; Seress, L. R.; Román-Salgado, C.; Trepte, K.; Atahan-Evrenk, S.; Er, S.; Shrestha, S.; Mondal, R.; Sokolov, A.; Bao, Z.; Aspuru-Guzik, A. *Energy Environ. Sci.* **2014**, *7*, 698.

Vita

Personal information

Name	Bei Zhang
Place of birth	Nanyang, China

Education

(expected) Ph.D. in Chemistry, Aug. 2012~Mar. 2018, University of Kentucky, USA
M.S. in Applied Chemistry, 2010, Dalian University of Technology, China
B.S. in Chemical Engineer, 2007, Northeast Petroleum University, China

Publications

- Thilanga Liyanage, A. D.; Milián-Medina, B.; **Zhang, B.**; Gierschner, J.; Watson, M. D. *Macromolecular Chemistry and Physics* 2016, 217, 2068.
- Yu, H.; Li, G.; **Zhang, B.**; Zhang, X.; Xiao, Y.; Wang, J.; Song, Y. *Dyes and Pigments* 2016,133, 93.